8-1983

A Machining System for Turning Nonaxisymmetric Surfaces

Spivey Stevens Douglass
University of Tennessee, Knoxville

To the Graduate Council:

I am submitting herewith a dissertation written by Spivey Stevens Douglass entitled "A Machining System for Turning Nonaxisymmetric Surfaces." I have examined the final electronic copy of this dissertation for form and content and recommend that it be accepted in partial fulfillment of the requirements for the degree of Doctor of Philosophy, with a major in Engineering Science.

Walter L. Green, Major Professor

We have read this dissertation and recommend its acceptance:

William T. Snyder, J. M. Bailey, Thomas G. Carley, Carl J. Remenyik

Accepted for the Council:
Dixie L. Thompson

Vice Provost and Dean of the Graduate School

(Original signatures are on file with official student records.)

To the Graduate Council:

I am submitting herewith a dissertation written by Spivey Stevens Douglass entitled "A Machining System for Turning Nonaxisymmetric Surfaces." I have examined the final copy of this dissertation for form and content and recommend that it be accepted in partial fulfillment of the requirements for the degree of Doctor of Philosophy, with a major in Engineering Science.

Walter L. Green

Walter L. Green, Major Professor

We have read this thesis
and recommend its acceptance:

William J. Snyder

J M Bailey

Thomas Carley

Carl J. Remenyi II

Accepted for the Council:

L W Minkel

The Graduate School

A MACHINING SYSTEM FOR TURNING NONAXISYMMETRIC SURFACES

A Dissertation

Presented for the

Doctor of Philosophy

Degree

The University of Tennessee, Knoxville

Spivey Stevens Douglass

August 1983

ACKNOWLEDGEMENT

I would first like to express my appreciation to the University of Tennessee and the graduate administration for the flexibility permitted in choosing and pursuing my graduate studies. My graduate committee members, Dr. J. M. Bailey, Dr. T. G. Carley, Dr. C. J. Remenyik and Dr. (now Dean) W. T. Snyder, were generous in their support and availability. My major professor and friend, Walter Green, has demonstrated that college teaching can extend far beyond the campus boundaries. Even without gaining the degree I would be thankful for his influence.

I certainly wish to recognize the support provided by my management at Union Carbide Corporation. Messrs. Hilton Tunnell, Fred Jones and Bill Dodson have been patient and steady and only with their help was my research possible. Quite a number of colleagues in the Y-12 Plant of Union Carbide Corporation in Oak Ridge, Tennessee are also due my gratitude, but space does not permit naming them individually. To all, I say "Thanks, again."

I do not know how to express to my mother, Mrs. Pearl Douglass, and to my deceased father, Nelson Douglass, my love and appreciation for their sacrifices in providing not only educational opportunities but much more. Likewise, brothers Nelson and Tom and their wives Rosemary and Thelma, have contributed greatly, both personally and financially; everyone should be blessed with such relations.

Finally, I cannot say anything to thank my wife Shelby adequately for her help. Maybe over the next fifty or so years I can partially repay her.

ABSTRACT

Aspheric reflecting surfaces possessing extremely high surface finish and contour accuracy are often demanded by the optics industry. Such reflectors have also been required in high energy gas laser systems used to trigger thermonuclear reactions in experiments connected with advanced electric power generation.

Historically, production of optical pieces of the quality described required many repetitions of selective hand-lapping, polishing and measuring. In the past ten years production of these pieces has been enhanced by machining with diamond cutting tools on precision numerically controlled (NC) turning machines. These machines are capable of generating axisymmetric surfaces competitive in quality to those produced by conventional means without the expensive hand-work. This experiment describes the design and testing of a prototype system for machining an off-axis parabolic sector by on-axis turning. The prototype system utilized an auxiliary slide which carried the cutting tool. The slide was supported by captive air bearings and was driven by a linear motor.

A transformation was performed on the parabola to describe the auxiliary slide motion in coordinates centered in the off-axis sector. A Fourier expansion resulted in a scheme which permits the slide position commands to be generated in real time. The use by the signal generator of position information from the base machine transverse slide along with zero position and tachometer signals from the spindle insured synchronization between all motions.

A test part was machined with the prototype system. The contour accuracy of the test part was measured between -.0005 and +.0009 inch. Surface finish varied from 7 microinches RMS near the part center to approximately 60 microinches near the outer edge.

Two important factors contributed to the workpiece inaccuracy. An electrical noise level equivalent to 15 to 20 microinches of vibration detracted from the surface finish and denied the use of a diamond cutting tool. A structural resonance in the linear motor prevented the use of higher position loop gain which resulted in increased following error. The system did serve as a proof-of-principle, however, and also produced a workpiece requiring less handwork than would have been required conventionally.

TABLE OF CONTENTS

LIST OF TABLES

LIST OF FIGURES

CHAPTER 1

INTRODUCTION

Turning constitutes one of the most important and frequently encountered manufacturing operations. Besides generating surfaces of revolution, turning provides an excellent combination of close-tolerance shaping and high material-removal rate. Consequently, extensive development effort has been invested in improving turning machines, tools, sensors, and other system components.

Although turning began prior to 26 BC (1), most of the important improvements started in the 18th century with the Industrial Revolution. Henry Maudslay invented the machine slide system in 1797 (1). Following his invention technology was soon developed for thread cutting as well as holding accurate dimensions in the presence of large tool forces that accompany high material-removal rates. The addition of slide control systems provided the capability for generating relatively complex surfaces of revolution, compared to flat, cylindrical, or tapered surfaces. This capability was extended by the introduction of the duplicator lathe (2) and later by numerically controlled machines (3). During the past twenty-five years, turning has been further advanced by such sophisticated components as: pressurized fluid bearings (4-12), laser interferometric position transducers (12-14), diamond cutting tools (8), and various drive mechanisms. These advances in metal-removal technology have provided the capability to produce parts with precise contours and surface finishes. Contour accuracies of less than 100 microinches and

surface finishes of less than one microinch can now be achieved with selected metals (8,15,16).

Currently turning operations are still largely confined to the generation of axisymmetric surfaces. In this case all cross sections perpendicular to the axis of symmetry are circular. To produce noncircular cross sections, one slide must be driven synchronously with the spindle rotation. However, spindles are usually operated at speeds greater than 100 rpm. There are two reasons for using such speeds: first, surface separation during cutting and hence the surface finish tend to deteriorate when the surface speed is below a material-dependent minimum; second, economic considerations demand the highest possible material-removal rates. Therefore, due to the requirements of a relatively high spindle speed, synchronization of slide motion to spindle motion is extremely difficult. Although the desired motion is mathematically describable with only two linear axes, physical realization of the required response is impossible due to the slide masses. The only known industrial turning machines operating in this manner are the "bottle" lathes used in the manufacture of molds for glass bottles. These machines typically operate at spindle speeds considerably below 100 rpm. Several applications exist for which high-speed slides, as just described, would be particularly valuable. These applications can generally be categorized as having either: (1) nonaxisymmetric surfaces or (2) special features (either elevations or depressions) on otherwise axisymmetric contours. Examples of the first category can be found in contoured reflectors used in the optics industry. In this case high accuracy is demanded in both shape and surface finish. An example of the second category might be seen as a groove in an otherwise round part necessitated by assembly with a mating part. Close-tolerance machining of this feature could

be required for reasons of strength or weight distribution. If this feature can be generated continuously with the surrounding surface, the cost of production will be reduced significantly.

Consider the "off-axis parabolic sector" illustrated by the shaded area in Figure 1-1. This particular sector is not a figure of revolution about any axis intersecting it and hence cannot be turned about its center. Generation of off-axis sectors by conventional means requires either that the part be turned about its principal axis in an interrupted cut, or that an expensive hand-working operation be applied to the nearest spherical surface approximating the desired sector. If the distance from the off-axis sector to the axis of symmetry is sufficiently large, the first alternative may be impossible because of insufficient machine capacity. A high-speed slide could, therefore, provide a strong economic improvement in the machining of these surfaces.

For focusing high energy laser beams onto small targets used in experimental laser fusion systems, extremely high quality parabolic reflectors are required. Thompson (17) first proposed the use of an auxiliary high-speed slide with conventional turning machines for production of off-axis sectors of these off-axis reflectors. Thompson's proposal described a machine configuration and the related mathematical transformations for producing these surfaces. The treatment was similar to that shown in Chapter 2.

The configuration of a typical, high-precision, numerically controlled (NC) turning machine is illustrated in Figure 1-2. The workpiece is mounted on the face of the spindle. The cutting tool is attached to the end of a boring bar which is mounted on the X slide. The X slide provides linear motion perpendicular to the spindle axis of rotation in a horizontal plane. The X slide is

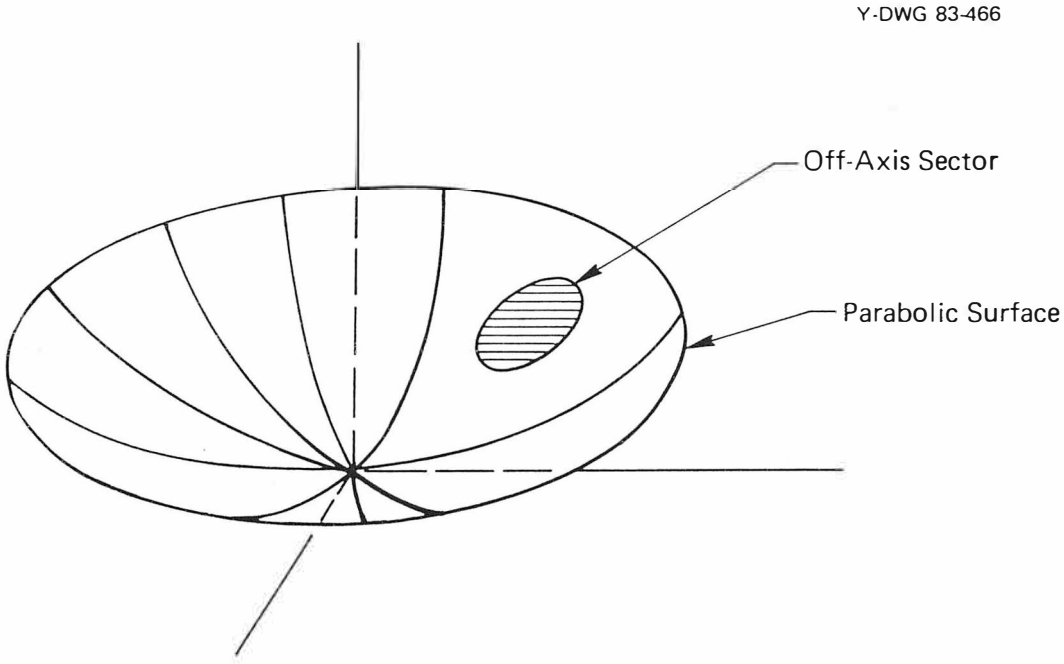

Figure 1-1. Off-axis sector of parabolic surface (concave upward).

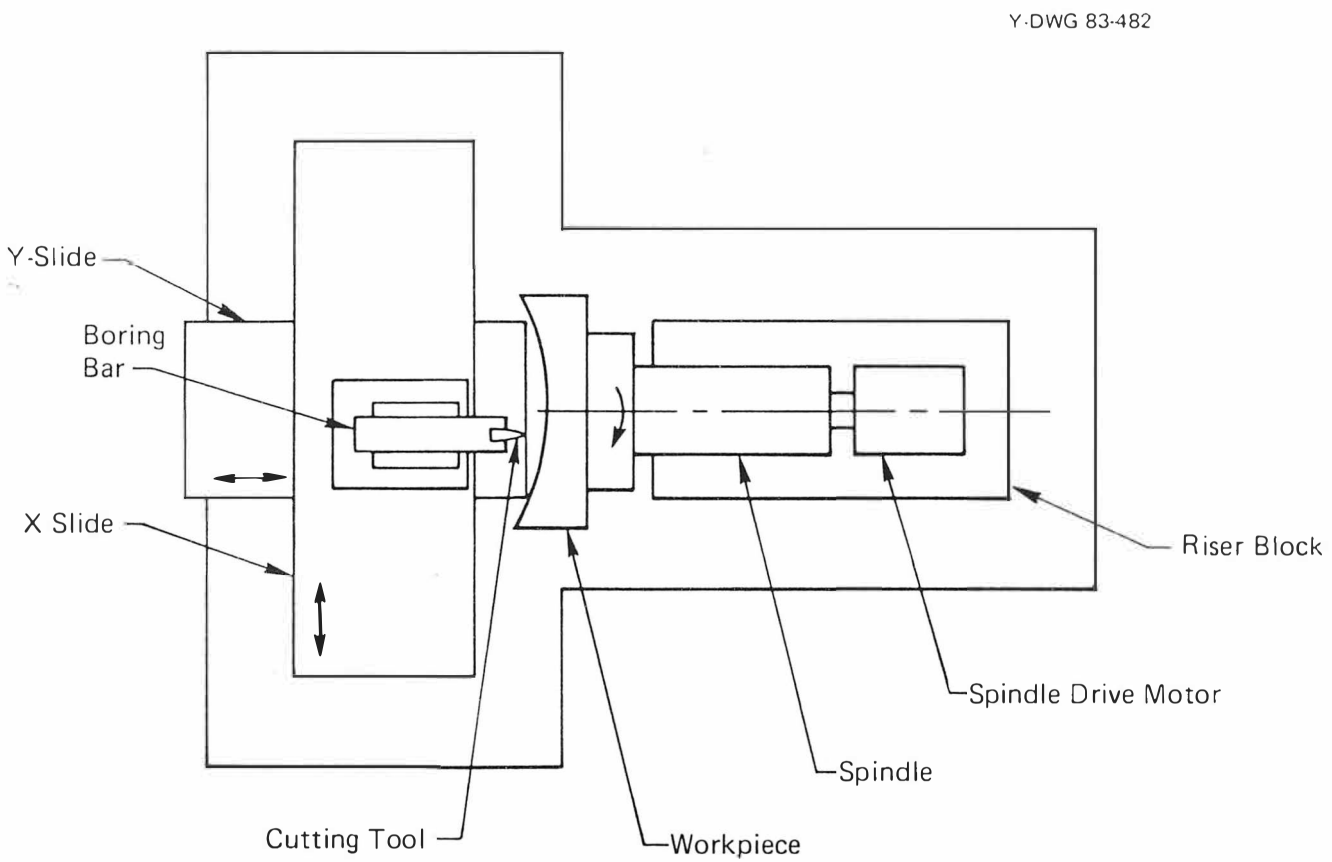

Figure 1-2. Typical numerically controlled (NC) turning machine.

carried on the Y slide which provides linear motion parallel to the spindle axis. Slide motions are provided by rotating a precision leadscrew within a nut fixed to the slide. Leadscrew rotation is driven by a motor (hydraulic or electric), controlled by the machine control unit (MCU). To follow a prescribed path at controlled velocities, information for each slide is read from a punched tape into the MCU. Feedback of the same quantities from slide sensors to the MCU closes the system loops. Since the slide motions are coupled only by command inputs, the accuracy of the generated surface depends on the ability of the MCU to match the motions in time. Generally, this requirement can be met since the slide response is usually much faster than the rate at which new commands are issued. The motions, therefore, are essentially steady-state.

For the most part MCU control of the spindle is limited to speed control through tachometer feedback. Except for machines possessing a threading capability, no effort is generally made to account for the spindle rotational position.

An indication of the success of the present control systems in performing their function is reflected by the quality of the generated surfaces. In a solid, easily machined metal part, a spherical surface can be produced to tolerances of less than 500 microinches. By incorporating the developments cited earlier, the accuracy can further be improved more than an order of magnitude.

The capability to generate nonaxisymmetric contours on an existing turning machine required a number of additions. Figure 1-3 illustrates the machining system used in this research. The existing X and Y slides were used to generate the primary linear motions while a third slide, denoted Z, was mounted on the X slide. The cutting tool was fixed to the end of the Z slide

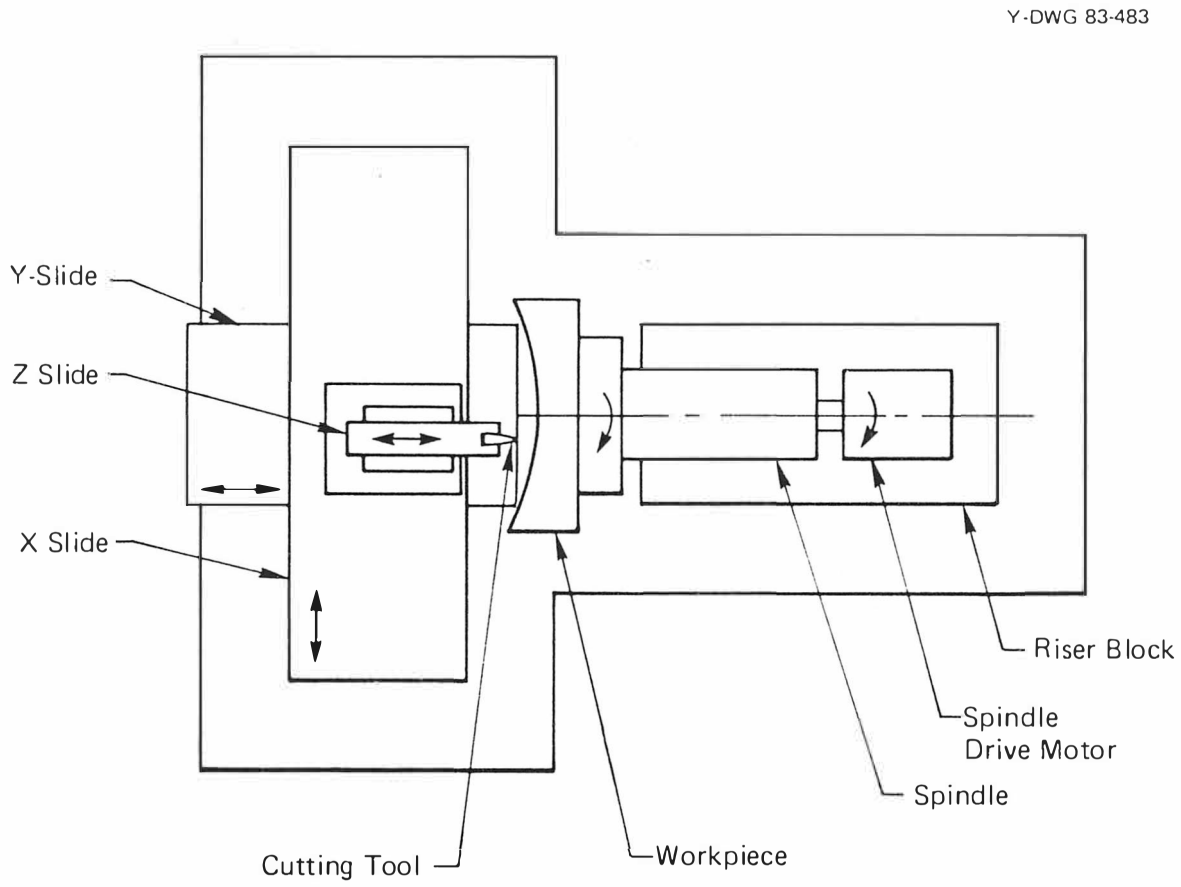

Figure 1-3. Modified NC turning machine.

rather than on the boring bar. A drive motor and position sensing equipment were required for the Z slide, along with spindle angle referencing equipment. Finally, electronic circuitry was required for generating commands to the Z slide, controlling the position of the Z slide, and synchronizing this position with that of the spindle and both primary slide motions.

For the purpose of this investigation the following problem statement was used to establish the performance goals:

It is desired to produce, by diamond turning, an off-axis parabolic sector defined by

1. A focal length of 79.15 inches;
2. A perpendicular distance from the sector center to the axis of the parabola of 28 inches; and
3. A sector diameter of approximately 16 inches.

Typical machining conditions will be defined as a 100 microinch depth of cut and a feedrate of 100 microinches per revolution at a spindle speed of 300 rpm. The desired surface will exhibit a finish of less than 5 microinches peak-to-valley and a contour accuracy of less than $\pm$ 30 microinches. It is emphasized that these are goals for the finished part and represent extremes in system performance. The machining system developed was not intended to compensate for errors in the base machine. The major thrust of this study lay in testing the feasibility of synchronizing a fast-response slide with the other machine motions as a means of producing nonaxisymmetric surfaces.

The chapters that follow describe the design, analysis and testing of the machining system. Chapter 2 presents the mathematical transformations associated with producing the off-axis parabolic sector. Included in this chapter are estimates of velocity and acceleration subsequently used in the design of

the control system and in choice of equipment. Chapter 3 details the modifications and additions made in the base machine and explains the design and selection of components used in the Z slide. The design and testing of the Z slide controls are described in Chapter 4. Final system testing by machining of test parts is discussed in Chapter 5 and includes a summary of actual measured surface errors. Chapter 6 consists of a summary of lessons learned during the investigation and recommendations for future work.

CHAPTER 2

MATHEMATICAL DESCRIPTION OF REQUIRED Z SLIDE MOTION

In this chapter the required Z-axis motion will be derived. This motion, which in synchronism with the spindle and X and Y slides, will theoretically generate the parabolic shape defined by the problem statement in Chapter 1. The derivation does not deal with slide dynamics, sensor accuracy or any other aspect of Z slide performance. Such considerations will be made in Chapter 3.

Development of Z Axis Motion

In this development three coordinate systems will be employed. The first will be denoted by subscript 1, the second by subscript 2, and the third by subscript 3.

A paraboloid of revolution about the z_1-axis with its vertex at the origin is defined by

$$Z_1 = \frac{x_1^2 + y_1^2}{4p} \tag{2-1}$$

where (0,0,p) are the coordinates of the focus and $z_1 = -p$ defines the plane of the directrix. Figure 2-1 illustrates a cross section of this surface.

A new coordinate system is desired to describe in a particular fashion a relatively small, off-axis sector of the parabolic surface. Let the sector of interest be centered at $(0,S_y,S_z)$. The desired coordinate system has its origin at this point. Furthermore, the transformed z_3-axis is normal to the surface of the paraboloid at the new origin. Two coordinate transformations, first pure

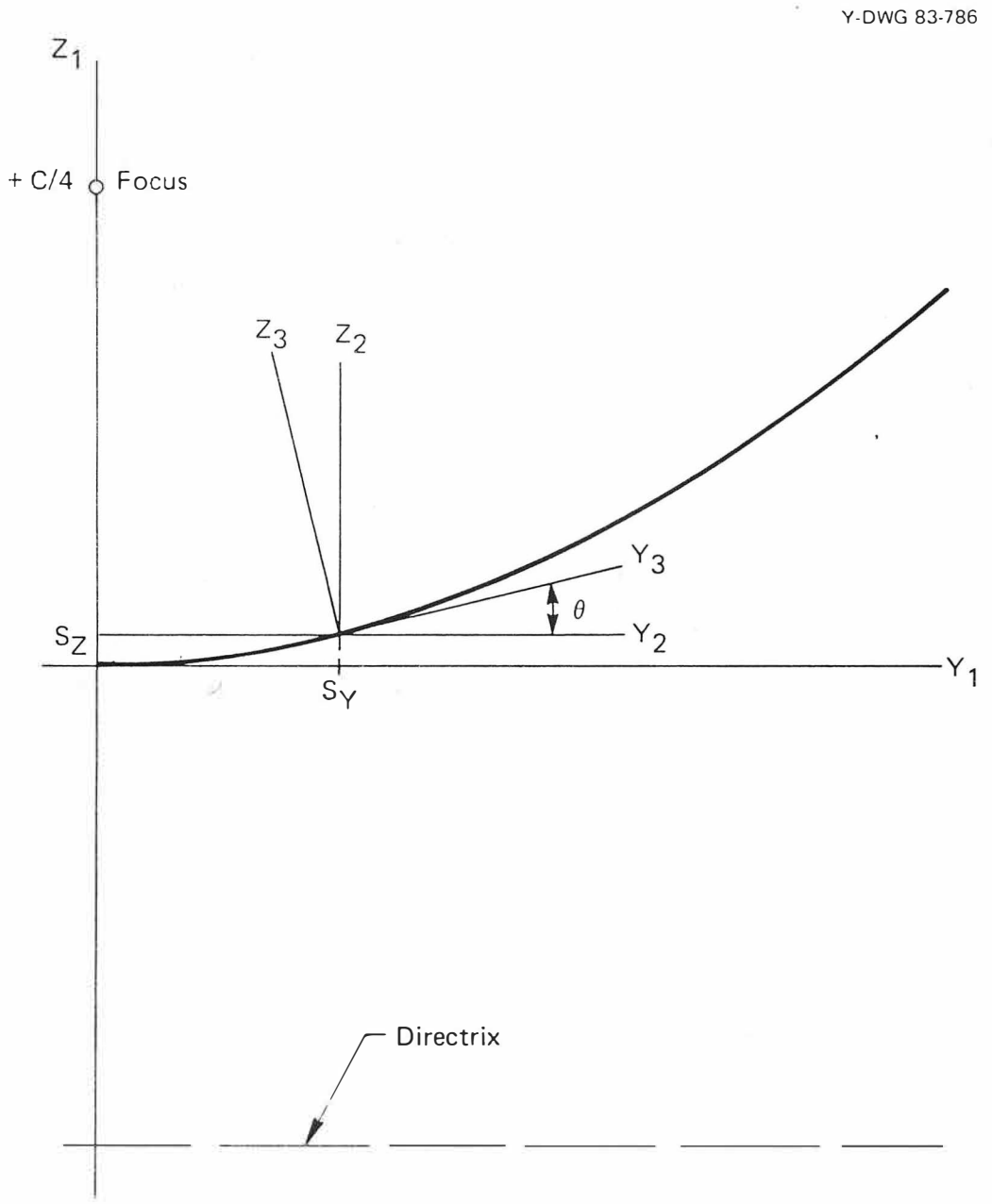

Figure 2-1. Definition of the coordinate systems.

translation and second pure rotation through an angle θ, produce the equation of the paraboloid in the new coordinate system.

For the translation:

$$\begin{aligned} x_1 &= x_2 \\ y_1 &= y_2 + S_y \\ z_1 &= z_2 + S_z \end{aligned} \tag{2-2}$$

where

$$S_z = z_1 \text{ at } x_1 = 0 \text{ and } y_1 = S_y$$

$$S_z = \frac{S_y^2}{c}$$

For the rotation:

$$\begin{aligned} x_2 &= x_3 \\ y_2 &= y_3\cos(\theta) - z_3\sin(\theta) \\ z_2 &= y_3\sin(\theta) + z_3\cos(\theta) \end{aligned} \tag{2-3}$$

where

$$\tan(\theta) = \frac{\partial z_2}{\partial y_2} \text{ at } x_2 = y_2 = 0$$

$$\tan(\theta) = \frac{2S_y}{c}.$$

Application of these transforming relations to Equation (2-1) yields

$$z_3 = \left(\frac{c^3}{8S_y^2\cos\theta}\right)\left\{\left[1 + \frac{4S_y^2}{c^2}\right] + \left[\frac{4S_y\cos\theta}{c^2}\right]y_3 - \left[\frac{4S_y}{c^2}\right] \times \left[\left(\frac{c^2}{2} + \frac{c^4}{16S_y^2} + S_y^2\right) + \left(\frac{c^2}{2S_y} + 2S_y\right)y_3\cos\theta - x_3^2\right]^{1/2}\right\} \tag{2-4}$$

If these rectangular coordinates are transformed into cylindrical coordinates by

$$\begin{aligned} x_3 &= R\cos(\phi) \\ y_3 &= R\sin(\phi) \\ z_3 &= z_3 \end{aligned} \tag{2-5}$$

Equation (2-4) takes the form

$$z_3 = \left(\frac{c^3}{8S_y^2\cos\theta}\right)\left\{\left(1 + \frac{4S_y^2}{c^2}\right) + \left(\frac{4S_y\cos\theta}{c^2}\right)R\sin\phi - \left(\frac{4S_y}{c^2}\right)\times \right.$$

$$\left[\left(\frac{c^2}{2} + \frac{c^4}{16S_y^2} + S_y^2\right) + \left(\frac{c^2}{2S_y} + 2S_y\right)R\cos\theta\sin\phi - \right.$$

$$\left.\left. R^2\cos^2\phi\right]^{1/2}\right\} \tag{2-6}$$

The R,ϕ,z_3 coordinate system represents the basic system to be employed by the turning machine in generating the off-axis sector of the paraboloid. At this point the axes will be re-labeled in order to conform with numerical control terminology. Let the R and z_3 designations be replaced by X and Y_t respectively. The basic turning machine motions then consist of:

1. The spindle, to which the workpiece is fixed and for which the rotational position is described by ϕ;

2. The X slide which carries the cutting tool and which represents the radial coordinate; and

3. The Y_t slide which carries the spindle and which represents the axial coordinate.

With this re-labeling Equation (2-6) becomes

$$Y_t(X,\phi) = \left(\frac{c^3}{8S_y^2\cos\theta}\right)\left\{\left(1 + \frac{4S_y^2}{c^2}\right) + \left(\frac{4S_y\cos\theta}{c^2}\right)X\sin\phi\right.$$

$$-\left(\frac{4S_y}{c^2}\right)\left[\left(\frac{c^2}{2} + \frac{c^4}{16}S_y^2 + S_y^2\right) + \left(\frac{c^2}{2S_y} + 2S_y\right)\cos\theta X\sin\phi - \right.$$

$$\left.\left.X^2\cos^2\phi\right]^{1/2}\right\} \qquad (2\text{-}7)$$

Since Y_t is a function of both X and ϕ, the off-axis sector cannot be a surface of revolution about the Y_t axis. Although the required Y_t motion is mathematically describable in terms of X and ϕ, the masses of the slides prevent their being driven in synchronism with the spindle at acceptable spindle speeds.

The machining system under study replaces the $Y_t(X,\phi)$ with two parallel motions. This is best exhibited by the expression

$$Y_t(X,\phi) = Y(X) + Z(X,\phi). \qquad (2\text{-}8)$$

Therefore, the new machining system utilizes the existing axial slide motion to provide the gross portion of $Y_t(X,\phi)$, while a third slide, the Z slide, provides only the ϕ-dependent motion required by the non-axisymmetry of the part surface. The Z slide is mounted on the X slide and carries the tool in short motions parallel to the Y slide.

If the Z slide is to provide only the within-rotation variations of the surface in the Y direction, a determination must now be made of the surface extrema at arbitrary but fixed X. Equation (2-7) can be re-written as

$$Y_t(X,\phi) = \frac{S_y}{\sin^3\theta} + \frac{X\sin\phi}{\tan\theta} - \left(\frac{S_y}{\sin^3\theta}\right) \times P(X,\phi) \qquad (2\text{-}9)$$

where

$$P(X,\phi) = \left[1 + \left(\frac{2\sin^2\theta\cos\theta}{S_y}\right)X\sin\phi - \left(\frac{\sin^4\theta}{S_y^2}\right)X^2\cos^2\phi\right]^{1/2}$$

The condition $\frac{\partial Y_t}{\partial \phi} = 0$ is applied.

$$\frac{\partial Y_t}{\partial \phi} = X\cot\theta\cos\phi \left\{1 - \frac{1 + \frac{2\sin\theta}{c}X\sin\phi}{P(X,\phi)}\right\} \qquad (2\text{-}10)$$

Extrema are located at $\phi = \pm n\pi/2$ $(n=1,3,5...)$. By equating to zero the quantity in braces in Equation (2-10), additional extrema are found where

$$\phi = \sin^{-1}\left[-\left(\frac{c}{2X\sin\theta}\right)\left\{1 - \left[1 - \left(\frac{X}{S_y}\right)^2\sin^2\theta\right]^{1/2}\right\}\right] \qquad (2\text{-}11)$$

To determine which of the extrema are minima and which are maxima, $\frac{\partial^2 Y_t}{\partial \phi^2}$ is evaluated at the various points of interest. Thus,

$$\frac{\partial^2 Y_t}{\partial \phi^2} = X\cot\theta\cos\phi\frac{\partial}{\partial\phi}\left\{1 - \frac{1 + \frac{2X\sin\theta}{c}\sin\phi}{P(X,\phi)}\right\}$$

$$-X\cot\theta\sin\phi\left\{1 - \frac{1 + \frac{2X\sin\theta}{c}\sin\phi}{P(X,\phi)}\right\}$$

which at $\phi = \pm \pi/2$ reduces to

$$\left(\frac{\partial^2 Y_t}{\partial \phi^2}\right)_{\phi=\frac{\pi}{2}} = -X\cot\theta \left\{1 - \frac{1 + \left(\frac{2X\sin\theta}{c}\right)}{\left[1 + \frac{2X\sin^2\theta\cos\theta}{S_y}\right]^{1/2}}\right\}$$

and

$$\left(\frac{\partial^2 Y_t}{\partial \phi^2}\right)_{\phi=-\frac{\pi}{2}} = X\cot\theta \left\{1 - \frac{1 - \left(\frac{2X\sin\theta}{c}\right)}{\left[1 + \frac{2X\sin^2\theta\cos\theta}{S_y}\right]^{1/2}}\right\}$$

Substitution of appropriate geometric parameters into these equations yields positive values at both points and therefore indicate that these points are minima. Furthermore, substitution of $\phi = \frac{\pi}{2}$ and $\phi = -\frac{\pi}{2}$ into Equation (2-9) shows that the absolute minimum occurs at $\phi = \frac{\pi}{2}$ and that

$$Y_{t,min}(X) = \left(\frac{S_y}{\sin^3\theta}\right)\left\{1 - \left[1 + \frac{2\sin^2\theta\cos\theta}{S_y}X\right]^{1/2}\right\} + X\cot\phi \quad (2\text{-}12)$$

A similar evaluation of ϕ at the extrema given by Equation (2-11) yields negative values and thus indicate maximum points. Substitution of Equation (2-11) into Equation (2-9) produces two equal maxima per revolution given by

$$Y_{t,max}(X) = \left(\frac{S_y}{\sin\theta}\right)\left[1 - \left(\frac{X}{S_y}\right)^2 \sin^2\theta\right]^{1/2} \quad (2\text{-}13)$$

For simplicity in computing the Z slide commands, the gross axial slide motion, Y(X), will be defined by $Y_{t,max}(X)$. Thus,

$$Y(X) \equiv Y_{t,max}(X) = \left(\frac{S_y}{\sin\theta}\right)\left[1 - \left(\frac{X}{S_y}\right)^2 \sin^2\theta\right]^{1/2} \qquad (2\text{-}14)$$

Use of this defining relationship in Equation (2-8) produces

$$Z(X,\phi) = Y_t(X,\phi) - Y(X)$$

or

$$Z(X,\phi) = \left(\frac{S_y}{\sin^3\theta}\right)\left\{1 - \left[1 + \left(\frac{2\sin^2\theta\cos\theta}{S_y}\right)X\sin\phi - \cdots \right.\right.$$

$$\left.\left. \cdots \left(\frac{\sin^4\theta}{S_y^2}\right)X^2\cos^2\phi\right]^{1/2}\right\} + (\cot\theta)X\sin\phi - Y(X) \qquad (2\text{-}15)$$

Figure 2-2 illustrates the dependence of Z on ϕ at various values of X. The expanded scale plots in the inserts display the Z behavior near the 0 and 180 degree points. The plots clearly indicate two dissimilar oscillations in Z in every spindle rotation. Further, the maximum motion of the Z slide is seen to be slightly less than 0.008 in. For purposes of "worst case" estimates, the motion can be assumed sinusoidal with half amplitude of 0.004 in. and frequency of 10 Hz (twice the maximum spindle speed). Accordingly, the maximum velocity and acceleration can be estimated as 0.25 in./sec. and 15.79 in./sec^2, respectively. These values will be used wherever such estimates are needed.

Generation of Z Slide Commands

Before determining a method for supplying commands to the Z slide, it must be recalled that the control of the X and Y slides is furnished by an

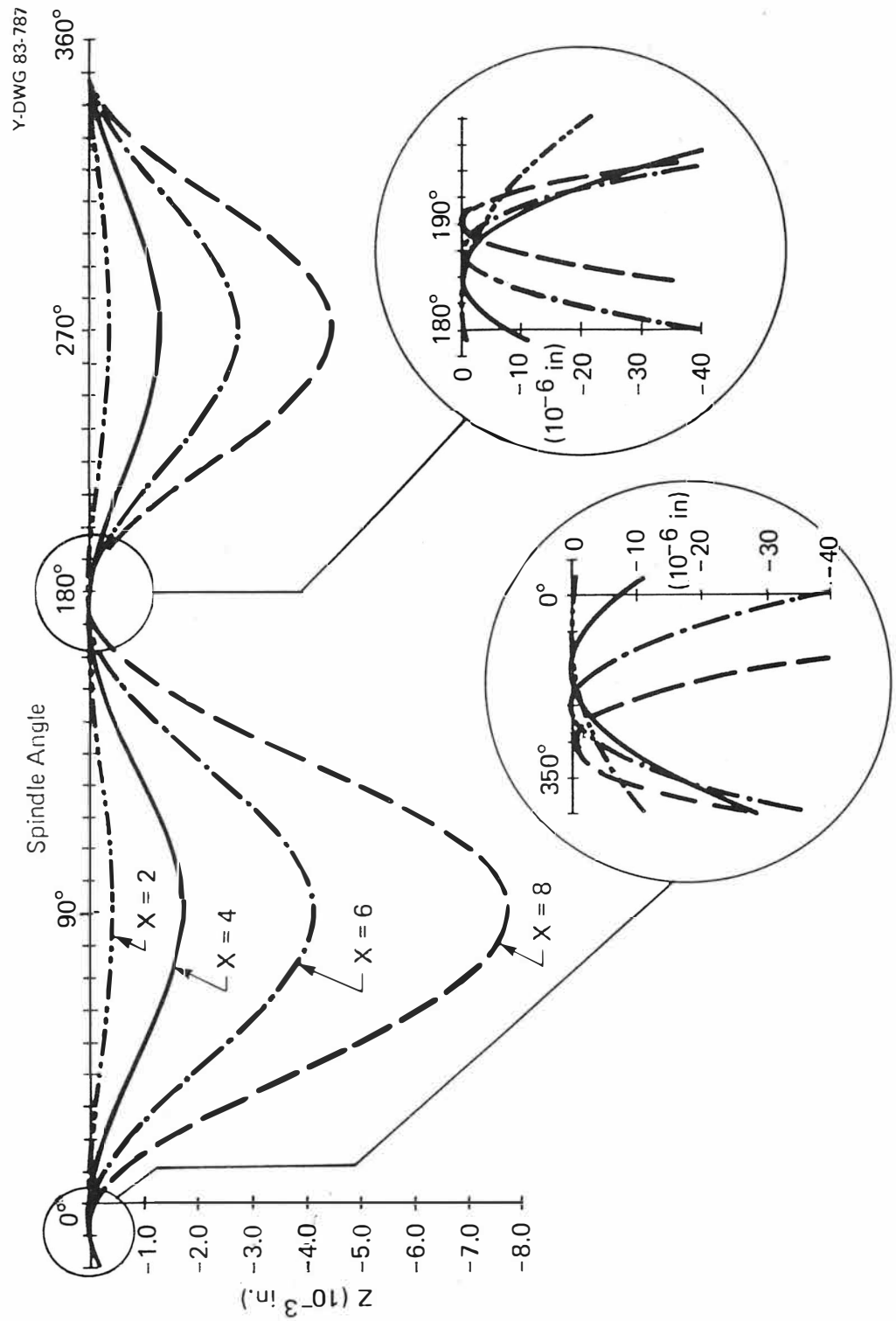

Figure 2-2. Z slide motion required for prescribed surface.

existing machine control unit. Therefore, it is desired that any additional controls have minimum impact on present equipment. Hence, if desired, the present base machine can be returned to original condition.

Obviously, the simplest means of supplying information to the Z slide would be by punched tape through an added channel in the existing control unit. When the rate of command inputs to the Z slide is considered, however, it is equally obvious that this alternative is not possible because of both the relatively slow speed of the tape reader and the amount of information that must be stored on tape. This pair of conditions virtually dictate that the Z slide commands be generated in real time rather than pre-computed off-line and stored.

A second approach for generating the Z slide commands is the use of a mini- or microcomputer to calculate the commands in real time. This technique also fails, however, due to the computation speed required. For example, the worst-case Z slide velocity was estimated earlier to be approximately 0.25 in./sec. If the computer could calculate the Z position commands (given by Equation (2-15)) in as short a time as 100 microseconds, the slide commands would be quantized to steps as large as 25 microinches. This condition would render the surface finish unacceptable and the contour accuracy marginal at best.

Close examination of Figure 2-2 revealed that perhaps the Z motion could be approximated in simpler form by combination of a low and high speed component. The high speed component would probably be ϕ-dependent, while the slower would be some function of X. Such an expression would have the form

$$Z(X,\phi) = \Xi(X)\Phi(\phi) \qquad (2\text{-}16)$$

Several unsuccessful attempts were made to derive a simple approximation of this form. Finally, Equation (2-15) was expanded in a Fourier series as follows.

$$Z(X,\phi) = C_0(X) + \sum_{i=1}^{N}\left[C_i(X)\cos(i\phi) + S_i(X)\sin(i\phi)\right] \qquad (2\text{-}17)$$

This expression was evaluated at the largest expected value of X (X = 8 inches). The purpose of this exercise was to determine the number of significant terms at the worst expected case (largest Z motion). The Fourier expansion was performed on a large digital computer using a library subprogram. The subprogram limits the value of N in Equation (2-17) to 19 terms. This was more than sufficient for the required accuracy. The coefficients resulting from this expansion, with N = 19 and X = 8 inches, are listed in Table 2-1.

Table 2-1. Coefficients of Fourier Expansions $Z(X,\phi)$ (X = 8 in.)

i	C_i	S_i
0	-3.129212 E-03	
1	-8.706122 E-10	-1.659055 E-03
2	3.009743 E-03	1.498976 E-09
3	1.636414 E-09	-1.283845 E-05
4	-5.471358 E-08	-2.409634 E-10
5	-1.803095 E-10	-9.868042 E-10
6	7.522339 E-10	-3.314755 E-10
7	-8.699309 E-10	4.801228 E-10
8	-1.186554 E-09	2.628988 E-10
9	6.358859 E-10	-6.323951 E-10
10	-1.153152 E-09	-1.005770 E-09
11	-1.263566 E-09	-1.317052 E-10
12	-1.030912 E-09	-4.570858 E-10
13	-1.370105 E-09	-6.901405 E-10
14	-7.919119 E-10	-7.132519 E-10
15	3.072071 E-10	-9.102900 E-10
16	1.231549 E-09	-8.889092 E-10
17	1.266274 E-09	6.782497 E-10
18	2.283308 E-10	5.107422 E-10
19	-6.987747 E-10	-6.062522 E-10

Because the position resolution for the system had been tentatively selected at the one microinch level, it was anticipated that truncation of the series might be exercised at coefficient values below 10^{-7} inches. The coefficient values listed in Table 2-1 show that the series intrinsically offered truncation at approximately this level, and hence the choice of significant terms was simplified.

The same expansion was performed at several other values of X over the range $0 < X < 8$ inches with similar results. In each case the terms of greatest significance are C_0, S_1, C_2, and S_3 as indicated in Table 2-1. Therefore, Equation (2-15) was approximated with the series

$$Z(X,\phi) = C_0(X) + S_1(X)\sin(\phi) + C_2(X)\cos(2\phi) + S_3(X)\sin(3\phi) \quad (2\text{-}18)$$

Without attempting to detail the hardware components involved in implementing Equation (2-18), the following general requirements are seen:

1. Represent to the command generator the spindle angle ϕ and X slide position;
2. Form the appropriate trigonometric function of spindle angle;
3. Generate the X-dependent coefficients; and
4. Form the indicated products and summations.

To satisfy the surface finish requirements, it is desired that quantization of the command signal be restricted to a maximum of less than one microinch. The hardware components are constrained accordingly.

Considerations of hardware implementation led to the conclusion that perhaps the series approximation given by Equation (2-18) might best be represented by the sum of terms in powers of $\sin(\phi)$. Thus, by employing the

trigonometric identities for $\cos(\phi)$ and $\sin(3\phi)$, the following series was formed:

$$Z(X,\phi) = C_{00}(X) + C_{01}(X)\sin(\phi) + C_{02}(X)\sin^2(\phi) + C_{03}(X)\sin^3(\phi) \quad (2\text{-}19)$$

where

$$C_{00}(X) = C_0(X) + C_2(X) \quad (2\text{-}20)$$

$$C_{01}(X) = S_1(X) + 3S_3(X) \quad (2\text{-}21)$$

$$C_{02}(X) = -2C_2(X) \quad (2\text{-}22)$$

$$C_{03}(X) = -4S_3(X) \quad (2\text{-}23)$$

Table 2-2 lists coefficient values of C_{00}, C_{01}, C_{02}, and C_{03} at 0.1 inch increments of X.

In comparison to the hardware components required previously, Equation (2-19) requires

1. Generating the sine of the spindle angle;
2. Generating the X-dependent coefficient values; and
3. Forming powers, products and summations.

The one microinch quantization constraint on the Z slide command signal will be shown to be satisfied quite easily with the hardware necessary to implement Equation (2-19).

Figures 2-3 and 2-4 illustrate the X-dependency of the coefficients. The initial desire was that perhaps a relatively simple general relationship might be established for mathematically representing the coefficients. Polynomial approximations up to second order were attempted without general success. It was then decided that linear interpolation between stored data points might provide the simplest acceptable means of generating the coefficient values.

Table 2-2. Coefficients Used in Equation (2-19)

X	C_{00}	C_{01}	C_{02}	C_{03}
0.0	0.0000000	0.0000000	0.0000000	0.0000000
0.1	-0.0000000	-0.0000000	-0.0000009	0.0000000
0.2	-0.0000000	-0.0000000	-0.0000038	0.0000000
0.3	-0.0000000	-0.0000001	-0.0000085	0.0000000
0.4	-0.0000000	-0.0000002	-0.0000151	0.0000000
0.5	-0.0000000	-0.0000004	-0.0000236	0.0000000
0.6	-0.0000000	-0.0000007	-0.0000340	0.0000000
0.7	-0.0000000	-0.0000011	-0.0000463	0.0000000
0.8	-0.0000000	-0.0000017	-0.0000604	0.0000001
0.9	-0.0000000	-0.0000024	-0.0000765	0.0000001
1.0	-0.0000000	-0.0000033	-0.0000944	0.0000001
1.1	-0.0000000	-0.0000044	-0.0001142	0.0000001
1.2	-0.0000001	-0.0000057	-0.0001360	0.0000002
1.3	-0.0000001	-0.0000073	-0.0001596	0.0000002
1.4	-0.0000001	-0.0000091	-0.0001850	0.0000003
1.5	-0.0000001	-0.0000112	-0.0002124	0.0000003
1.6	-0.0000002	-0.0000136	-0.0002417	0.0000004
1.7	-0.0000002	-0.0000163	-0.0002728	0.0000005
1.8	-0.0000003	-0.0000194	-0.0003059	0.0000006
1.9	-0.0000004	-0.0000228	-0.0003408	0.0000007
2.0	-0.0000005	-0.0000266	-0.0003776	0.0000008
2.1	-0.0000006	-0.0000308	-0.0004163	0.0000009
2.2	-0.0000007	-0.0000354	-0.0004569	0.0000011
2.3	-0.0000008	-0.0000404	-0.0004994	0.0000012
2.4	-0.0000010	-0.0000459	-0.0005437	0.0000014
2.5	-0.0000011	-0.0000519	-0.0005900	0.0000016
2.6	-0.0000013	-0.0000584	-0.0006381	0.0000018
2.7	-0.0000016	-0.0000654	-0.0006881	0.0000020
2.8	-0.0000018	-0.0000729	-0.0007400	0.0000022
2.9	-0.0000021	-0.0000810	-0.0007938	0.0000025
3.0	-0.0000024	-0.0000897	-0.0008495	0.0000027
3.1	-0.0000027	-0.0000990	-0.0009070	0.0000030
3.2	-0.0000031	-0.0001089	-0.0009665	0.0000033
3.3	-0.0000035	-0.0001194	-0.0010278	0.0000036
3.4	-0.0000039	-0.0001306	-0.0010910	0.0000040
3.5	-0.0000044	-0.0001425	-0.0011561	0.0000043
3.6	-0.0000049	-0.0001550	-0.0012231	0.0000047
3.7	-0.0000055	-0.0001683	-0.0012919	0.0000051
3.8	-0.0000061	-0.0001823	-0.0013627	0.0000055
3.9	-0.0000068	-0.0001971	-0.0014353	0.0000060
4.0	-0.0000075	-0.0002127	-0.0015098	0.0000064
4.1	-0.0000083	-0.0002290	-0.0015862	0.0000069
4.2	-0.0000091	-0.0002462	-0.0016645	0.0000075
4.3	-0.0000100	-0.0002642	-0.0017446	0.0000080
4.4	-0.0000110	-0.0002831	-0.0018266	0.0000086
4.5	-0.0000120	-0.0003028	-0.0019106	0.0000092

Table 2-2 (continued).

X	C_{00}	C_{01}	C_{02}	C_{03}
4.6	-0.0000131	-0.0003235	-0.0019964	0.0000098
4.7	-0.0000143	-0.0003450	-0.0020840	0.0000105
4.8	-0.0000155	-0.0003675	-0.0021736	0.0000111
4.9	-0.0000169	-0.0003910	-0.0022650	0.0000118
5.0	-0.0000183	-0.0004154	-0.0023583	0.0000126
5.1	-0.0000198	-0.0004408	-0.0024535	0.0000134
5.2	-0.0000214	-0.0004673	-0.0025506	0.0000142
5.3	-0.0000231	-0.0004947	-0.0026495	0.0000150
5.4	-0.0000249	-0.0005233	-0.0027503	0.0000158
5.5	-0.0000268	-0.0005529	-0.0028530	0.0000167
5.6	-0.0000288	-0.0005836	-0.0029576	0.0000177
5.7	-0.0000309	-0.0006154	-0.0030640	0.0000186
5.8	-0.0000331	-0.0006484	-0.0031724	0.0000196
5.9	-0.0000354	-0.0006825	-0.0032826	0.0000207
6.0	-0.0000379	-0.0007178	-0.0033946	0.0000217
6.1	-0.0000405	-0.0007543	-0.0035086	0.0000228
6.2	-0.0000432	-0.0007920	-0.0036244	0.0000240
6.3	-0.0000461	-0.0008310	-0.0037421	0.0000252
6.4	-0.0000491	-0.0008712	-0.0038616	0.0000264
6.5	-0.0000522	-0.0009126	-0.0039831	0.0000276
6.6	-0.0000555	-0.0009554	-0.0041064	0.0000289
6.7	-0.0000589	-0.0009995	-0.0042316	0.0000303
6.8	-0.0000625	-0.0010449	-0.0043586	0.0000316
6.9	-0.0000663	-0.0010917	-0.0044875	0.0000330
7.0	-0.0000702	-0.0011399	-0.0046183	0.0000345
7.1	-0.0000743	-0.0011894	-0.0047510	0.0000360
7.2	-0.0000786	-0.0012404	-0.0048855	0.0000375
7.3	-0.0000831	-0.0012928	-0.0050219	0.0000391
7.4	-0.0000877	-0.0013467	-0.0051601	0.0000408
7.5	-0.0000926	-0.0014020	-0.0053003	0.0000424
7.6	-0.0000976	-0.0014588	-0.0054422	0.0000441
7.7	-0.0001029	-0.0015172	-0.0055861	0.0000459
7.8	-0.0001083	-0.0015771	-0.0057318	0.0000477
7.9	-0.0001140	-0.0016385	-0.0058794	0.0000496
8.0	-0.0001199	-0.0017015	-0.0060288	0.0000515

Such interpolation could be provided by a small digital processor with output through digital-to-analog converters (DACs) to the remainder of the command circuitry. Since the interpolation scheme involves hardware limitations, the interpolation grid and its associated accuracy will be described in Chapter 3.

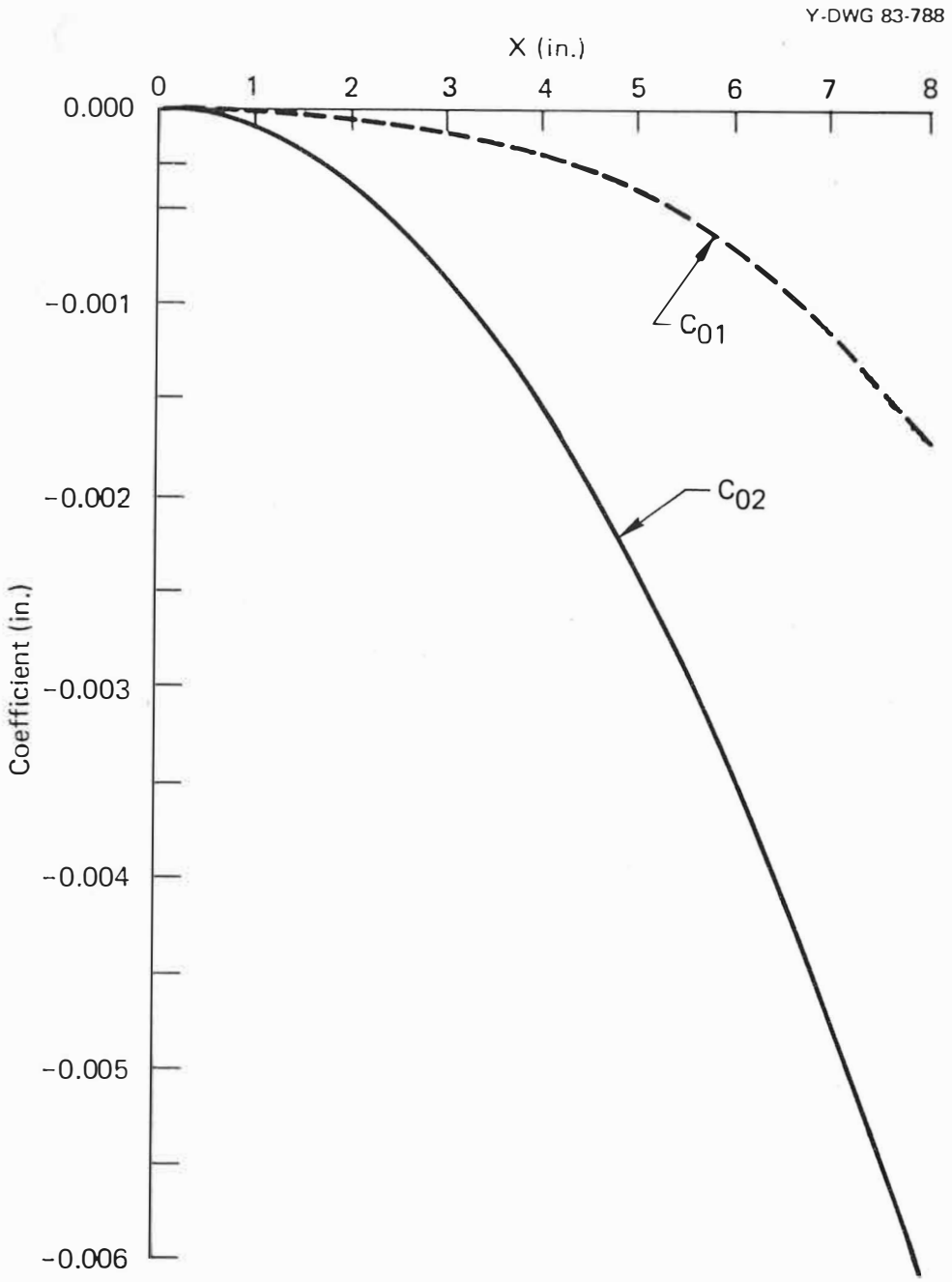

Figure 2-3. Variation of Coefficients C_{01} and C_{02} with radius.

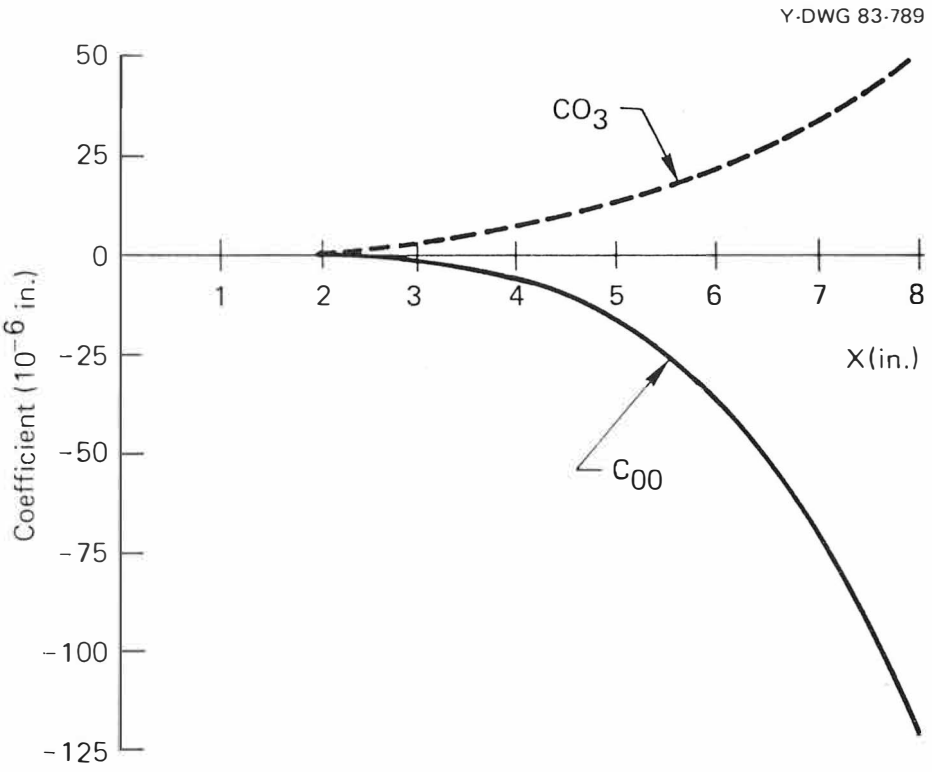

Figure 2-4. Variation of Coefficients C_{00} and C_{03} with radius.

The command signal representing Equation (2-15) is approximated by Equation (2-19) where the coefficient values are generated via interpolation from Table 2-2. The accuracy of the approximation was compared with the true values as given by Equation (2-15) in a Fortran simulation. Figure 2-5 illustrates the results of this simulation with values selected as typical and/or worst-case. The maximum deviation from theoretical $Z(X,\phi)$ is seen to be 0.1 microinch at the interpolation endpoints. Not surprisingly, the maximum error occurs approximately midway between the interpolation endpoints and varies up to slightly less than one-half microinch.

Information flow for generation of Z slide commands is illustrated in general form in Figure 2-6. X position information and spindle angle information are required inputs to the calculations.

This chapter has presented the mathematical development of the Z-axis command signal. Chapter 3 will describe the hardware components utilized in generating this command along with measurements of accuracy of the actual command signals.

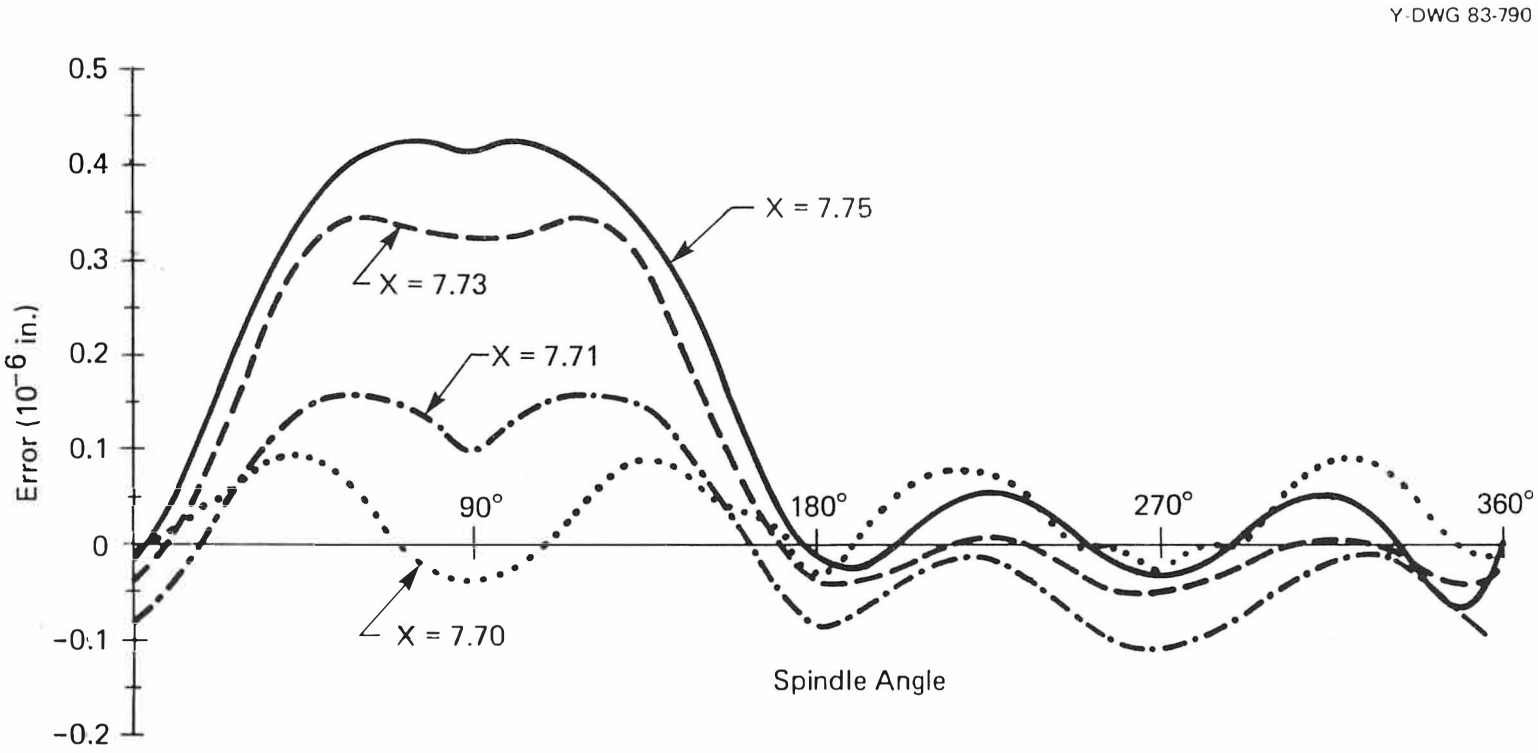

Figure 2-5. Series approximation errors.

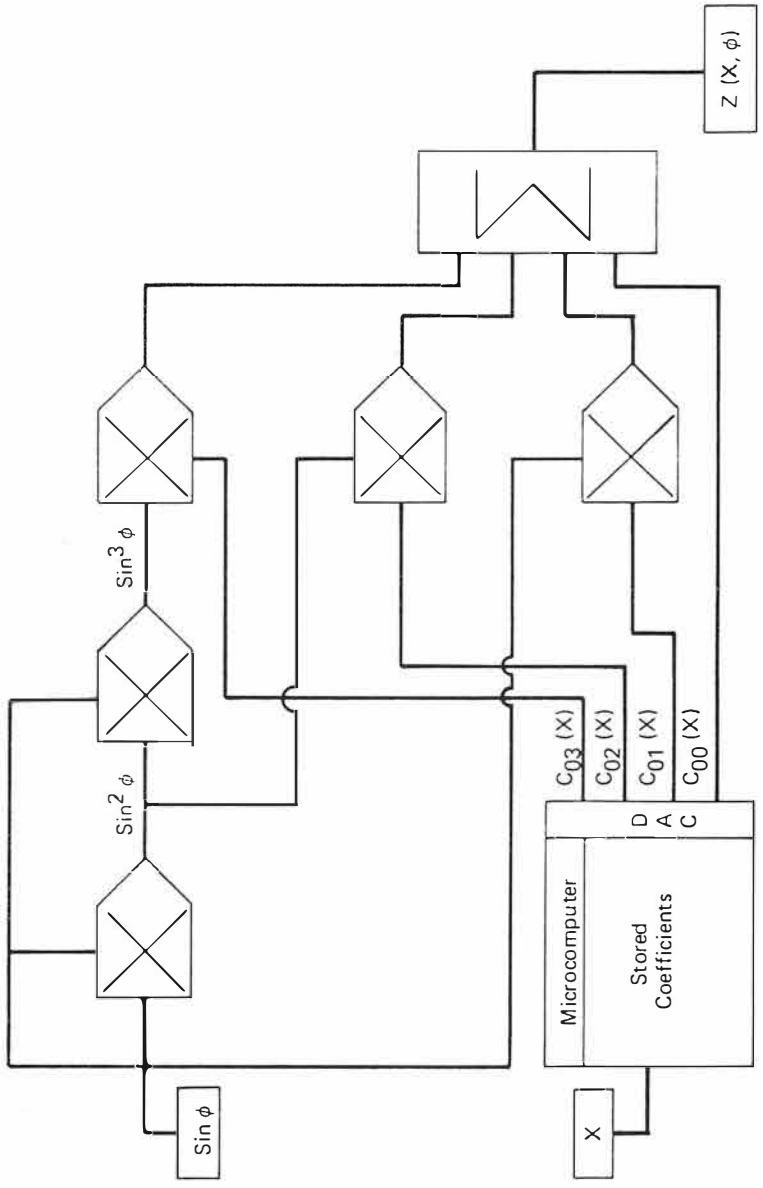

Figure 2-6. Schematic of command signal formation.

CHAPTER 3

DESCRIPTION OF HARDWARE

This chapter describes the equipment utilized in producing the combination of relative motions between cutting tool and workpiece. A general description of the base machine is provided first followed by a presentation of the components comprising the Z-axis add-on system. Details of the base machine modifications were omitted because this work was not the focus of this paper. The Z slide coverage, however, includes not only a description of the components but also the rationale for their selection

Base Machine

The base machine is a Moore No. 3 Measuring Machine which was modified and upgraded to provide the needed basic capabilities. A vendor illustration of the original machine is shown in Figure 3-1. As originally configured the machine slides were driven manually with handcranks connected to extremely precise leadscrews with which linear displacements were measured. The machine was utilized because of its basic accuracy in motion straightness.

A photograph of the machine as modified is shown in Figure 3-2. Among the required modifications were:

1. Replacement of the measuring column with a riser block, air bearing spindle, and spindle drive;

2. Conversion of the slides from oil hydrodynamic bearings to externally pressurized air films;

3. Addition of anti-backlash biasing weights to remove slack from the drive train;

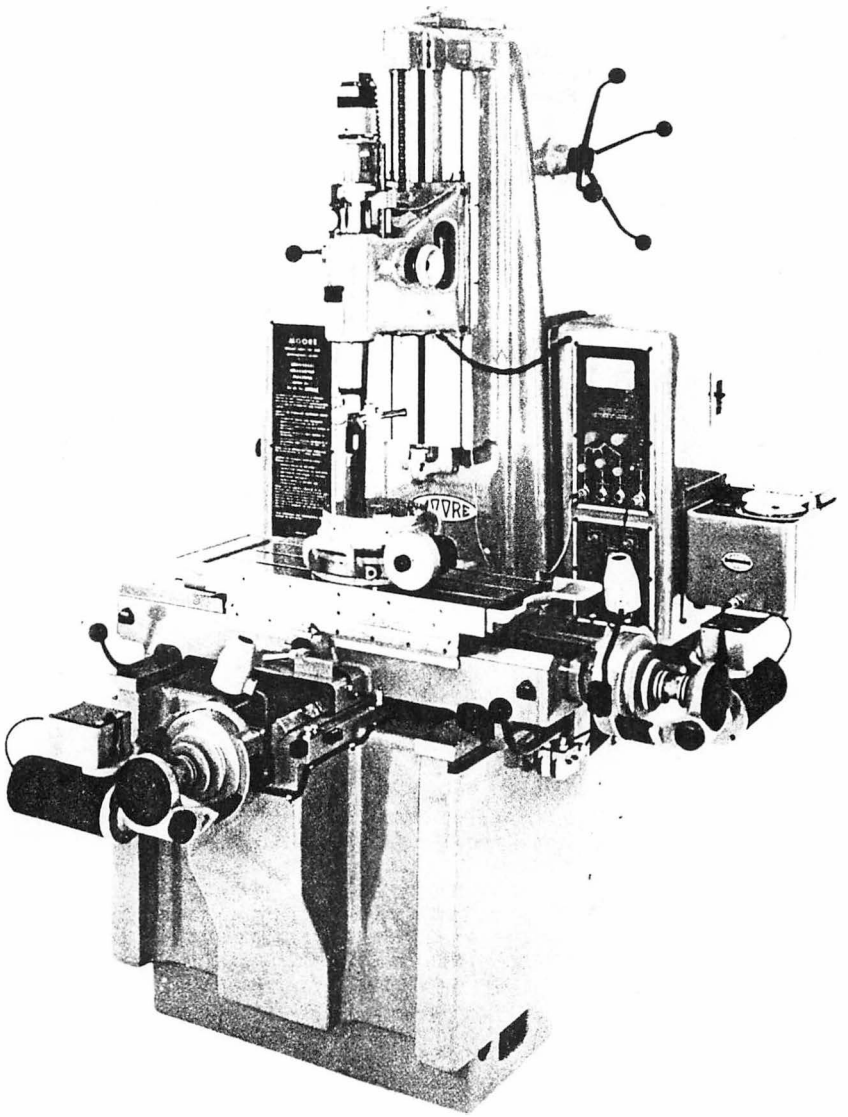

Figure 3-1. Moore machine as originally configured (without drive motors).

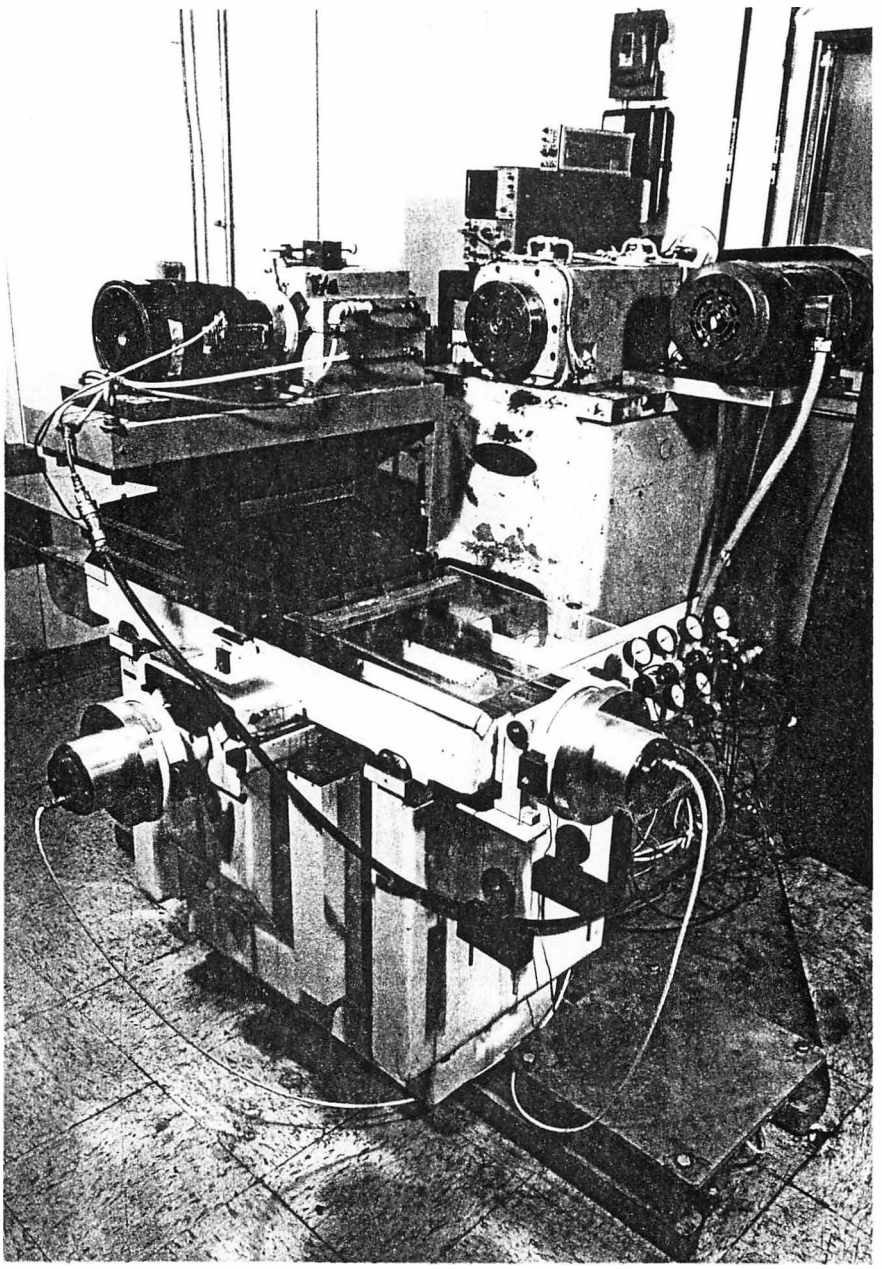

Figure 3-2. Moore machine as modified.

4. Addition of laser interferometric position transducers for slide position and velocity feedback;

5. Addition of torque motors directly coupled to the leadscrew shafts;

6. Addition of a two-axis numerical control (NC) machine control unit (MCU) which provides automatic control of the machine via punched tape;

7. Addition of necessary electronics and power to drive and control the slides to the desired accuracies; and

8. Addition of a vibration isolation system to isolate the machine from building structural vibrations.

Most of these modifications and additions were required to convert the machine slides from manual handcrank drive to continuous path, closed loop numerical control. The slide bearing modifications and biasing weights were necessary both for the elimination of the destabilizing effects of backlash and for reducing the discontinuous nonlinearity associated with Coulomb friction.

The basic components in the slide control systems are illustrated in Figure 3-3. Slide position and velocity commands are read from punched tape by the MCU tape reader. This information is converted into a train of command pulses whose time spacing is determined by the velocity command. Simultaneously, a similar pulse train is fed back from the slide laser interferometric position transducers to the MCU. An analog position error signal eventually results and is filtered by an outer loop compensator before passing to the minor, or velocity, loop.

The MCU was originally designed to operate at a wiring-selectable, least unit of resolution of either 10 or 100 microinches. In this case 10 microinch resolution was used which resulted in command pulse values of 10 microinches. However, the MCU was originally designed to accept pulses

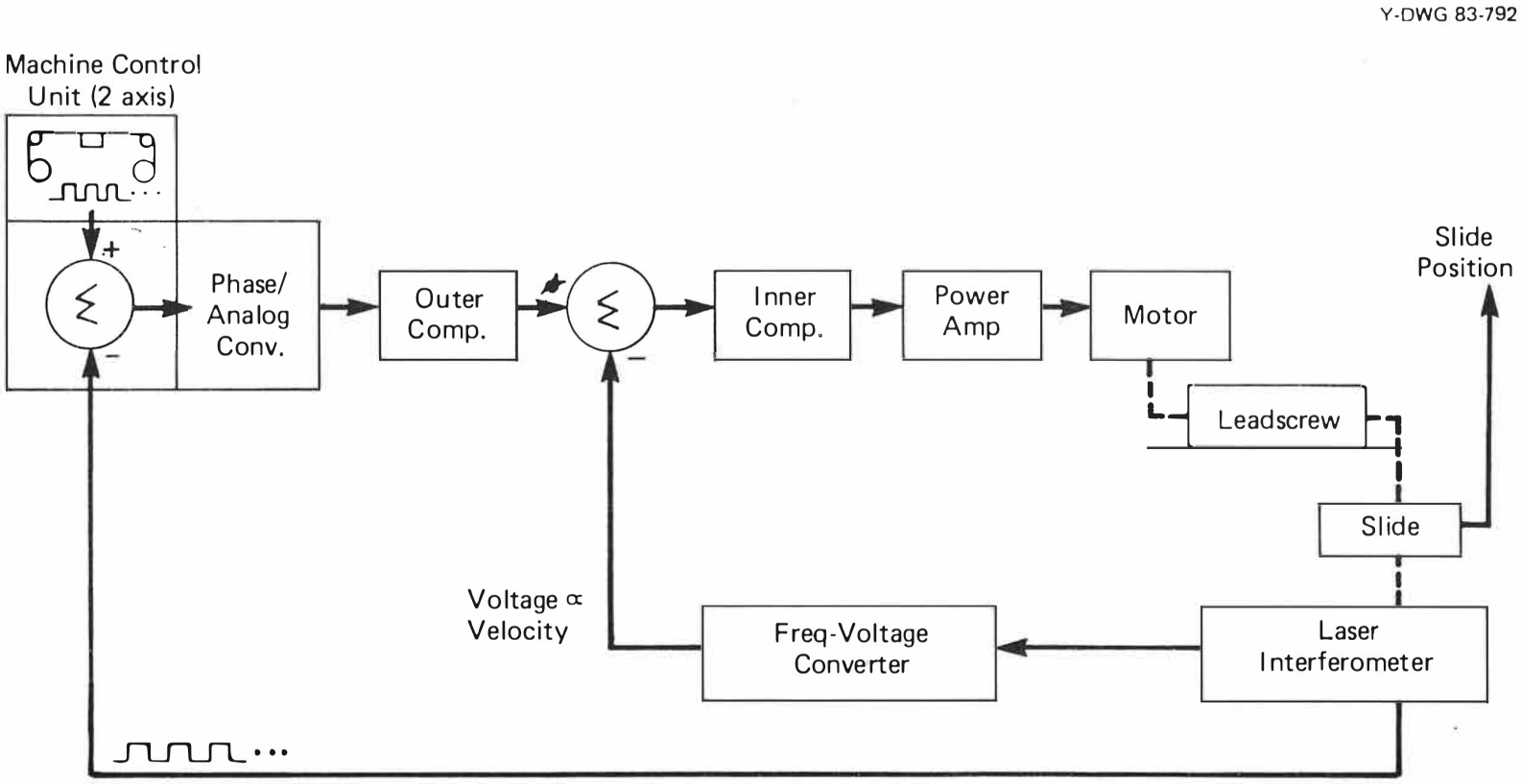

Figure 3-3. Symbolic diagram of base machine slide control system.

representing position changes of one-eighth wavelength, $\lambda/8$, of a Perkin-Elmer helium-neon laser. The wavelength of this light in vacuum is 24.9209232 microinches. The original MCU circuitry also performed the fringe-to-inch conversion (with temperature and barometric pressure compensation of wavelength) and repetitively subtracted the resulting pulses from the position error register. When overflow occurred in this register, a pulse representing 10 microinches of slide motion was issued to the command-minus-feedback summing point.

The laser interferometers used in this experiment for slide position feedback were Hewlett-Packard model 5100 laser transducers with associated electronics. Rather than issuing pulses representing one-eighth wavelengths, the Hewlett-Packard equipment in this configuration issues pulses representing 1 microinch (automatically compensated for temperature and barometric pressure changes). The error register therefore issued pulses corresponding to position changes of $80/\lambda$. This represents the actual least unit of resolution of the slide control system.

The difference in weights of command and feedback pulses necessitated a departure from the routine tape programming procedure. The closed loop machine control system seeks to null the number or position pulses rather than actual distances. For example, a slide position increment of 20 microinches causes two command pulses to be issued and is nulled by two feedback pulses representing only $80/\lambda$. This difficulty is overcome by simply scaling up command values, in this case by a factor of $\lambda/8$, such that the desired motion is realized. After being compensated for temperature, barometric pressure and relative humidity, the $\lambda/8$ factor was 3.1143367 microinches (18).

The velocity loop is formed for the dual purposes of increasing both system damping and stiffness. Conventionally, slide velocity feedback is provided by attaching a tachometer to the slide leadscrew. Because the laser interferometer provides position pulses at a rate proportional to slide velocity, it was decided to form the velocity feedback signal by passing these pulses to two frequency-to-voltage (F/V) converters (one each for positive and negative directions). The outputs of the F/V converters provide an analog signal proportional to slide velocity.

Design of the inner loop compensator of both slides required consideration of the dynamics created by structural resonances in the machine baseplate. The character of these resonances is described in (19). Lag compensators were finally used to permit gain increases with the attendant improvement in system stiffness. The filtered signal is amplified by a wide-band linear servo amplifier to power the slide drive motors.

Auxiliary Slide and Drive System

An exploded view of the auxiliary slide is shown in Figure 3-4. The slide itself is made of aluminum and has a square cross-section with a hole bored through its length for mass reduction. Approximately three inches of slide travel were provided. Figure 3-4 shows that a total of eight porous graphite air pads were used to form the captive air bearing system. The slide housing was machined from cast iron into the shape shown with holes drilled to allow the pressurized air to flow into the back of each pad. The eight pads were rough-machined to approximately the same thickness and glued into place in the slide housing. The slide was assembled with shims placed between the two housing halves such that the assembly was snug. The slide was then

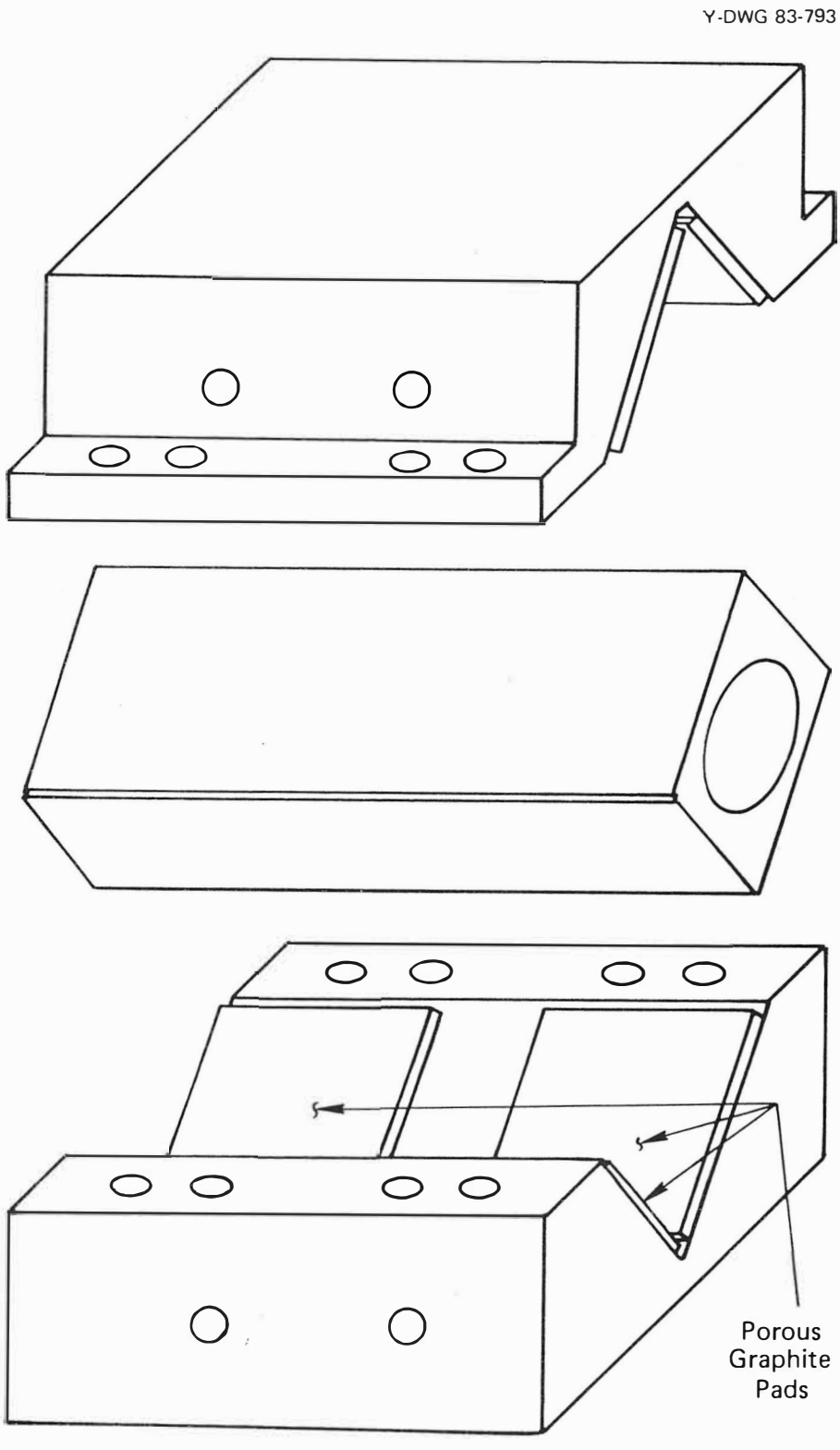

Figure 3-4. Exploded view of air bearing auxiliary slide.

reciprocated to lap the graphite pads until uniform contact with the slide was produced across the face of each pad. The shims were then adjusted to provide a 100 microinch gap between the slide and the graphite pads. With air pressure of 80 to 90 psig slide deflection of approximately 1 microinch was measured with a one pound load. The force required to initiate movement of the slide longitudinally was on the order of a few grams.

The slide is driven by a directly coupled linear motor of a type commonly used to drive the read/write head on computer disk storage systems. It was chosen for its relatively high force constant and low armature mass. The motor is powered by a linear power amplifier.

Z-slide position is monitored by a capacitance gage which provides an analog signal for feedback to the slide control electronics. The measuring range of the capacitance gage is .020 in. This gage was chosen here for its high resolution, relatively low noise, moderate linearity and analog output. The .020 in. gaging range is sufficient for the part to be machined.

The auxiliary slide control system is illustrated in symbolic form in Figure 3-5. The differentiating network shown in the minor loop feedback path represents the use of rate feedback for damping and stiffening benefits. Several forms of rate feedback were considered and will be described in the discussion of slide compensation. The slide controls are seen to be subdivided into the two principal areas of command signal generation and closed loop control system.

Figure 2-6 illustrated conceptually how the Z slide commands are generated. The command generator is seen to consist of the relatively slower speed, digital elements associated with X-dependent series coefficients and the more rapidly changing analog elements involving trigonometric functions of

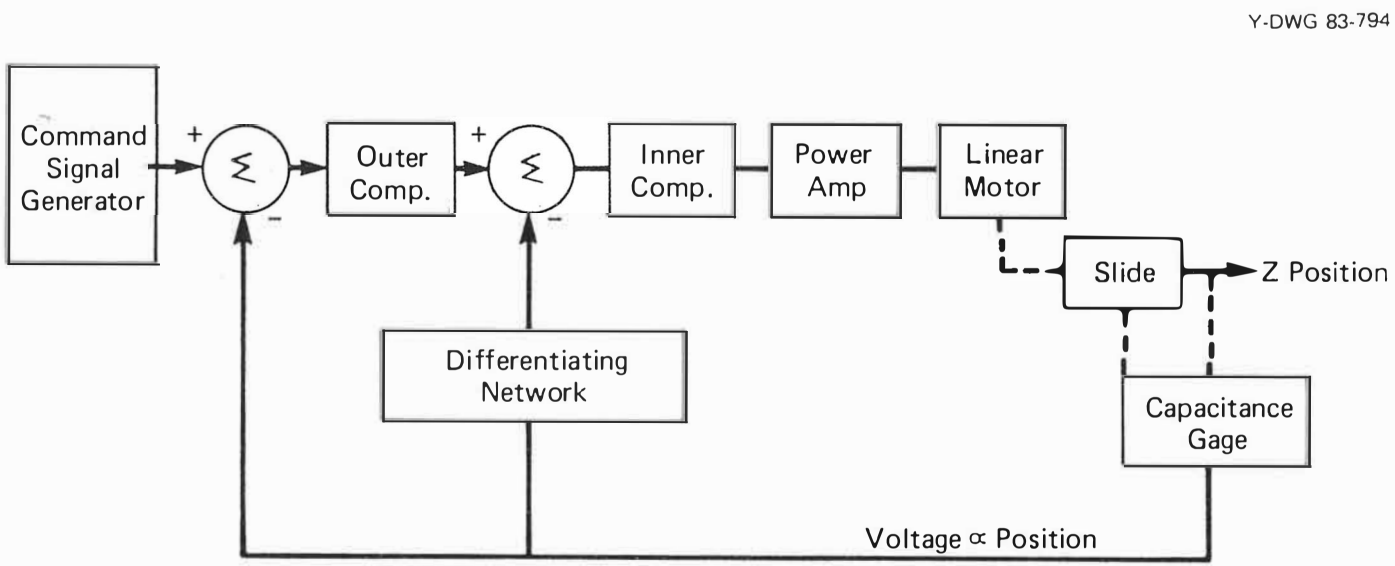

Figure 3-5. Symbolic diagram of auxiliary slide control system.

spindle angle. The digital section shows input of digital X slide position data. These data are furnished to the microcomputer by the position counter associated with the X slide laser interferometer.

Essential to the real-time command generation scheme is the sine ϕ function generator shown in Figure 3-6 as an input to the analog multipliers. After no commercially manufactured variable frequency sinusoidal oscillator was found in the needed under 10 Hz range, it was decided to build a function generator to produce the sine of the spindle angle. Wong and Ott (20) describe a circuit, shown in Figure 3-6, which provides a 10 volt amplitude sine wave. The frequency of the sinusoid is proportional to a dc voltage furnished by a tachometer driven by the spindle. The diode circuitry on the output integrator is used to prevent saturation of the circuit at very low frequencies and holds the output to ± 10 volts.

Regardless of the accuracy of the components used in the circuit shown in Figure 3-6 the likelihood of unacceptable error was considered to be strong over the course of many thousand cycles. Since the rotational synchronization of the part and tool depends totally on the stability of the sine function generator, some means must be provided for preventing the accumulation of error in rotational angle ϕ. To eliminate this cumulative error the integrators in Figure 3-6 were replaced with Teledyne model 4850 three-mode integrator modules. These modules have the capabilities of zero reset and initial condition input as well as integration. A Frost photodiode was used to furnish a reset signal to the integrators by sensing a zero position mark on the rear of the spindle. Figure 3-7 is a photograph both of this photosensor and the spindle tachometer which provided the voltage signal to the oscillator circuit to control the frequency of the sinusoid. Thus, in each rotation, on receiving the "reset" signal

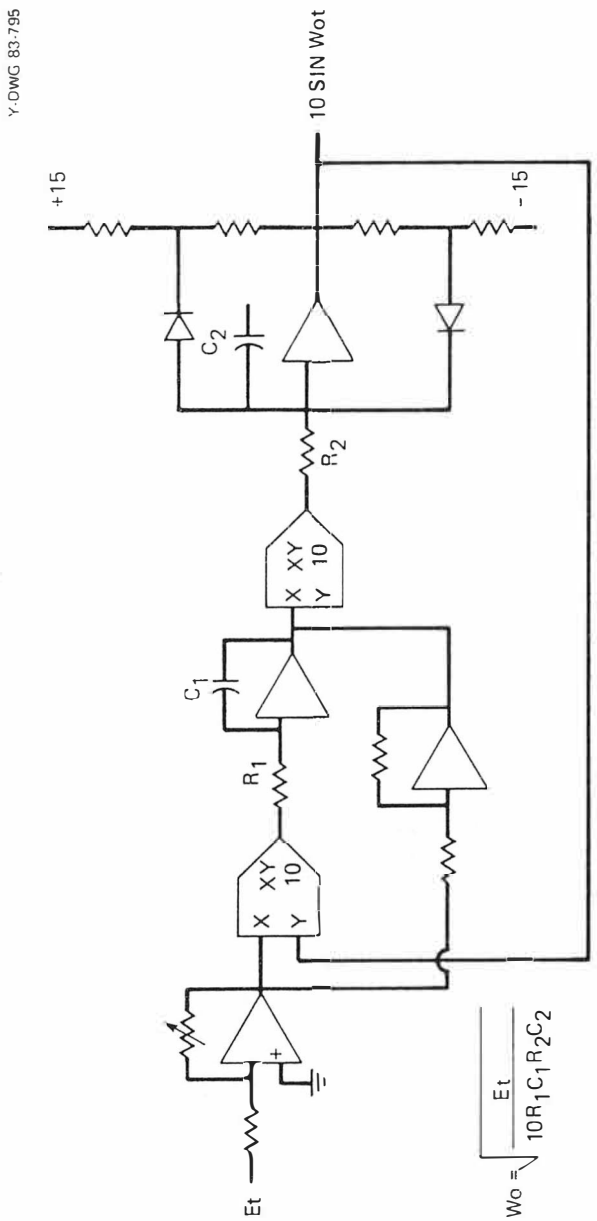

Figure 3-6. Sinusoid generator of Wong and Ott.

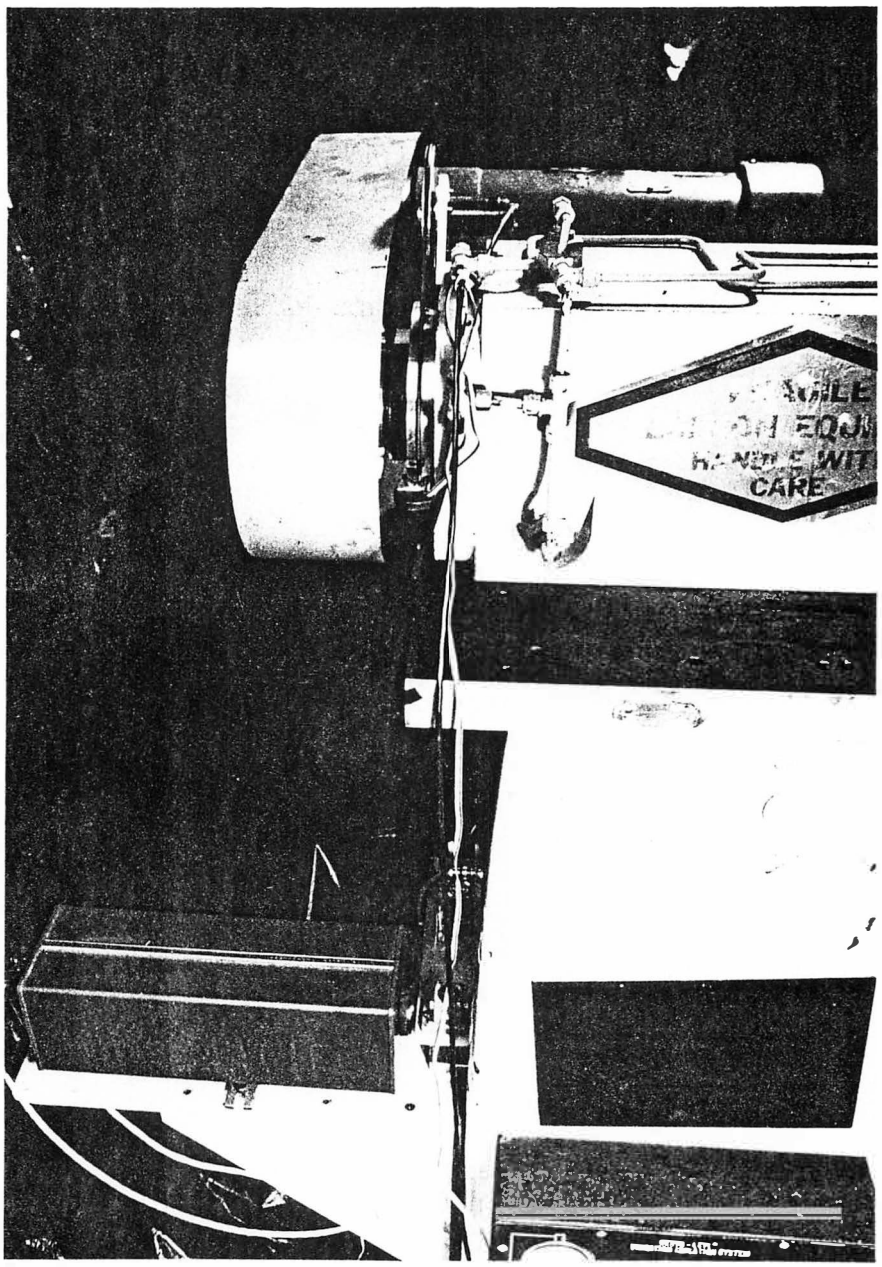

Figure 3-7. Photograph of tachometer and photodiode.

from the photodiode, the integrators are reset to initial conditions (in this case, zero) and then immediately are placed in the "operate" mode to produce the sine (ϕ) function.

Figure 3-8 is a schematic diagram of the sine wave generator. The tachometer signal was attenuated to yield a calibrated +5 volts at 300 rpm of the spindle (5 rev/sec). This signal is fed to one of the analog multipliers while its inverted to the other. The photodiode is shown driving the reset circuitry through the one-shots to provide short, jitter-free reset signals to the integrators. The output of the integrators is given by the manufacturer's data sheet as

$$e_o(t) = \frac{1}{R_i C_f} \int_0^t e_i(\tau) d\tau + KE_{ic}$$

where

R_i = input resistance

C_f = integrating capacitance

E_{ic} = arbitrary initial value at t = 0

K = 1 for R_{ic} = 10k Ω.

With the initial conditions on both integrators set equal to zero,

$$e_{o2}(t) = - \frac{1}{R_{i2}C_{f2}R_{i1}C_{f1}} \int_0^t E_t(\tau_1) \left[\int_0^{\tau_1} E_t(\tau_2) e_{o2}(\tau_2) d\tau_2 \right] d\tau_1 \quad . \tag{3-1}$$

The attenuated tachometer output signal E_t is shown as a function of time, and hence yields a nonlinear differential equation in E_{02}. To void this nonlinearity E_t must change very slowly. The integration period t represents one rotation of

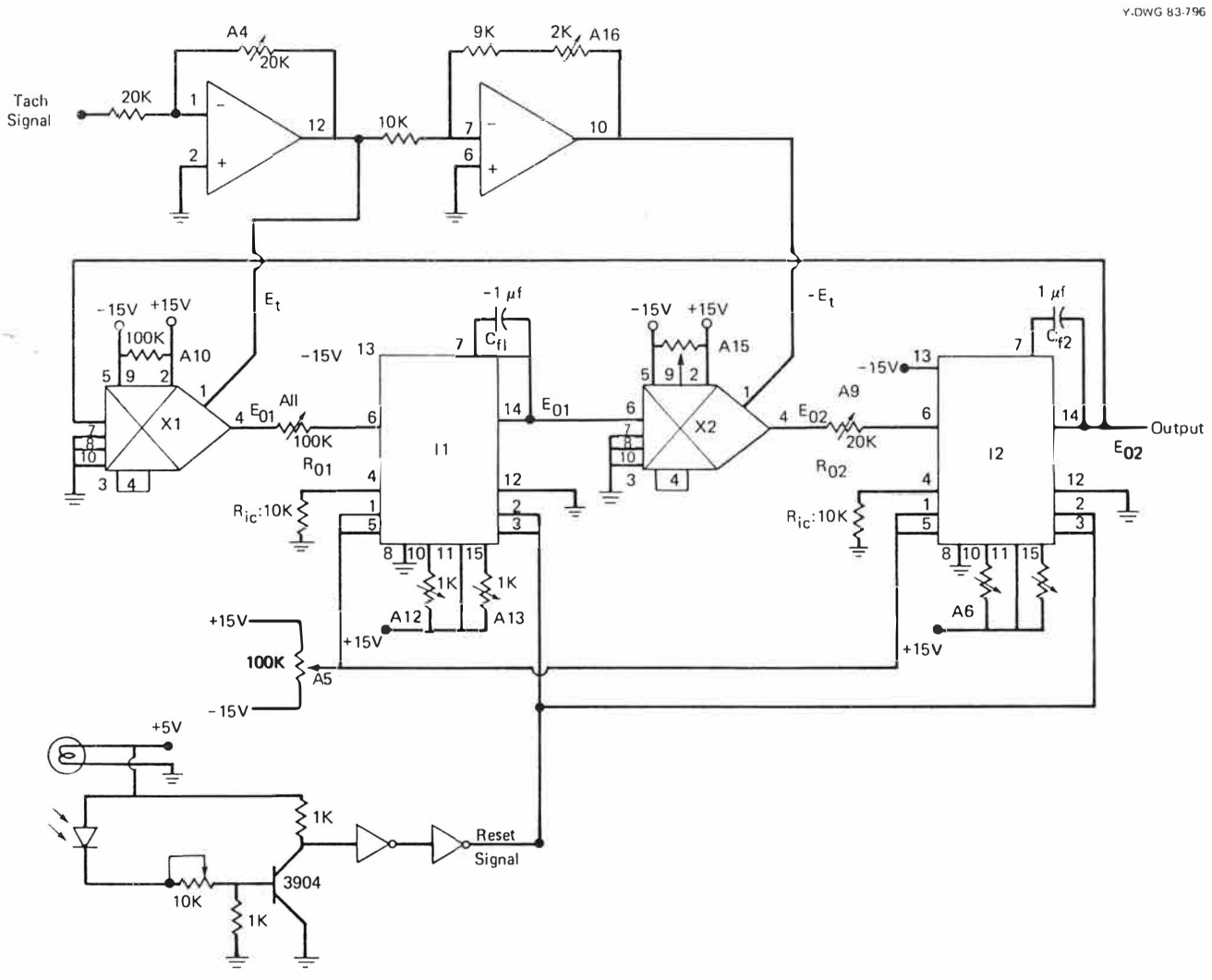

Figure 3-8. Final sinusoid generator schematic.

the spindle. By permitting E_t to vary only 1 or 2 percent over the period t, Equation (3-1) is reduced to

$$e_{o2}(t) = - \frac{E_t^2}{R_{i2}C_{f2}R_{i1}C_{f1}} \int_0^t \int_0^{\tau_1} e_{o2}(\tau_2) d\tau_2 d\tau_1 \quad . \tag{3-2}$$

If differentiated twice with respect to t, the familiar form of the differential equation for a sinusoidal oscillator results.

$$\frac{d^2 e_{o2}(t)}{dt^2} + \left(\frac{E_t^2}{R_{i2}C_{f2}r_{i1}C_{f1}} \right) e_{o2}(t) = 0 \tag{3-3}$$

The frequency of the oscillator is given by

$$\omega = \frac{E_t}{R_{i2}C_{f2}R_{i1}C_{f1}} \quad . \tag{3-4}$$

Thus, the circuit shown in Figure 3-8 is designed to produce a sinusoid of frequency, ω, given by Equation (3-4). In reality the circuit is affected by nonlinearities in the multipliers and integrators, as well as by the minor variation of E_t during a revolution of the spindle. The variation of the sinusoid from theoretical was measured and will be described in Chapter 4. The powers of the sine terms are formed with analog multipliers and further multiplied by the X-dependent coefficients represented in equation (2-19).

The coefficients are stored in a microcomputer at predetermined intervals in X and are output through digital-to-analog converters (DACs) on interrupt from circuitry connected to the X slide interferometer display. Before describing the equipment, however, the requirements of this digital portion of the command signal generator should be considered.

Figures 2-3 and 2-4 show that all four coefficients and their rates of change increase monotonically with X. The maximum values for the defined parabola are

$C_{00} = -.0001195$

$C_{01} = -.0016976$

$C_{02} = -.0060195$

$C_{03} = .0000514$

and occur at X = 8 inches. The resolution in the microcomputer was desired to be such that a microinch be represented by at least one bit which would permit one microinch or smaller steps. The largest of the coefficients, C_{02}, at the one bit per microinch level would require at least 13 bits. Consequently, it was decided to utilize the scaling used by the capacitance gage in position feedback; i.e., + 10 volts correspond to + .010 inch. Furthermore, the .020 inch range would be represented by a 16 bit counter to yield a resolution of 3.2768 bits/microinch. Use of this resolution over the ranges of coefficient values results in the word length requirements shown in Table 3-1.

Table 3-1. Coefficient Word Lengths

Coefficient	Number of Bits
C_{00}	9
C_{01}	13
C_{02}	15
C_{03}	8

The other chief requirements of the microcomputer system concern the rate of update of the coefficient values and the width of the intervals over which interpolation is performed. Coefficient updates were sought to yield motion steps not exceeding one microinch. If a maximum X slide velocity of .2

inch/minute is anticipated, an approximation of coefficient update rate can be obtained.

Table 2-2 shows that for a change in X from 7.9 to 8.0 inches, C_{00} changes by -5.9 microinches, C_{01} by -62.9 microinches, C_{02} by -149.2 microinches, and C_{03} by +2.0 microinches. From these maximum rates of change it was concluded that 200 updates per .1 inch were convenient and sufficient for C_{02}. Likewise, choices of 100, 10, and 10 updates per .1 inch change in X were made for C_{01}, C_{00}, and C_{03} respectively. These correspond to updates at X intervals of .0005, .001, .010, and .010 inch respectively. At an X velocity of .2 inch per minute C02 must then be re-evaluated each .150 second. Additionally, at X positions of integral multiples of .010 inch, all other coefficients must also be updated, effectively reducing the update time to less than .040 second.

The width of the interval over which interpolations were to be executed was examined to determine how coarse the interpolation grid could be made before producing unacceptable error in the command signal. Only convenient intervals were chosen for ease of use in later computation schemes. Excess errors (greater than 1 microinch) were found for interval widths of .25 and .2 inch, so the .1 inch intervals shown in Table 2-2 were used.

After it had been shown that interpolation for coefficient values could mathematically produce commands with error less than .5 microinch, it was necessary to design a hardware system capable of implementing this scheme. An Intel SBC 80/10 microcomputer was chosen as the basis for this system. The function of the microcomputer was to monitor the X slide position, recall the interpolated value or perform the interpolation, and output the value through the appropriate port to the Digital-to-Analog Converter.

At this point it was necessary to decide whether the interpolation should be performed by the microcomputer itself or performed off-line by a large computer with each individual value stored in microcomputer memory. The former approach requires a greater program cycle time but a relatively small amount of computer memory. The latter uses the microcomputer only as a look-up table and hence requires only a short program cycle. However, the amount of memory needed by the second method could grow very large for a parabola whose surface rate of change is high. This limitation was examined since the SBC 80/10 is limited to 64 Kbytes of computer memory.

Table 3-1 shows that only the C_{03} coefficient can be represented by one byte of memory; the other three coefficient values each require two bytes. The most rapidly changing coefficient, C_{02}, required updates each .0005 inch or 16001 times over the 8 inches of travel in the X direction. C_{01} required half that number, or 8001 updates. C_{00} required updates at .010 inch intervals for a total of 801. These 24803 updates represent 49606 bytes of memory. With the 801 bytes required by C_{03}, a grand total 50407 bytes of memory must be available for data storage.

Even with the drawbacks of inflexibility and memory requirements noted above, it was initially decided to perform the interpolation off-line and store the coefficients in Programmable, Read-only Memory (PROM). The primary reason for this decision was a concern over the limitation on the cycle time of the operating program noted above. However, before this system was put into use, a fast floating-point arithmetic board for the computer was found which permitted real-time interpolation in a few milliseconds per coefficient.

Figure 3-9 is a schematic of the X slide laser interferometer position counter. The counter consists of nine Binary-Coded-Decimal (BCD) counter

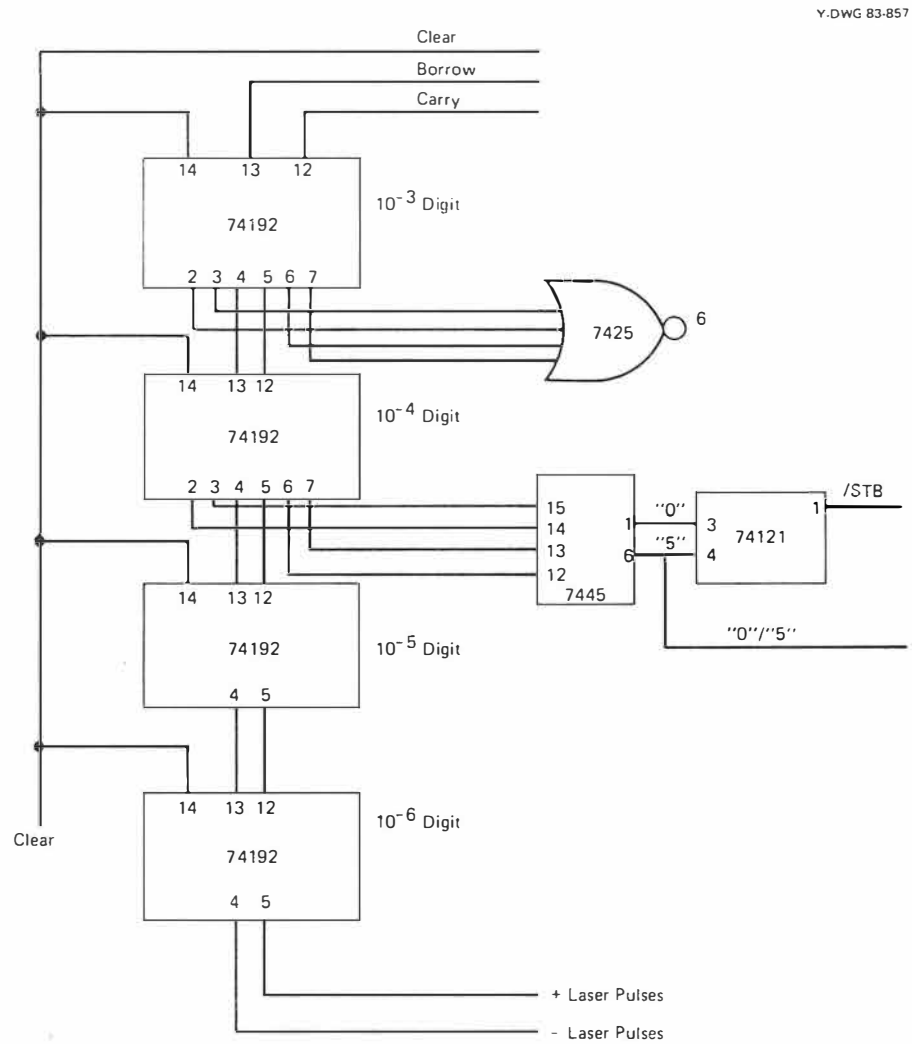

Figure 3-9. Schematic diagram of interferometer display.

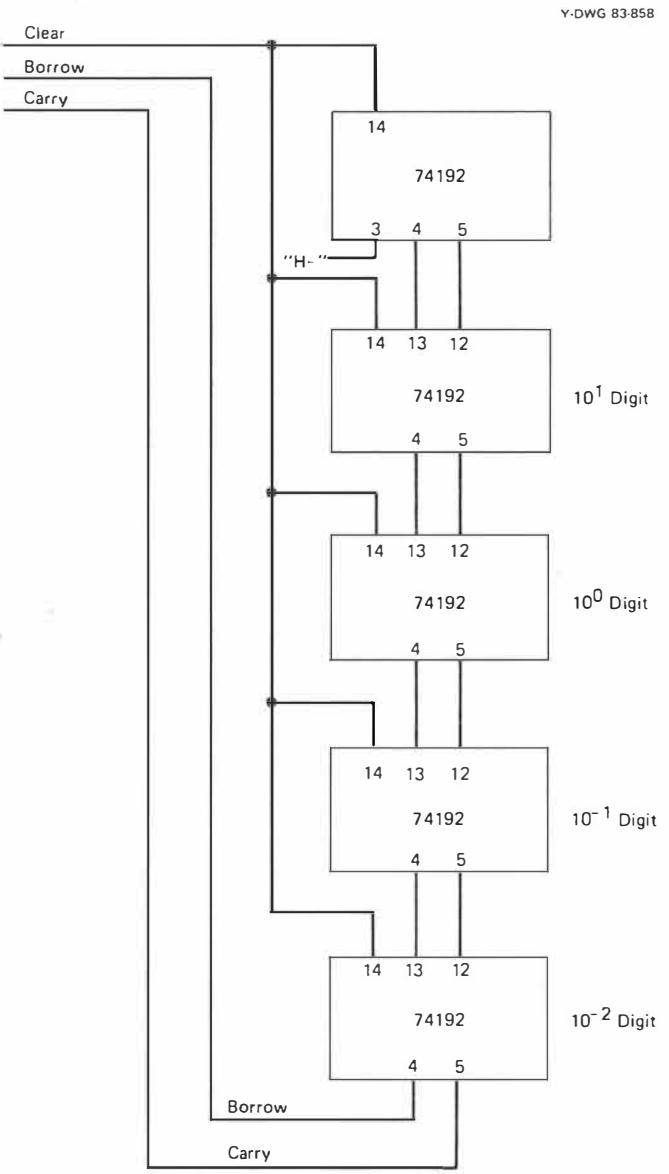

Figure 3-9 (continued).

chips, the first of which is driven positively by up counts from the laser interferometer circuitry and negatively by down counts. The remaining chips are connected in serial fashion with the up counts driven by the carry signal output from the previous chip and the down counts driven by the corresponding borrow signal. Each chip also has four BCD output lines which are used to drive numeric displays of slide position. These lines were also used to convey the necessary position data to the computer from four of the chips. Also shown in Figure 3-9 are digital logic circuits driven by the BCD lines on the chips representing the third and fourth digits right of the decimal.

The C_{02} coefficient is recalled to require updates at X intervals of .0005 inch. The use of the interrupt capability of the microcomputer was thought to provide the surest method of initiating updates for all coefficients appropriately. In Figure 3-9 a BCD-to-decimal decoder is seen at the output of the BCD chip representing the fourth decimal digit. The "0" and "5" lines output from the decoder to monostable multivibrator (SN74121) furnish a pulse to the interrupt circuitry of the microcomputer. Simultaneously this pulse is used to latch the readings of the desired four display digits into the registers at the computer input ports. The "5" line at the output of the decoder chip is passed to the computer also to permit the computer to discriminate between the half-mil and whole-mil states. Similarly, the four output lines from the BCD chip representing the third decimal (mil) digit are passed to a NOR gate to indicate to the computer when the mil digit is zero. Thus, at each half-mil increment in X position an interrupt signal is passed to the computer along with two flags which indicate the presence of the zero state of the third and fourth decimal digits. At the interrupt signal the computer immediately reads the four BCD chips representing the "d.ddd" number. At all interrupts the C_{02} coefficient is

retrieved while C_{01} is retrieved only when the fourth digit is zero. Similarly, C_{00} and C_{03} are returned only when the third digit is zero.

An Intel SBC 80/10 single-board microcomputer with memory and input/output extension boards was used to implement the interpolation scheme. This computer is based on the Intel 8080A microprocessor and has among its features:

1. Six 8-bit general purpose registers and an 8-bit accumulator;
2. A 16-bit program counter which allows direct addressing of 64 Kbytes of memory;
3. 1 Kbyte of static Random Access Memory(RAM);
4. A serial communications interface;
5. Six 8-bit programmable parallel input/output ports.

The SBC 80/10 also possesses four sockets for up to 4 Kbytes of onboard Read Only Memory (ROM). Two of these sockets were used for the system monitor which was used for activating short programs for hardware testing during the various stages of system development. The system operating program and the coefficient data were stored on Eraseable, Programmable Read Only Memory (EPROM) chips mounted on an Intel SBC-816 Memory Expansion board.

Before describing the details of the computer hardware configuration, the required and desired features of the system should first be discussed. The basic input/output specifications were given in Chapter 2 and are summarized as follows.

1. Inputs to the computer from four binary-coded decimal (BCD) digits of the X slide laser interferometer display;

2. Inputs to the computer from the logic circuitry which flag the occurrence of a "0" or "5" in the ten-thousandths inch digit of the same display; and

3. Outputs from the computer to the four digital-to-analog Converters (DAC's) whose outputs represent the coefficient values C_{00}, C_{01}, C_{02} and C_{03}.

Table 3-1 showed that all C_{03} coefficient values can be represented by eight or fewer bits while the other coefficients require between nine and sixteen bits. If allocated in eight bit blocks, computer output to the DACs is then seen to occupy 16 lines for each of C_{00}, C_{01} and C_{02} and an additional 8 lines for C_{03} for a total of 56 data output lines. Provision for a strobe output was also desired so that data conversion for all updated coefficient values could be initiated simultaneously.

The four BCD laser display digits each occupy four lines of input for a total of 16 lines. The interrupt logic driven by the laser display require a line to signify whether the interrupt represents a "0" or "5" ten-thousandths digit. An additional line was initially desired to detect the presence of a "0" in the thousandths inch digit. It was also desired to use the interrupt signal to latch the values of all inputs simultaneously.

A total of 18 input and 56 output lines was thus required which exceeded the total available 48 input/output lines resident on the SBC 80/10 board. An Intel SBC 508 I/O Expansion Board with capability for 32 input and 32 output lines was used to satisfy the input/output capacity not provided by the SBC 80/10.

The six 8-bit ports on the SBC 80/10 board can be arranged in several configurations. The Intel Hardware Reference Manual (21) describes the details for programming and control of the multiplicity of input/output combi-

nations available with these ports. Basically, the six ports are divided into two groups and are designated group 1, ports A, B and C and similarly for group 2. Ports A and B of both groups can be programmed for normal or latched/strobed input/output. Port A of group 1 is permanently configured as bidirectional. Port C of both groups can only be used in normal input/output modes but can also be further subdivided into two independent 4-bit ports under certain circumstances. However, for both groups under conditions of latched/strobed input/output to ports A and B, some of the lines of port C are needed for controlling the other ports.

Figure 3-10 illustrates the final system input configuration. Coefficient updates are triggerred at half-mil intervals in X by furnishing the interrupt signal to group 1, port C, lines 2 and 4. Ports A and B of this group are configured for latched input. The half- or whole-mil state is transmitted via port A, line 6 while the "0" mil condition is read on line 7 of this port. Group 1, port B is utilized to read the one-mil and ten-mil BCD display digits. Input Port 00 of the I/O Expansion Board was used to read the two most significant BCD display digits.

Originally these latter two digits were to be read with latched input through port A with the logic inputs read through port C, lines 6 and 7. However, as system testing began, the behavior of the laser up-down counters made it necessary to latch the interrupt logic inputs through port A. This behavior will be described in the software discussion. The result of moving the higher order display digits to the unlatched port 00 on the I/O Expansion Board was inconsequential because their rates of change are sufficiently slow.

Analog Devices model 1136 DACs were chosen for use in the system. These 16-bit DACs are mounted on cards and each is equipped with gain and

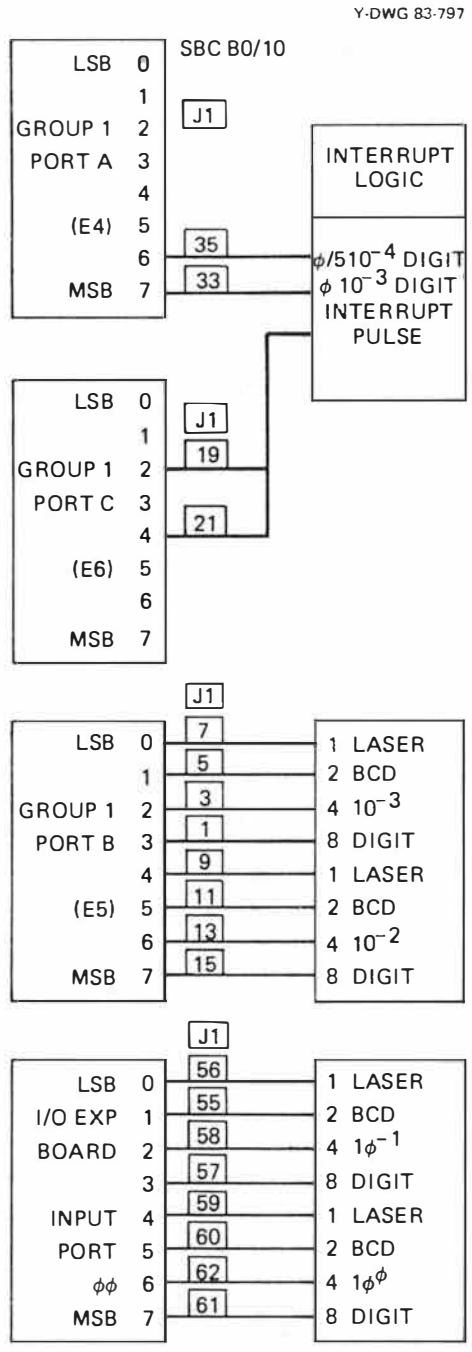

Figure 3-10. Microcomputer input port configuration.

offset adjustments and a 16-bit register to which data can be transferred and stored. Data conversion can also initiated by use of a strobe signal from the computer.

Figure 3-11 depicts the output port configuration. The SBC 80/10 group 2, ports A and B were interfaced to the C_{00} DAC while port C was tied to the eight least significant bits of the C_{03} DAC. Ports 00 and 01 and ports 02 and 03 of the SBC 508 board were used for output to the C_{01} and C_{02} DACs respectively. All output to these ports is unstrobed so that all of port C lines were available for use with the DACs. Note that the C_{03} coefficient is made permanently non-negative by grounding the most significant bit of the DAC. The next seven most significant bits are tied to +5 v to hold the maximum output of this DAC to +.078 v.

The most significant bit of the C_{00} DAC was tied to +5 v. Since the output of this DAC is always to be negative, the most significant bit of group 2, port A was used for a strobe signal. Updates of the coefficients are thus executed sequentially and written to their ports. These data do not actually reach the storage register associated with each DAC until clocked with the positive-going strobe signal at pin U on each DAC card.

The flowcharts for the system operating program and principal subroutines are shown in Figures 3-12 through 3-16. These figures are not intended to reflect assembly language coding details, but rather are intended to show the main functions of the program in receiving X slide position data and updating coefficient data through the DACs. The program begins with the initializing of the stack pointer, I/O ports and floating point mathematics board as well as storing interrupt branch instructions and the interrupt starting address. This interrupt initialization involves not only the preparation of the

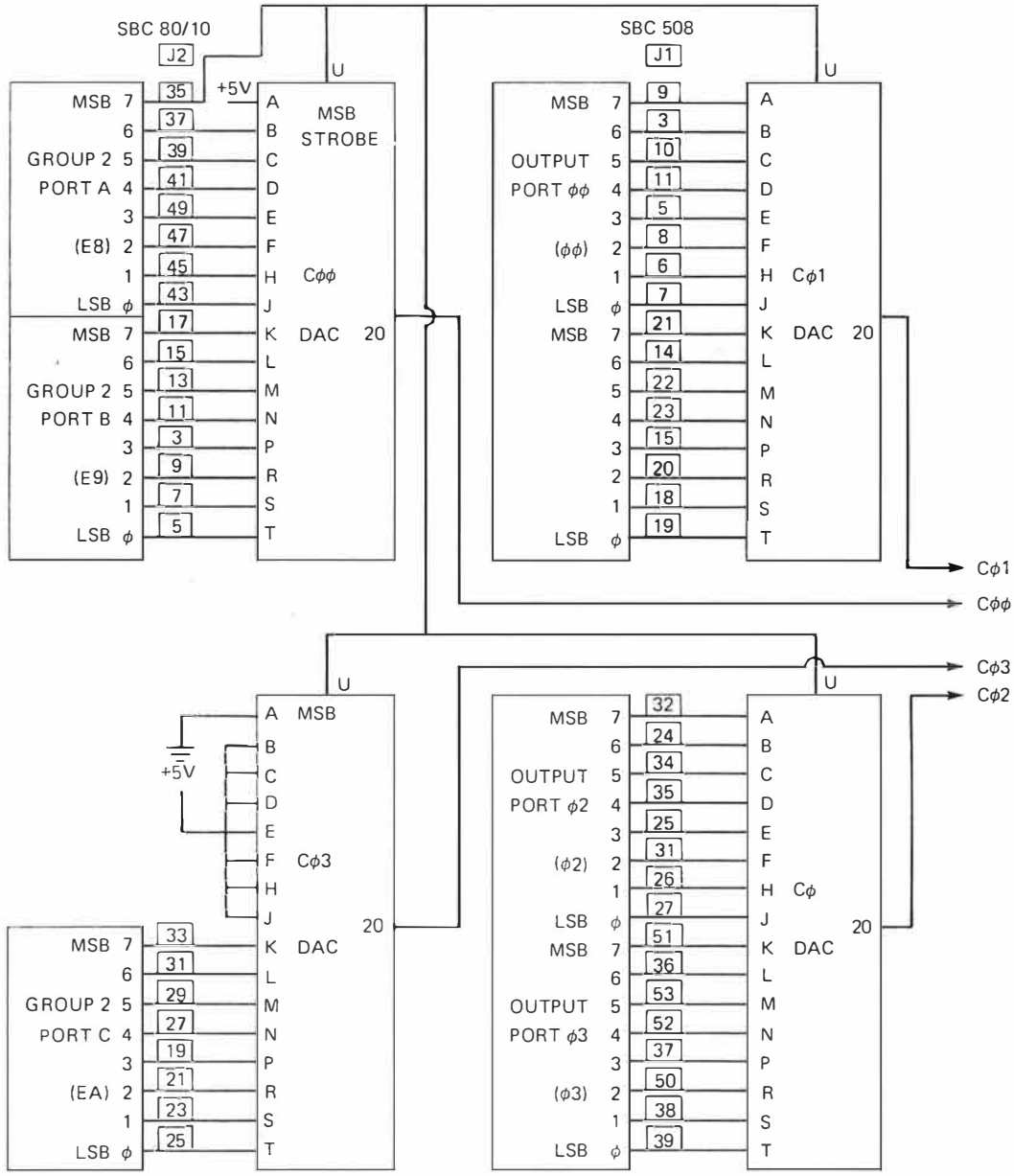

Figure 3-11. Microcomputer output port configuration.

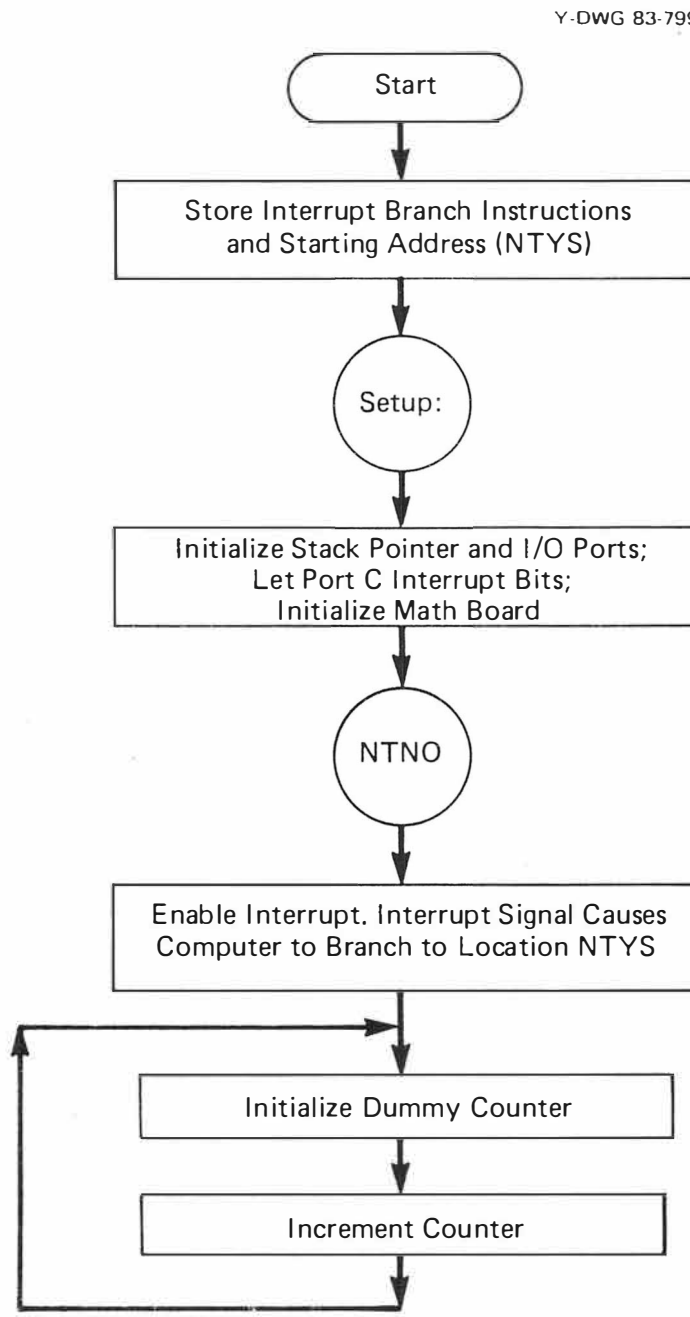

Figure 3-12. Flowchart of operating program.

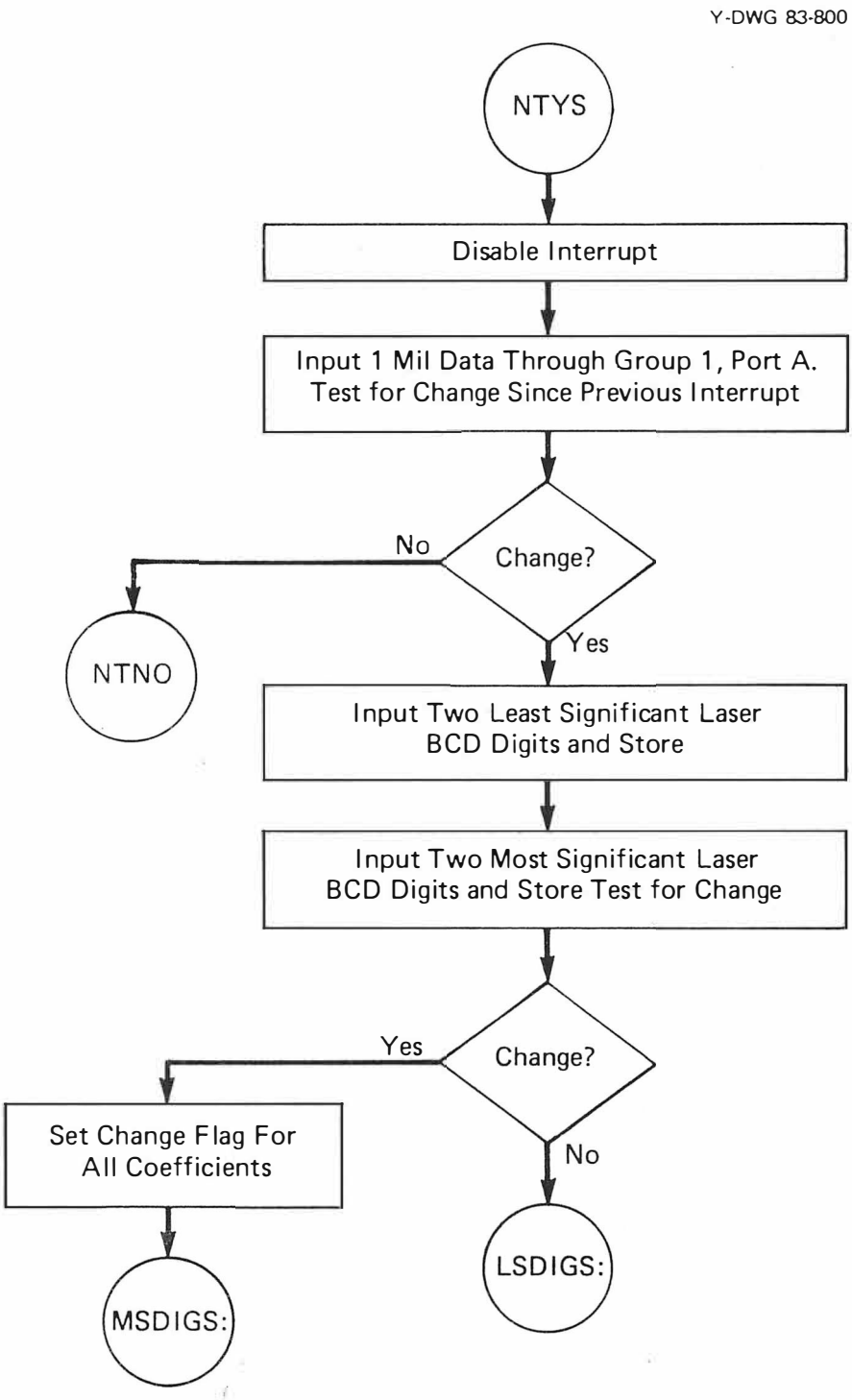

Figure 3-12 (continued).

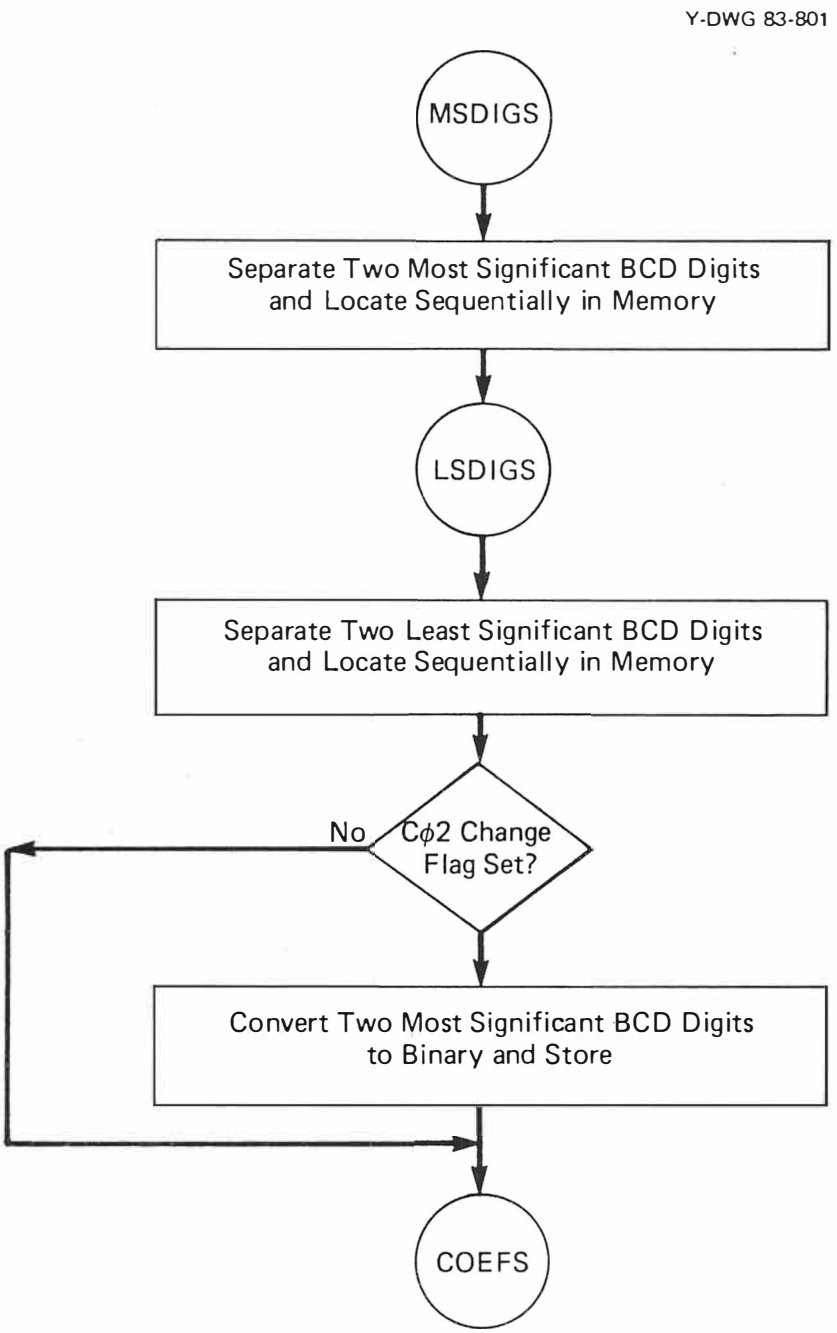

Figure 3-12 (continued).

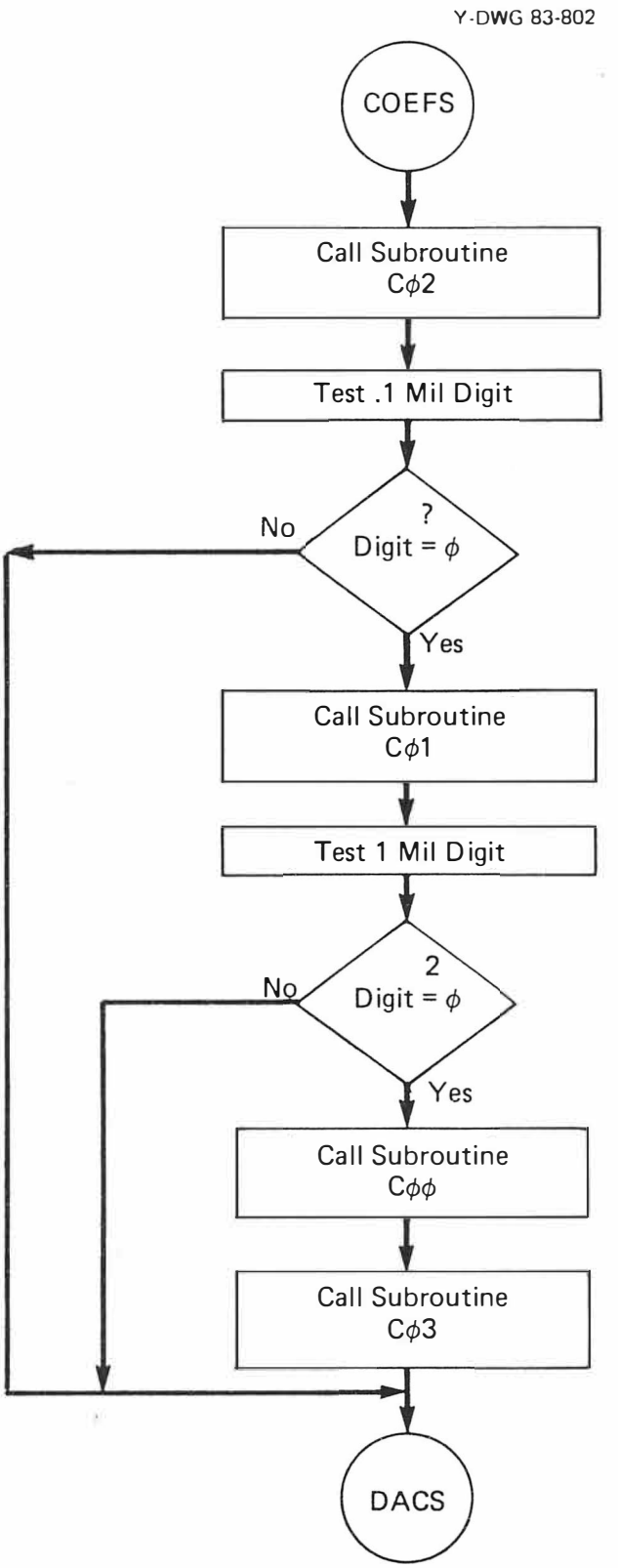

Figure 3-12 (continued).

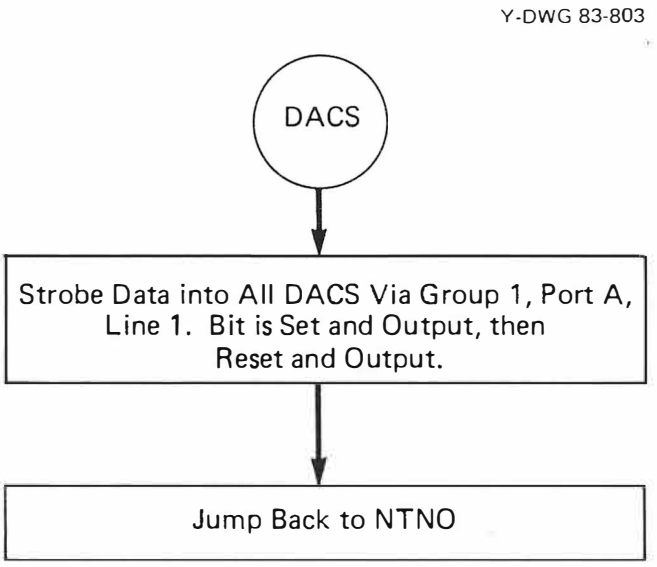

Figure 3-12 (continued).

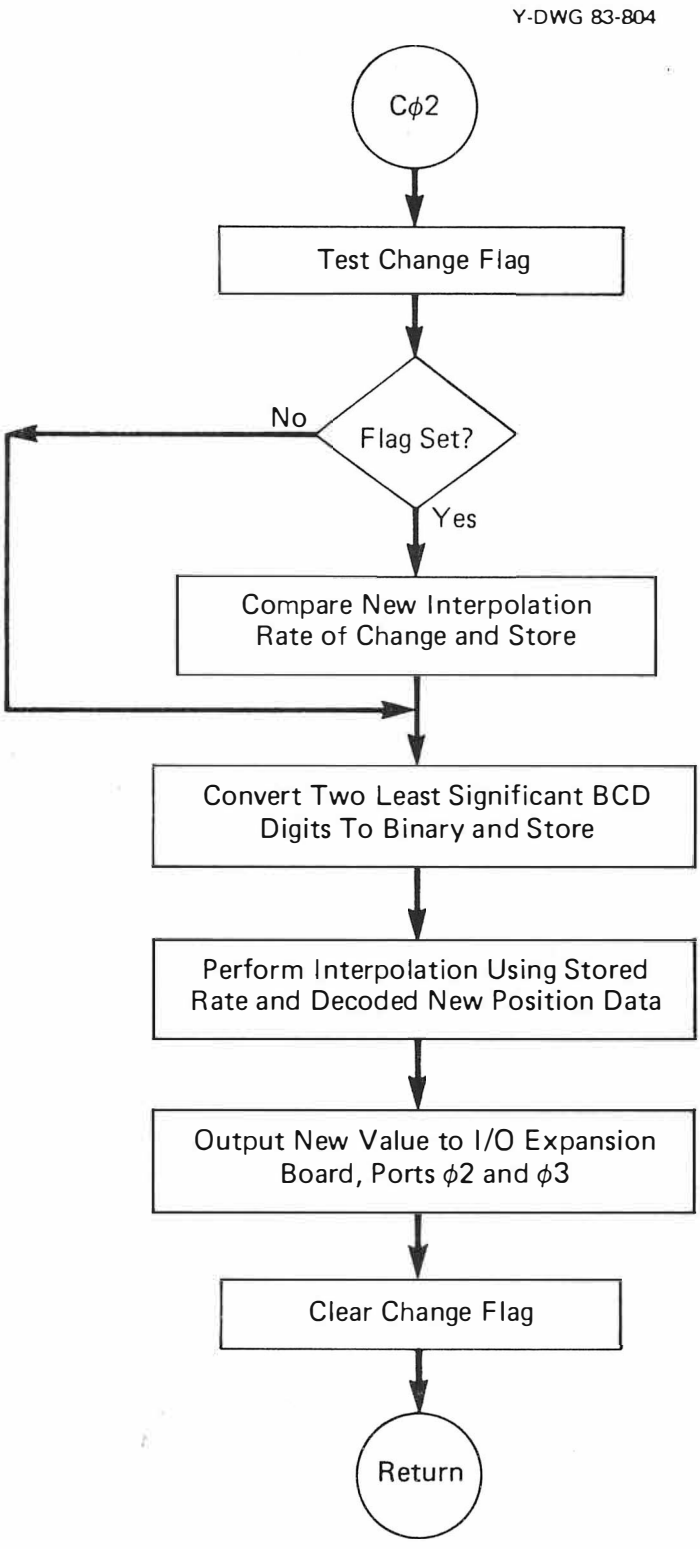

Figure 3-13. C_{02} output subroutine flowchart.

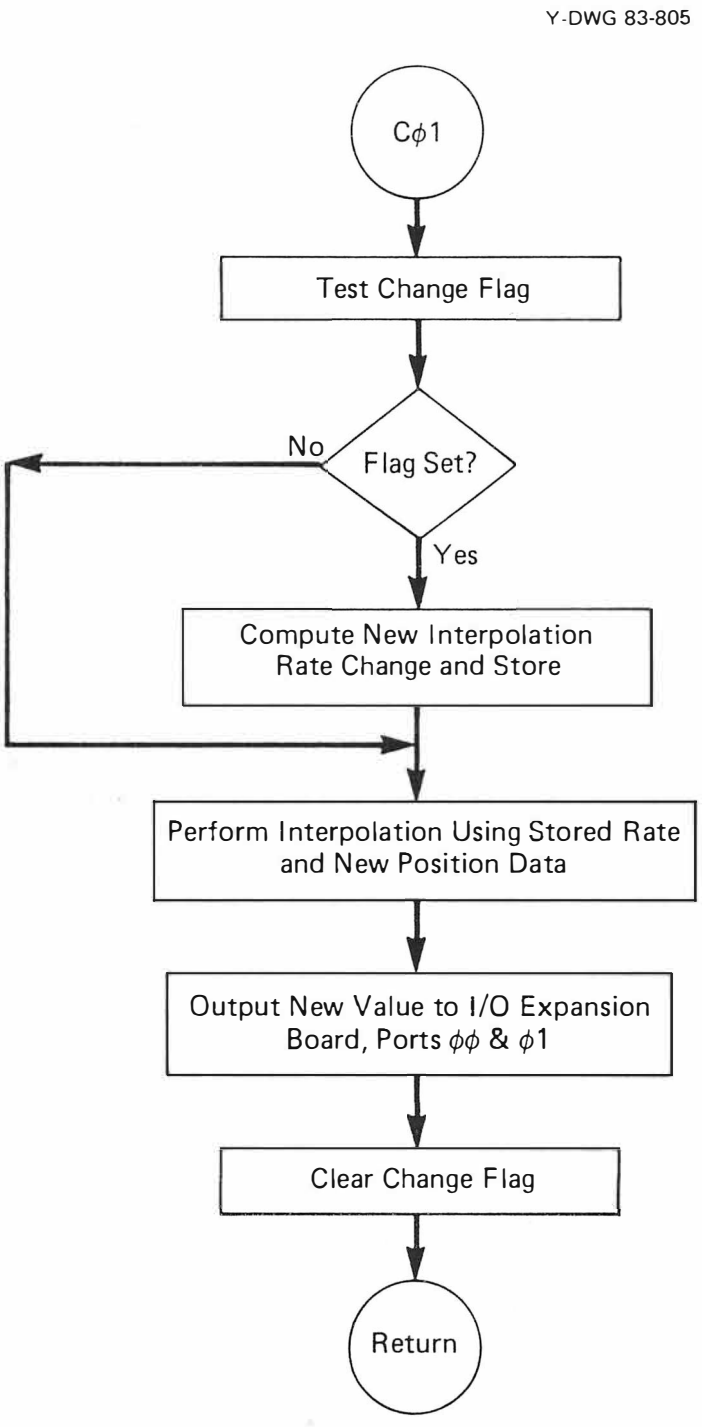

Figure 3-14. C_{01} output subroutine flowchart.

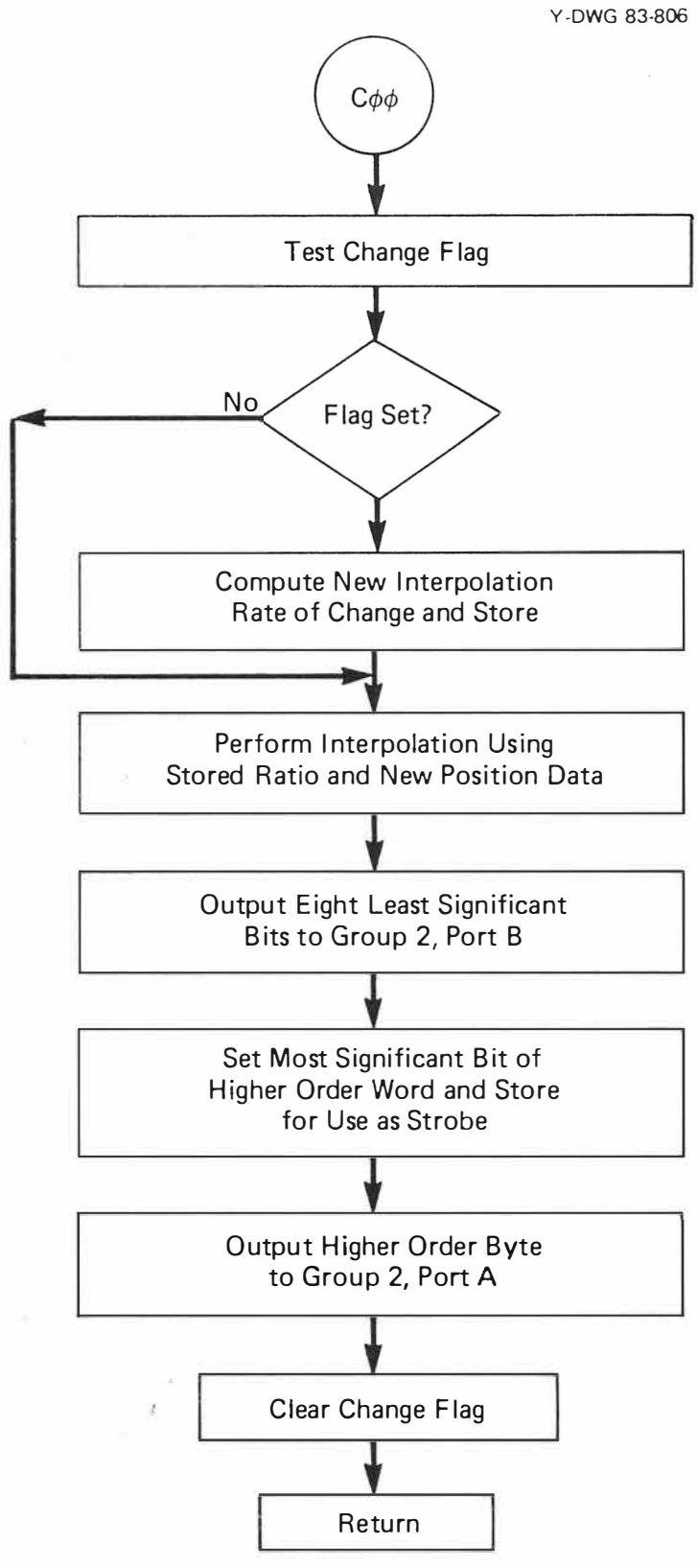

Figure 3-15. C_{00} output subroutine flowchart.

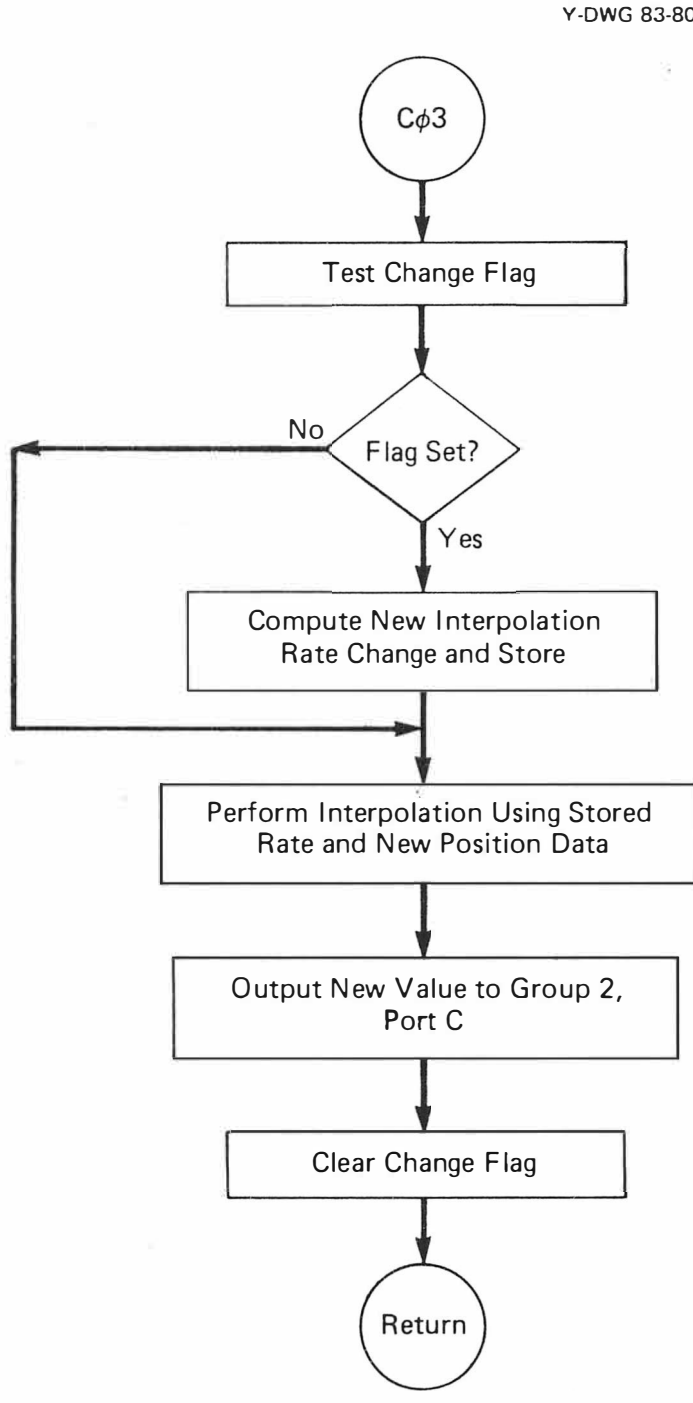

Figure 3-16. C_{03} output subroutine flowchart.

computer itself to respond to the interrupt signal but also the enabling of two bits in group 1, port C which allows the latching of inputs to ports A and B.

After initialization the computer enables the interrupt (see NTNO on flowchart) and enters a loop where a counter is incremented until an interrupt signal is received. At this point the computer branches to a location called NTYS where, after temporarily disabling the interrupt structure, the data at the logic circuitry is input through Group 1, Port A. The 0.1 mil value on line 6 is examined to determine whether any change has occurred since the last interrupt. This step was found to be necessary when it was discovered that momentary, very fast direction changes in the laser up-down position counters were resulting in flase interrupts to the computer. If no change was detected in this value the program returned to the interrupt loop. If a change was detected, the two least significant laser BCD digits were received and stored. The two most significant digits were then input and stored and also were tested to see if their values had changed since the last interrupt. If change had occurred, a flag was set for each coefficient.

In Chapter 2 the interpolation scheme was shown to employ a grid of values whose X spacing is .1 inch. Thus, only the two most significant laser digits are required to reference the end points of interpolation. Furthermore, the interpolation rate of change (the change in coefficient value from endpoint to endpoint divided by the number of interpolations in the .1 inch interval) is constant provided the two most significant laser digits do not change. This means that the rate of change must be computed once for each coefficient at each new interpolation interval. Software flags were used to indicated the need for a new coefficient rate of change computation.

The most and least significant pairs of BCD digits are separated and stored sequentially in memory in preparation for decoding to binary numbers. Although the least significant pair requires decoding at each interrupt, the most significant pair is decoded only after changes occur (as detected by the C_{02} change flag).

The new value of the C_{02} coefficient is computed and output at every interrupt. The .1 mil indicator bit is then tested. If this digit is zero, the C_{01} coefficient is similarly updated. Finally, the 1 mil digit is tested. If zero, the C_{00} and C_{03} coefficients are updated. As C_{00} is updated, the higher order byte is stored for later use in strobing all data into the DACs simultaneously. This strobing is accomplished by first setting the most significant bit and outputting to the port, clearing this bit and repeating the cycle. After strobing new data into the DACs, the program returns to the interrupt-await loop.

The coefficient subroutines represented in Figures 3-13 through 3-16 are basically similar. Decoding of the least significant pair of BCD digits to binary form is required in interpolation of the C_{02} and C_{01} coefficients and hence is performed only in the C_{02} subroutine. The C_{00} and C_{03} subroutines require only the use of the mil digit. Interpolation is accomplished by multiplying the rate of change by the position increment furnished by the least significant pair of BCD digits read from the laser display. This product is added to the coefficient value at the lower end of the interval. All subroutines utilize the floating point mathematics board for greatly increased computation speed.

The operating program was generated on an Intel Corporation Intellect 8 microcomputer development system along with an Intel PROM Programmer. This development system possesses all the software and hardware necessary to create and edit files, assemble and link assembly language programs and place

the result in the proper format for transmitting to the PROM Programmer. The PROM Programmer then fixes the binary code into nonvolatile memory chips. The listing of the assembly language can be seen in Appendix A.

This chapter has provided a description of the hardware utilized in the experiment excluding the Z slide closed loop control system. This last topic is presented in the next chapter.

CHAPTER 4

Z SLIDE CONTROL SYSTEM DESIGN AND TESTING

In this chapter the design and testing of the Z slide closed loop controls are described. A theoretical model of the system plant (slide, drive motor, servo amplifier and capacitance gage) is derived. This derivation is followed by a description of the measurements taken to validate and/or modify the model. The series of compensation techniques is presented followed by a description of the performance of slide controls as finally configured.

As described earlier the tool is mounted on a hollow aluminum slide supported by a pressurized air film and driven by a directly connected linear motor. The free-body diagram shown in Figure 4-1 illustrates the forces acting on the slide in the longitudinal direction. The frictional force, df_f, is a distributed force consisting of the breakaway, or Coulomb, friction component and a viscous friction component arising from shear in the pressurized air film. The Coulomb friction force is only a few grams and hence will be neglected in this analysis. A force balance in the longitudinal, or Z, direction yields

$$f_m(t) - df_f(t) = M\frac{d^2z(t)}{dt^2}$$

or

$$f_m(t) - f_f(t) = M\frac{d^2z(t)}{dt^2} \quad . \tag{4-1}$$

The viscous friction component f_f is difficult both to measure and to compute. This difficulty arises from the inaccuracy of instrumentation and analytical

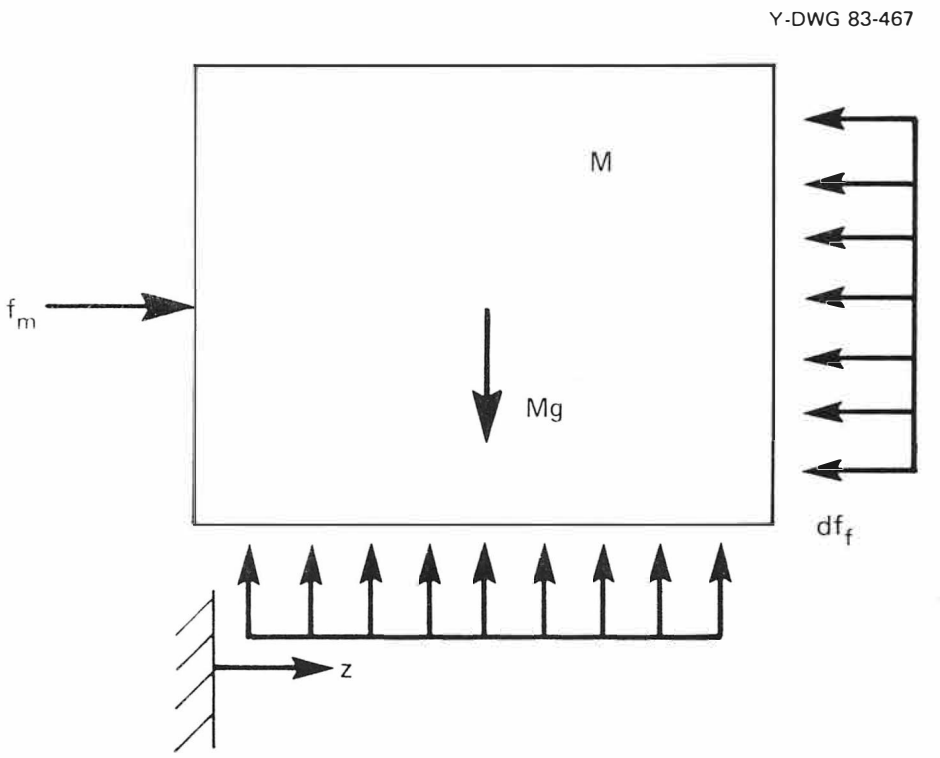

Figure 4-1. Free-body diagram of slide and motor.

characterization of the air flow through the porous graphite pads. The air flow and slide velocity, however, are sufficiently low that the flow is in the laminar region and can be represented by

$$f_f(t) = B\frac{dz(t)}{dt}$$

so that

$$f_m(t) = M\frac{d^2z(t)}{dt^2} + B\frac{dz(t)}{dt}.$$

The Laplace transformation of this equation yields (with zero initial conditions)

$$F_m(s) = Ms^2Z(s) + BsZ(s). \tag{4-2}$$

The slide was driven initially by an Information Magnetics Model 14 linear motor (later changed to a Model 15 due to structural problems). The force, $f_m(t)$, generated by the linear motor is illustrated in Figure 4-2. The voltage, $e_m(t)$, applied to the motor terminals is opposed by the motor back emf, $e_b(t)$, which depends linearly on the slide velocity. The force, $f_m(t)$, generated by the motor is proportional to motor current, $i_m(t)$, and is given by

$$f_m(t) = K_f i_m(t). \tag{4-3}$$

The motor current is represented by

$$e_m(t) - e_b(t) = Ri_m(t) + L\frac{di_m(t)}{dt}. \tag{4-4}$$

With

$$e_b(t) = K_b\frac{dz(t)}{dt} \tag{4-5}$$

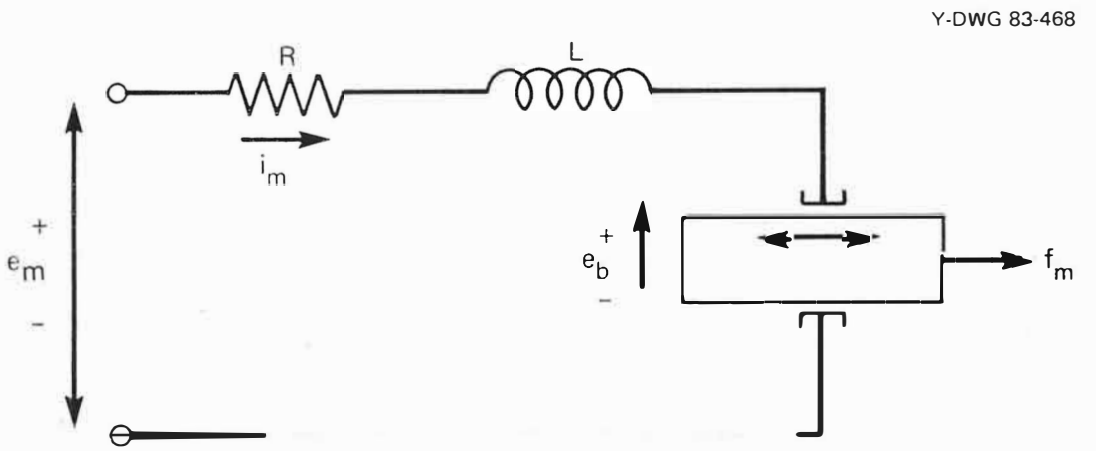

Figure 4-2. Electrical model of linear motor.

Equation (4-4) becomes

$$e_m(t) - K_b\frac{dz(t)}{dt} = Ri_m(t) + L\frac{di_m(t)}{dt} \tag{4-6}$$

If a Laplace transformation is performed on Equation (4-6) the result (again, with zero initial conditions) is

$$E_m(s) - K_bsZ(s) = RI_m(s) + LsI_m(s)$$

or

$$I_m(s) = \frac{E_m(s) - K_bsZ(s)}{R + Ls} \tag{4-7}$$

The transformed motor force, $F_m(s)$, is thus given by

$$F_m(s) = K_fI_m(s)$$

or

$$F_m(s) = K_f\left[\frac{E_m(s) - K_bsZ(s)}{R + Ls}\right] \tag{4-8}$$

If the motor force expressions in Equations (4-2) and (4-8) are equated, there results

$$Ms^2Z(s) + BsZ(s) = K_f\left[\frac{E_m(s) - K_bsZ(s)}{R + Ls}\right] \tag{4-9}$$

or

$$sZ(s) = K_f\left[\frac{E_m(s) - K_bsZ(s)}{(Ms + B)(Ls + R)}\right] \tag{4-10}$$

Equation (4-10) is deliberately left in this form for use with the block diagram shown in Figure 4-3. The output of the plant is left in the sZ(s), or Z velocity, form because of its use in subsequent controls description.

The plant transfer function is reduced from Equation (4-10) to

$$\frac{sZ(s)}{E_m(s)} = \frac{K_f}{MLs^2 + \left[MR + BL\right]s + \left[BR + K_fK_b\right]}$$

or

$$\frac{sZ(s)}{E_m(s)} = \frac{\frac{K_f}{ML}}{s^2 + \left[\frac{R}{L} + \frac{B}{M}\right]s + \left[\frac{BR + K_fK_b}{ML}\right]} \qquad (4\text{-}11)$$

All of the parameters appearing in Equation (4-11) are either published in manufacturers specifications or are easily measured except for the viscous friction coefficient B. The values of these parameters are:

1. Force constant, $K_f = 4.0$ lbf/amp
2. Back emf constant, $K_b = 5.52$ volt-sec/ft
3. Driven mass, $M = 6.25$ lbm $= 0.194$ slug
4. Coil DC Resistance, $R = 3.2$ ohm
5. Coil inductive time constant, $\tau_e = L/R = .00026$ sec

Without knowing the value of B an attempt was made to scale at least the order of magnitude of this quantity. The difficulty of computing flow parameters associated with porous graphite air bearings was discussed by Park, et al, (22). In a sensitivity analysis they attribute a major cause of the disagreement between computed and measured flow parameters to nonuniformity in graphite porosity. Measurement of the viscous frictional force is also diffi-

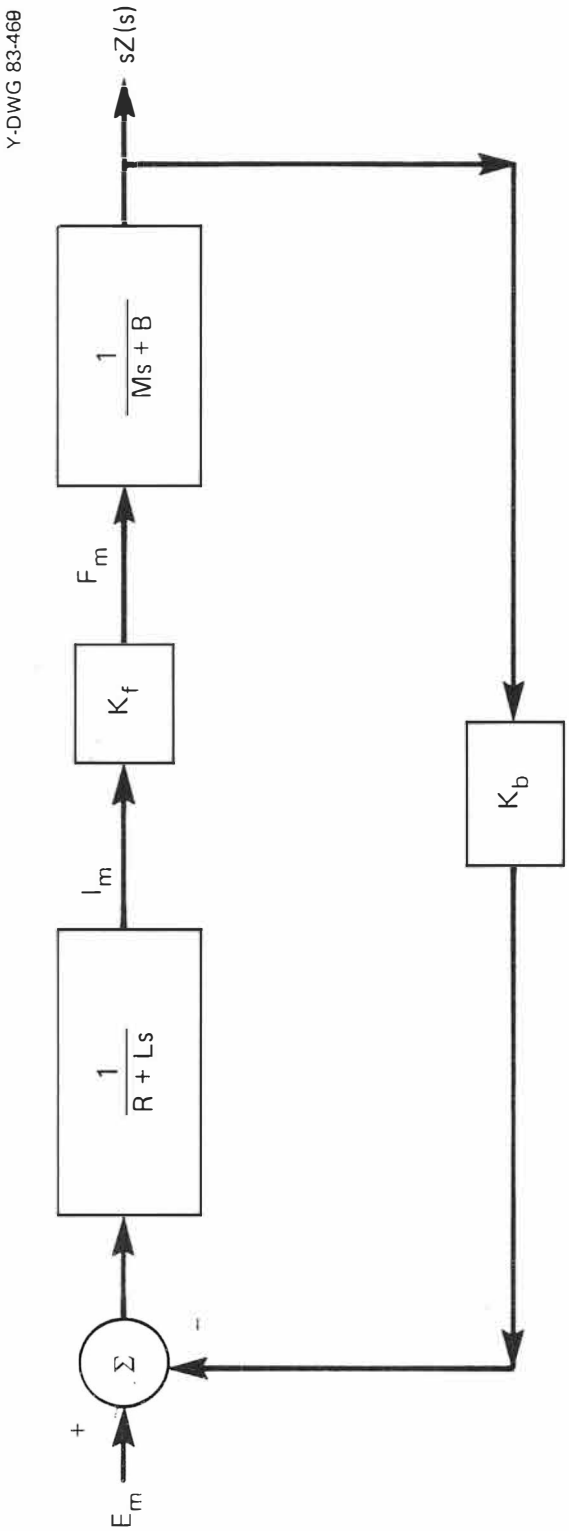

Figure 4-3. Block diagram of plant.

cult because of the very small values. An attempt was therefore made to estimate, by "feel", a value for B and to determine the significance of this term. Previously the breakaway friction was quoted as on the order of a few grams. Continued application of a force thought to approximate this breakaway force was observed to move the slide at a rate exceeding 1 in/sec. If this frictional force were as large as, 1 ounce, or .0625 lbf, B is no larger than 0.75 lbf-sec/amp.

The coefficient of the first degree term in s in the denominator of Equation (4-11) is seen to be heavily dominated by the $\frac{R}{L}$ term, and hence the $\frac{B}{M}$ term can be ignored without real consequence. Similarly, in the zero degree term the BR product is smaller than $K_f K_b$ by more than an order of magnitude. This indicates that the deletion of both appearances of B in Equation (4-11) should not seriously affect the system model. Thus, Equation (4-11) is reduced to

$$\frac{sZ(s)}{E_m(s)} = \frac{\frac{K_f}{ML}}{s^2 + \left(\frac{R}{L}\right)s + \left(\frac{K_f K_b}{ML}\right)} \qquad (4\text{-}12)$$

Substitution of the parameter values into Equation (4-11) yields the following characteristic equation

$$s^2 + 3846s + 136791 = 0 \qquad (4\text{-}13)$$

with two real roots at $s = -35.9$ and $s = -3810$. The transfer function of Equation (4-12) is also seen to have a dc gain of $1/K_b$ or approximately 1 ft/volt-sec.

At this point it was desired to perform tests on the slide and motor to verify this model. With the very low slide friction and absence of direct, non-influencing velocity transducers, open loop testing of the plant was not practical. Use of the differentiated capacitance gage signal did not provide a solution because the slide drifted sufficiently in open loop to saturate the capacitance gage and the associated electronics. Characterization of the plant was therefore accomplished by derivation from measurements of the closed velocity loop.

A simple test control system was designed in which the slide and drive motor were placed in the control loops illustrated by the block diagram in Figure 4-4. The K_o and K_A factors represent the outer (position) loop proportional gain and power amplifier gain respectively. The plant transfer function, G_p, is followed by the factor 12000/s which represents the conversion of slide displacement units to mils and the integration of velocity to yield displacement. The capacitance gage used for position feedback produces 1 volt per mil of displacement for a gain of 1. Velocity feedback was provided by placing a differentiating network accompanied by a low pass filter at the output of the capacitance gage. This transfer function was given by

$$H_v(s) = \frac{K_{fv}s}{1 + \frac{s}{\omega_{fv}}} \qquad (4\text{-}14)$$

The purpose of the low pass filter was to reduce the effect of noise produced by differentiation. Since the desired system bandwidth was 100 Hz, it was felt that the break frequency of this filter should be located at 1000 Hz or beyond. The transfer function of the closed velocity loop, therefore, is

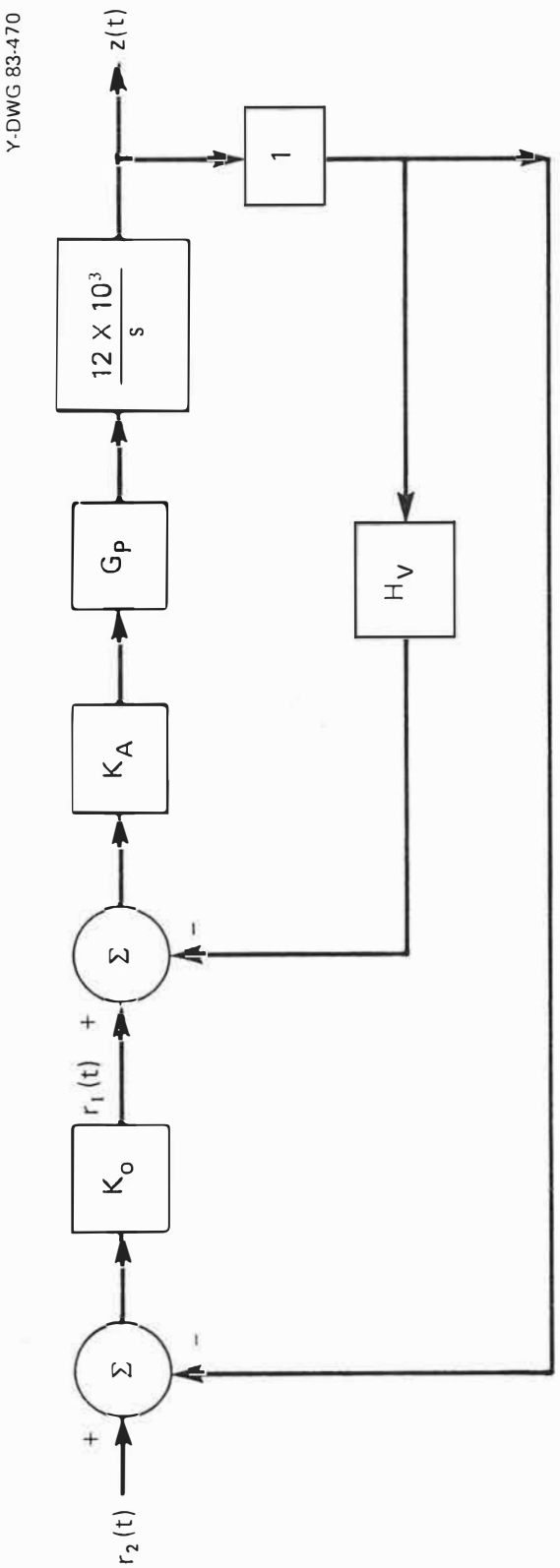

Figure 4-4. Initial Z slide block diagram (z in inches).

$$\frac{Z(s)}{R_1(s)} = \frac{K_A G_p\left(\frac{12000}{s}\right)}{1 + K_A G_p\left(\frac{12000}{s}\right) H_v} \tag{4-15}$$

which produces

$$\frac{Z(s)}{R_1(s)} = \frac{492804000K_A\left(s + \omega_{fv}\right)}{s\left[s^3 + \left(3846 + \omega_{fv}\right)s^2 + \cdots\right.}$$

$$\cdots \left.\left(136791 + 3846\omega_{fv}\right)s + \left(136791 + 492804000K_A K_{fv}\right)\omega_{fv}\right] \tag{4-16}$$

With $K_A = 10$

$$\frac{sZ(s)}{R_1(s)} = \frac{4928040000\left(s + \omega_{fv}\right)}{s^3 + \left(3846 + \omega_{fv}\right)s^2 + \cdots}$$

$$\cdots \left(136791 + 3846\omega_{fv}\right)s +$$

$$\cdots \left(136791 + 4928040000K_{fv}\right)\omega_{fv} \tag{4-17}$$

Although no true velocity loop is seen in Figure 4-4, the equivalent loop is obvious in Figure 4-5. The outer loop transfer function is produced similarly

$$\frac{Z(s)}{R_2(s)} = \frac{4928040000\left(s + \omega_{fv}\right)}{s^4 + \left(3846 + \omega_{fv}\right)s^3 + \cdots}$$

$$\cdots \left(136791 + 3846\omega_{fv}\right)s^2 + \left[\left(136791 + 4928040000K_{fv}\right)\omega_{fv} \cdots\right.$$

$$\left. + 4928040000K_o\right]s + 4928040000K_o\omega_{fv} \tag{4-18}$$

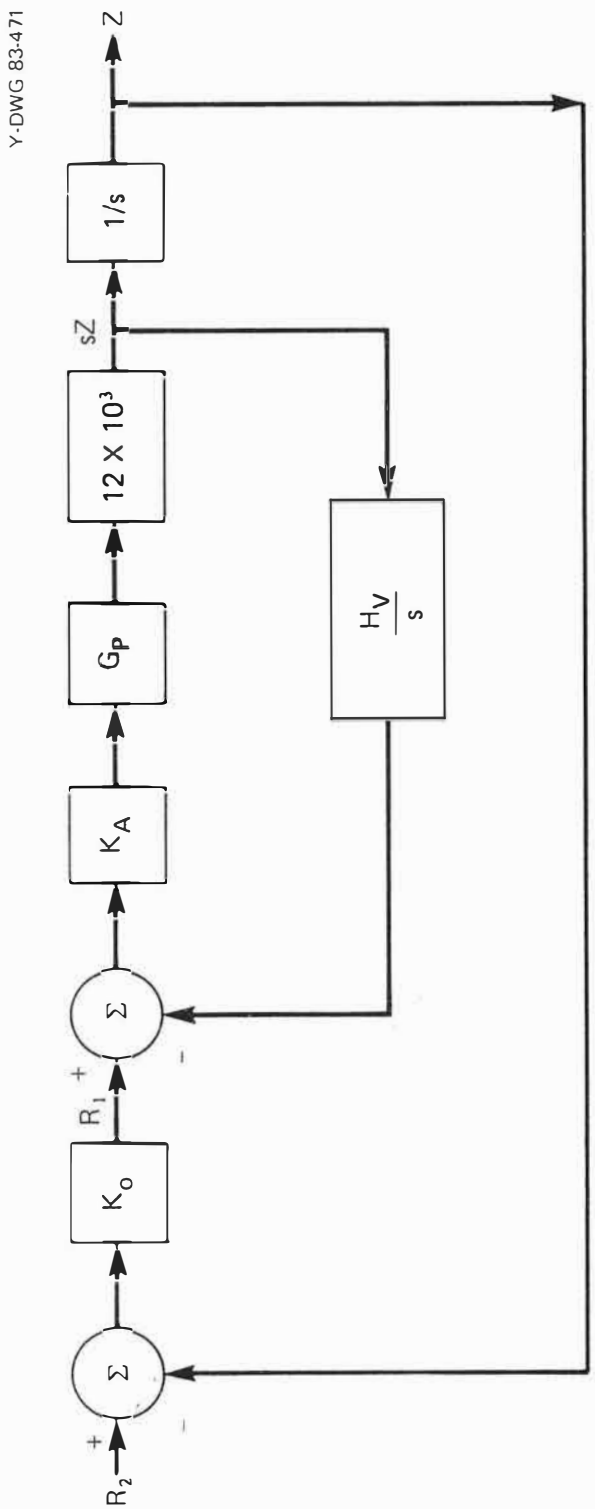

Figure 4-5. Equivalent Z slide block diagram.

The transfer functions for both the velocity and position loops were left in symbolic form for comparison with the root locus diagrams shown in Figures 4-6 and 4-7. For fixed ω_{fv} the locus of roots in the velocity loop are seen in Figure 4-6 to approach zeros at infinity along asymptotes at 60, 180 and 300 degrees as K_{fv} approaches infinity. These asymtotes intersect at the real point

$$s = -\frac{\left(3846 + \omega_{fv}\right)}{3} \tag{4-19}$$

For fixed K_{fv} the effect of shifting ω_{vf} in the negative direction is to shift the intersection of asymtotes negatively also. Simultaneously, with fixed K_{fv}, the complex roots show increasing natural frequency with decreasing damping.

The root locus diagram for the position loop, Figure 4-7, assumes that two of the roots of the velocity loop characteristic equation are complex. Three of the closed loop roots are again seen to approach zeros at infinity along asymtotes at 60, 180, and 300 degrees. The fourth root, originating from the open loop pole at the origin, approaches the zero at ω_{fv}.

A FORTRAN computer program (Appendix B-2) was written to permit selection of values of ω_{fv}, K_{fv}, and K_O which would yield reasonable roots for the closed velocity and position loops. Since the filter frequency, ω_{fv}, was desired to be 1000 Hz or larger, it was set at 100000 rad/sec for convenience. The gain factors, K_{fv} and K_o were selected to be relatively small to prevent too rapid saturation of the electronics and of the capacitance gage. With K_{fv} = .002 and K_o = 1.5 the closed velocity loop was found to have a real root at -100102 rad/sec and a pair of complex roots with natural frequency of 3164 rad/sec and damping coefficient of 0.59. The closed position loop calculation

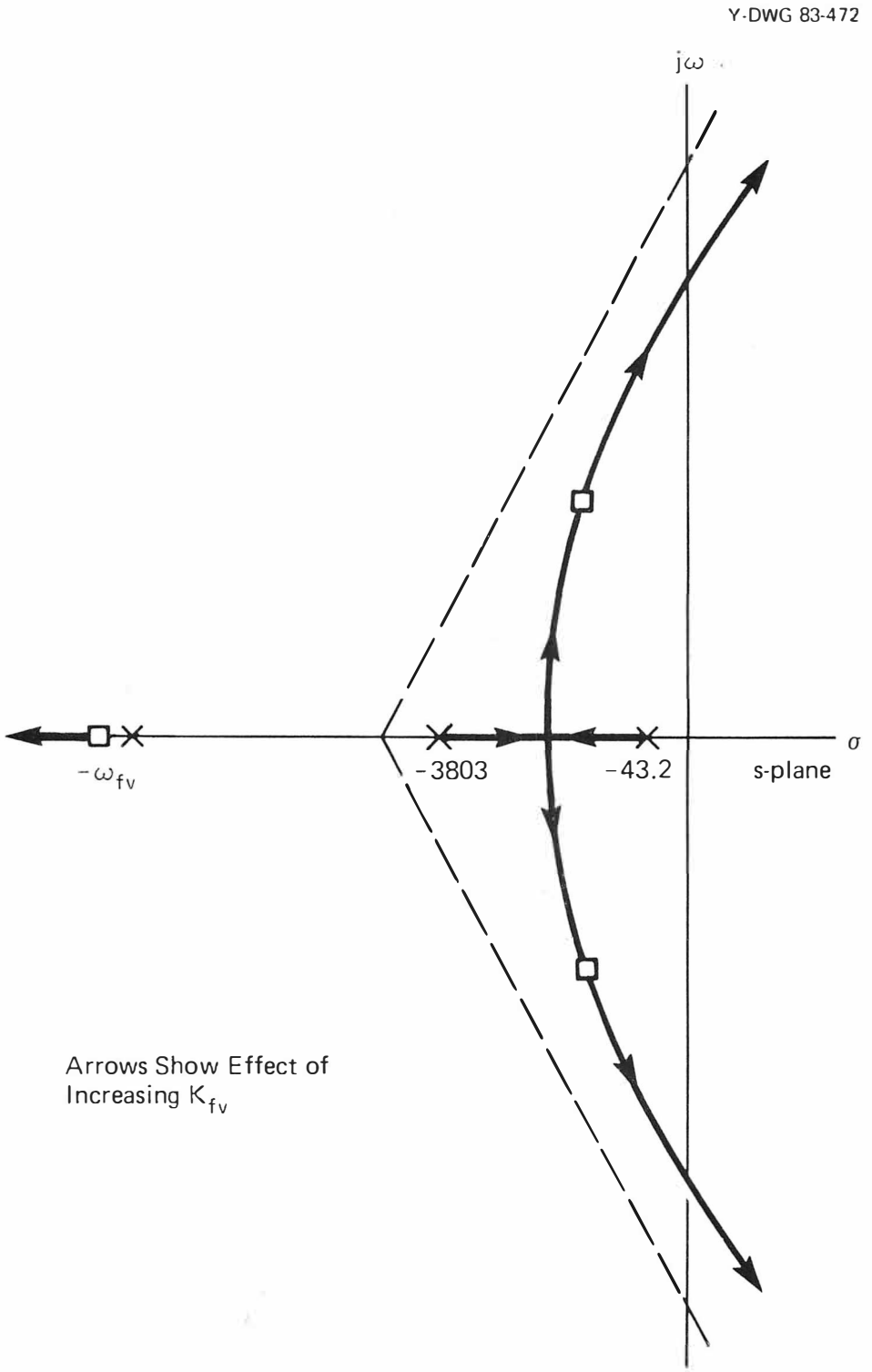

Figure 4-6. Root locus diagram of closed velocity loop (not to scale).

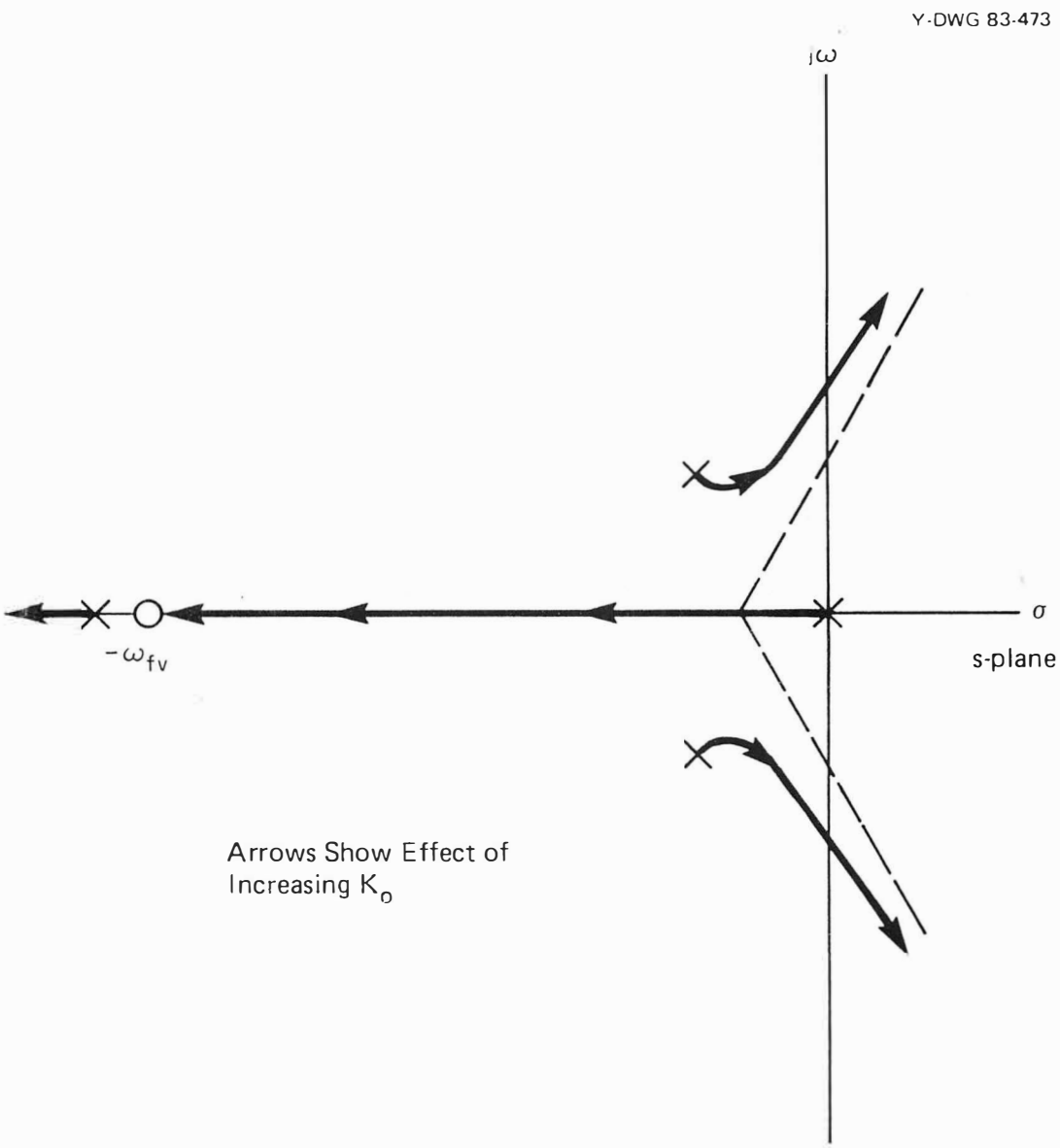

Figure 4-7. Root locus diagram of closed position loop (not to scale).

produced the same three roots plus another real root at s = -0.7379. The transfer function of the closed position loop thus appeared as

$$\frac{Z(s)}{R_2(s)} = \frac{4928040000\left(s + \omega_{fv}\right)}{(s + 100102)(s + .7379)\left(s^2 + 3743s + 10007563\right)}$$

The large pole and zero values were nearly identical which permitted the loop dynamics to be approximated by the third order function

$$\frac{Z(s)}{R_2(s)} = \frac{4928040000}{(s + .7379)\left(s^2 + 3743s + 10007563\right)} \qquad (4\text{-}20)$$

Because the real root at -0.7379 is more than three orders of magnitude nearer the origin than the real parts of the complex pole pair, it was expected to dominate the response of the system. Response to a step input should thus have exponentially approached the final value with a settling time (four time constants) of nearly 5.5 seconds.

The test system was constructed according to this design. The power amplifier, drive motor, and capacitance gage were connected into the system and power was applied. Although the system was stable, two undesirable characteristics were noticed immediately. First, the stiffness of the system was poor -- obviously insufficient to withstand the forces of metal cutting. This condition was not viewed as terribly serious since no attempt had been made to design for stiffness.

The second characteristic is displayed in the oscilloscope trace in Figure 4-8. The position error of the test system was viewed while the controls maintained the slide at the null position; ie, with zero position command. A 120 Hz, 5 mV noise signal is seen which over wider time traces appeared as 10 mV

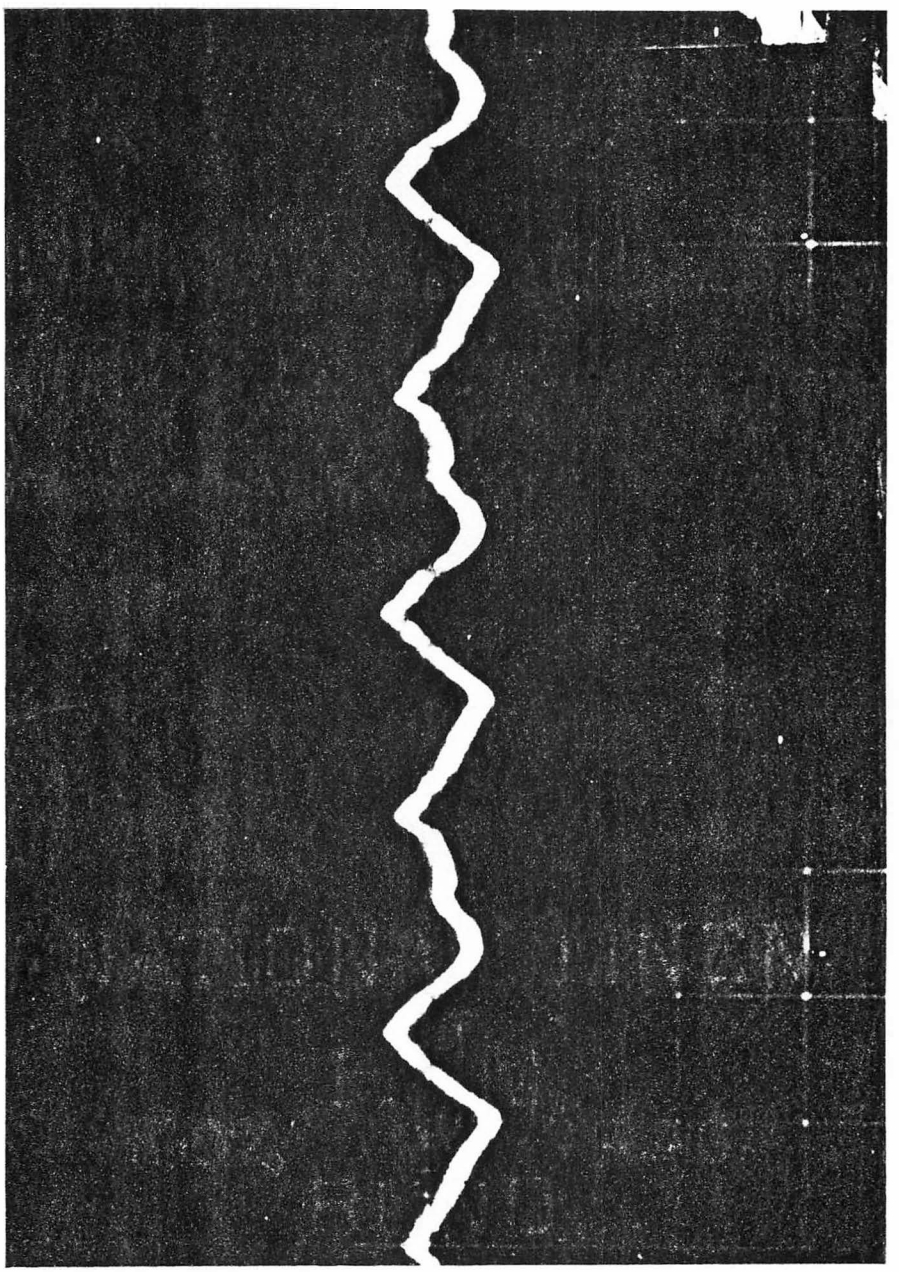

Figure 4-8. Actual position error signal with null command input.

and could not be eliminated with the test circuitry. This noise, of course, translated directly into microinches of displacement. Since the source of this noise was unknown, it was not known whether this noise could be eliminated. The noise later proved to be a critical factor in the performance of the slide.

An 8 volt step command, corresponding to an 8 mil position change, was applied to the position input. The response was markedly different from that postulated above. The system was seen to overshoot approximately 16 percent before settling to within a few percent of final value in approximately .010 sec. The time to first peak was measured as approximately .004 sec, while the 10 to 90 percent rise time was roughly .002 sec. This response can be viewed in Figure 4-9. When excited with a variable frequency sinusoid, the system indicated a bandwidth of more than 150 Hz.

A few calculations were made at this point to determine if these measurements were compatible. Because behavior similar to that of second order systems had been observed, formulae for second order systems were used (23). From

$$\text{Percent Overshoot} = 100\, e^{\frac{-\pi\zeta}{\sqrt{1-\zeta^2}}} \tag{4-21}$$

the 16 percent overshoot translated into a damping ratio of 0.5. From this damping ratio and the time-to-first-peak measurement, the undamped natural frequency was computed from

$$t_p = \frac{\pi}{\omega_n\sqrt{1-\zeta^2}} \tag{4-22}$$

This computation yielded a value of 145 Hz for the undamped natural frequency, ω_n. The bandwidth, given by (24)

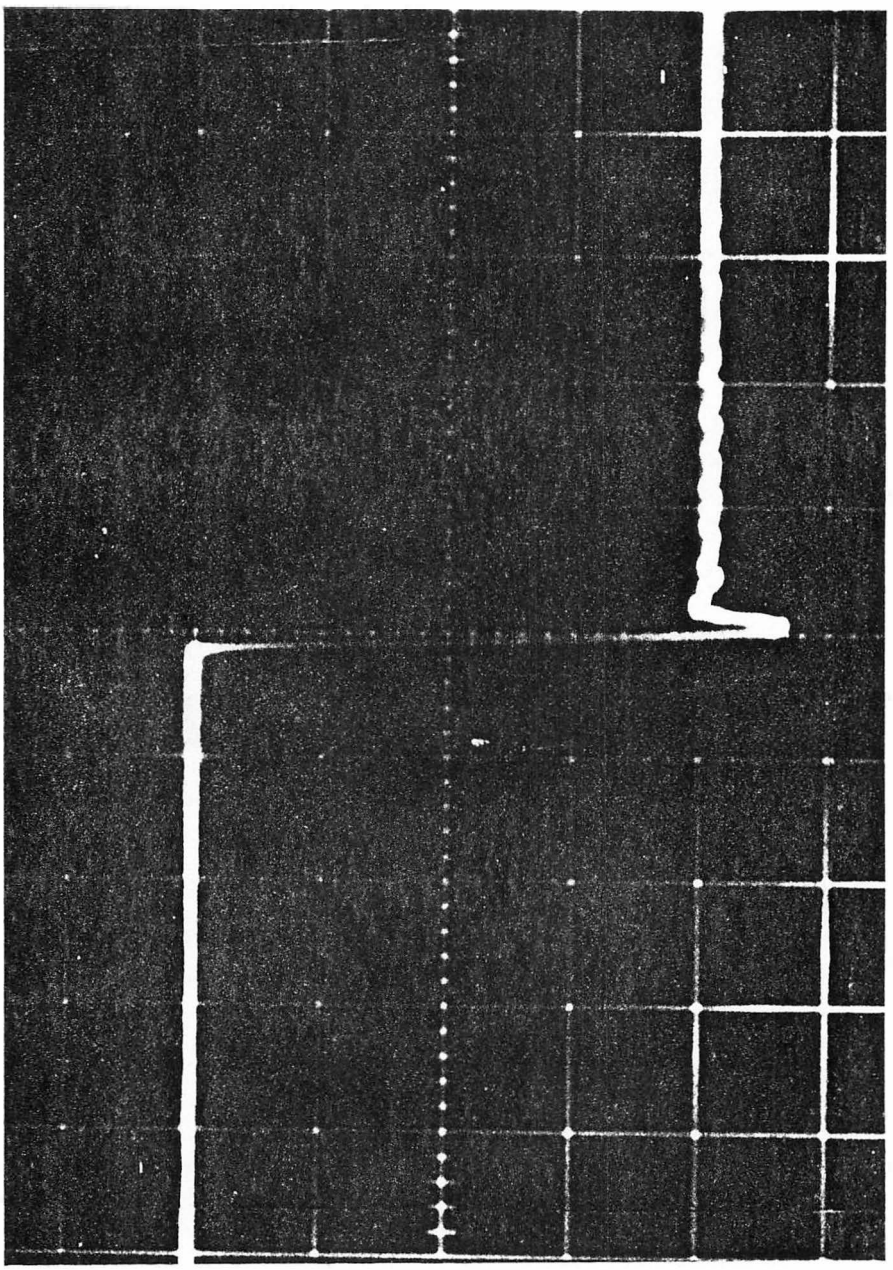

Figure 4-9. Response of initial test system to step input.

$$\omega_{BW} = \omega_n\left[\left(1 - 2\zeta^2\right) - \sqrt{4\zeta^4 - 4\zeta^2 + 2}\ \right]^{1/2} \qquad (4\text{-}23)$$

was then computed as 169 Hz. The rise time, t_r, can be approximated by

$$t_r \approx \frac{1 + 1.1\zeta + 1.4\zeta^2}{\omega_n} \qquad (4\text{-}24)$$

which produced a value of .0021 sec and compared quited favorably with the measured value of .002 sec.

The system was then driven with a 4 volt half-amplitude sine wave command of 10 Hz frequency. Figure 4-10 is a photograph of an oscilloscope trace of the position error signal during this sinusoidal excitation. The position error is seen to be roughly sinusoidal with a half-amplitude of .4 volts with higher frequency, low amplitude ripples superimposed.

With the pronounced differences in predicted and measured response of the test system, it was obvious that the model had unacceptable flaws that required reconciliation. With the simplicity and small number of components in the test system it was felt that the discrepancy must lie either in the manufacturer's specifications or in the assumption that viscous friction was negligible. The motor coil resistance and inductance were measured and found to support the quoted values. The motor back emf, which depends linearly on the force constant, could not be measured directly and accurate force measuring equipment was not available. Even if the force constant was in error by a factor of two, however, the difference would not have been sufficient to account for the measured behavior. The assumption regarding the viscous friction was therefore reconsidered.

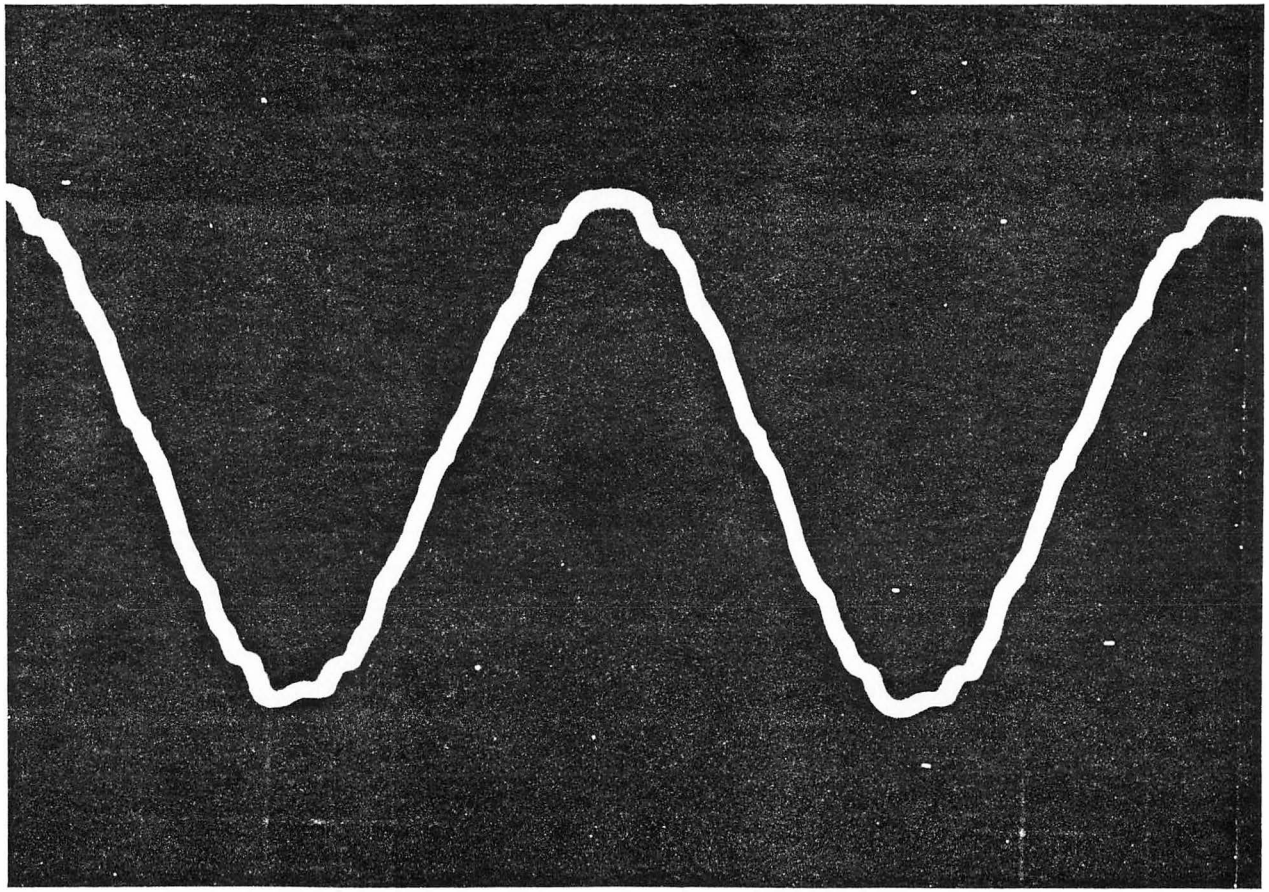

Figure 4-10. Position error of initial system under sinusoidal excitation.

Equation (4-11) can be rewritten as

$$G_p(s) = \cdots \left[\frac{ML}{BR + K_f K_b} \right] s^2 \Bigg]$$

or, more simply

$$G_p(s) = \frac{a_1}{1 + a_2 s + a_3^2} \tag{4-25}$$

where

$$a_1 = \frac{K_f}{BR + K_f K_b}$$

$$a_2 = \frac{MR + BL}{BR + K_f K_b}$$

$$a_3 = \frac{ML}{BR + K_f K_b}$$

If the closed velocity and position loops are carried out in this symbolic form, there result

$$\frac{sZ(s)}{R_1(s)} = \frac{120000a_1 \left(1 + \frac{s}{\omega_{fv}}\right)}{\left(1 + 240a_1\right) + \left[a_2 + \frac{1}{\omega_{fv}}\right] s + \cdots} \tag{4-26}$$

$$\cdots \left[a_3 + \frac{a_2}{\omega_{fv}}\right] s^2 + \left[\frac{a_3}{\omega_{fv}}\right] s^3$$

and

$$\frac{Z(s)}{R_2(s)} = \frac{120000K_o a_1\left(1 + \frac{s}{\omega_{fv}}\right)}{\left(120000K_o a_1\right) + \left(\frac{120000K_o a_1}{\omega_{fv}} + 1 + 240a_1\right)s + \cdots}$$

$$\cdots \left(a_2 + \frac{1}{\omega_{fv}}\right)s^2 + \left(a_3 + \frac{a_2}{\omega_{fv}}\right)s^3 + \left(\frac{a_3}{\omega_{fv}}\right)s^4 \qquad (4\text{-}27)$$

The forward path transfer function in the position loop is given by

$$G_f(s) = \frac{K_o}{s}\left[\frac{sZ(s)}{R_1(s)}\right] \qquad (4\text{-}28)$$

The velocity constant, K_v, of this Type 1 system is, therefore

$$K_v = \lim_{s\to 0} sG_f = \lim_{s\to 0} K_o\left[\frac{sZ(s)}{R_1(s)}\right]$$

or

$$K_v = \frac{120000a_1K_o}{1 + 240a_1} \qquad (4\text{-}29)$$

Since K_o was known to be 1.5, the test system velocity error constant reduced to

$$K_v = \frac{180000K_o}{BR + K_f\left(240 + K_b\right)} \qquad (4\text{-}30)$$

At this point the system should have been driven with a ramp, or constant velocity, command to permit a true measurement of steady-state error, e_{ss}. Because the slide travel was limited to .020 inch, the test command signal would have had to be a sawtooth wave with a frequency which was

small compared to the system bandwidth. This waveform was not available on the function generator, however, so the test was approximated with a sinusoid. The system bandwidth had been determined experimentally earlier as roughly 179 Hz. At the 10 Hz excitation rate represented by the position error signal shown in Figure 4-10, the system should have been operating at nearly steady-state conditions throughout the sinusoid. Of course, since the velocity was varying throughout the cycle, the following error varied nearly proportionately. The following error was seen to peak at roughly .4 volt (400 microinches) at the point where velocity peaked at

$$4 \text{ volt} \times 20\pi \text{ rad/sec} = 251.3 \text{ volt/sec}$$

Thus,

$$K_v = \frac{\left(\frac{dr_2}{dt}\right)}{e_{ss}} = \frac{251.3 \frac{v}{sec}}{.4 \text{ v}} \tag{4-31}$$

$$= 628.3 \text{ sec}^{-1}$$

This experimentally derived value of the velocity error constant was substituted into Equation (4-30) along with the other previously detailed system parameters to obtain the viscous friction coefficient, B.

$$B = \frac{K_f}{R}\left[\frac{120000K_o}{K_v} - 240 - K_f\right] \tag{4-32}$$

$$B = 51.2 \text{ lbf}-\text{sec/ft}$$

This value of viscous friction is seen to exceed the assumed value by more than a factor of 60 which invalidates the initial assumption regarding friction in the

system plant. Use of this derived value of B in Equation (4-11) produces the plant transfer function

$$G_p(s) = \frac{24781.9}{s^2 + 4110.1s + 1151836.3} \tag{4-33}$$

or

$$G_p(s) = \frac{24781.9 \quad \frac{ft}{v-sec}}{(s + 302.5)(s + 3807.6)} \tag{4-34}$$

Substitution of B into Equation (4-26) produces the closed velocity loop transfer function

$$\frac{sZ}{R_1} = \frac{2973830293(s + 100000)}{s^3 + 104110.1s^2 + 412159000.8s + 7.0995242\times10^{11}} \tag{4-35}$$

In factored form this appears as

$$\frac{sZ}{R_1} = \frac{2973830293(s + 100000)}{(s + 100061.9)\left(s^2 + 4048.1s + 7095129.5\right)} \tag{4-36}$$

which over the frequency range of interest can reasonably be reduced to

$$\frac{sZ}{R_1} = \frac{2973830293}{s^2 + 4048.1s + 7095129.5} \tag{4-37}$$

or

$$\frac{sZ}{R_1} = \frac{419.14}{1 + 2(.75988)\left(\frac{s}{2663.668}\right) + \left(\frac{s}{2663.668}\right)^2} \tag{4-38}$$

This relation was used in subsequent control system design.

With the model of the plant experimentally established--at least to a first approximation--the design of the permanent control circuitry could begin.

Before describing this procedure the system design goals should first be reviewed. The finished machined part was desired to possess a surface finish of 5 microinches or less and a surface contour error not to exceed 8 microinches. Recalling also that the worst case command compares to a 10 Hz, 8 mil pk-to-pk sinusoid, the maximum Z slide velocity anticipated was 0.25 inch/sec. If this maximum velocity were seen as a ramp input to the position loop, a velocity error constant, K_v, in excess of 30000 sec^{-1} would be required to satisfy the contour error requirement. It was felt that the large increase in position loop gain indicated by this requirement would simultaneously improve the stiffness of the system. The measured 10 microinches of noise superimposed on the position error signal directly affects the surface finish. This noise obviously had to be reduced to satisfy the finish requirement.

These part feature requirements themselves, of course, do not translate directly into recognizable control system parameters, particularly for the inner loop. It was noted during the description of the initial test circuitry that the system stiffness was much too low. This observation might indicate that the inner loop gain needed to be increased, but it is quickly seen that increasing the forward gain of the inner loop has very little effect on the closed inner loop gain. The test system had shown reasonably fast response (estimated $\zeta = .5$, $\omega_n = 145$ Hz). The inner loop was therefore accepted as it was except for the differentiating network.

Figure 4-11 shows the Bode diagram of the uncompensated forward path of the position loop described by Equation (4-38). The free s factor, indicated by the 90 degree phase lag and -20 dB/dec magnitude slope, represents the integration of velocity into position. The two underdamped poles are

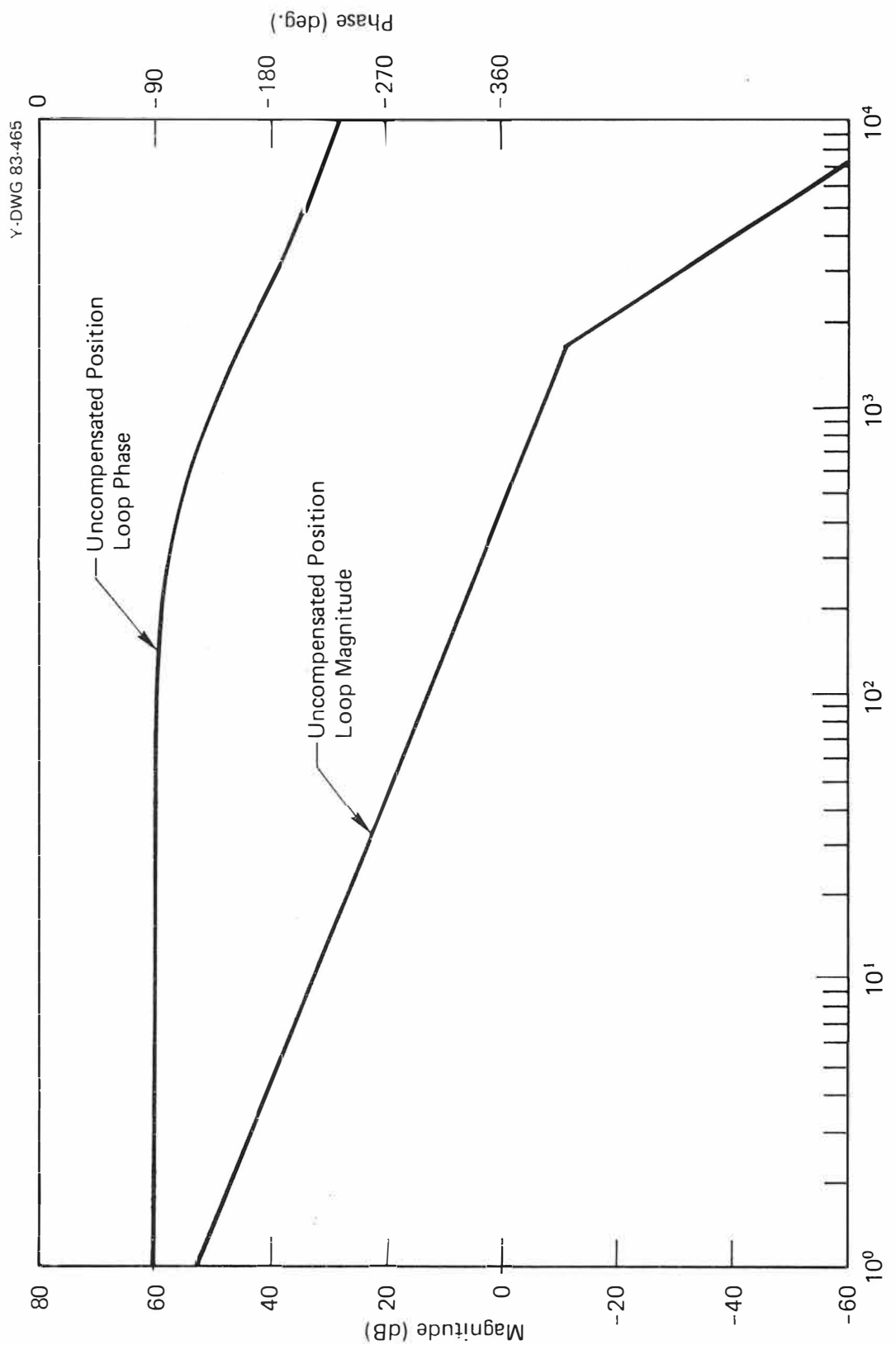

Figure 4-11. Bode diagram of uncompensated position loop.

shown at $\omega = 2664$ rad/sec, and the root locus gain at $\omega = 1$ rad/sec is 419 which is also the magnitude of the velocity error constant, K_v. Thus, the forward path required a gain increase of approximately 75 (37.5 dB) to achieve a $K_v = 30000$ sec^{-1}. Such a gain increase without additional compensation would obviously result in an unstable system. The magnitude plot shows that gain crossover occurs at about 430 rad/sec at a slope of -20 dB/dec, while the phase crossover frequency is 2664 rad/sec. To achieve the desired system bandwidth of at least 100 Hz (628 rad/sec), the open loop crossover frequency also needed to be increased. The resonant poles obviously played a constraining role on this design goal.

A general purpose control circuit board was fabricated to allow a variety of forms of compensation in both the velocity and position loops. Figure 4-12 shows the schematic diagram of this board. It is obvious that the primary consideration in building this board was to provide a versatile means of testing compensation rather than to conserve components. Two feedback input lines were also provided. The first, shown at edge connector pins 7 and 8, provided for the capacitance gage signal, while the second was furnished to allow for inputs from alternative sources such as vibration or current sensors.

Compensation design began with the primary intent of increasing the velocity error constant to a value sufficient to satisfy the following error goal. The first compensator attempted was a series lag compensator in the outer loop. The block diagram for the system is shown in Figure 4-13 and is seen to utilize the closed velocity loop transfer function as derived in Equations (4-37) and (4-38). The lag compensator was designed with corner frequencies of 2.9 and 290 rad/sec. The Bode diagram of the compensator is shown in the dotted curves in Figure 4-14. The total open loop frequency response with the addi-

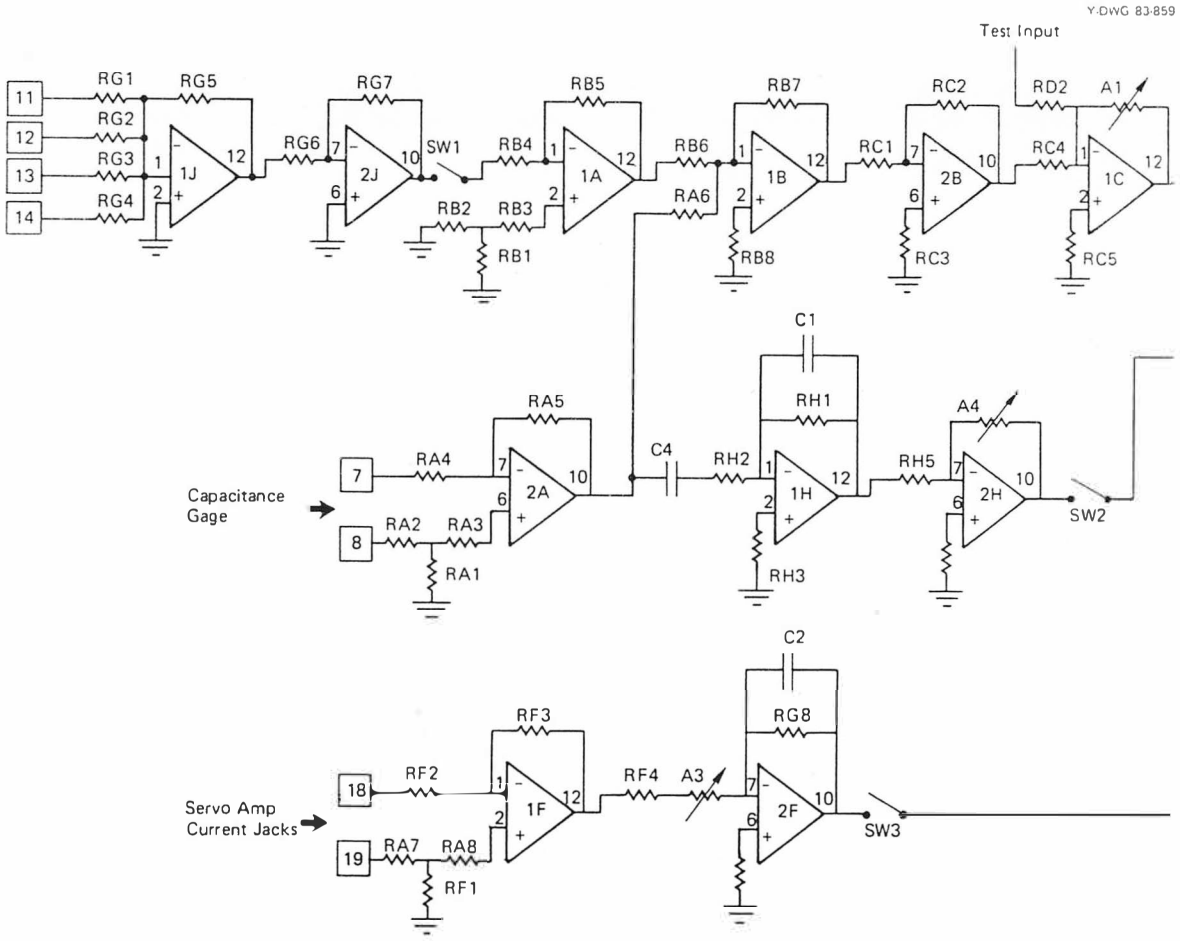

Figure 4-12. Schematic diagram of controls circuitry.

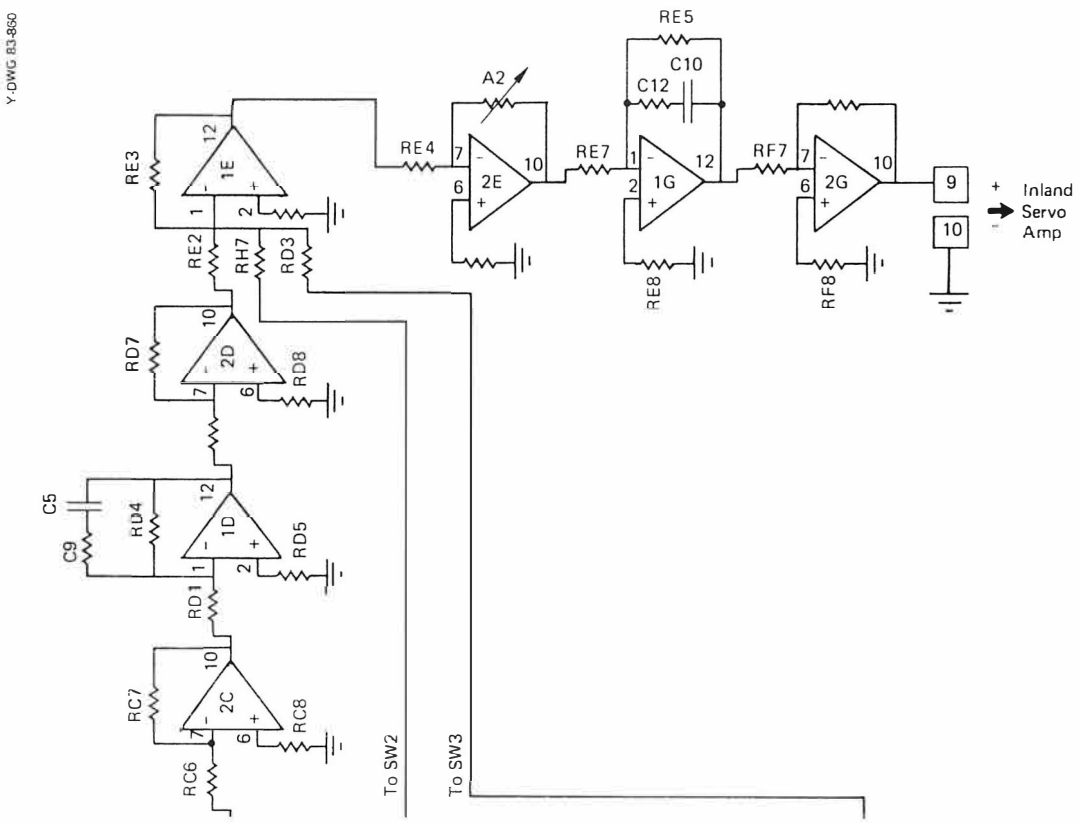

Figure 4-12 (continued).

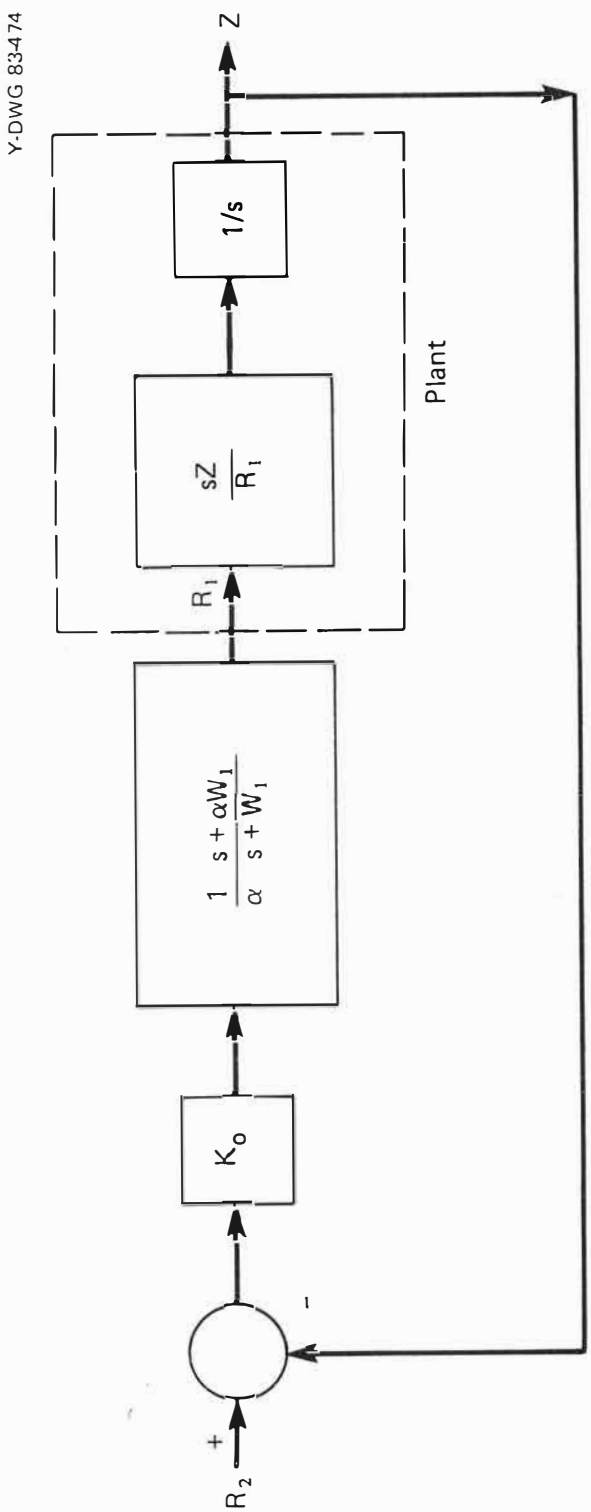

Figure 4-13. Block diagram of lag-compensated position loop.

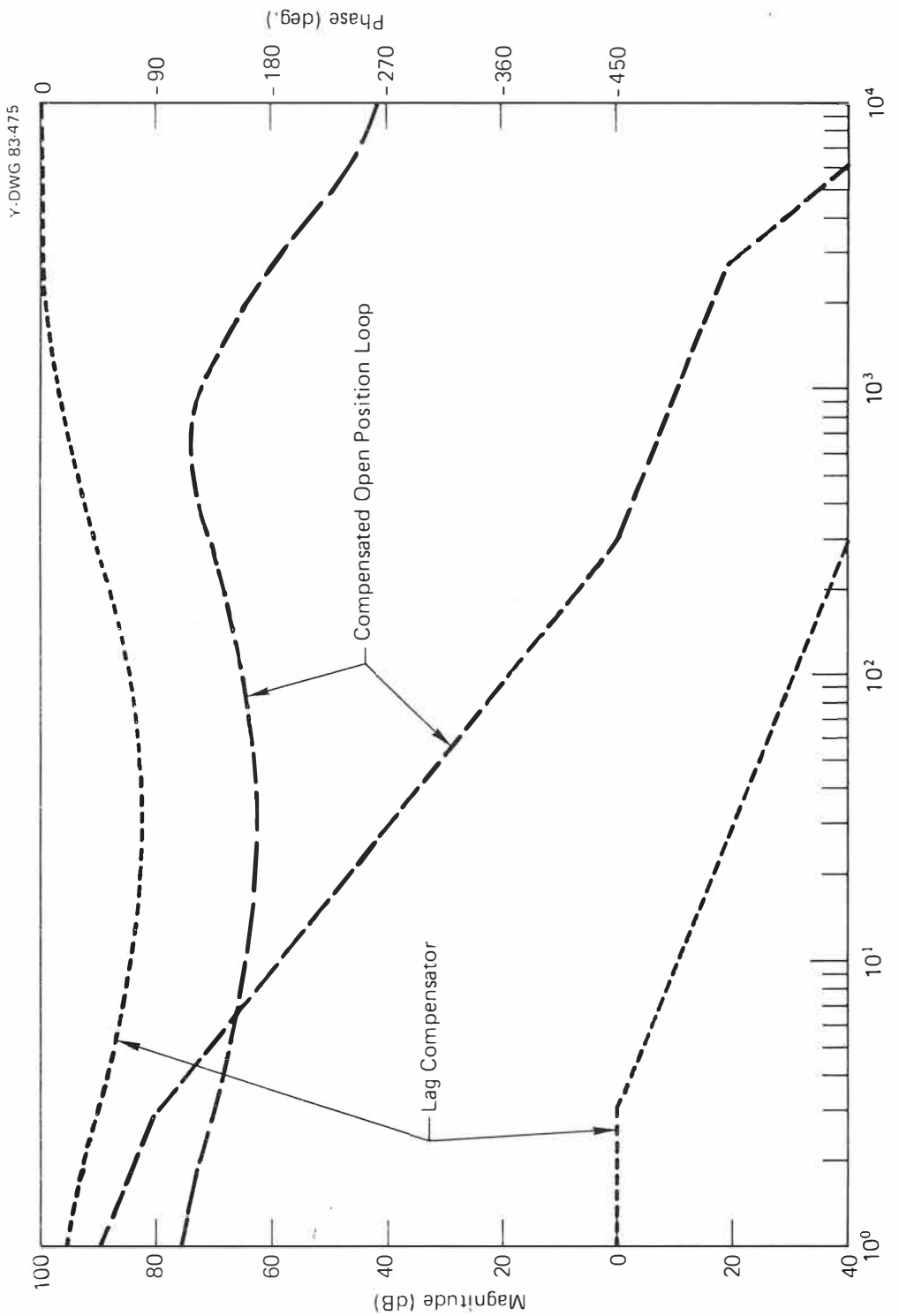

Figure 4-14. Bode diagram of lag-compensated position loop.

tion of proportional gain of 38 dB is shown as the dashed line in Figure 4-14. The compensated open loop system is seen to have approximately 45 degrees of phase margin and 20 dB gain margin.

From the above considerations it appeared that the lag compensator would provide a stable closed position loop with adequate system gain to satisfy the following error goal. However, the network was further tested via digital simulation with the Continuous Systems Modeling Program (CSMP) software (26). The program and the print-plotted output are shown in Appendices C-1 and C-2. Simulated response of the system to both step and ramp inputs indicated the system would be stable and would perform in an acceptable fashion. The compensation was therefore built into the circuit board for testing.

As soon as power was applied to the control system, the system oscillated quite audibly. The gain was reduced until finally, with an outer loop gain of only 20, the system stopped oscillating. At this point it was not known what caused the oscillation -- only that the slide and drive system must contain some dynamic elements not previously recognized.

The next compensation scheme eliminated the velocity feedback loop and used a lead-lag compensator to attempt to widen the system bandwidth while raising the loop gain. The block diagram of this system is shown in Figure 4-15. The plant transfer function is given by

$$G_p = \frac{sZ}{R_1} = \frac{2582}{\left(1 + \frac{s}{302.5}\right)\left(1 + \frac{s}{3808}\right)} \qquad (4\text{-}39)$$

and its Bode diagram appears in Figure 4-16. It is seen that elimination of velocity feedback changes the plant poles from complex to real. The compensator was designed to take advantage of this characteristic. A lead network

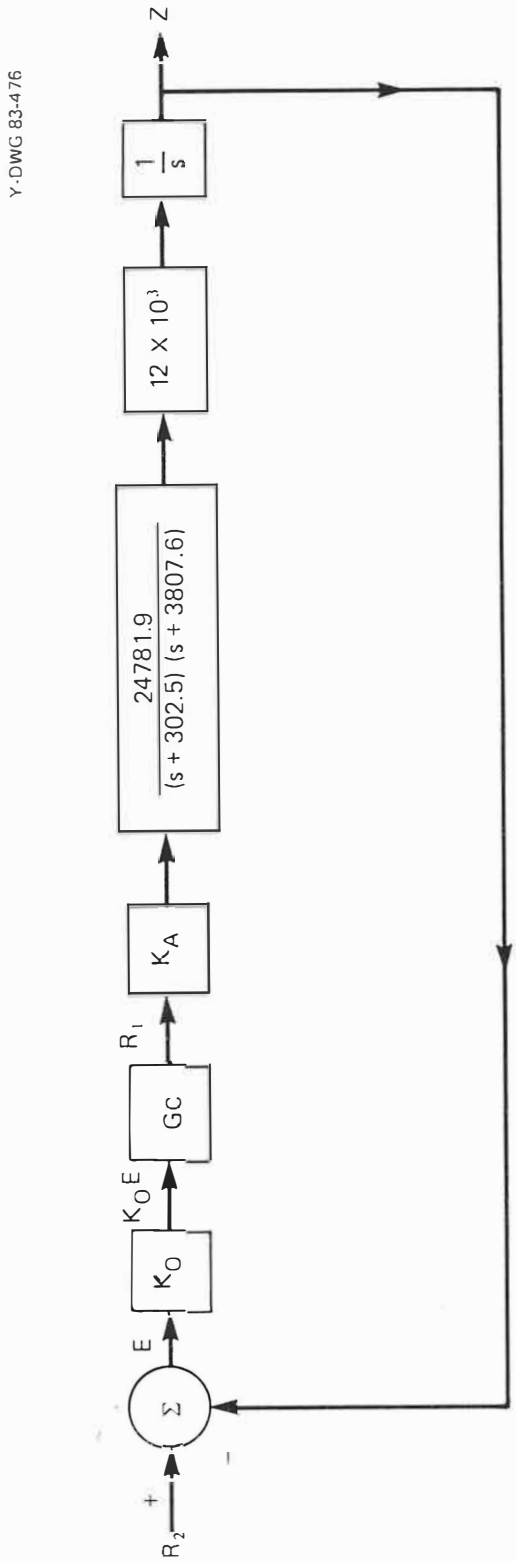

Figure 4-15. Block diagram of lead-lag compensated system.

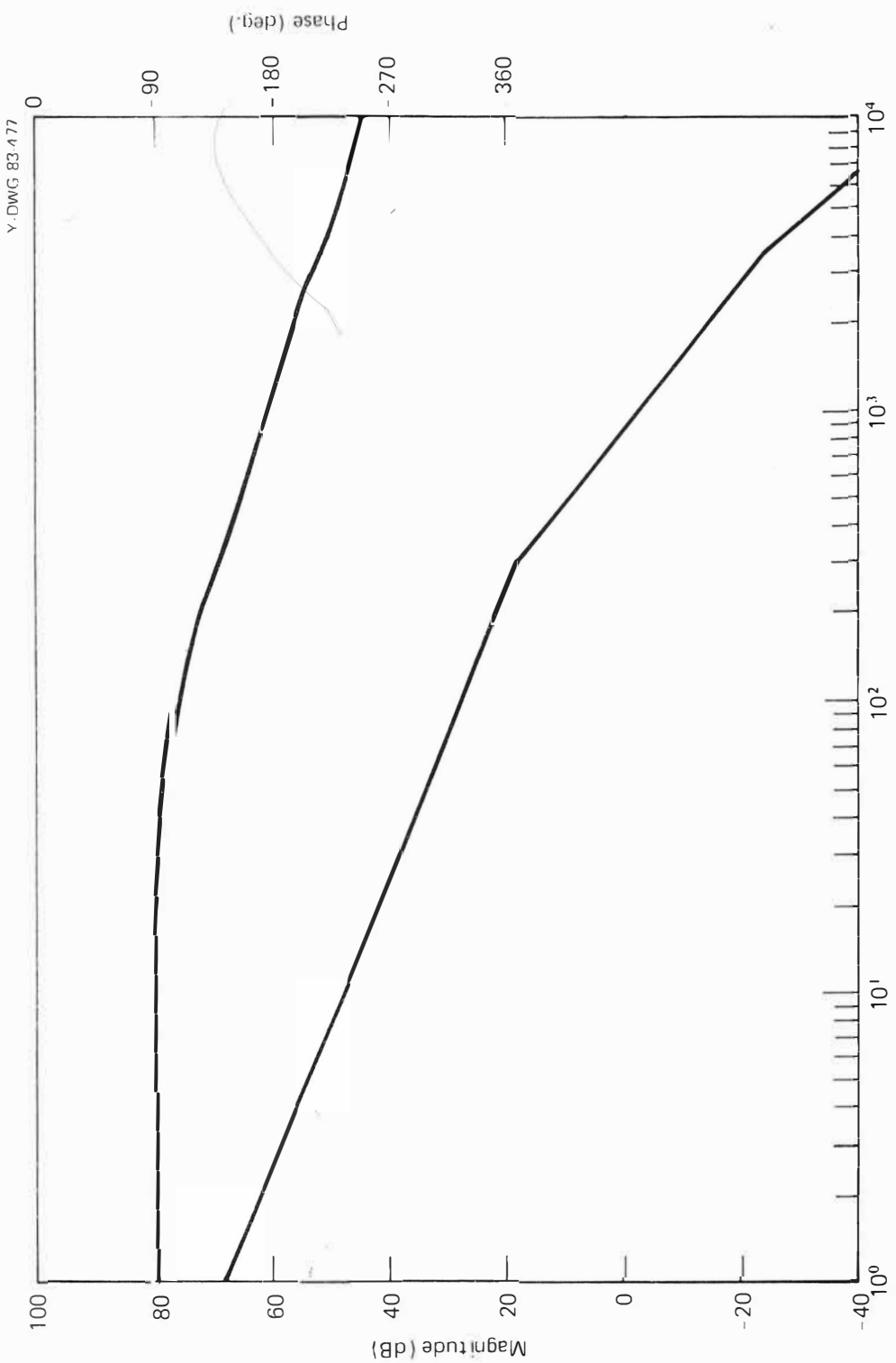

Figure 4-16. Bode diagram of uncompensated plant.

was placed to produce a -20 dB/dec slope in the frequency range where gain crossover was to occur after the addition of proportional gain. The lag network of course was used to increase the steady-state gain. This compensator is represented by

$$G_c = \frac{\left(1 + \frac{s}{35}\right)\left(1 + \frac{s}{100}\right)}{\left(1 + s\right)\left(1 + \frac{s}{3500}\right)} \tag{4-40}$$

and its Bode diagram is shown in the dotted curves in Figure 4-17. The compensated open loop network is also plotted in Figure 4-17 in the dashed curves. A proportional gain factor of 7.75 was used which yielded a velocity error constant of 20000 sec^{-1}. This gain factor was not sufficient to satisfy the following error goal and hence represented a compromise of design goals. Gain crossover of the compensated system occurred at 1500 rad/sec with approximately 50 degrees of phase margin. Gain margin of about 10 dB also resulted.

This test system was also simulated with CSMP using step and ramp inputs. Details of the simulation are in Appendices C-3 and C-4, but the results confirmed that the system response would be consistent with the above parameters.

Power was again applied to the system. It was stable with the gain setting of 7.75 noted above. Response to a step input compared well with the CSMP simulation. The following error (under 10 Hz, 8 mil pk-to-pk sinusoidal excitation) was approximately 12 microinches (masked with about 10 microinches of noise). However, the system stiffness was very low--certainly insufficient to withstand the forces generated in metal cutting.

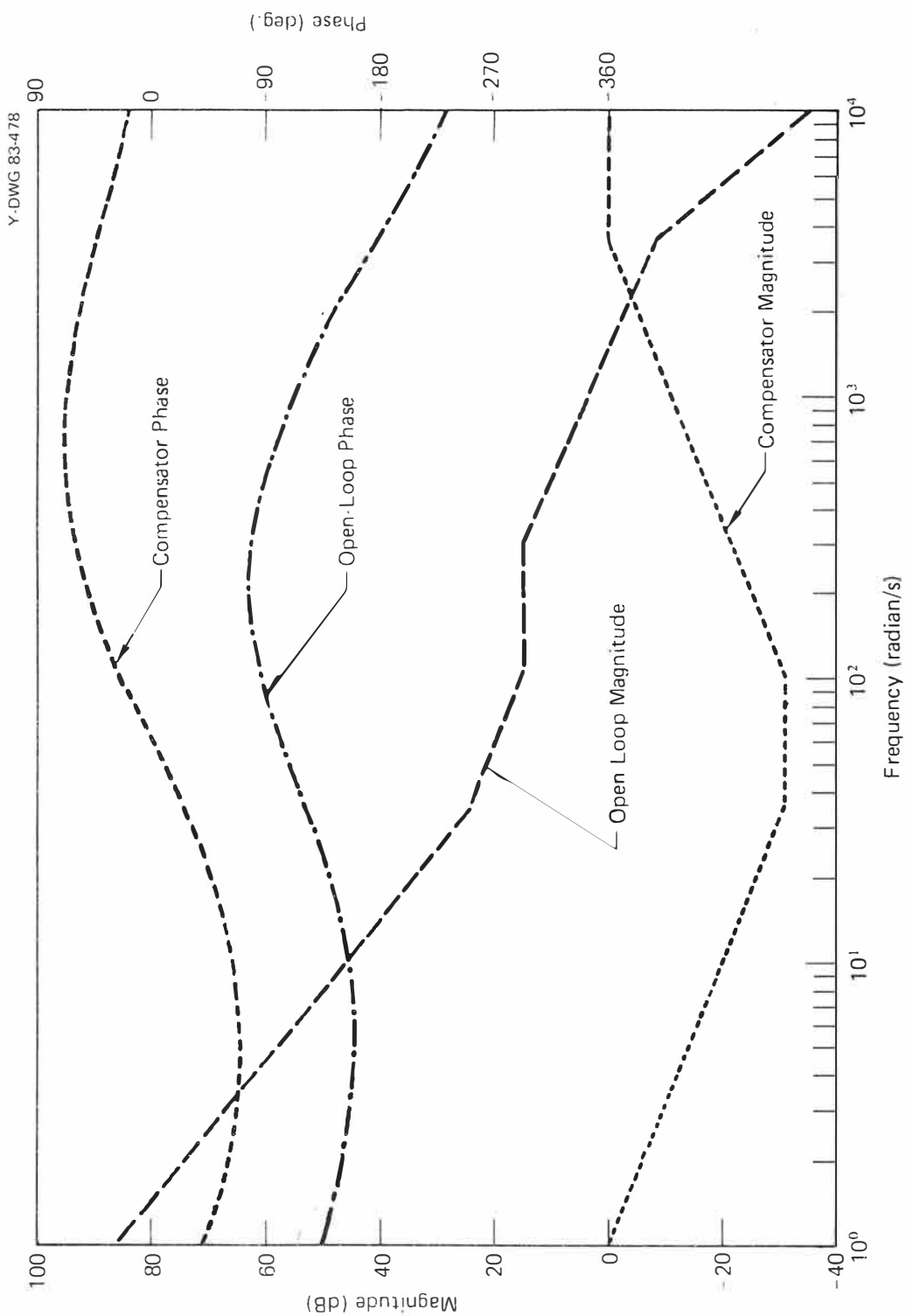

Figure 4-17. Bode diagram of lead-lag compensated system.

The next compensation scheme considered involved the use of acceleration rather than velocity feedback. The block diagram of this system is shown in Figure 4-18. The closed inner loop transfer function that results is

$$\frac{sZ}{R_1} = \frac{2973828000}{s^2 + \left(4110.1 + 2973828000K_{acc}\right)s + 1151836.3} \qquad (4\text{-}41)$$

It is seen that the roots of the characteristic equation occur at -302.5 and -3808 with $K_{acc} = 0$. As K_{acc} is increased, the first of these roots becomes more positive while the second becomes more negative. Since the intended use of the network was to move both roots in the negative direction, the network was judged not to provide the desired change in pole location.

A similar attempt was made with the use of current feedback. Although the characteristic equation of this network is slightly different from that of acceleration feedback, the effect of increasing the feedback gain is similar.

Parenthetically, it might be added that even if one of these networks had appeared attractive theoretically, realization of the feedback scheme would have been unlikely. Acceleration feedback by double position differentiation would undoubtedly have produced too much noise. No servo accelerometers were available for direct measurement and feedback. Observation of the motor current on an oscilloscope during earlier testing revealed a very low level signal which exhibited sufficient noise to have required some type of smoothing. Because of these conditions, further investigation as to the desirability of combining one of these networks with other compensations schemes was not made.

Because the most satisfactory control network yet tried employed velocity feedback with an outer loop lag compensator, the same network was

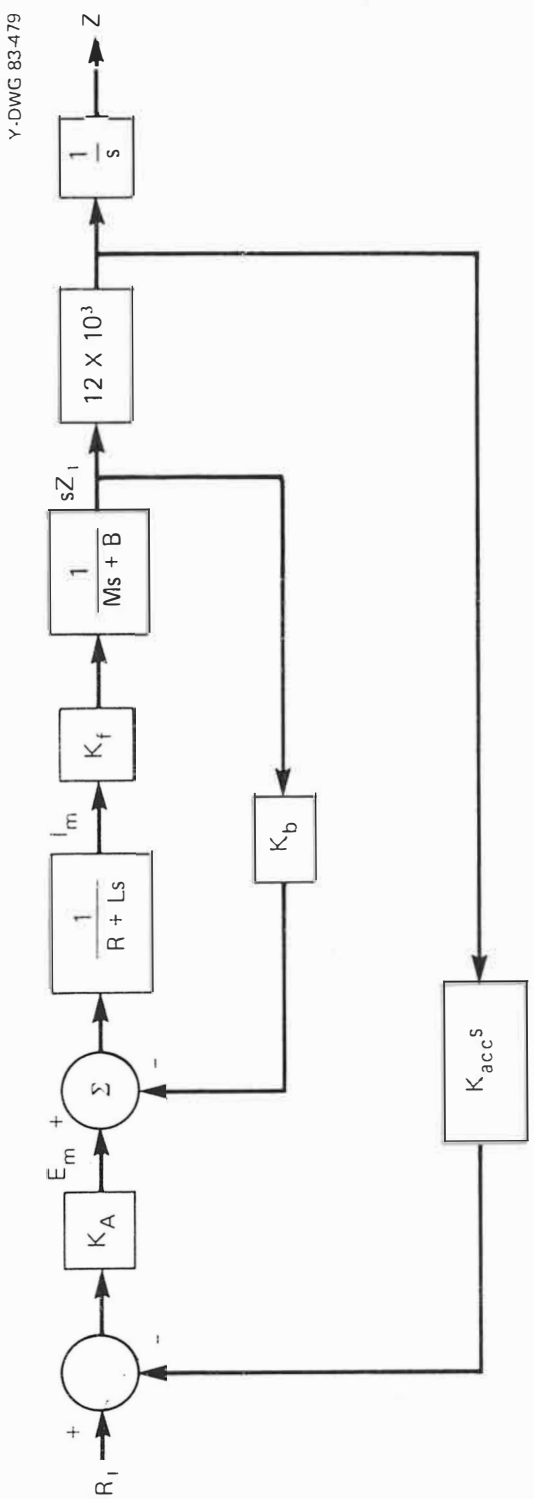

Figure 4-18. Block diagram of acceleration of feedback network.

attempted with an inner loop lag compensator. The block diagram of this system is shown in Figure 4-19a. The purpose of this addition was to provide additional system stiffness and hopefully to permit the use of greater outer loop gain. The plant transfer function was given by Equation (4-39). The block diagram is shown manipulated slightly in Figure 4-19b to produce a unity negative velocity feedback to facilitate analysis. The velocity feedback network so employed utilized a lower frequency lowpass filter than that used in initial tests. Computations indicated that the break frequency could be reduced by an order of magnitude to 10000 rad/sec without seriously affecting the slide dynamics. The intent, of course, was to reduce the effect of noise on system performance. Simultaneously, the gain in the feedback loop was reduced from .002 to .0005. This action permitted a corresponding increase in the forward loop gain without changing the system poles. The result of this action was larger forward gain in the position loop.

The dashed curve in Figure 4-20 is a Bode plot of the velocity loop as manipulated in Figure 4-19b. Also shown in Figure 4-20 is the compensated open velocity loop. The lag compensator was placed with its pole at 25 rad/sec and its zero to cancel the plant pole at 302.5 rad/sec. The magnitude curve is shown as the dotted curve in Figure 4-20. The compensated loop is shown in the solid curve in the figure. A gain increase of a factor of 12 is indicated.

The closed velocity loop transfer function resulting from this compensation is given by

$$\frac{Z}{R_1} = \frac{1.1797468 \times 10^{10}\left(s + 10^4\right)}{s^4 + 13832.6s^3 + 38424190s^2 + 5.9969239 \times 10^{10}s} \qquad (4\text{-}42)$$

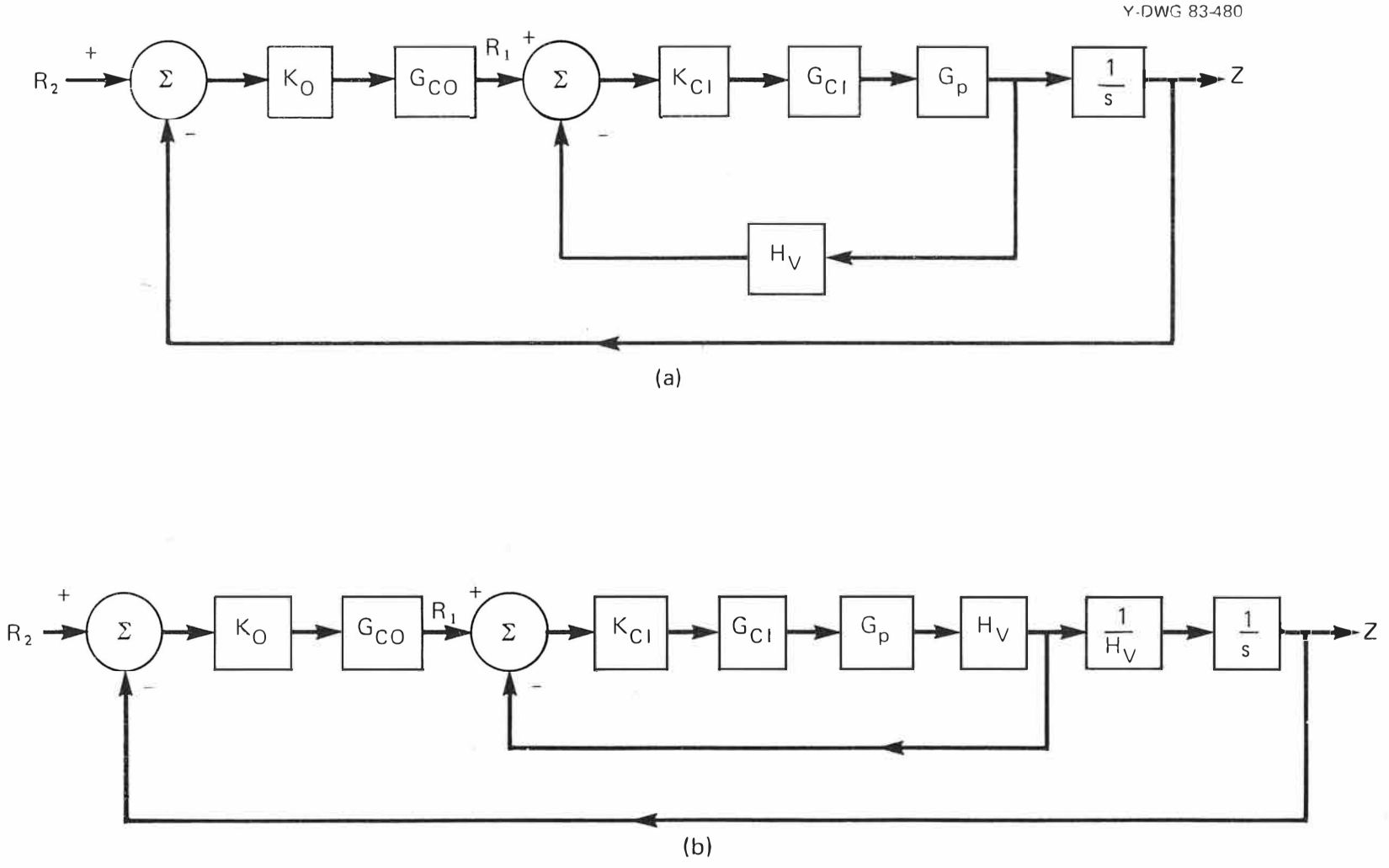

Figure 4-19. Block diagram of system using velocity feedback.

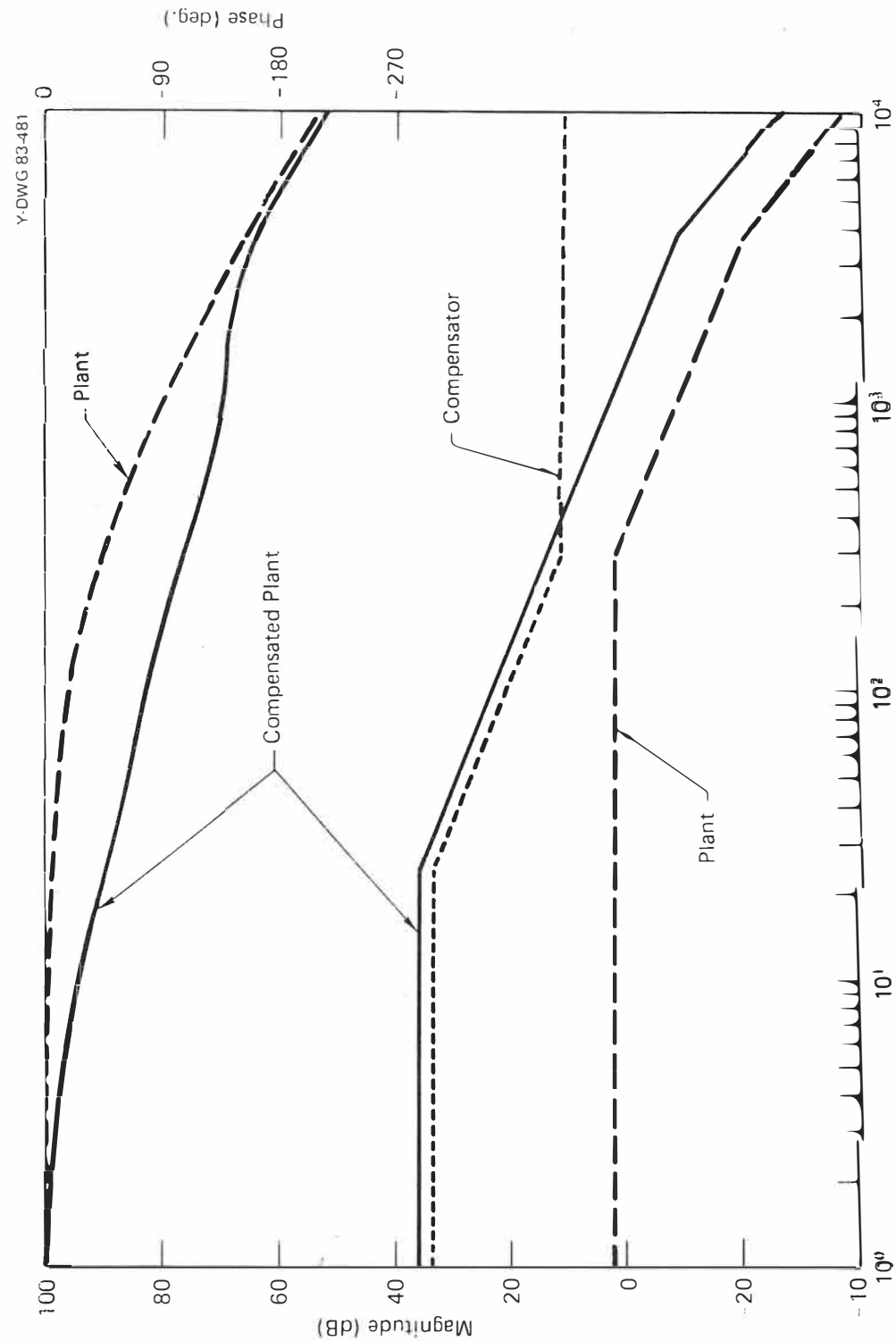

Figure 4-20. Bode diagram of open velocity loop.

When coupled with the velocity-to-position integral and the 1/Hv factor shown in the block diagram, the uncompensated open loop transfer function results.

$$\frac{Z}{R_1} = \frac{1967.2532\left(1 + \frac{s}{10000}\right)}{s\left(1 + \frac{s}{10785.6}\right)\left[1 + 2(.6461)\left(\frac{s}{2358}\right) + \left(\frac{s}{2358}\right)^2\right]} \tag{4-43}$$

The Bode diagram representing Equation (4-43) is shown as the dashed line in Figure 4-21. The outer loop compensator was chosen to be a relatively low frequency, wide span lag compensator to permit a wide range of gain values to be used. An outer loop gain value greater than 15 was needed to attain the desired value of at least 30000 sec^{-1} for the velocity error constant.

As seen in the magnitude plot (dotted curve in Figure 4-21), the compensator was designed with a pole at 1 rad/sec and a zero at 100 rad/sec (Actually the compensator was constructed in two stages with cancelling pole and zero at 10 rad/sec.). Figure 4-22 illustrates the closed position loop frequency response at outer loop gain values ranging from 5 through 30. The system is seen to yield greater magnitude peaking at the lower gain value. It was decided to build and test the compensator.

The compensator was built with a gain value of 30 and power was applied as before. Immediately the system oscillated audibly as had been experienced previously. The gain was reduced as previously until, at a value of approximately 10, the oscillation ceased. Figure 4-22 indicates that with K_o = 10 magnitude peaking of roughly 2.2 dB should occur at a frequency of about 16 Hz. A crude measurement of the magnitude ratio was performed on the system by exciting the system with a varying frequency wave and measuring the output with an oscilloscope. The results of these measurements are plotted

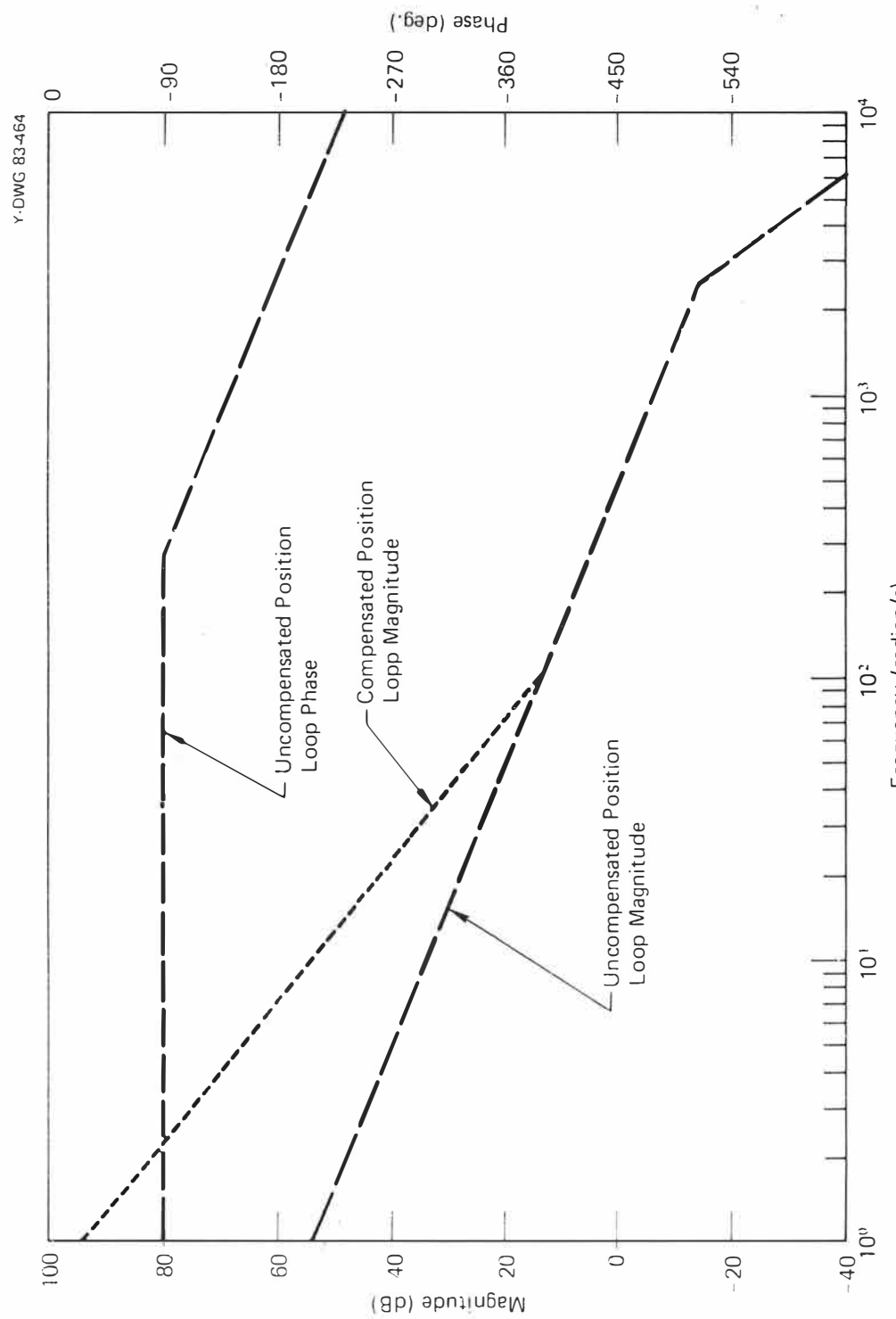

Figure 4-21. Bode diagram of open position loop.

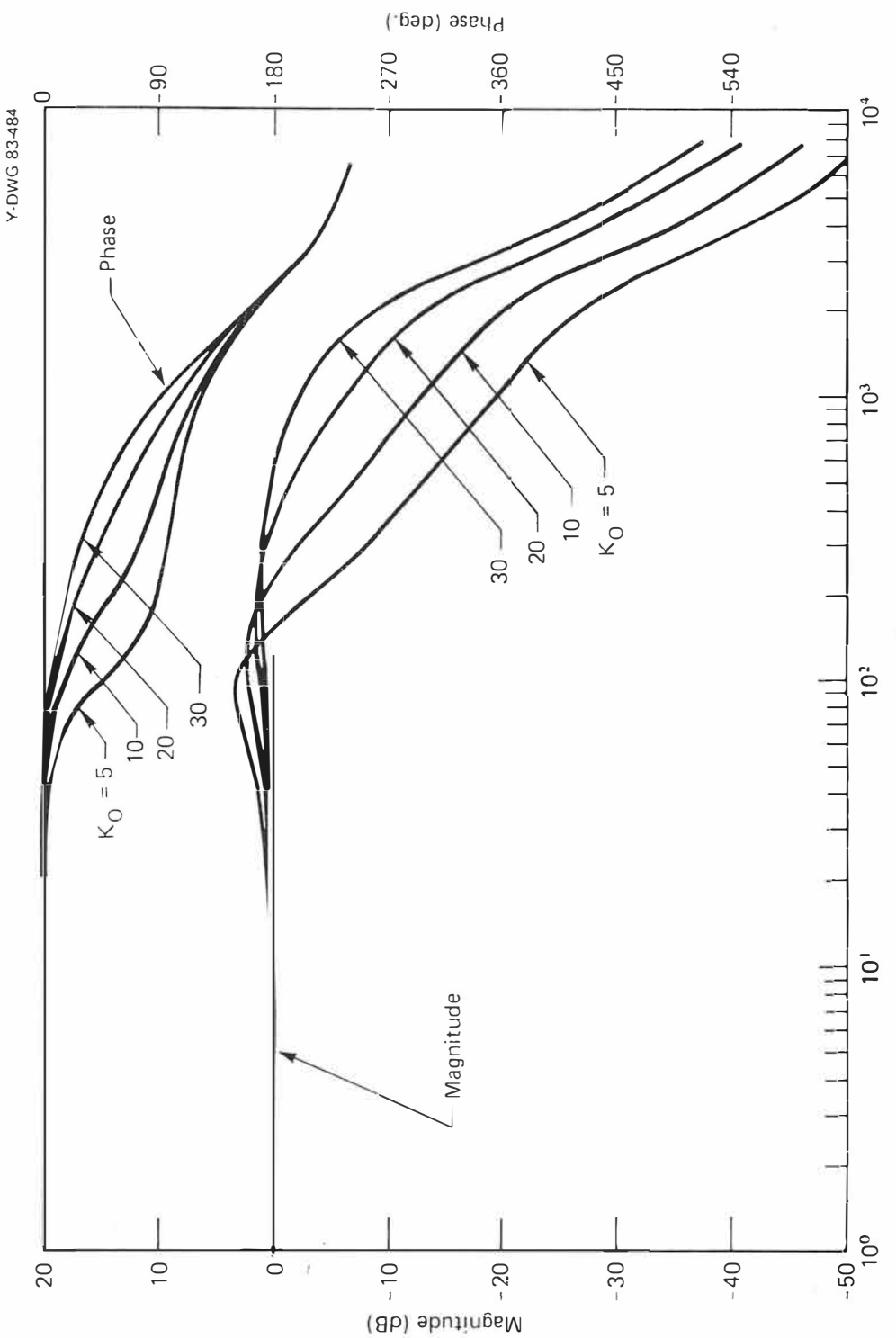

Figure 4-22. Bode diagram of closed position loop.

in Figure 4-22 and show peaking of only about 1.5 dB occurring at nearly 30 Hz.

The occurence of the unanticipated system oscillation with several different compensation schemes was particularly disturbing because it was unexplained. An attempt was made to reduce the system noise noted earlier by improving the differentiating network which provided the velocity feedback signal. A technical note from National Semiconductor (27) suggests that differentiating circuits like the one used here need an additional low pass filter designed around the gain characteristic of the operational amplifiers employed. Figure 4-23 shows the gain-frequency characteristic (28) for the uA747C dual op-amps used in the control circuitry. Superimposed on this curve is the magnitude plot for the differentiating network used in the test. It is seen that the gain of the circuit exceeds the op-amp characteristic at frequencies above 10 kHz. The National note recommends that a second filter be placed so that the circuit gain attenuates at a rate sufficient to stay within the op amp characteristic. The purpose of this addition is to prevent potential higher frequency oscillations under certain excitation. A second low pass filter is shown in the figure which satisfies this condition. Both filters were placed at roughly 1050 Hz.

The new differentiating network was installed in the control system using the previous compensation system, and power was applied. No noticeable change was observed in the system performance. The oscillation occurred again at approximately the same gain values as previously. It was concluded that the differentiating network was not the source of the oscillation.

Although the system performance was a disappointment from the standpoint of achievement of desired velocity error constant, one highly desirable

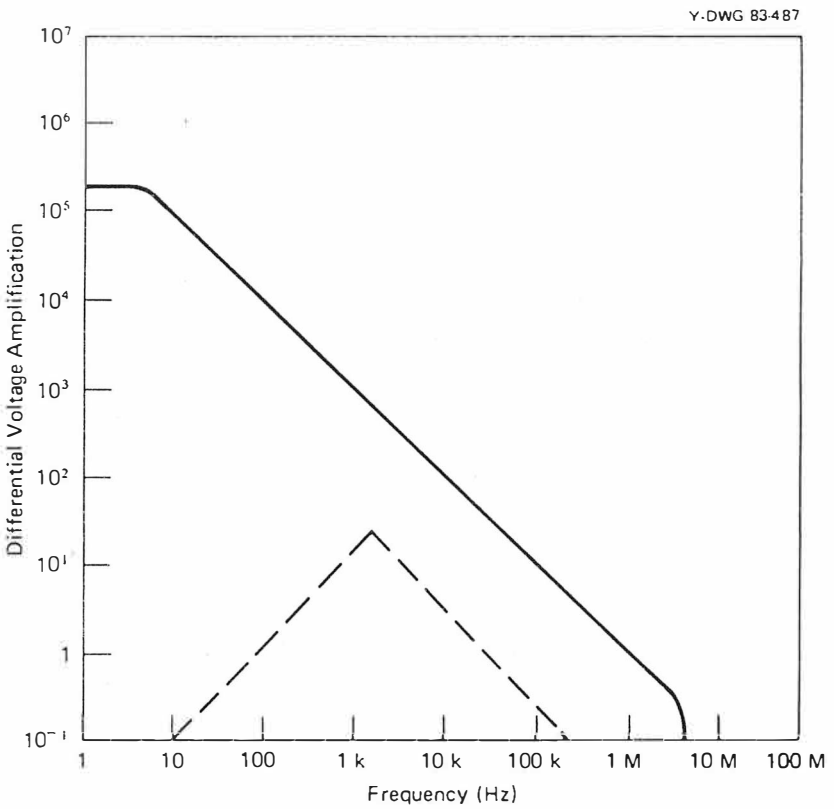

Figure 4-23. Operational amplifier gain-frequency characteristic.

characteristic was observed. The stiffness of the system was much superior to that observed with any control scheme attempted to date. In fact, the stiffness may have been too good for the health of the equipment because additional testing resulted in a structural failure of the linear motor in the joint between the armature and its coupling frame with the slide. Fortunately, a spare linear motor, Infomag Model 15, with similar characteristics had been obtained as a backup. All further work was performed with this motor. Its characteristics were:

Force constant, K_f = 2.9 lbf/amp

Back emf, K_b = 4.002 lbf-sec/ft

Driven Mass, M = 6.25 lbm = .2 slug

Coil DC resistance, R = 1.4 ohm

Coil inductive time constant, = L/R = .00026 sec.

A Hewlett-Packard model 5420 Digital Signal Analyzer (DSA) was purchased which greatly facilitated the experimental characterization of the control systems. Together with a digital plotter and a desktop computer (HP models 9872 and 9825, respectively) the new instrumentation permitted rapid measurement, analysis and documentation of dynamic phenomena such as vibrational parameters as well as control systems. A photograph of this equipment is shown in Figure 4-24. Before proceeding with the narrative of controls development a description of this equipment will be given.

The digital signal analyzer is essentially a minicomputer based, two channel spectrum analyzer with additional computational capability for calculating auto and cross correlations and transfer functions as well as their counterparts in the time domain. A small CRT display exhibits the measurements in a variey of familiar formats such as real and imaginary values versus fre-

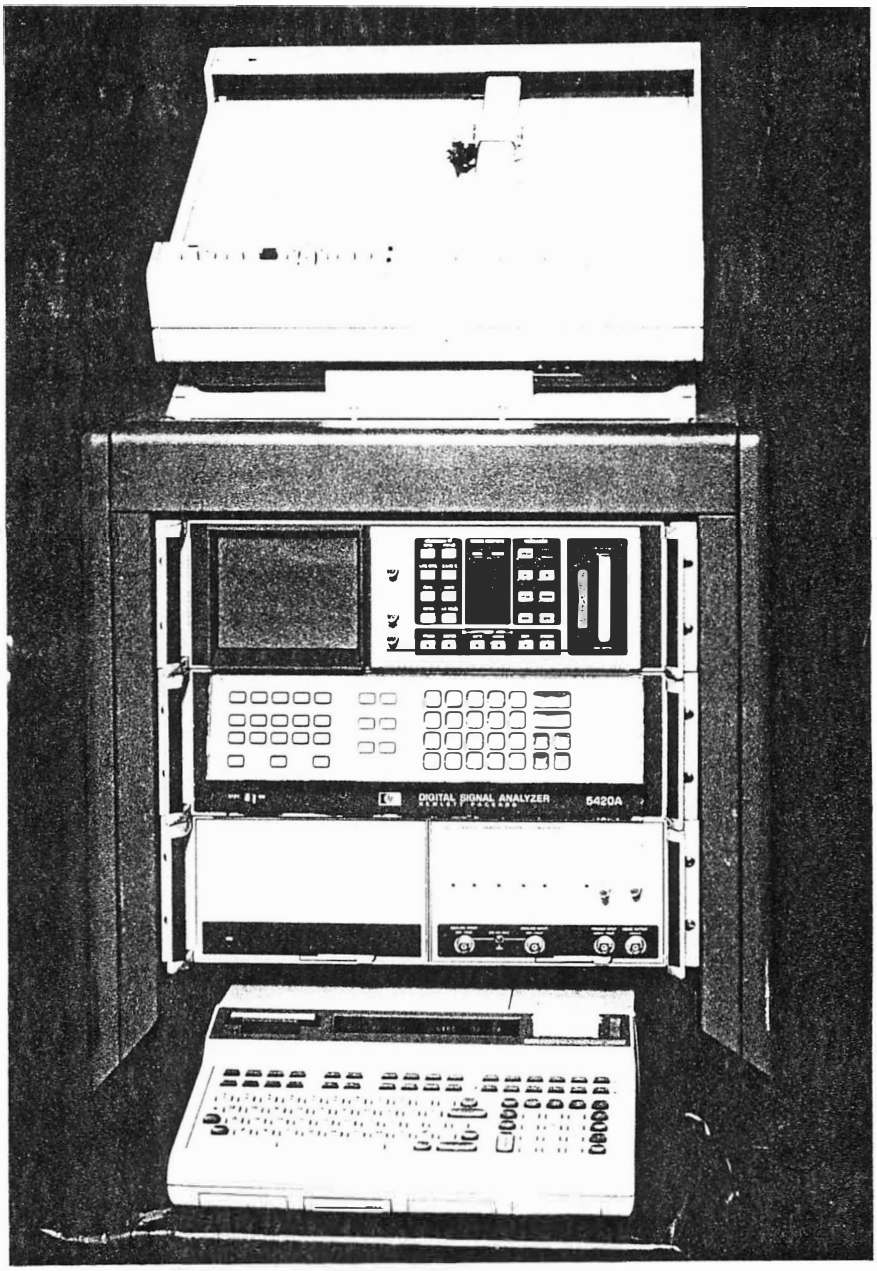

Figure 4-24. Digital signal analyzer, plotter and desktop computer.

quency, Bode, Nyquist and Nichols plots. The analysis range can vary from less than one Hz to 25.6 kHz. The built-in two channel analog-to-digital converters are accompanied by a broadband noise generator. Averaging of measurements can be performed in a number of ways and over a chosen number of samples. Finally, the analyzer is also equipped with a cassette recorder for storage of data and pertinent setup information.

Measurement of transfer functions is performed by exciting the system with the noise generator and by passing both this signal and the system output signal to the input channels of the analyzer. The computed transfer functions are averaged over a pre-selected number of measurements. As the number of measurements increases, the average is smoothed until the resulting model closely approximates the model which would have been derived from measurements using sinusoidal excitation.

The analyzer is also equipped with a General Purpose Interface Bus (IEEE 488-1975) so that it can be controlled by an external computer as well as transmitting data in both directions. This interface bus provides the communication link with the plotter and desktop computer.

After replacing the damaged linear motor it was necessary to re-characterize the system plant. Ideally, with the signal analyzer available the measurement could be made directly by exciting the power amplifier with the noise signal and measuring the output at the capacitance gage. No feedback would be employed in this measurement. It was quickly discovered that this approach was not feasible, however, because of the short measurement range of the capacitance gage. Therefore, the transfer function of the closed velocity loop was measured and used in further design.

Testing of the velocity loop was begun with the injection of the noise into the summing junction of the velocity loop and measuring the response at the capacitance gage. Testing was performed over 400, 1600, and 3200 Hz analysis ranges. Figure 4-25 shows the 1600 Hz test. The labels on the scales refer to values at the outer tick marks. The legend at the top indicates that both curves are transfer function measurements stored on record number 1 on the cassette and that each data point plotted represents the average of 80 measurements. Several comments concerning the plots are in order. First, the lowest frequency data point is often erroneous and probably should be ignored. Second, the phase plot shows a positive 360 degree phase shift which actually exists only by the nature of the phase angle computation. Lastly, the data shows considerably more scatter at the higher frequencies due to the very low magnitudes of the data. The plot shows a decrease in amplitude of 80 dB over the 1600 Hz frequency range.

As would be expected, the curves show the presence of a pole at the origin in the velocity loop transfer function. A real pole is also indicated by the 45 degree phase change near 140 Hz. A second real pole is seen as probable between 500 and 1000 Hz, but the curves become too ragged to approximate the transfer function accurately beyond this point.

The velocity loop was analyzed again in a slightly different fashion. Noise was again injected at the summing amplifier, but the response of the loop was measured at the output of the differentiating network in the feedback path. Again the test was performed over several ranges. These responses were then divided by corresponding measured responses of the differentiating networks. The 1600 Hz analysis is shown in Figure 4-26. Because the dynamic ranges in both measurements used to form this ratio were much smaller than

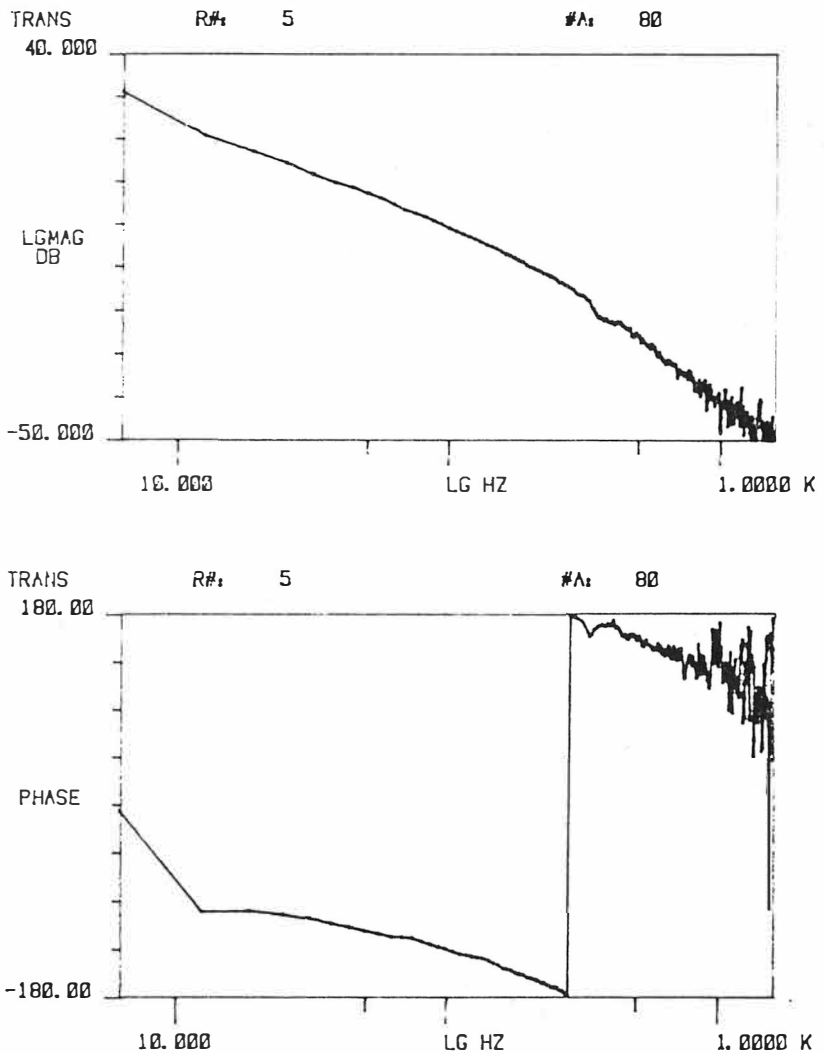

Figure 4-25. Measured frequency response of closed velocity loop (direct measurement).

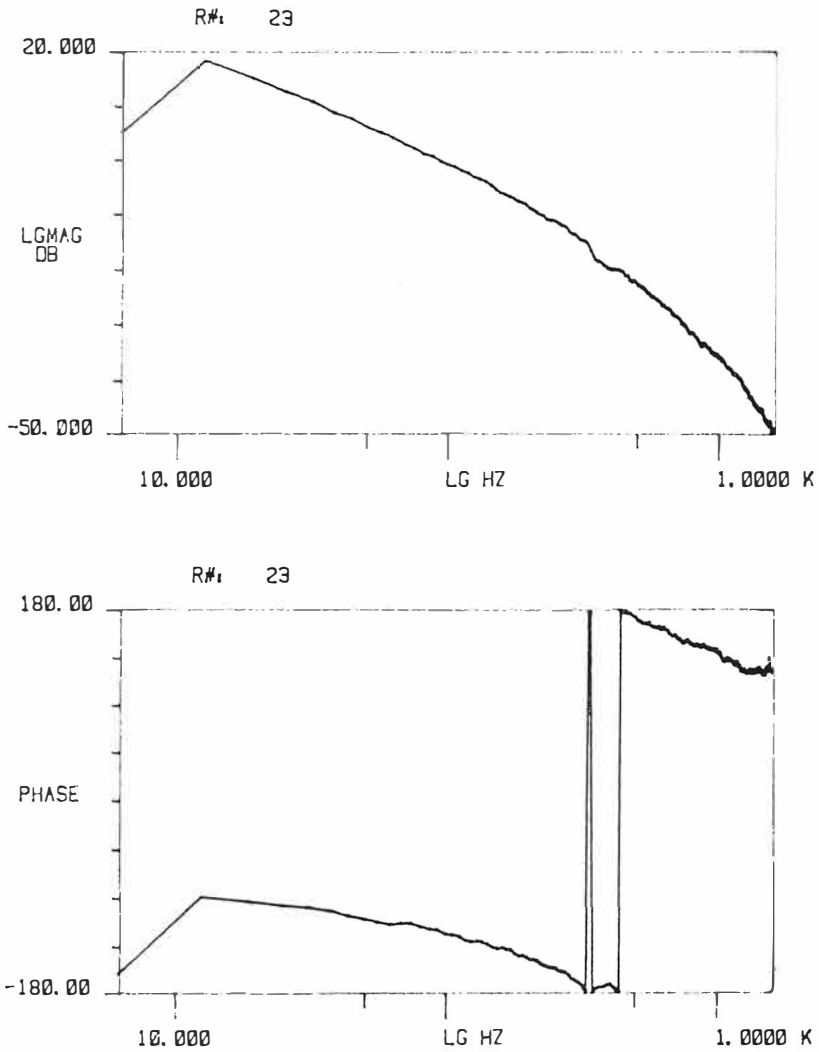

Figure 4-26. Measured frequency response of closed velocity loop (inferred).

seen in the first test, the data in Figure 4-27 are seen to possess much less scatter. Consequently, these derived data were used in subsequent design. Both the magnitude and the phase curves display small "kinks" near 450 HZ which represent small resonances and/or anti-resonances. This second order effect was not considered important in the design of compensation.

The computational capabilities of the signal analyzer were used at this point to synthesize transfer functions which could approximate the measured frequency responses shown in Figures 4-25 and 4-26. Figure 4-27 shows the comparison of the measured data with the synthesized transfer function

$$\frac{Z}{R_1} = \frac{674}{s\left(1 + \frac{s}{1162.4}\right)\left(1 + \frac{s}{7634.1}\right)} \qquad (4\text{-}44)$$

The magnitude component of Equation (4-44) is re-plotted in Figure 4-28. A lag compensator was placed at more than two decades below the system pole at -1162.4 rad/sec. The compensator is given by

$$G_{oc} = \frac{\left(1 + \frac{s}{4.16667}\right)}{\left(1 + \frac{s}{.378788}\right)}$$

The compensated magnitude curve in Figure 4-28 shows magnitude crossover occurs at approximately 60 rad/sec. The slope of this curve at crossover is -20 dB/dec. The plot indicates that a total gain of approximately 16 can be applied before crossover occurs at a steeper slope.

To attenuate the noise a simple pole was also added near 500 Hz (The use of convenient components resulted in a corner frequency of 3030.3

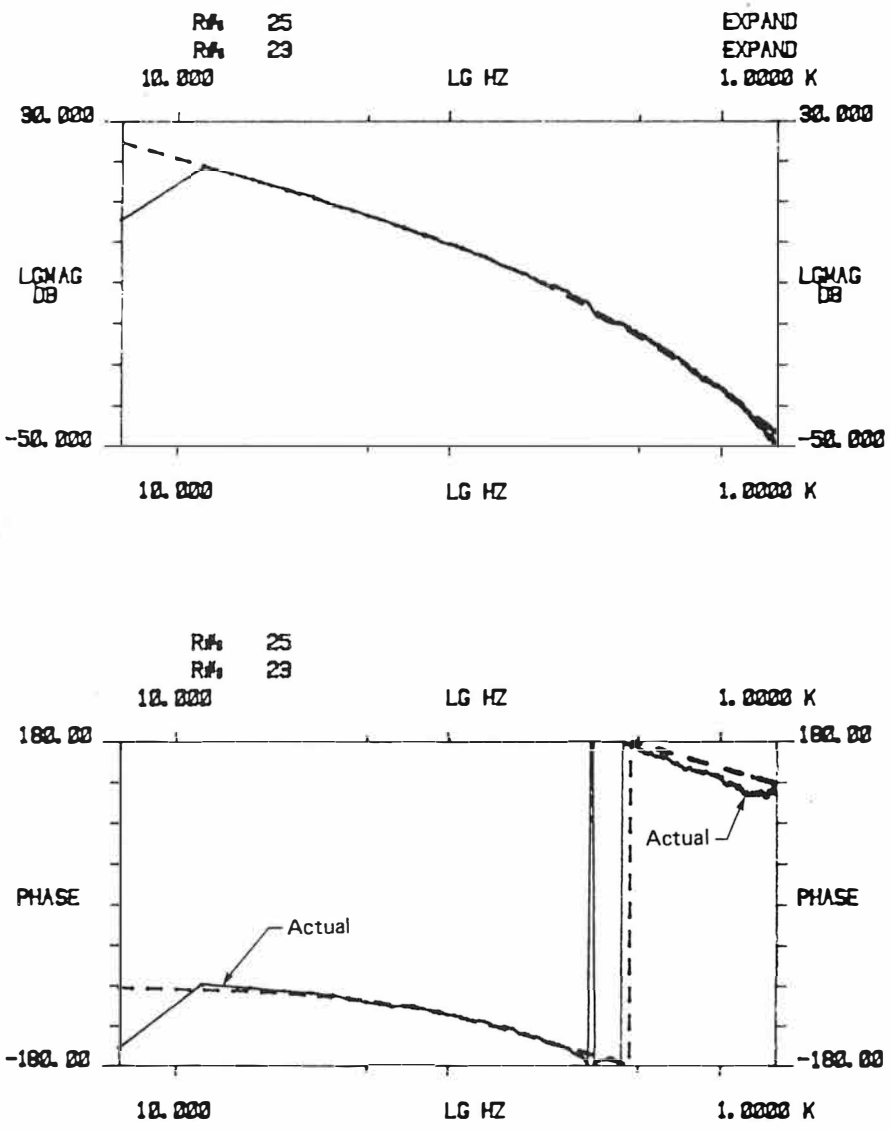

Figure 4-27. Comparison of synthesized and measured velocity loop transfer functions.

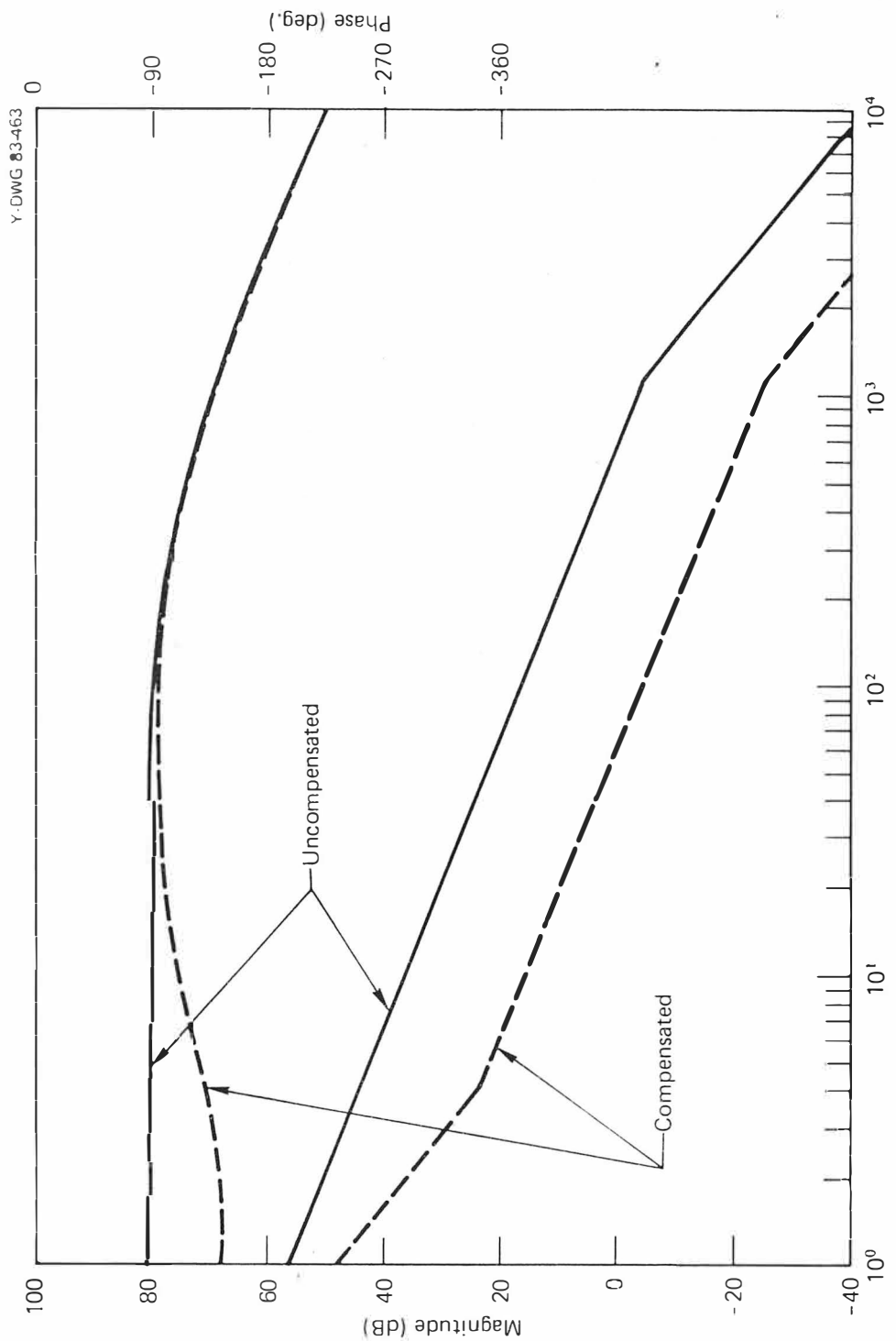

Figure 4-28. Bode diagram of final open position loop.

rad/sec.). The filter, of course, did not treat the major noise source, the power supplies. The 120 Hz noise stemming from the power supplies was difficult to treat because it was almost within the desired system bandwidth. Construction of the compensator included a gain of 12. Attenuation of this gain was provided elsewhere. The compensator thus appeared as

$$G_{oc} = \frac{12K_o\left(1 + \frac{s}{4.16667}\right)}{\left(+ \frac{s}{.378788}\right)\left(1 + \frac{s}{3030.3}\right)} \tag{4-45}$$

The open loop transfer function resulting from these factors is

$$\frac{Z}{Z - R_2} = \frac{K_o\left(1.9771851 \times 10^{13}\right)(s + 4.16667)}{s(s + .378788)(s + 3030.3)(s + 1162.4)(s + 7634.1)} \tag{4-46}$$

The root locus diagram associated with this transfer function is shown in Figure 4-29. The closed position loop transfer function was formed to select an acceptable range of values for K_o.

$$\frac{Z}{R_2} = \frac{K_o\left(1.9771851\times10^{13}\right)(s + 4.16667)}{s^5 + c_5s^4 + c_4s^3 + c_3s^2 + c_2s + c_1} \tag{4-47}$$

where

$$c_1 = 8.2382777\times10^{13}K_o$$

$$c_2 = 1.0185803\times10^{10} + 1.9771851\times10^{13}K_o$$

$$c_3 = 2.690397\times10^{10}$$

$$c_4 = 3.5534392\times10^{7}$$

$$c_5 = 1.1827179\times10^{4}$$

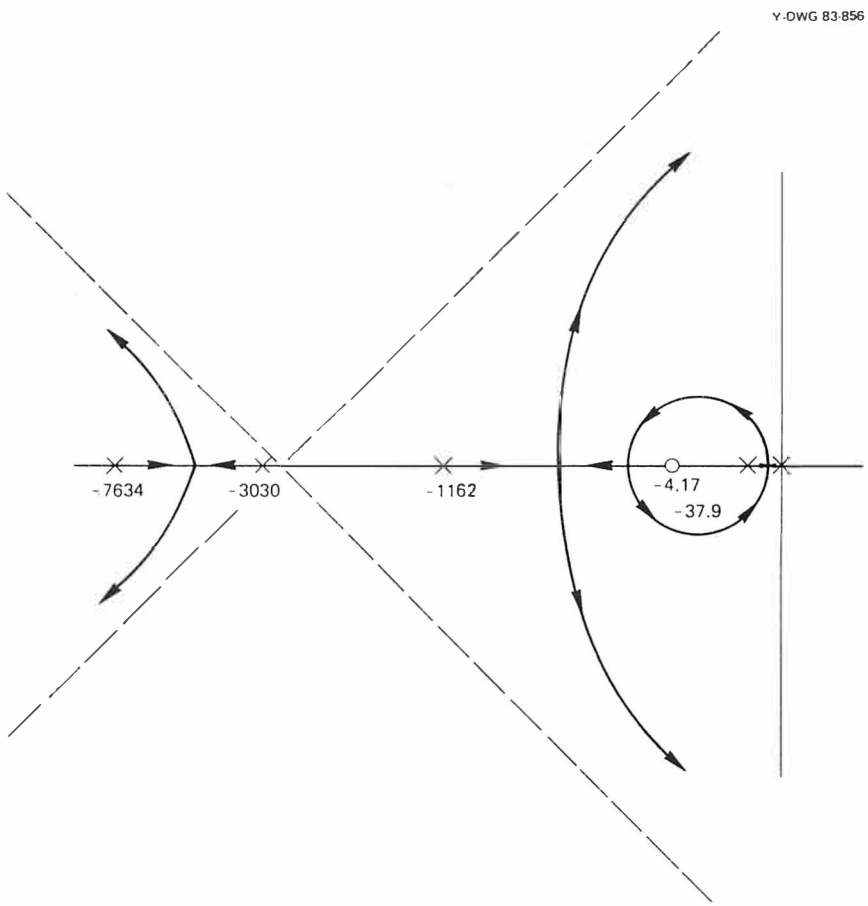

Figure 4-29. Root locus diagram of position loop (from Equation 4-45).

The Routh-Hurwitz criterion was applied to the characteristic equation. A maximum value of approximately 3.9 was found for K_o which limited the total gain to 46.0.

A value of K_o was chosen which would provide a reasonably flat frequency response. A root solving routine, similar to that shown in Appendix B-2, was helpful in selecting a trial value of K_o. A value of approximately 0.5 was used initially to achieve an acceptable set of real closed loop poles at -4.17, -3386.5, and 7582.6 rad/sec and a complex pole pair of natural frequency 663.5 rad/sec and damping coefficient of .64. The low frequency pole was essentially cancelled so that the closed loop transfer function could be simplified to

$$\frac{Z}{R_2} = \frac{K_o\left[1.9771851 \times 10^{13}\right]}{(s + 3386.5)(s + 7582.6)\left[s^2 + 2(.64)(663.5)s + (663.5)^2\right]} \tag{4-48}$$

The slide responded approximately as expected from the above considerations. As the gain was increased, the system exhibited the same audible oscillation heard previously. Since the oscillation occurred at a gain value well below the point anticipated earlier from the Routh test, the adequacy of the model expressed by Equation (4-48) was judged insufficient. With repetition of this condition over a wide variety of controllers and two drive motors, a logical conclusion was that the system possessed some property which should be measureable with the signal analyzer.

The position loop was broken and testing of the velocity loop was repeated over 3200 and 6400 Hz analysis ranges with the response taken at the output of the differentiating network. The test over the 3200 Hz range is

shown in Figure 4-30. Near the high end of the frequency range the data again displays scatter. A strong upward thrust of nearly 180 degrees is seen in the phase at about 3100 Hz.

Figure 4-30 shows the synthesized transfer function for this case. The high frequency spike was found to be represented by the ratio of a lightly damped complex zero pair to a lightly damped complex pole pair. Since this relation is frequently encountered in mechanical resonances, it was concluded that the source of this resonance might well be a structural vibration.

A modal analysis was performed on the slide and motor structure. Using a force instrumented hammer for input to the first channel of the analyzer and an accelerometer for channel two input, a set of transfer functions was formed between each pair of points on the structure. A preliminary search was made of the frequencies of interest by examining the accelerometer frequency distribution for peaking which indicate resonancies. At each of these chosen frequencies the entire set of transfer functions is manipulated to indicate the relative displacements of all the points in the connectivity matrix. The distortion of the structure at each frequency can then be viewed from any perspective either in animation on the analyzer CRT display or in hardcopy from the plotter. The software for performing this analysis (MAAP) was developed by personnel at the University of Cincinnati (29).

The velocity loop measurement indicated a resonance was likely near 3000 Hz. Thus, this frequency region was of primary concern. A resonance was found to match the velocity loop transfer function indication. Figure 4-31 illustrates the vibration mode. The predominant displacement is seen to occur in the motor armature shell. Some axial motion of the structure is seen, however, and it is this motion which is of greatest influence on the performance of

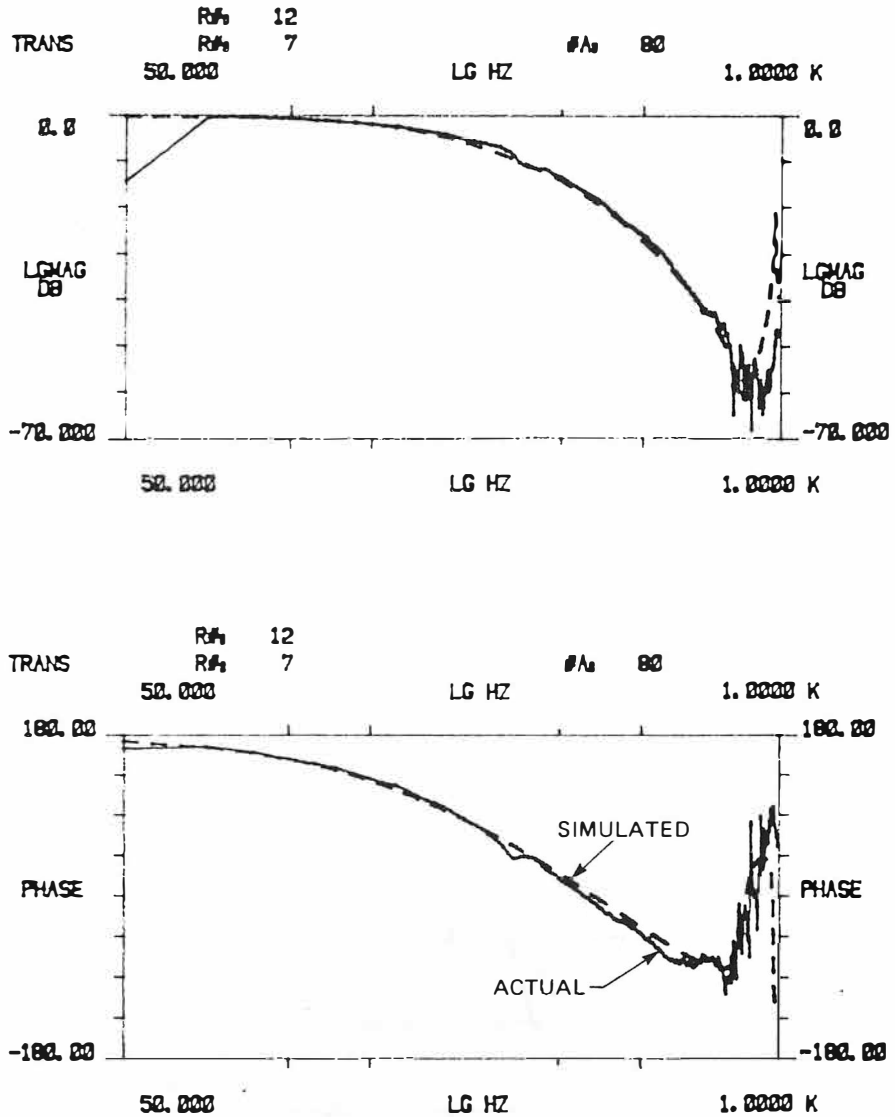

Figure 4-30. Comparison of synthesized and measured frequency responses for the velocity loop.

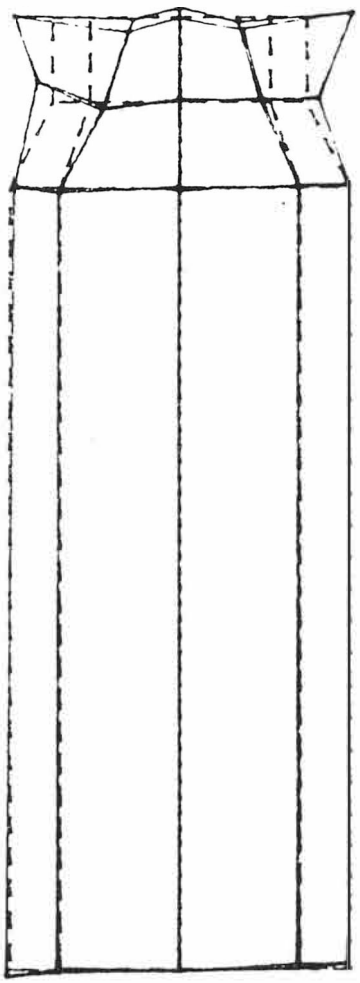

Figure 4-31. Vibratory motion of slide and motor at 3150 Hz mode.

the slide. The greatest axial deflection of the flange fastened to the slide occurred near the point used by the capacitance gage to indicate position. The capacitance gage had been fixed to the slide housing approximately at the ten o'clock position viewing from the rear of the motor. The capacitance gage was moved to the 7 o'clock position, which yielded a less pronounced displacement. The direction of position indication was required to be reversed from positive Z to negative. Further changes were required in the command generator. This procedure is described in Chapter 5. In any event, the effect of vibration at the probe was reduced, but the basic structural difficulty could not be eliminated.

Another compensator was designed with consideration given to the structural anomaly. The gain was fine-tuned to yield the frequency response shown in Figure 4-32. A system bandwidth of greater than 100 Hz is seen along with magnitude peaking of roughly 1.8 dB. This transfer function was synthesized as

$$\frac{Z}{R_2} = \frac{1}{\left(1 + \frac{s}{2827.4}\right)\left(1 + \frac{s}{9110.6}\right)\left[1 + 2(.5)\left(\frac{s}{691.2}\right) + \left(\frac{s}{691.2}\right)^2\right]} \quad (4\text{-}49)$$

A comparison of this synthesis with the measured value is shown in Figure 4-33.

The response of the system to a step input was studied even though this type of command input was not contemplated for the slide. Figure 4-34 illustrates a portion of the slide response to a two mil amplitude, 20 Hz square wave. The time to first peak was seen to be .005 sec and the 1.8 % settling time approximately .012 sec. The overshoot was 22 %. With $\zeta = 0.5$ and ω

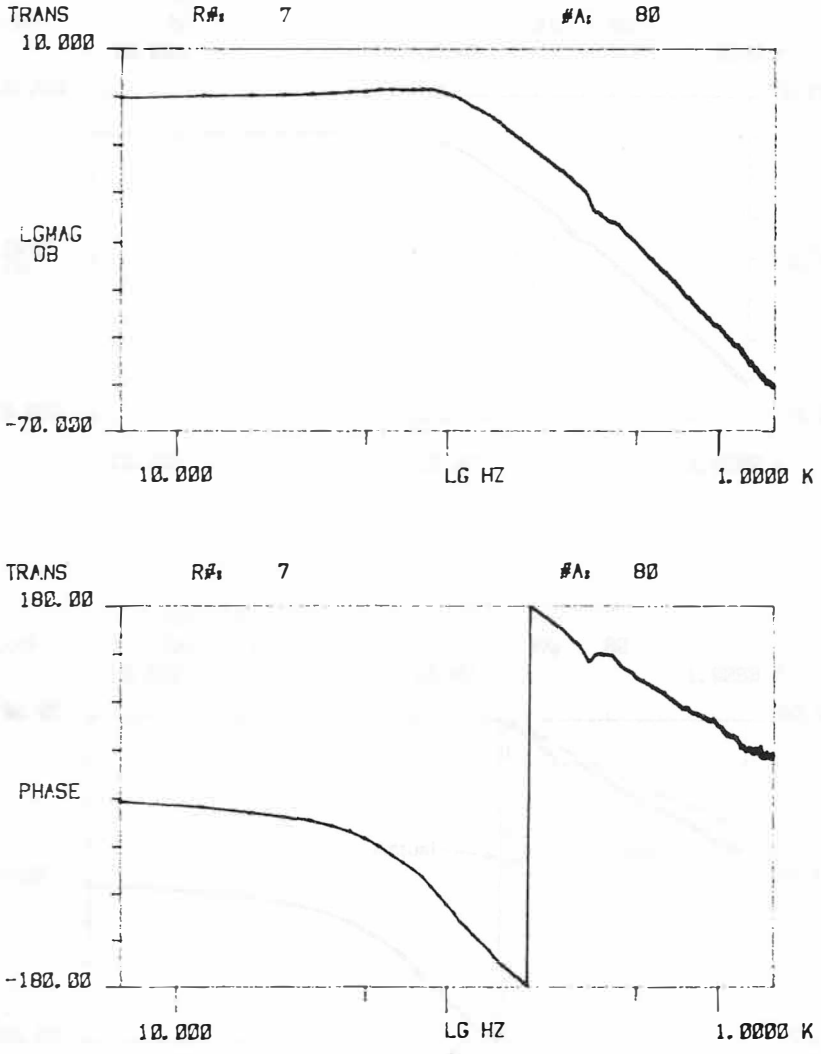

Figure 4-32. Frequency response of final system.

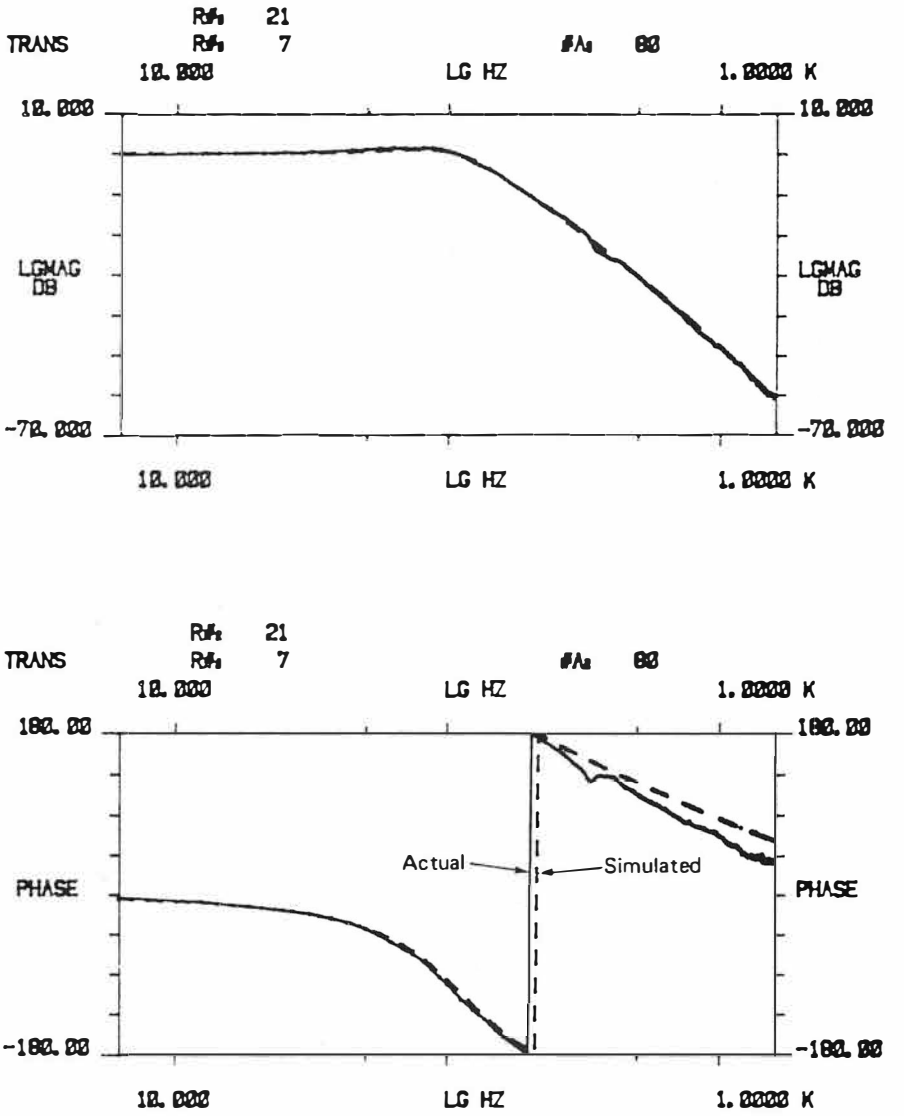

Figure 4-33. Comparison of synthesized and measured frequency responses of final closed position loop.

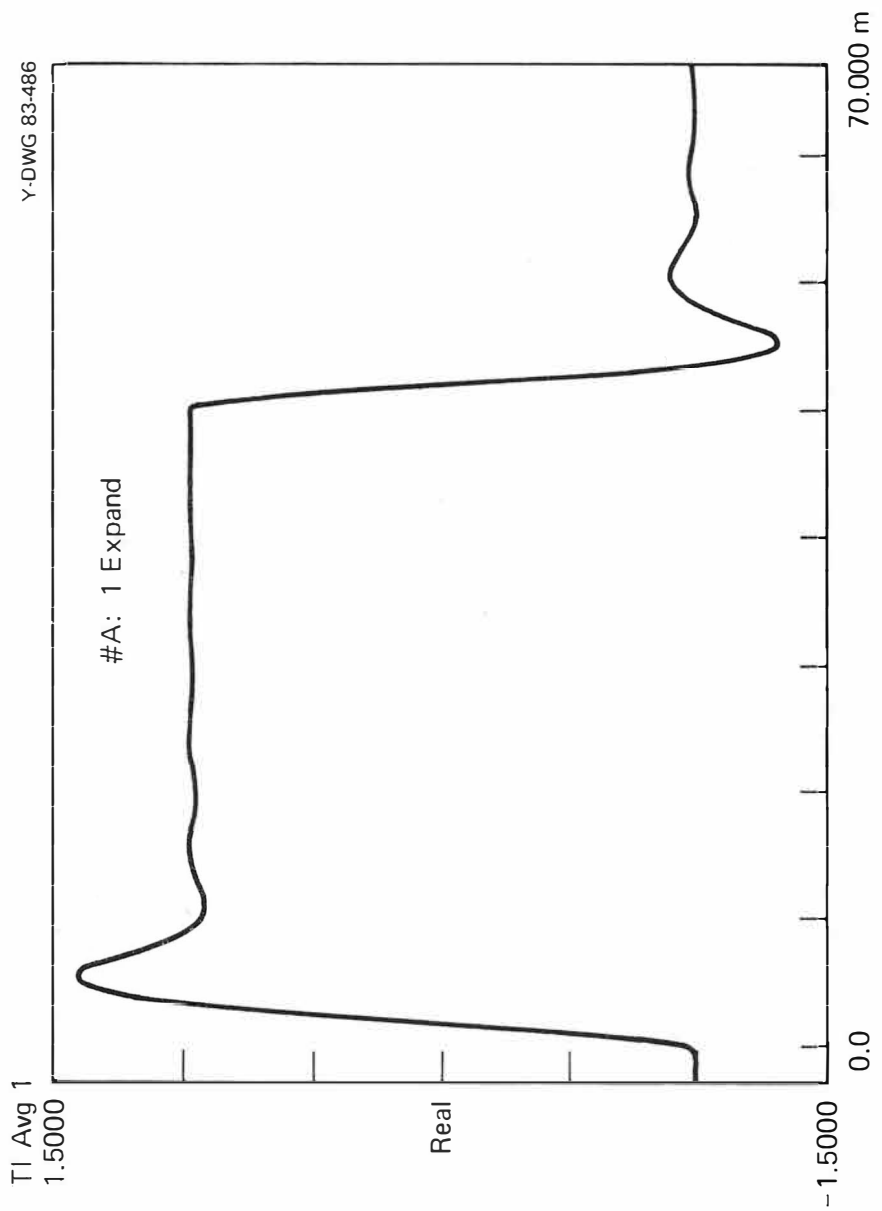

Figure 4-34. Response of slide to step input.

= 691 rad/sec estimated in Equation (4-49) a second order system estimate of the slide would predict the time to first peak of

$$t_p = \frac{\pi}{\omega_n\sqrt{1 - \zeta^2}} = .00525\text{sec} \tag{4-50}$$

and a 1.8 % settling time of

$$t_s = \frac{4}{\zeta\omega_n} = .0115\text{sec} \tag{4-51}$$

Percent overshoot is given by Equation (4-21) or

$$\text{Percent Overshoot} = 16.3\% \tag{4-52}$$

The time to first peak and the settling time tend to confirm the synthesized form, while the measured overshoot was slightly greater than expected.

The compensator was judged to be acceptable for machining of the test part. The final system represented a compromise in design goals. The velocity error constant, K_v, of the system about 4800 sec^{-1} rather than the 30000 sec^{-1} originally sought. Furthermore, the noise in the system was sufficiently large to rule out the use of diamond cutting tools and degrade the surface finish expectations. It was felt, however, that the design of the controls was presently limited by the choice of equipment and that different components must be used to improve the design significantly.

In summary, the analysis and testing of the control system, as presented in this chapter, revealed a combination of electrical noise and structural limitations. The effects of these factors are assessed in Chapter 5 which describes the testing of the entire system through actual metal cutting.

CHAPTER 5

MACHINING OF THE TEST PART

In this chapter the machining tests utilizing all system components is presented. Before describing the machining operation itself, however, the test part is defined and the procedure for machining is explained. Finally, the results of the machining tests are quantified by measurements of the finished part surface on a coordinate inspection machine.

In Chapter 2 the desired off-axis parabolic sector was stated as having a diameter of sixteen inches. Because of limitations imposed by a combination of base machine travel in the X slide and the tool setting procedure, this diameter was reduced to 15 inches. Furthermore, the actual contoured portion of the part was only 14.5 inches due to the need for the machining of a setup surface on the part to facilitate measurement of the surface on the inspection machine. Figure 5-1 illustrates this setup surface or part "face". The disk was held in place on the spindle faceplate by eight bolts countersunk in the surface of the part to be machined. The diameter of the faceplate was eight inches. Because of the length of the structure supporting the Z slide the travel of the Y slide was restricted to only about three inches. Thus, the thickness of the test part was limited to only two inches. This condition, together with the amount of "overhang" of the part from the spindle faceplate, was later seen to have a pronounced effect on part rigidity during machining.

It was stated in Chapter 2 that a diamond tool is required to produce the desired high quality surface finish. A 0.125 inch radius diamond tool was originally planned for finish machining so that a tungsten carbide "button" tool

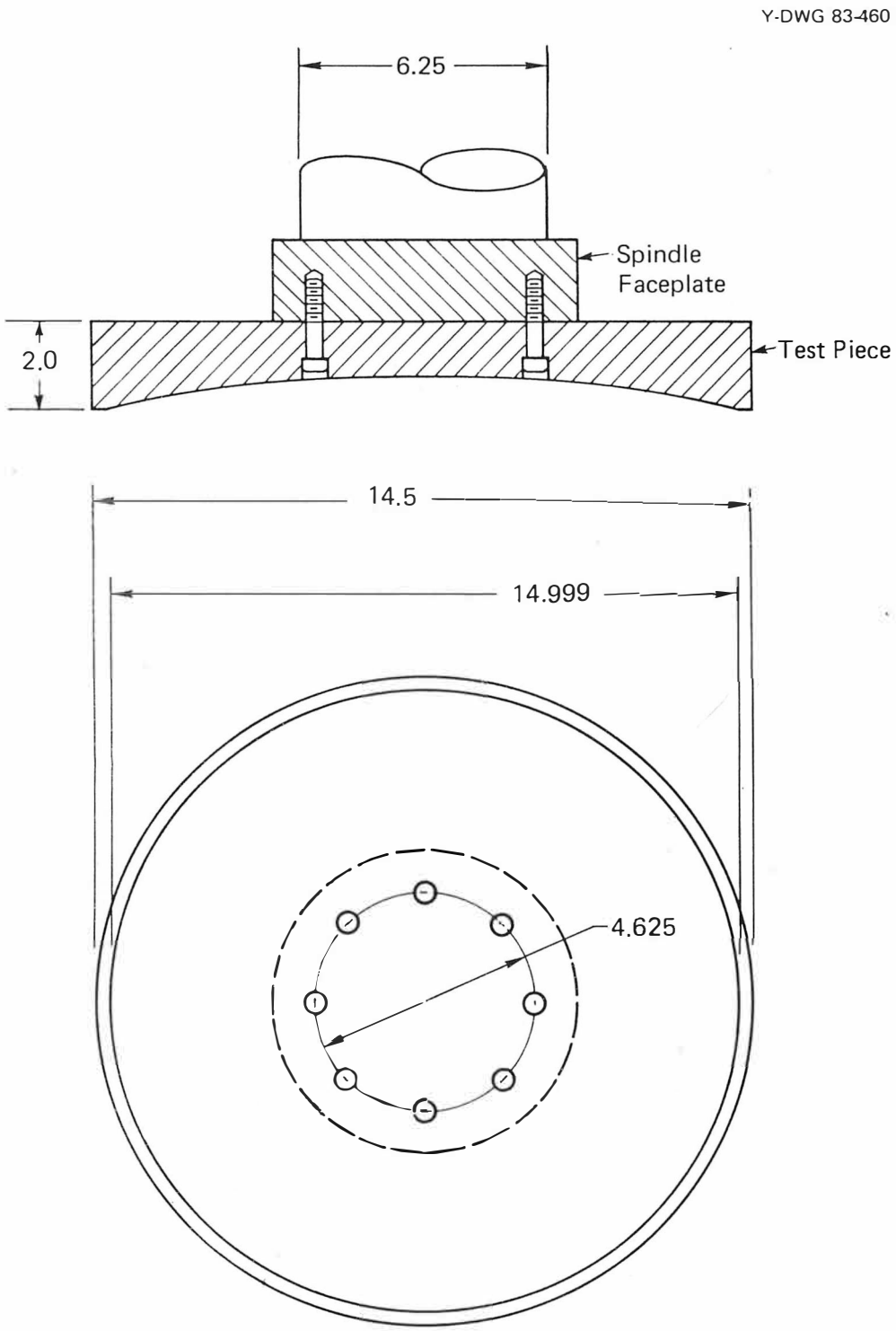

Figure 5-1. Mounting of test part for machining.

of the same size could be used for rough machining. This particular tool has a positive rake angle and is capable of generating reasonably high quality surfaces with relatively low cutting forces. With the noise level excluding the use of the diamond tool, the carbide tool was also used for finish machining. A photograph of the tool is shown in Figure 5-2.

Figure 5-3 illustrates the path followed by the center of the tool as provided by the punched tape driving the X and Y slides of the Moore machine. (This does not include the motion of the Z slide.) The curved portion of the motion represents the gross motion described in Chapter 2 and defined by Equation (2-14). From its starting point the tool first moves in the Y direction toward the part and then proceeds in the X direction to allow a cut across the face of the part. After clearing the inner edge of the part face the tool backs away from the part and moves out along X until the tool intersects the projection of the contoured portion of the part. At this point the tool follows the contour inward until the center of the tool reaches the spindle centerline. The tool then returns to the starting point and ceases motion until re-started.

Before initiating a machining operation it was first required that the Z slide controls be activated. The procedure for this activiation was as follows. First, the command signal generator was switched out of the summing junction of the closed position loop. Next, the Z slide was manually positioned to its null position as indicated on the capacitance gage panel meter. The power amplifier was switched into the circuit to place the slide under control. The manual positioning of the slide was required because failure to do so resulted in a position error signal sufficiently large to trip out the power amplifier.

The accuracy accompanying the tool path of NC machines is generally quite good. However, this accuracy can be no better than the accuracy with

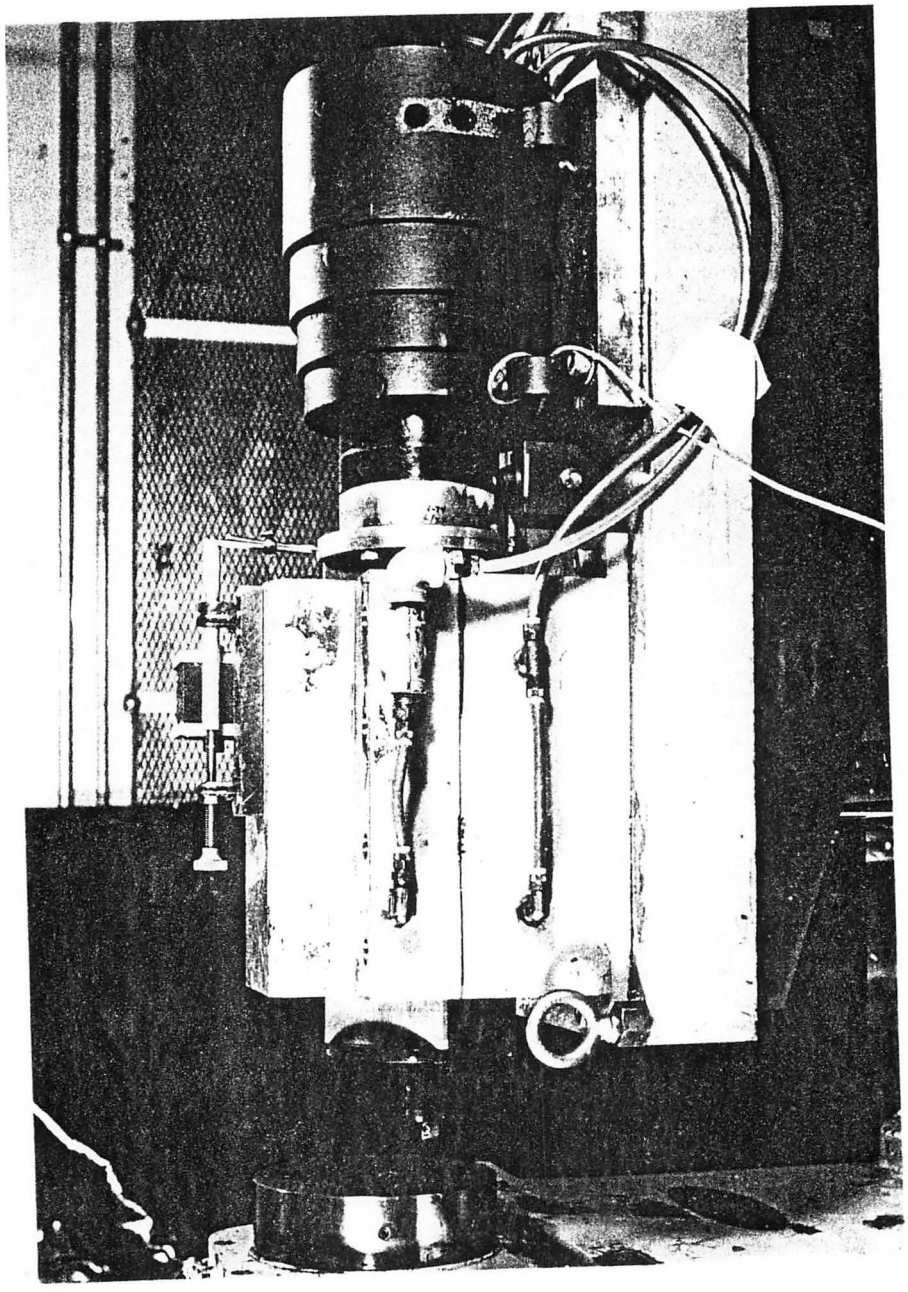

Figure 5-2. Photograph of mounted cutting tool.

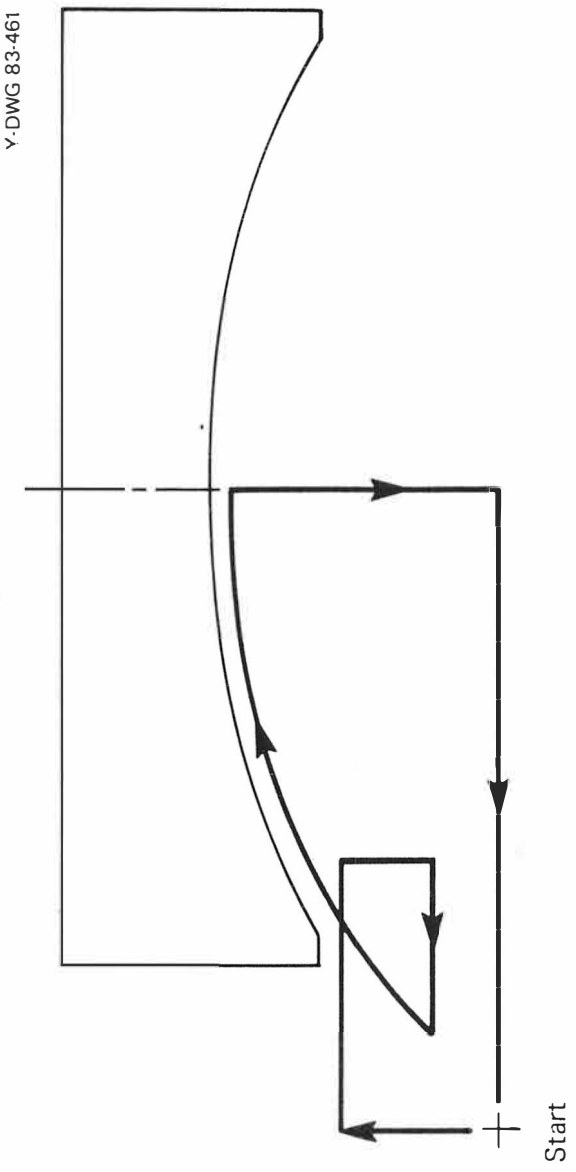

Figure 5-3. Path of tool during cutting cycle.

which the tool starting point is located. Because the Moore machine used did not have an automatic tool setter, a manual tool setting technique was required. First, a very light cut was made on the outer (cylindrical) surface of the part. This produced a very smooth surface which could be measured and henceforth used as a standard. Thus, in the future if the tool was caused to just touch this surface the location of the tool relative to the spindle centerline was known within the limits of the diameter measurement and the skill employed in touch-up.

To establish a reference surface for use in the Y direction a similar approach was taken. Since the tool is moved successively inward along Y while roughing and since the face of the part is machined with the contour, this standard is not quite so critical.

Before the finished contour could be machined into the part, it was first necessary to rough-machine the part to the full depth controlled by the tape. This roughing procedure required only that the Z slide be maintained at null position. The roughing sequence, therefore, consisted of activating the Z slide at the null position, touching-up the tool on the two reference surfaces and moving the tool to the starting position before activating the NC control. After each cutting pass the tool was moved inward along the part axis. After beginning with a flat face across the part, each cutting pass thus increased the depth and diameter of the part concavity.

The depth of the surface after rough machining was approximately 0.205 inch. With depths of cut generally no greater than 0.010 inch, the rough machining stage provided considerable opportunity to observe the Z slide behavior under cutting conditions. Several of these observations are worth reporting.

During the early stages of Z slide control system testing an oscilloscope was used to monitor several signals in the controls circuitry, in particular the position command, feedback and error signals. The use of this oscilloscope was continued while machining and proved to be very useful. With the slide active at the null position the display of error signal showed approximately 20 mV, and hence, 20 microinches, of noise.

The Z slide power amplifier was equipped with an ammeter which measured the flow of current to the motor. Under conditions of heaviest cuts (10 mils or more), this meter indicated current flow of three to four amps. Since both the power amplifier and linear motor were limited to, and fused for, eight amps, it was expected that the system should function well at depths of cut under five mils. The system was observed to weather continuous cuts of this depth well. It was also found that even small loads suddenly placed on the system could sometimes cause the power amplifier to overload and turn itself off.

Earlier in this chapter the test part was described as a disk approximately 15 inches in diameter and two inches thick. Since it was attached to an eight inch diameter spindle faceplate, the part was unsupported over its outer 3.5 inches. The undesirability of this condition became very obvious as soon as the rough machining operation reached the point where the tool made contact with the part at a radius larger than that of the faceplate. A ringing tone was produced by the excitation of the tool cutting forces. This tone was later measured as the natural frequency of the part as supported by the spindle. These oscillations were of relatively low magnitude. The instantaneous position displayed on the oscilloscope showed a widening in the noise on the position error signal to approximately 40 to 50 microinches. A correspond-

ing increase in surface roughness was also visible in this outer region of the part surface.

The eight holes in the surface of the part had a strong effect on Z slide behavior as the tool moved over them. A typical sketch of the oscilloscope display of the slide position error signal is shown in Figure 5-4 for a single revolution of the part at a 300 rpm spindle speed. As the tool began moving over the holes the error spikes emerged. The spikes represent the forward motion of the slide when the cutting force was suddenly removed at the edge of the bolt hole. The magnitude of these error spikes varied with the depth of cut but was of the order of several hundred microinches. The effect of this tool "overshoot" could be seen at the edge of holes where cutting resumed. These rear edges were bevelled, indicating that the slide position recovery had not been completed when the rear edge of the hole was encountered by the tool. The periodic sound of the resumption of cutting could be readily heard. This interrupted cut provided the greatest limitation on the depths of cut possible. When the error spikes became sufficiently large, overload conditions became large enough to produce an overload condition in the power amplifier protection system to shut down the slide control system. This required complete reinitialization of the cutting cycle, including tool setting. This procedure caused a considerable loss of time.

The rough machining procedure was complete when metal cutting was continuous across the part face and over the concavity to the center of the part. At this point the Z slide command could be switched on to cause the slide to start driving rather than merely hold its null position. This required an additional procedure in tool initialization. The coefficient data were tabulated in computer memory as varying with X slide position which increases from a

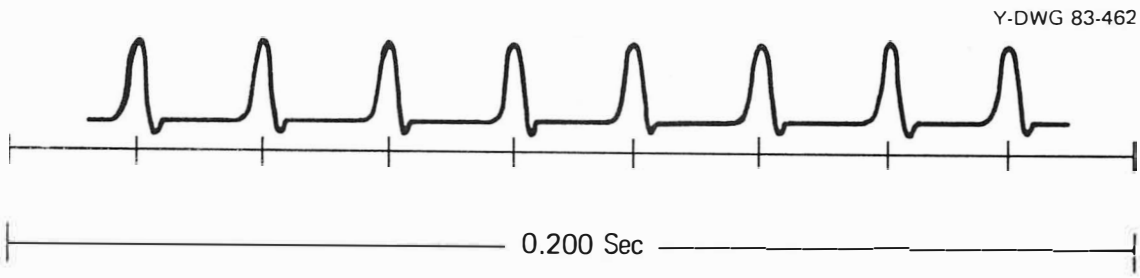

Figure 5-4. Position error signal while cutting over bolt holes.

zero value at the part center. After tool "touch-up" on the part reference diameter the X slide was moved manually to center the tool on the part axis. The Y slide was moved to a point corresponding to its most positive (inward) point in the path controlled by the punched tape. At this point the laser position displays were set to zero to reference the coefficient data properly. The tool was then moved manually to the starting point shown in Figure 5-3.

In Chapter 2 it was stated that the maximum travel of the Z slide in producing this parabolic surface was approximately 8 mils. This maximum, however, applied to a contour of 8 inch radius. With the part size limitations previously described, the maximum travel was reduced to approximately 6.4 mils. Even this amount was more than desired in a single pass. Therefore, several machining passes were taken before the entire surface was machined continuously.

The operating program in the microcomputer was written so that for X greater than 7.2 inches all coefficient values were set to zero. This caused the Z slide to be nulled for tool setting and part facing. Thus since the face of the part was machined in the same pass as the full contour, the flat face could be used as a reference surface when the part was measured.

In addition to the difficulties cited previously concerning rough machining another problem was encountered during the machining after the Z slide motion was activated. At the outer portion of the contour the varying depth of cut caused a sufficient torque resisting spindle motion that the spindle speed could not be maintained at the desired 300 rpm. It was found that a speed of 360 rpm could be held acceptably. This condition, of course, was not related to the Z slide controls, but rather reflected the absence of a closed loop spindle speed control system.

The photograph shown in Figure 5-5 was taken after two passes across the part. The portion of the surface seen at the top and bottom of the part had not been machined during these first two passes. The area in the center is the freshly machined surface and demonstrates the nonaxisymmetric character of the machining action. The surface finish of these areas is seen to be not strikingly different. Thus, the finish did not seem to be influenced by the fact that the slide was being driven rather than merely holding the null position.

Also seen in Figure 5-5 are a series of concentric circles or portions of circles. The spacing of these circles was measured to be approximately 0.1 inches. It was first thought that these lines represented the initiation of a new command block by the NC controller. An examination of the NC tape command listing showed that new commands were being read from the tape at intervals of roughly .032 inch and, hence, were not the source of the circular grooves. It was then thought that the .1 inch lead on the threads of the leadscrew of the base machine X slide might be related to these grooves. Closer examination showed that the grooves were not present on the rough machined surface. Since the only difference in machine tool action from this portion of the surface to the other was the activation of the Z slide command generator, it was concluded that the command generator was the source of the abnormality. The difficulty was traced to the .1 inch grid spacing in the interpolation scheme. A slight change was made in the interpolation algorithm to affect only the updates at the endpoints. Subsequent passes showed that the grooving action was indeed eliminated by this software change.

After sufficient passes were made to "clean up" the surface, a new tool was used to provide the final cut with the best possible surface finish (with this type of cutting tool). This tool change required, of course, that the tool setting

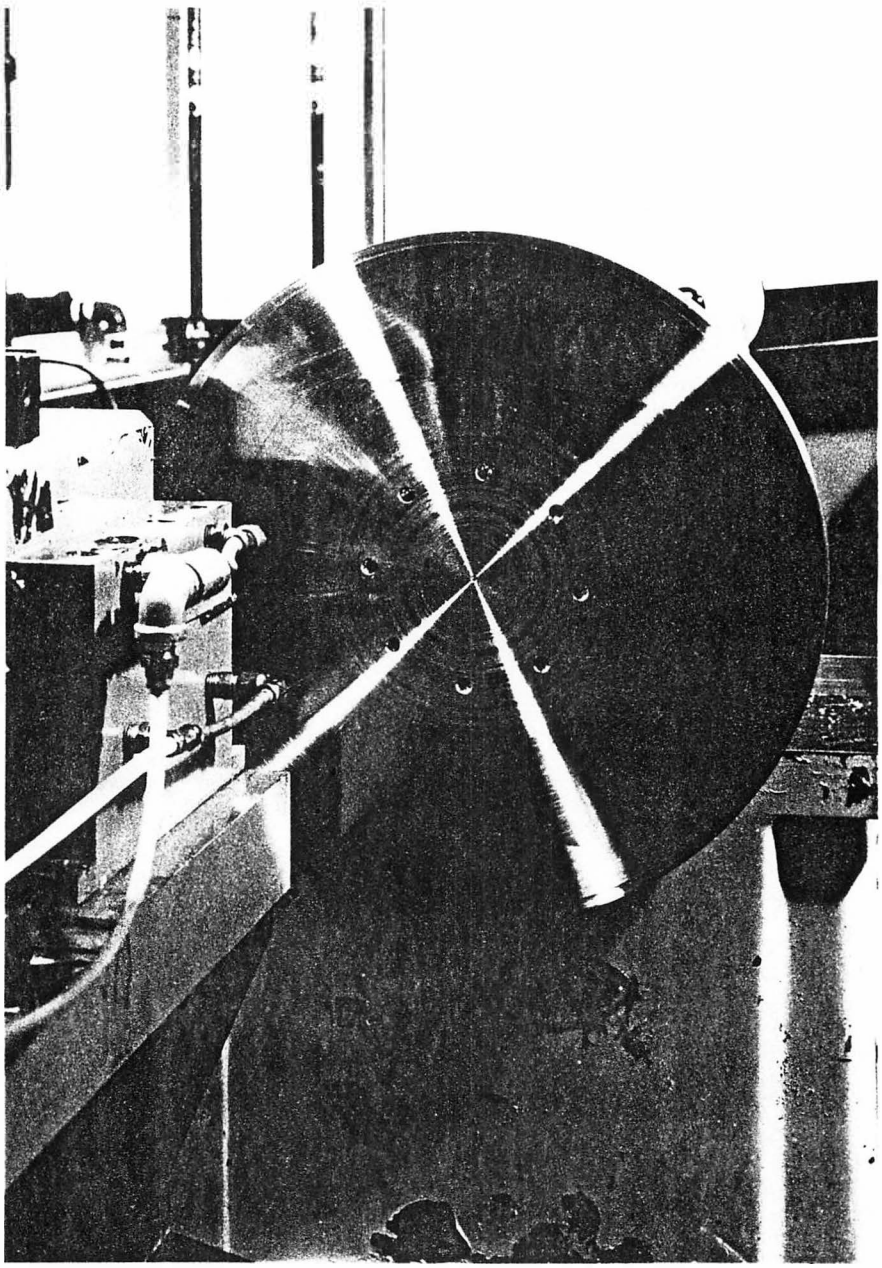

Figure 5-5. Appearance of surface before complete cleanup.

and X slide display initiation procedures be repeated. A depth of cut of about .0003 inch was used to insure that the surface was machined continuously.

The finished part was placed on a Renault coordinate measuring machine to characterize the error in the machined surface. The part was aligned by contacting a three-dimensional gaging probe at several points on the periphery of the part as well as three points on the machined face. With these points the alignment error of the part with the machine axes was known and could be used to correct the measured errors for the misalignment. The probe was moved to the center of the part to initiate measurements. From the center the probe was moved under NC control to a grid of points in space which are defined by the parabola of interest. The grid was formed of points on 1 inch radial and 10 degree angular spacing. At each point the probe contacted the part and indicated the deviation of the machined surface from nominal. These deviations were corrected for the alignment errors as described earlier.

The surface measurement showed errors of a magnitude and character totally unexpected. A quick examination of these data indicated that the errors in the part surface were greater than would have been incurred if the Z slide had not been driven at all. Still closer examination showed that the error at each point was very nearly twice the Z slide command. It was then realized that the sign had been reversed on the Z slide command generator. A new set of measurements was made on the part with coordinates derived with an inversion of sign on the Z slide motion. The results of this part inspection are shown in Table 5-1 and confirmed the suspicion about the sign reversal. Note that errors are within a $\pm$ .0006 in. band. about the nominal. The surface error data are plotted in Figure 5-6. Note that the errors are both more constant and more positive toward the center of the part. Because the slide dis-

Table 5-1. Measured Contour Error in First Machined Part

	Part Contour Error (Mils)						
ϕ	X=1	X=2	X=3	X=4	X=5	X=6	X=7
0	0.51	0.47	0.35	0.31	0.31	0.35	0.28
10	0.51	0.47	0.39	0.31	0.35	0.43	0.39
20	0.51	0.43	0.39	0.39	0.43	0.51	0.51
30	0.47	0.47	0.43	0.43	0.47	0.51	0.47
40	0.47	0.47	0.39	0.39	0.47	0.51	0.47
50	0.55	0.43	0.39	0.39	0.47	0.51	0.43
60	0.55	0.43	0.35	0.35	0.43	0.39	0.39
70	0.51	0.47	0.31	0.31	0.31	0.31	0.24
80	0.51	0.35	0.31	0.24	0.20	0.20	0.12
90	0.51	0.35	0.20	0.20	0.12	0.08	-0.04
100	0.43	0.35	0.24	0.08	0.12	-0.04	-0.12
110	0.43	0.39	0.16	0.08	0.04	-0.04	-0.12
120	0.47	0.35	0.20	0.12	0.04	-0.04	-0.08
130	0.47	0.43	0.24	0.16	0.04	-0.04	-0.04
140	0.55	0.47	0.31	0.16	0.16	-0.04	0.00
150	0.47	0.47	0.28	0.20	0.16	0.12	0.08
160	0.51	0.43	0.31	0.24	0.20	0.20	0.16
170	0.51	0.47	0.39	0.24	0.20	0.24	0.24
180	0.51	0.47	0.35	0.31	0.24	0.28	0.20
190	0.55	0.43	0.39	0.28	0.31	0.28	0.24
200	0.55	0.47	0.31	0.31	0.31	0.31	0.20
210	0.63	0.43	0.35	0.39	0.35	0.35	0.24
220	0.59	0.12	0.39	0.35	0.31	0.35	0.20
230	0.59	0.43	0.31	0.28	0.24	0.28	0.08
240	0.55	0.47	0.28	0.28	0.20	0.16	-0.08
250	0.55	0.35	0.24	0.16	0.20	0.12	-0.20
260	0.55	0.39	0.24	0.12	0.00	-0.12	-0.39
270	0.55	0.35	0.12	0.04	-0.08	-0.20	-0.51
280	0.55	0.31	0.16	0.04	-0.16	-0.20	-0.59
290	0.55	0.35	0.16	0.00	-0.12	-0.31	-0.55
300	0.55	0.31	0.20	0.04	-0.12	-0.28	-0.55
310	0.59	0.43	0.16	0.04	-0.08	-0.20	-0.47
320	0.59	0.43	0.24	0.12	0.00	-0.12	-0.31
330	0.55	0.43	0.28	0.20	0.12	0.04	-0.16
340	0.63	0.39	0.31	0.24	0.16	0.16	0.04
350	0.55	0.43	0.39	0.28	0.31	0.28	0.16

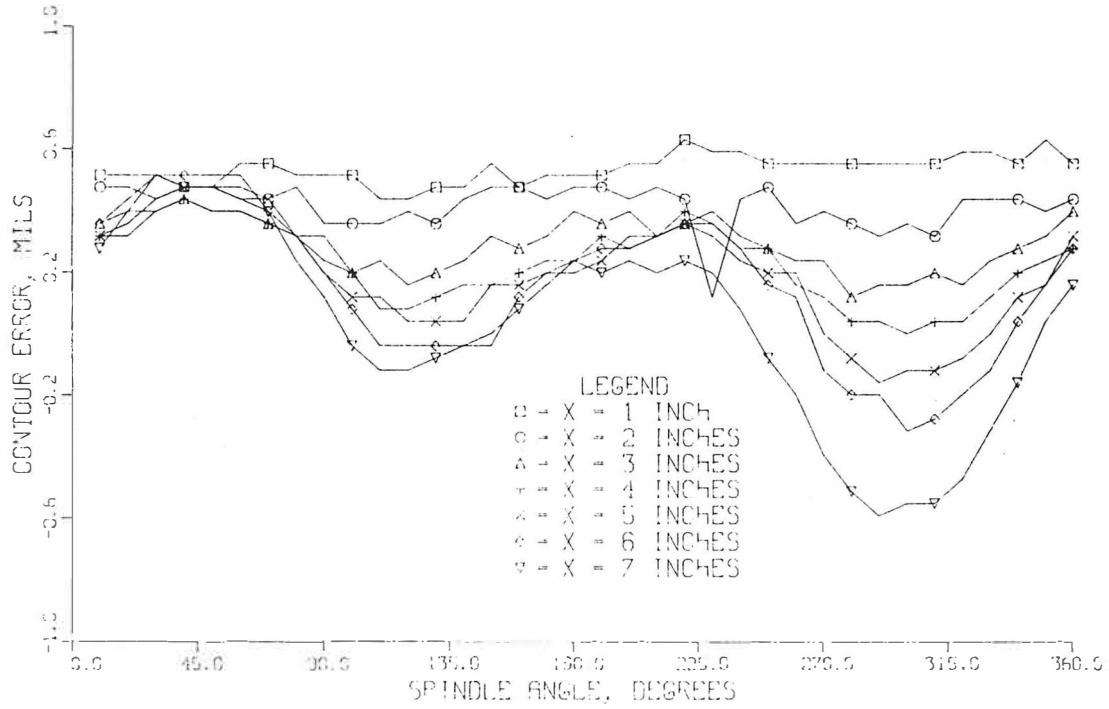

Figure 5-6. Measured error in first machined part.

placement, and hence velocity, decreases with part radius, it was anticipated that variation in surface error would also be smaller in the center region. It was not anticipated, however, that the error would become increasingly positive in this region. Since positive error in this measurement indicates excess stock, the data reflect higher tool forces near the part center. The only known explanation for this characteristic is that the relative velocity between tool and part (known as 'surface speed') decreases with radius and permits less time for relief of tool cutting forces.

Figure 5-7 illustrates the comparison of measured surface deviations at a 7 inch radius with the deviations predicted by computer simulation. The comparison is seen to be within .0002 inch for more than the first 90 degrees in ϕ. Over the next 225 degrees of rotation the character of the measured error appears to be quite different from that expected from the simulation. This departure from the expected is presumably due to the unknown influence of the tool force on the behavior of the slide and control system.

The sign inversion error of the command signal generator was corrected and the part was re-machined. Before machining was begun, however, the bolt holes in the part surface were filled with a cast material to eliminate, or at least reduce, the effect of the interrupted cut on the slide controls. The part was again measured on the Renault measuring machine. The result of this measurement is shown in Table 5-2 and Figure 5-8. The error band is seen to be slightly larger than that seen after the first machining pass and ranges from - .0005 to + .0009 inch. Again, the error toward the center of the part shows a positive bias, which decreases with increasing radius. The measured errors at a 7 inch radius were again plotted with the errors predicted from computer simulation. This comparison is shown in Figure 5-9. The two curves are seen

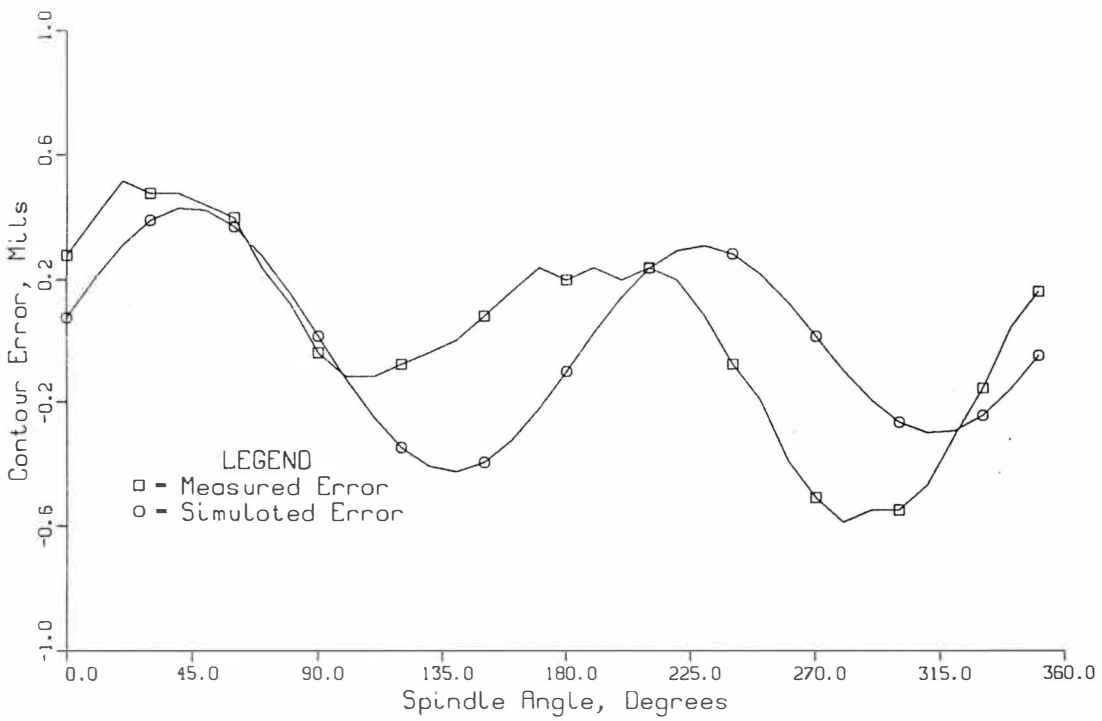

Figure 5-7. Comparison of measured and simulated errors in first part.

Table 5-2. Measured Contour Error in Second Machined Part

	Part Contour Error (Mils)						
ϕ	X=1	X=2	X=3	X=4	X=5	X=6	X=7
0	0.39	0.35	0.20	0.08	-0.08	0.04	-0.08
10	0.39	0.35	0.35	0.24	0.04	-0.04	-0.08
20	0.47	0.47	0.24	0.16	0.00	-0.04	-0.20
30	0.47	0.35	0.24	0.00	-0.08	-0.04	-0.28
40	0.55	0.47	0.20	0.04	0.04	-0.20	-0.20
50	0.59	0.43	0.24	0.08	0.04	-0.08	-0.12
60	0.59	0.39	0.28	0.16	0.00	0.12	-0.08
70	0.51	0.43	0.28	0.16	0.12	0.28	0.20
80	0.59	0.39	0.28	0.24	0.28	0.28	0.43
90	0.67	0.39	0.35	0.35	0.31	0.51	0.43
100	0.59	0.55	0.47	0.39	0.47	0.71	0.55
110	0.59	0.51	0.47	0.43	0.51	0.75	0.83
120	0.63	0.51	0.51	0.55	0.63	0.67	0.87
130	0.63	0.63	0.47	0.47	0.51	0.63	0.75
140	0.63	0.59	0.51	0.47	0.47	0.63	0.55
150	0.51	0.43	0.47	0.43	0.39	0.39	0.55
160	0.43	0.55	0.43	0.35	0.31	0.31	0.20
170	0.43	0.47	0.31	0.35	0.28	0.20	0.08
180	0.59	0.47	0.31	0.12	0.08	0.00	-0.16
190	0.43	0.47	0.31	0.16	-0.08	-0.08	-0.24
200	0.47	0.39	0.28	0.16	0.00	-0.08	-0.31
210	0.47	0.35	0.24	0.12	-0.08	-0.28	-0.51
220	0.43	0.51	0.28	0.00	-0.16	-0.31	-0.43
230	0.43	0.43	0.28	0.00	-0.16	-0.24	-0.39
240	0.39	0.43	0.20	0.08	-0.08	-0.08	-0.31
250	0.39	0.51	0.16	0.12	0.12	0.00	-0.20
260	0.47	0.55	0.16	0.16	0.12	0.20	-0.35
270	0.59	0.55	0.20	0.20	0.20	0.31	0.24
280	0.51	0.51	0.35	0.24	0.31	0.55	0.31
290	0.47	0.51	0.35	0.43	0.39	0.43	0.43
300	0.47	0.55	0.55	0.43	0.39	0.43	0.59
310	0.47	0.55	0.47	0.31	0.35	0.43	0.55
320	0.51	0.51	0.43	0.43	0.35	0.47	0.35
330	0.59	0.43	0.47	0.39	0.39	0.35	0.39
340	0.55	0.43	0.35	0.31	0.31	0.39	0.31
350	0.47	0.47	0.39	0.20	0.16	0.20	0.08

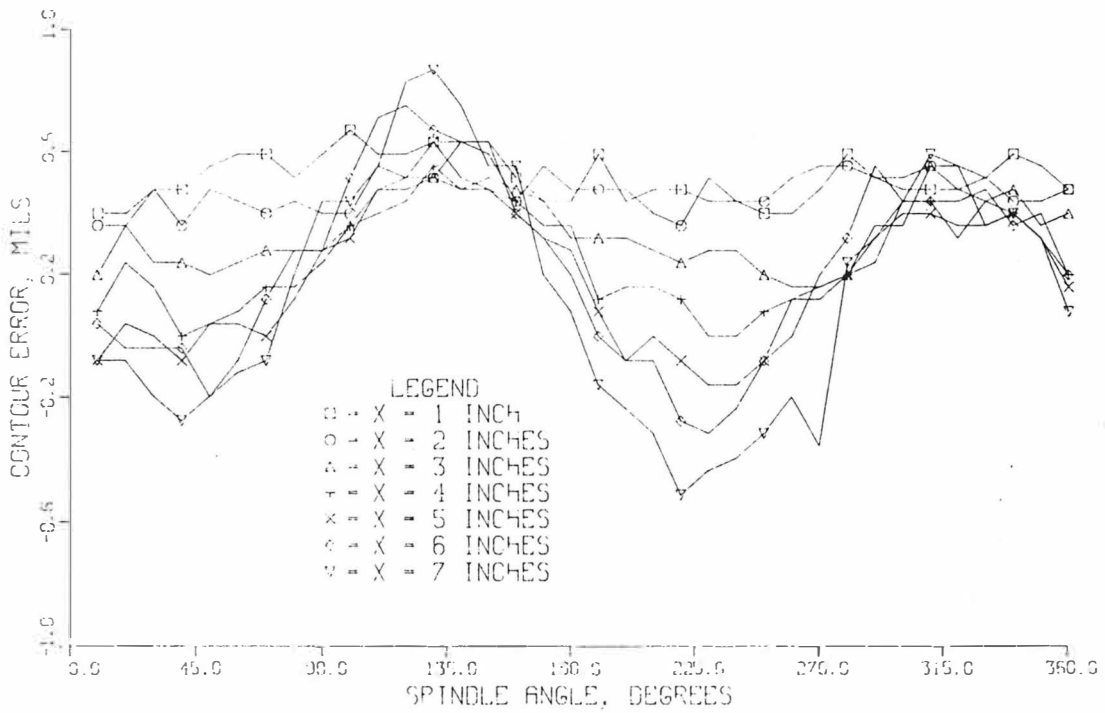

Figure 5-8. Measured error in second machined part.

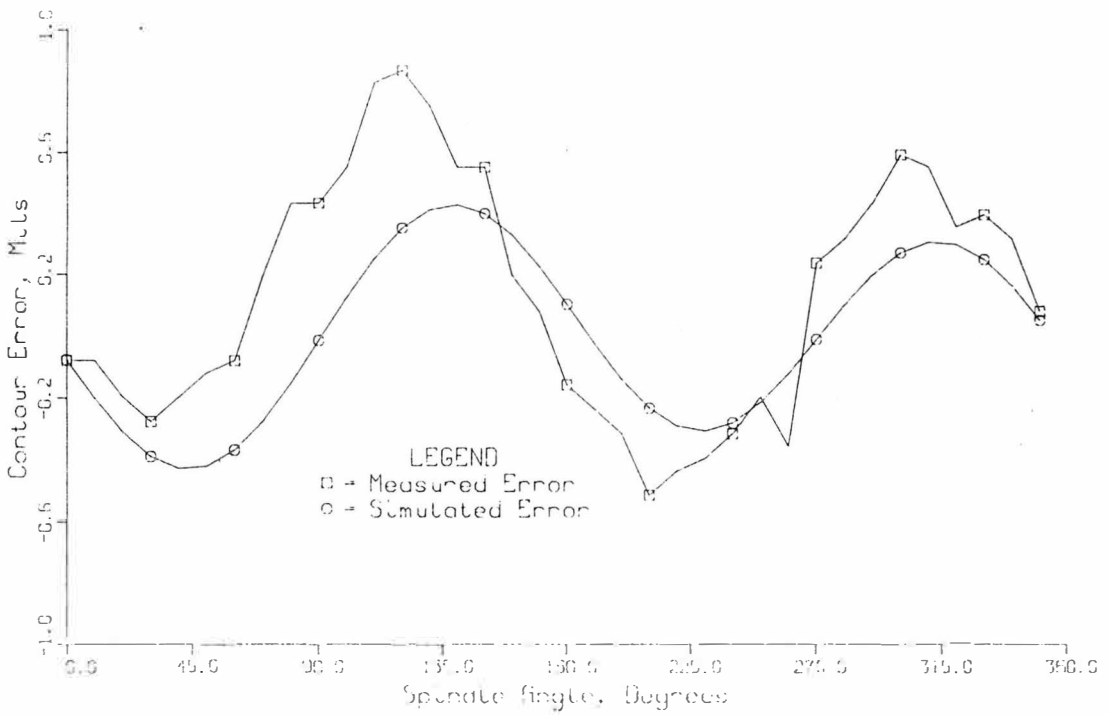

Figure 5-9. Comparison of simulated and measured errors in second part.

to display a similar character although the actual errors are of greater magnitude. A photograph of the finished part is shown in Figure 5-10. This photograph was taken after the surface had been polished lightly for cosmetic effect. Before the surface was polished, the surface finish was measured with a profilometer. The finish varied from approximately 7 microinches RMS near the part center to about 60 microinches at the outer region of the contoured surface.

Both the surface finish and contour error exceeded the target values by considerable margin. Both of these excesses stemmed principally from the choice of the drive mechanism. Although the linear motor used in this experiment is apparently quite sufficient for positioning computer disk read/write heads, the mechanical resonances described in Chapter 4 limited the position loop gain such that the dynamic position error could not be reduced to the desired level.

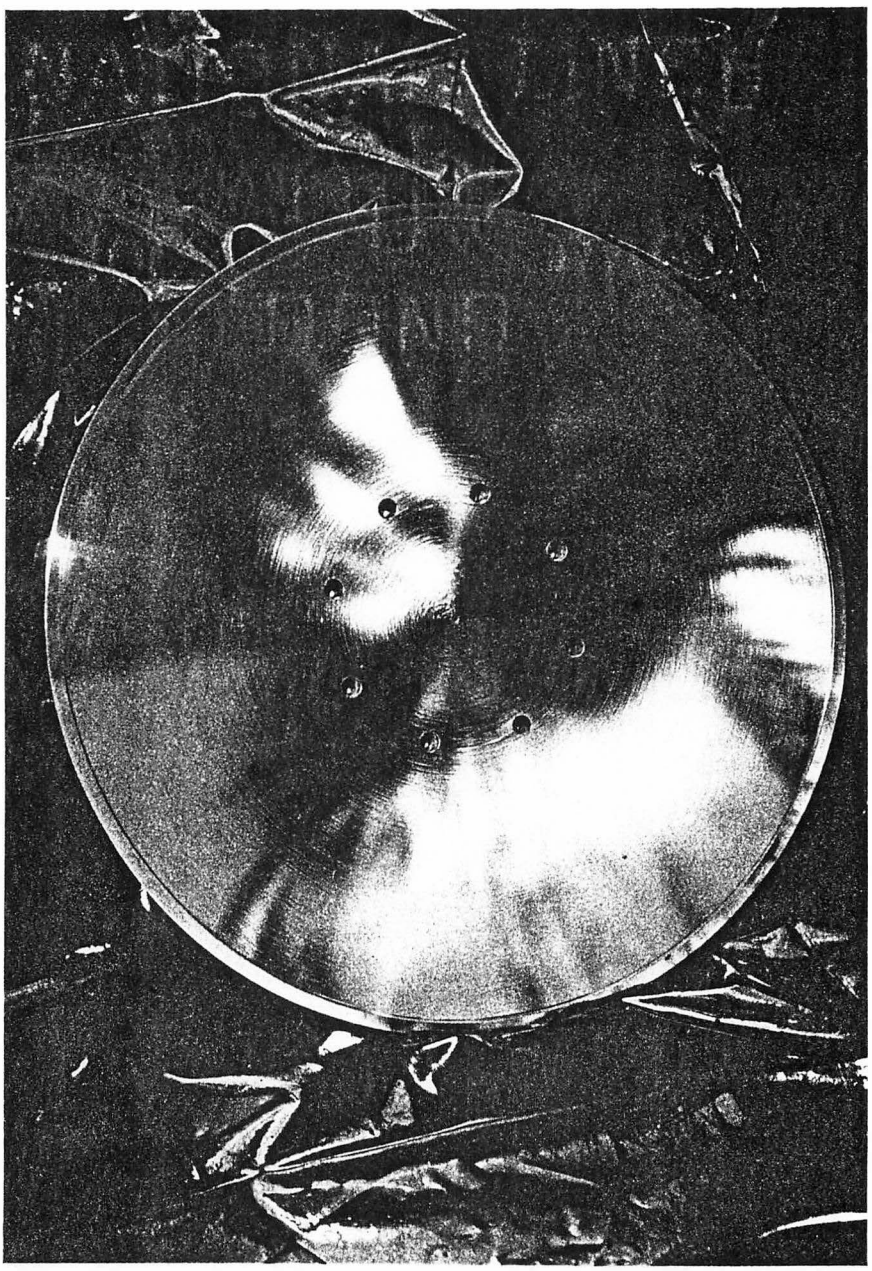

Figure 5-10. Photograph of finished part.

CHAPTER 6

CONCLUSIONS AND RECOMMENDATIONS

Comparison of the results of the finished part measurements with the design goals would, on first glance, indicate the project had failed. The surface finish goal of 5 microinches peak-to-valley was exceeded by over an order of magnitude. The desired maximum contour error of ± 30 microinches was exceeded by a factor of approximately 30. As was mentioned at the end of the previous chapter, this disappointment could be attributed principally to two factors: the use of the linear motor as a drive mechanism and the excessive amount of electrical noise in the controls. These topics, together with other suggestions for improvements, will be treated in this chapter.

It is felt that the source of much of the noise in the control circuitry was the supplies of 12 volt power to the printed circuit board components and in the power converter in the capacitance gage electronics. Tests on the output of this gage alone revealed noise of approximately 10 millivolts as allowed by the manufacturer's specification. The low pass filter used in the forward path of the position loop was intended to attenuate the effect of this noise, as was the op amp network through which the capacitance gage feedback signal was passed. Even with the use of these two measures the signal sent to the servo amplifier still displayed at least 20 millivolts, corrresponding to 20 microinches, of noise. This condition precluded the use of diamond cutting tools which automatically reduced further the opportunity for very high surface finish.

Another contributor to the low quality surface finish was the method by which the part was fixed to the spindle. As was described in Chapter 5 the

part was bolted directly to the spindle surface plate, the diameter of which was only about one-half that of the part. This lack of support behind the part was very obvious during machining because of the ringing sound heard while metal was being cut. After the cut passed within the diameter of the faceplate, the ringing sound stopped, and a corresponding improvement was observed in the measured surface finish. Because of space restrictions between the end of the tool holder and the faceplate, it was not possible to use an intermediate part-holding fixture of larger diameter to provide greater support to the outside of the part. Undoubtedly the inability to use the diamond cutting tool resulted in greater vibration excitation because of the higher cutting forces associated with the button tool. The effects of excessive noise thus were found to have been compounded.

The consequences of the use of the linear motor as a drive mechanism have already been cited. This device was chosen because of its linear characteristic and simplicity in implementation. The limiting factor with the motor was found to be the rigidity of its coil frame. This condition was not anticipated and could hardly have been without prior experience with this particular equipment. The literature supplied by the manufacturer did not show sufficient construction detail to have triggered concern about rigidity of the structure. Perhaps if the Digital Signal Analyzer had been available earlier in the program, either an alternate drive motor or more sophisticated compensation measures might have been employed to improve the performance of the control system.

From the standpoint of compensation it is quite likely that better compensator design could have been used, particularly if time and money permitted greater experimentation with other sensing equipment. Aside from the direct

effect of noise in position feedback, the differentiation of this signal to provide velocity feedback was certainly not a desirable approach. An alternate, and probably superior, technique could have made use of a servo accelerometer. This signal could have been integrated to provide the velocity signal thus resulting in smoothed, rather than amplified, noise content. In addition, the acceleration signal might have been used in connection with the velocity feedback to combat the vibrational resonance. One disadvantage of the use of the servo accelerometer is that these devices are generally fairly heavy and would thus have resulted in a larger driven mass to be controlled. Even if the accelerometer weighed as much as a half-pound, the total mass would have been increased by only about eight per cent. Such a change of mass should not have presented undue additional difficulties.

The spindle drive system could also have been improved. No velocity or torque control was provided to the drive motor other than simple rheostat control over voltage input. The description of the cutting tests indicated that the drive motor could not maintain the desired spindle speed while the cut was at the outer area of the contour. This limitation required machining at a higher than desired spindle speed simply to realize a sufficiently high surface speed throughout the cut. The addition of a simple automatic speed control system should have helped this condition considerably.

Although the microcomputer portion of the command signal generator worked adequately for this experiment, the scheme could certainly have been improved from the standpoint of flexibility. This hardware would be much more permissive of changes in contour geometry if a disk drive were added. Such storage has the non-volatility desired of EPROM memory, while permitting rapid change in geometry.

The analog portion of the command generator also displayed limitations. The sine wave generator required that the amplitude be tuned to a specific spindle speed. The design of a constant amplitude generator was attempted but not completed successfully. The use of better components and improved noise guarding would also have improved the output of the command generator.

Regardless of the problems described above, the project resulted in a number of accomplishments not previously seen and worthy of note.

First, the system as finally tested represents an improvement over any equipment available today in the application of interest here. There is no marketed machining system which permits the turning of nonaxisymmetric surfaces to the precision quoted here. Although the system will not produce finished surfaces to the desired quality, it will yield a semifinished product of this type more quickly than any other known equipment. Because lapping and polishing are already required for these surfaces, the use of this turning system permits starting of the handwork with a more accurate surface.

Second, the basic scheme for on-line command generation worked quite satisfactorily. Although improvements were suggested in the hardware, the fact is that the concept and its hardware representation functioned as designed even when machining at a higher than desired spindle speed.

Third, if more rigid fixturing had been used, the surface finish measured in the inner surface of the part would probably have been realized over the entire surface. The quality of the surface finish in this region was actually quite gratifying.

Fourth, the contour accuracy of the machined part may have been poor in a relative sense, but in absolute terms was not so very bad. If following

error is used as a measure of "goodness", the control system is better than would normally be found in a conventional numerical control system. It is quite common for such systems to permit one to two mils of position error per inch/minute of slide speed. The control system used here allowed less than a mil at a slide speed of approximately .24 in/sec or over 14 in/min. The difference in the two control systems is that following error in conventional machine tools appears tangent to the machined surface, while that in the system under test was directly reflected in the part surface.

In summary, a prototype machining system was designed and built which provided proof of the principle of nonaxisymmetric turning. It is felt that with the experience gained to date, a second generation machine could be built which would come much closer to satisfying the demanding goals sought in this work. Furthermore, the availability of analytical tools such as the signal analyzer make possible the design of much more sophisticated compensation measures than have been practical before. These considerations thus indicate that the experiment was a success.

LIST OF REFERENCES

LIST OF REFERENCES

[1] Armarego, E. J. A. and Brown, R. H.; *The Machining of Metals*; Prentice-Hall, Inc (1969).

[2] Dall, Albert H.; "Machine Hydraulics: Part V. Sensitive Servos and Tracers", *Machine Design, 18*, (12); December 1946.

[3] Howe, R. E.; Editor; *Introduction to Numerical Control in Manufacturing*; American Society of Tool and Manufacturing Engineers, Detroit, Michigan (1969).

[4] Lewis, T. G.; *Hydrostatic Gas Bearings and Metroloty in Ultra Precision Machine Design*; ASME Lubrication Symposium, New York, New York; June 6-9, 1965.

[5] Gross, W. A.; "A Review of Developments in Externally Pressurized Gas Bearing Technology Since 1959", *Journal of Lubrication Technology, Transactions of ASME*, pp 161-165; January 1969.

[6] Steger, P. J.; *Air Bearing Spindle for Machine Tools-Spherical Design*, Y-1581; Union Carbide Corporation - Nuclear Division, Oak Ridge Y-12 Plant, Oak Ridge, Tennessee; September 1967.

[7] Steger, P. J. and Abbatiello, L. A.; *Air Bearing Spindle for Production Machine Tools*, Y-1578; Union Carbide Corporation - Nuclear Division, Oak Ridge Y-12 Plant, Oak Ridge, Tennessee; September 1967.

[8] Whitten, L. G. and Lewis, T. G.; *Machining and Measurement to Submicron Tolerances*; Seventh International Machine Tool Design and Research Conference, The University of Birmingham, England; September 12-16, 1966.

[9] Wunsch, H. L.; *Air Bearing Applications to Machine Tools and Measuring Instruments*, Paper 68-Lub S-23; Presented at the ASME Lubrication Symposium, Las Vegas, Nevada; June 17-20, 1968.

[10] Sneck, H. J.; *A Survey of Gas-Lubricated Porous Bearings*, Paper 68-Lub S-36; Presented at the ASME Lubrication Symposium, Las Vegas, Nevada; June 17-20, 1968.

[11] Rieger, N. F. and Wilcox, D. F.; "Hydrostatic Gas Bearings", *Machine Design*; March 31, 1966.

[12] Richards, J. B.; *Application of Automatic Tool Setting, Air Bearing Spindles and Laser Interferometer Feedback to Contour Machining*; Seventh International Machine Tool Design and Research Conference, The University of Birmingham, England; September 12-16, 1966.

[13] Schede, R. W.; *Laser Interferometric Feedback for Numerical Control*; Presented at the 19th Annual IEEE Machine Tool Conference, Detroit, Michigan; October 27-29, 1969.

[14] Woodall, N. D.; *Application of Air Bearings and Laser Interferometry to an Inspection Machine*; Presented at the ASME Winter Annual Meeting and Energy Systems Exposition, New York, New York; November 29 - December 3, 1970.

[15] Steger, P. J. and Baldwin, R. R.; *Precision Machining with Diamond Tools*; Presented at the 1969 ASTME Engineering Conference and Tool Exposition, Chicago, Illinois; May 5-9, 1969.

[16] Lewis T. G.; *Ultra Precision Machine Tool Elements and Machining Processes,* Y-1611; Union Carbide Corporation - Nuclear Division, Oak Ridge Y-12 Plant, Oak Ridge, Tennessee; October 1968.

[17] Thompson, D. C.; "Theoretical Tool Movement Required to Diamond Turn an Off-Axis Paraboloid on Axis"; *Proceedings of the Society of Photo-Optical Instrumentation Engineers*, No. 93, San Diego, California, August 26-27, 1976.

[18] Hewlett-Packard Corporation; 5501A System Operating and Service Manual; March, 1977.

[19] Douglass, S. S., Babelay, E. F., Green, W. L., Igou, R. E., and Woodard, L. M.; "Control Systems Improvements in a Coordinate Measuring Machine", *Proceedings of the Joint Automatic Control Conference*; San Francisco, California, August 13, 1980.

[20] Wong, Y. J. and Ott, W. E.; *Function Circuits--Design and Applications*; McGraw-Hill Book Company; New York, New York (1976).

[21] Intel Corporation; *Hardware Reference Manual*

[22] Park, J. E., Giles, G. E., Jr, Rasnick, W. H., and Steger, P. J.; *Computation and Measurement of Flow Rate and Load Capacities for Graphite-Fed Externally Pressurized Gas Bearings*; K/CSD/TM-7; Union Carbide Corporation - Nuclear Division, Oak Ridge Gaseous Diffusion Plant, Oak Ridge, Tennessee; 1978.

[23] Gupta, S. C. and Hasdorff, Lawrence; *Fundamentals of Automatic Control*; John Wiley and Sons, Inc, New York (1970).

[24] Kuo, B. C.; *Automatic Control Systems*, third edition; Prentice-Hall Associates, Inc, Englewood Cliffs, New Jersey (1975).

[25] International Business Machines Corporation; *Continuous Systems Modeling Program III (CSMP III) Program Reference Manual*; IBM Corp. (1972).

[26] Speckart, F. H. and Green, W. L.; *A Guide to Using CSMP, the Continuous System Modeling Program*; Prentice-Hall, Inc., Englewood Cliffs, New Jersey, (1976).

[27] National Semiconductor Corporation; "An Applications Guide for Op Amps", *Linear Applications Handbook*, pp AN20-1,2; National Semiconductor Corp, Santa Clara, California (February, 1969).

[28] Texas Instruments Corporation; *Linear Integrated Circuits*, pp 133-136; Texas Instruments Corp, Dallas, Texas (1976).

[29] Hewlett-Packard Corporation; *Modal Analysis Application Program (MAAP) Operating Note*; HP Technical Note 02-5952-7106.

[30] Barkman, W. E., Brown, R. J., Gerth, H. L. and Green, W. L.; *Interfacing the Linear Motor Slide Drive to a Precision Machine Tool*; Report Y-2180, Union Carbide Corporation - Nuclear Division, Oak Ridge Y-12 Plant; Oak Ridge, Tennessee, April, 1979.

[31] Stoneking, J. E., Gerth, H. L. and Dorris, W. J.; *Analysis of Diamond-Turned Reflective Optics (The Diamond Turning Process - Machining and Analysis Techniques)*; Presented at ASME Winter Annual Meeting, San Francisco, California; December 10-15, 1978.

[32] Gerth, H. L., Sladky, R. E., Bezik, M. J. and Washington, C. A.; *Fabrication of Off-Axis Parabolic Mirrors*; Proceedings of the Society of Photo-Optical Instrumentation Engineers Seminar, v 159; San Diego, California; August 30-31, 1978.

[33] Brehm, P. D.; *Linear Air Bearings for Precision Applications*; Proceedings of Society of Manufacturing Engineers meeting, Dearborn, Michigan; December 30,1970.

[34] Gorez, R. and Szwarcman, M.; *Hydrostatic Slider Gas Bearing Fed Through a Row of Porous Discs*; International Journal of Machine Tool Design and Research v11, n2, pp 89-108; June, 1971.

[35] Barkman, W. E.; *Linear Induction Motor Slide Drive*; Proceedings of Instrument Society of America annual meeting, Philadelphia, Pennsylvania; October 16, 1978.

[36] Rasnick, W. H.; *Air Bearing Rework and Impregnation*; Precision Machining and Gaging Seminar sponsored by the Society of Manufacturing Engineers; Oak Ridge, Tennessee; November 14, 1972.

[37] Burleson, R. R.; *Interferometric Correction System for a Numerically Controlled Machine*; patent application filed by the Department of Energy, October 11, 1977.

APPENDIXES

APPENDIX A

MICROCOMPUTER OPERATOR PROGRAM

APPENDIX A

MICROCOMPUTER OPERATING PROGRAM

```
LOC  OBJ CODE  LINE NO.  SOURCE STATEMENT          COMMENTS
                   01                              ;
                   02                              ;PROGRAM EQUATES
                   03                              ;
3C50               04 SP0       EQU 3C50H
3C62               05 DAT0      EQU 3C62
3C63               06 OLDH      EQU 3C63H
3C64               07 DGP0      EQU 3C64H
3C65               08 DGM1      EQU 3C65H
3C66               09 DGM2      EQU 3C66H
3C67               10 DGM3      EQU 3C67H
3C68               11 BN1       EQU 3C68H
3C6A               12 BN2       EQU 3C6AH
3C6C               13 FLG2      EQU 3C6CH
3C6D               14 FLG1      EQU 3C6DH
3C6E               15 FLG0      EQU 3C6EH
3C6F               16 FLG3      EQU 3C6FH
3C70               17 FLDF2     EQU 3C70H
3C74               18 FLDF1     EQU 3C74H
3C78               19 FLDF0     EQU 3C78H
3C7C               20 FLDF3     EQU 3C7CH
3C80               21 TEMPC     EQU 3C80H
3C84               22 FLT       EQU 3C84H
3C88               23 BASE      EQU 3C88H
3C8A               24 DVSR      EQU 3C8AH
3C8C               25 BTAD      EQU 3C8CH
3C8E               26 BTAD2     EQU 3C8EH
3C90               27 BTAD1     EQU 3C90H
3C92               28 BTAD0     EQU 3C92H
3C94               29 BTAD3     EQU 3C94H
3C96               30 TEMPA     EQU 3C96H
3C98               31 BTNO      EQU 3C98H
3C9A               32 BTNO2     EQU 3C9AH
3C9C               33 BTNO2     EQU 3C9CH
3C9E               34 BTNO0     EQU 3C9EH
3CA0               35 BTNO3     EQU 3CA0H
3CA2               36 TEMPB     EQU 3CA2H
3CA4               37 SUM2      EQU 3CA4H
3CA6               38 SUM1      EQU 3CA6H
3CA8               39 SUM0      EQU 3CA8H
3CAA               40 SUM3      EQU 3CAAH
```

```
3CAC            41 STRO     EQU 3CACH
3CAD            42 CONTR    EQU 3CADH
00BF            43 CW1      EQU 0BFH
0080            44 CW2      EQU 80H
00E7            45 CRA1     EQU 0E7H
00EB            46 CRA2     EQU 0EBH
0000            47 P0DA     EQU 00H
00E4            48 P1DA     EQU 0E4H
00E5            49 P2DA     EQU 0E5H
00E6            50 P3DA     EQU 0E6H
00E8            51 P4DA     EQU 0E8H
00E9            52 P5DA     EQU 0E9H
00EA            53 P6DA     EQU 0EAH
0000            54 P7DA     EQU 00H
0001            55 P8DA     EQU 01H
0002            56 P9DA     EQU 02H
0003            57 PADA     EQU 03H
0005            58 BS2      EQU 05H
0009            59 BS4      EQU 09H
0008            60 FLTDS    EQU 08H
0003            61 FDIV     EQU 03H
0002            62 FMUL     EQU 02H
0009            63 FIXSD    EQU 09H
0005            64 FSUB     EQU 05H
FFF0            65 MEBS     EQU 0FFF0H
0010            66 IOBS     EQU 10H
0001            67 BUSY     EQU 01H
0007            68 ECODE    EQU 07H
01E8            69 CO       EQU 01E8H
01D5            70 CI       EQU 01D5H
00F0            71 MSKF0    EQU 0F0H
000F            72 MSK0F    EQU 0FH
1544            73 TWO0     EQU 1544H
14A2            74 ONE0     EQU 14A2H
1400            75 ZER0     EQU 1400H
15E6            76 TRE0     EQU 15E6H
00F0            77 MEMLO    EQU 0F0H
00FF            78 MEMHI    EQU 0FFH
3C3D            79 USRBR    EQU 3C3DH
1000            80          ORG 1000H
                81                          ;
                82                          ;ON INTR, BRCH
1000  3CE3       83          MVI A,0C3H      ;TO NTYS
1002  323D3C     84          STA USRBR
1005  212D10     85          LXI H,NTYS
1008  223E3C     86          SHLD USRBR+1
                87                          ;
                88                          ;INIT SP, SET
                89                          ;I/O PT MODES.
                90                          ;INIT MATH BRD
                91                          ;MEM BASE
```

```
100B  31503C   92 SETUP:  LXI SP,SP0
100E  3EBF     93        MVI A,CW1      ;PTS 1,2:
1010  D3E7     94        OUT CRA1       ;MD1 IN
1012  3E80     95        MVI A,CW2      ;PTS 4,5,6:
1014  D3EB     96        OUT CRA2       ;MD0 OUT
1016  3E05     97        MVI A,BS2      ;ENAB I/O CHIP
1018  D3E7     98        OUT CRA1       ;INTERRUPT
101A  3E09     99        MVI A,BS4
101C  D3E7     100       OUT CRA1
101E  3EF0     101       MVI A,MEMLO    INIT MATH BRD.
1020  D311     102       OUT IOBS+1
1022  3EFF     103       MVI A, MEMHI
1024  D312     104       OUT IOBS+2
               105                      ;
               106                      ;LOOP, AWAIT INT
               107                      ;
1026  FB       108 NTNO: EI
1027  0600     109       MVI B, 00H
1029  04       110       INR B
102A  C32910   111       JMP $-1
102D  C1       112 NTYS: POP B
102E  F3       113       DI
102F  DBE4     114       IN P1DA        ;GET .1 MIL DATA
1031  2F       115       CMA
1032  21623C   116       LXI H,DAT0
1035  BE       117       CMP M
1036  CA2610   118       JZ NTNO
1039  32623C   119       STA DAT0
103C  DBE5     120       IN P2DA        ;GET 2 LS
103E  32613C   121       STA DAT0-1     ;LASER DGT
1041  DB00     122       IN P0DA        ;GET 2 MS
1043  2F       123       CMA            ;LASER DGT
1044  32603C   124       STA DAT0-2
1047  47       125       MOV B,A
1048  FE72     126       CPI 72H
104A  FA7410   127       JM SKP0
104D  21FF7F   128       LXI H,32767
1050  22A43C   129       SHLD SUM2
1053  CD6F11   130       CALL OPUT2
1056  21FF7F   131       LXI H,32767
1059  22A63C   132       SHLD SUM1
105C  CDE811   133       CALL OPUT1
105F  21FFFF   134       LXI H,0FFFFH
1062  22A83C   135       SHLD SUM0
1065  CD6512   136       CALL OPUT0
1068  210000   137       LXI H,0
106B  22AA3C   138       SHLD SUM3
106E  CDE912   139       CALL OPUT3
1071  C3E510   140       JMP DACS
1074  78       141 SKP0: MOV A,B
1075  21633C   142       LXI H,OLDH     ;CMPR 2 MS DGT
1078  BE       143       CMP M          ;WI OLD VALS.
```

```
1079  CAA210  144           JZ LSDIGS       ;SET FLGS=1
107C  3E01    145           MVI A,01H       ;IF DIFF.
107E  326C3C  146           STA FLG2
1081  326D3C  147           STA FLG1
1084  326E3C  148           STA FLG0
1087  326F3C  149           STA FLG3
108A  78      150           MOV A,B
108B  32633C  151           STA OLDH
108E  3A603C  152 MSDIGS:   LDA DAT0-2      ;SEP 2 MS DGT.
1091  E6F0    153           ANI MSKF0       ;STR MS DGT AT
1093  0F      154           RRC             ;DGP0
1094  0F      155           RRC
1095  0F      156           RRC
1096  0F      157           RRC
1097  32643C  158           STA DGP0
109A  3A643C  159           LDA DAT0-2      ;STR NEXT MS
109D  E60F    160           ANI MSK0F       ; AT DGM1
109F  32653C  161           STA DGM1
10A2  3A613C  162 LSDIGS:   LDA DAT0-1      ;STR 3RD MS
10A5  E6F0    163           ANI MSKF0       ;DGT AT DGM2
10A7  0F      164           RRC
10A8  0F      165           RRC
10A9  0F      166           RRC
10AA  0F      167           RRC
10AB  32663C  168           STA DGM2
10AE  3A613C  169           LDA DAT0-1      ;STR LS DGT
10B1  E60F    170           ANI MSK0F       ;AT DGM3
10B3  32673C  171           STA DGM3
              172                           ;
              173                           ;LSR BCD TO BIN
              174                           ;
10B6  3A6C3C  175           LDA FLG2
10B9  FE01    176           CPI 01H
10BB  C2C910  177           JNZ COEFS
10BE  3E02    178           MVI A,2
10C0  11643C  179           LXI D,DGP0
10C3  CD9313  180           CALL DECODE
10C6  22683C  181           SHLD BN1
10C9  CDF310  182 COEFS:    CALL C02        ;OUT C02 TO
10CC  3A623C  183           LDA DAT0        ;PTS 9,10
10CF  E640    184           ANI 40H
10D1  CAE510  185           JZ DACS
10D4  CD7E11  186           CALL C01        ;IF .1 MIL DGT
10D7  3A673C  187 SKP1:     LDA DGM3        ;=0 OUT C01
10DA  E60F    188           ANI OFH         ;IF MIL DGT=0,
10DC  C2E510  189           JNZ DACS        ;OUT C00 AND C03
10DF  CDF711  190           CALL C00
10E2  CD7B12  191           CALL C03
10E5  3AAC3C  192 DACS:     LDA STRO        ;STRB ALL DATA
10E8  E67F    193           ANI 7FH         ;OUT OF DACS
10EA  D3E8    194           OUT P4DA
```

```
10EC  C680    195          ADI 80H
10EE  D3E8    196          OUT P4DA
10F0  C32610  197          JMP NTNO        ;AWAIT INT.
10F3  3A6C3C  198 C02:     LDA FLG2
10F6  FE01    199          CPI 01H
10F8  C22B11  200          JNZ OLDIF2
10FB  214415  201          LXI H,TWO0
10FE  22883C  202          SHLD BASE
1101  CDF312  203          CALL BASNO
1104  2A8C3C  204          LHLD BTAD
1107  228E3C  205          SHLD BTAD2
110A  22963C  206          SHLD TEMPA
110D  2A983C  207          LHLD BTNO
1110  229A3C  208          SHLD BTNO2
1113  22A23C  209          SHLD TEMPB
1116  21C800  210          LXI H,200
1119  228A3C  211          SHLD DVSR
111C  CD0713  212          CALL DFRNC
111F  2A803C  213          LHLD TEMPC
1122  22703C  214          SHLD FLDF2
1125  2A823C  215          LHLD TEMPC+2
1128  22723C  216          SHLD FLDF2+2
112B  3E02    217 OLDIF2:  MVI A,2
112D  11663C  218          LXI D,DGM2
1130  CD9313  219          CALL DECODE
1133  226A3C  220          SHLD BN2
1136  29      221          DAD H
1137  3A623C  222          LDA DAT0
113A  E640    223          ANI 40H
113C  CA4011  224          JZ$+4
113F  23      225          INX H
1140  22F0FF  226          SHLD MEBS
1143  210000  227          LXI H,0
1146  22F2FF  228          SHLD MEBS+2
1149  3E08    229          MVI A,FLTDS
114B  CDBA13  230          CALL OPCODE
114E  2A703C  231          LHLD FLDF2
1151  22F4FF  232          SHLD MEBS+4
1154  2A723C  233          LHLD FLDF2+2
1157  22F6FF  234          SHLD MEBS+6
115A  3E02    235          MVI A,FMUL
115C  CDBA13  236          CALL OPCODE
115F  3E09    237          MVI A,FIXSD
1161  CDBA13  238          CALL OPCODE
1164  2AF0FF  239          LHLD MEBS
1167  EB      240          XCHG
1168  2A9A3C  241          LHLD BTNO2
116B  19      242          DAD D
116C  22A43C  243          SHLD SUM2
116F  3AA43C  244 OPUT2:   LDA SUM2
1172  D303    245          OUT PADA
1174  3AA53C  246          LDA SUM2+1
```

```
1177  D302     247          OUT P9DA
1179  AF       248          XRA A
117A  326C3C   249          STA FLG2
117D  C9       250          RET
117E  3A6D3C   251 C01:     LDA FLG1
1181  FE01     252          CPI 01
1183  C2B611   253          JNZ OLDIF1
1186  21A214   254          LXI H,ONE0
1189  22883C   255          SHLD BASE
118C  CDF312   256          CALL BASNO
118F  2A8C3C   257          LHLD BTAD
1192  22903C   258          SHLD BTAD1
1195  22963C   259          SHLD TEMPA
1198  2A983C   260          LHLD BTNO
119B  229C3C   261          SHLD BTNO1
119E  22A23C   262          SHLD TEMPB
11A1  216400   263          LXI H,100
11A4  228A3C   264          SHLD DVSR
11A7  CD0713   265          CALL DFRNC
11AA  2A803C   266          LHLD TEMPC
11AD  22743C   267          SHLD FLDF1
11B0  2A823C   268          LHLD TEMPC+2
11B3  22763C   269          SHLD FLDF1+2
11B6  2A6A3C   270 OLDIF1:  LHLD BN2
11B9  22F0FF   271          SHLD MEBS
11BC  210000   272          LXI H,0
11BF  22F2FF   273          SHLD MEBS+2
11C2  3E08     274          MVI A,FLTDS
11C4  CDBA13   275          CALL OPCODE
11C7  2A743C   276          LHLD FLDF1
11CA  22F4FF   277          SHLD MEBS+4
11CD  2A763C   278          LHLD FLDF1+2
11D0  22F6FF   279          SHLD MEBS+6
11D3  3E02     280          MVI A,FMUL
11D5  CDBA13   281          CALL OPCODE
11D8  3E09     282          MVI A,FIXSD
11DA  CDBA13   283          CALL OOPCODE
11DD  2AF0FF   284          LHLD MEBS
11E0  EB       285          XCHG
11E1  2A9C3C   286          LHLD BTNO1
11E4  19       287          DAD D
11E5  22A63C   288          SHLD SUM1
11E8  3AA63C   289 OPUT1:   LDA SUM1
11EB  D301     290          OUT P8DA
11ED  3AA73C   291          LDA SUM1+1
11F0  D300     292          OUT P7DA
11F2  AF       293          XRA A
11F3  326D3C   294          STA FLG1
11F6  C9       295          RET
11F7  3A6E3C   296 C00:     LDA FLG0
11FA  FE01     297          CPI 01
11FC  C22F12   298          JNZ OLDIF0
```

```
11FF  210014  299          LXI H,ZER0
1202  22883C  300          SHLD BASE
1205  CDF312  301          CALL BASNO
1208  2A8C3C  302          LHLD BTAD
1208  22923C  303          SHLD BTAD0
120E  22963C  304          SHLD TEMPA
1211  2A983C  305          LHLD BTNO
1214  229E3C  306          SHLD BTNO0
1217  22A23C  307          SHLD TEMPB
121A  210A00  308          LXI H,10
121D  228A3C  309          SHLD DVSR
1220  CD0713  310          CALL DFRNC
1223  2A803C  311          LHLD TEMPC
1226  22783C  312          SHLD FLDF0
1229  2A823C  313          LHLD TEMPC+2
122C  227A3C  314          SHLD FLDF0+2
122F  3A663C  315 OLDIF0:  LDA DGM2
1232  32F0FF  316          STA MEBS
1235  AF      317          XRA A
1236  32F1FF  318          STA MEBS+1
1239  210000  319          LXI H,0
123C  22F2FF  320          SHLD MEBS+2
123F  3E08    321          MVI A,FLTDS
1241  CDBA13  322          CALL OPCODE
1244  2A783C  323          LHLD FLDO0
1247  22F4FF  324          SHLD MEBS+2
124A  2A7A3C  325          LHLD FLDF0+2
124D  22F6FF  326          SHLD MEBS+6
1250  3E02    327          MVI A,FMUL
1252  CDBA13  328          CALL OPCODE
1255  3E09    329          MVI A,FIXSD
1257  CDBA13  330          CALL OPCODE
125A  2AF0FF  331          LHLD MEBS
125D  EB      332          XCHG
125E  2A9E3C  333          LHLD BTNO0
1261  19      334          DAD D
1262  22A83C  335          SHLD SUM0
1265  3AA83C  336 OPUT0:   LDA SUM0
1268  D3E9    337          OUT P5DA
126A  3AA93C  338          LDA SUM0+1
126D  E67F    339          ANI 7FH
126F  C680    340          ADI 80H
1271  32AC3C  341          STA STRO
1274  D3EB    342          OUT P4DA
1276  AF      343          XRA A
1277  326E3C  344          STA FLG0
127A  C9      345          RET
127B  3A6F3C  346 C03:     LDA FLG3
127E  FE01    347          CPI 01H
1280  C2B312  348          JNZ OLDIF3
1283  21E615  349          LXI H,TRE0
1286  22883C  350          SHLD BASE
```

```
1289  CDF312  351          CALL BASNO
128C  2A8C3C  352          LHLD BTAD
128F  22943C  353          SHLD BTAD3
1292  22963C  354          SHLD TEMPA
1295  2A983C  355          LHLD BTNO
1298  22A03C  356          SHLD BTNO3
129B  22A23C  357          SHLD TEMPB
129E  210A00  358          LXI H,10
12A1  228A3C  359          SHLD DVSR
12A4  CD0713  360          CALL DFRNC
12A7  2A803C  361          LHLD TEMPC
12AA  227C3C  362          SHLD FLDF3
12AD  2A823C  363          LHLD TEMPC+2
12B0  227E3C  364          SHLD FLDF3+2
12B3  3A663C  365 OLDIF3:  LDA DGM2
12B6  32F0FF  366          STA MEBS
12B9  AF      367          XRA A
12BA  32F1FF  368          STA MEBS+1
12BD  210000  369          LXI H,0
12C0  22F2FF  370          SHLD MEBS+2
12C3  3E08    371          MVI A,FLTDS
12C5  CDBA13  372          CALL OPCODE
12C8  2A7C3C  373          LHLD FLDF3
12CB  22F4FF  374          SHLD MEBS+4
12CE  2A7E3C  375          LHLD FLDF3+2
12D1  22F6FF  376          SHLD MEBS+6
12D4  3E02    377          MVI A,FMUL
12D6  CDBA13  378          CALL OPCODE
12D9  3E09    379           MVI A,FIXSD
12DB  CDBA13  380          CALL OPCODE
12DE  2AF0FF  381          LHLD MEBS
12E1  EB      382          XCHG
12E2  2AA03C  383          LHLD BTNO3
12E5  19      384          DAD D
12E6  22AA3C  385          SHLD SUM3
12E9  3AAA3C  386 OPUT3:   LDA SUM3
12EC  D3EA    387          OUT P6DA
12EE  AF      388          XRA A
12EF  326F3C  389          STA FLG3
12F2  C9      390          RET
12F3  2A883C  391 BASNO:   LHLD BASE
12F6  EB      392          XCHG
12F7  2A683C  393          LHLD BN1
12FA  29      394          DAD H
12FB  19      395          DAD D
12FC  228C3C  396          SHLD BTAD
12FF  5E      397          MOVE,M
1300  23      398          INX H
1301  56      399 MOV D,M
1302  EB      400          XCHG
1303  22983C  401          SHLD BTNO
1306  C9      402          RET
```

```
1307  2AA23C  403 DFRNC:  LHLD TEMPB
130A  22F0FF  404         SHLD MEBS
130D  210000  405         LXI H,0
1310  22F2FF  406         SHLD MEBS+2
1313  3E08    407         MVI A,FLTDS
1315  CDBA13  408         CALL OPCODE
1318  2AF0FF  409         LHLD MEBS
131B  22843C  410         SHLD FLT
131E  2AF2FF  411         LHLD MEBS+2
1321  22863C  412         SHLD FLT+2
1324  2A963C  413         LHLD TEMPA
1327  23      414         INX H
1328  23      415         INX H
1329  5E      416         MOV E,M
132A  23      417         INX H
132B  56      418         MOV D,M
132C  EB      419         XCHG
132D  22F0FF  420         SHLD MEBS
1330  210000  421         LXI H,0
1333  22F2FF  422         SHLD MEBS+2
1336  3E08    423         MVI A,FLTDS
1338  CDBA13  424         CALL OPCODE
133B  2A843C  425         LHLD
133E  22F4FF  426         SHLD MEBS+4
1341  2A863C  427         LHLD FLT+2
1344  22F6FF  428         SHLD MEBS+6
1347  3E05    429         MVI A,FSUB
1349  CDBA13  430         CALL OPCODE
134C  2AF0FF  431         LHLD MEBS
134F  22843C  432         SHLD FLT
1352  2AF2FF  433         LHLD MEBS+2
1355  22863C  434         SHLD FLT+2
1358  2A8A3C  435         LHLD DVSR
135B  22F0FF  436         SHLD MEBS
135E  210000  437         LXI H,0
1361  22F2FF  438         SHLD MEBS+2
1364  3E0B    439         MVI A,FLTDS
1366  CDBA13  440         CALL OPCODE
1369  2AF0FF  441         LHLD MEBS
136C  22F4FF  442         SHLD MEBS+4
136F  2AF2FF  443         LHLD MEBS+2
1372  22F6FF  444         SHLD MEBS+6
1375  2A843C  445         LHLD FLT
1378  22F0FF  446         SHLD MEBS
137B  2A863C  447         LHLD FLT+2
137E  22F2FF  448         SHLD MEBS+2
1381  3E03    449         MVI A,FDIV
1383  CDBA13  450         CALL OPCODE
1386  2AF0FF  451         LHLD MEBS
1389  22803C  452         SHLD TEMPC
138C  2AF2FF  453         LHLD MEBS+2
138F  22823C  454         SHLD TEMPC+2
```

```
1392  C9        455             RET
1393  4F        456 DECODE:     MOV C,A
1394  210000    457             LXI H,0
1397  AF        458             XRA A
1398  CDA113    459 LOOP:       CALL BCD
A398  CDA113    460             INX D
139C  0D        461             DCR C
139D  C29813    462             JNZ LOOP
13A0  C9        463             RET
13A1  D5        464 BCD:        PUSH D
13A2  E5        465             PUSH H
13A3  47        466             MOV B,A
13A4  29        467             DAD H
13A5  8F        468             ADC A
13A6  29        469             DAD H
13A7  8F        470             ADC A
13A8  D1        471             POP D
13A9  19        472             DAD D
13AA  88        473             ADC B
13AB  29        474             DAD H
13AC  8F        475             ADC A
13AD  47        476             MOV B,A
13AE  D1        477             POP D
13AF  1A        478             LDAX D
13B0  85        479             ADD L
13B1  6F        480             MOV L,A
13B2  7C        481             MOV A,H
13B3  CE00      482             ACI 0
13B5  67        483             MOV H,A
13B6  78        484             MOV A,B
13B7  CE00      485             ACI 0
13B9  C9        486             RET
13BA  D310      487 OPCODE:     OUT IOBS
13BC  DB17      488 WAIT:       IN IOBS+7
13BE  E601      489             ANI BUSY
13C0  C2BC13    490             JNZ WAIT
13C3  DB11      491             IN IOBS+1
13C5  E607      492             ANI ECODE
13C7  C8        493             RZ
13C8  FE07      494             CPI 07H
13CA  C8        495             RZ
13CB  C630      496             ADI 30H
13CD  4F        497             MOV C,A
13CE  CDE801    498             CALL CO
13D1  0E0D      499             MVI C,0DH
13D3  CDE801    500             CALL CO
13D6  0E0A      501             MVI C,0AH
13D8  CDE801    502             CALL CO
13DB  C9        503             RET
                504             END
```

APPENDIX B

FORTRAN PROGRAMS

APPENDIX B-1

FOURIER EXPANSION OF EQUATION (2-25)

```
C     FOREX4.FOR
C
C     COMPUTES FOURIER COEFFICIENTS FOR THE PRESCRIBED
C     FUNCTION AT 0.1 INCH INTERVALS AND STORES THESE
C     DATA IN FILE FOR30.DAT
C
      IMPLICIT REAL*8(A-H,O-Z)
      DIMENSION X12(81),CO(5),SI(5),C00(81),C01(81),
     1 C02(81),C03(81)
      COMMON A,A1X,A2X2,A3X,Y
      EXTERNAL FORIF,FUN
      N=360
      M=4
      C=316.7
      SY=28.0
      RT=.125
      STH=2.0*SY/DSQRT(C*C+4.0*SY*SY)
      CTH=C/DSQRT(C*C+4.0*SY*SY)
      A=C/(2.0*CTH*STH**2)
      A1=2.0*CTH/(A*STH)
      A2=2.0*CTH/(A*C)
      A3=C/(2.0*SY)
      DO 2 I11=1,81
      X=(I11-1)*.1
      X12(I11)=X
      ITER1=0
      X1=X
1000  ITER1=ITER1+1
      A1X=A1*X1
      A2X2=A2*X1*X1
      A3X=A3*X1
      Y=(C/(2.0*CTH))*(1.0-DSQRT(1.0-(X1*STH/SY)**2))
      DY=X1
      DX=(SY/STH)-Y
      ALPHA=DATAN(DY/DX)
      XTC=X1-RT*DSIN(ALPHA)
      IF(ITER1.EQ.3) GO TO 1001
      X1=X+X1-XTC
      GO TO 1000
1001  YTC=Y+RT*DCOS(ALPHA)
      CALL FORIF(FUN,N,M,CO,SI,IER)
      C0=CO(1)
      S1=SI(2)
      C2=CO(3)
```

```
      S3=SI(4)
      C00(I11)=(C0+C2)
      C01(I11)=(S1+3.0*S3)
      C02(I11)=(-2.*C2)
      C03(I11)=(-4.0*S3)
      WRITE(5,202) I11,X1,Y,XTC,YTC
202    FORMAT(1H ,I2,4(3X,F20.10))
2     CONTINUE
      WRITE(30,203) (X12(I12),C00(I12),C01(I12),
     1 C02(I12),C03(I12),I12=1,81)
203    FORMAT(F4.1,'ϟ,F10.7,'ϟ,F10.7,'ϟ,F10.7,
     1 'ϟ,F10.7)
      END
      FUNCTION FUN(PHI)
      IMPLICIT REAL*8(A-H,O-Z)
      COMMON A,A1X,A2X2,A3X,Y
      SPH=DSIN(PHI)
      FUN=A*(1.0-DSQRT(1.0+A1X*SPH+A2X2*SPH**2-A2X2))
     1 +A3X*SPH-Y
      RETURN
      END
      SUBROUTINE FORIF(FUN,N,M,A,B,IER)
      IMPLICIT REAL*8(A-H,O-Z)
      DIMENSION A(5),B(5)
      IER=0
20     IF(M) 30,40,40
30     IER=2
      RETURN
40     IF(M-N) 60,60,50
50     IER=1
      RETURN
60     AN=N
      COEF=2.0/(2.0*AN+1.0)
      CONST=3.141593*COEF
      S1=DSIN(CONST)
      C1=DCOS(CONST)
      C=1.0
      S=0.0
      J=1
      FUNZ=FUN(0.0)
70     U2=0.0
      U1=0.0
      AI=2*N
75     X=AI*CONST
      U0=FUN(X) + 2.0*C*U1 - U2
      U2=U1
      U1=U0
      AI=AI-1.0
      IF(AI) 80,80,75
80     A(J)=COEF*(FUNZ + C*U1-U2)
      B(J)=COEF*S*U1
      IF(J-(M+1)) 90,100,100
```

```
90     Q=C1*C - S1*S
       S=C1*S + S1*C
       C=Q
       J=J+1
       GO TO 70
100    A(1)=A(1)*.5
       RETURN
       END
```

APPENDIX B-2

FORTRAN PROGRAM FOR SELECTION OF GAIN AND FILTER VARIABLES

```
      IMPLICIT REAL*8(A-H,O-Z)
      DIMENSION XCOF(37),COF(37),ROOTR(36),ROOTI(36)
      WRITE(5,100)
100    FORMAT(1H ,'F(S) = C1 + C2*S + C3*S**2 +
     1 C4*S**3 + ...')
      WRITE(5,101)
101    FORMAT(1H ,'ORDER OF POLYNOMIAL = ',$)
      ACCEPT *,KO
100    WRITE(5,102)
102    FORMAT(1H ,'INPUT COEFFICIENTS')
      DO 1 I=1,KO+1
      WRITE(5,103) I
103    FORMAT(1H ,'C(',I2,') = ',$)
1     ACCEPT *,XCOF(I)
      CALL POLRT(XCOF,COF,KO,ROOTR,ROOTI,IER)
      WRITE(5,104)
104    FORMAT(1H ,3X,'REAL ROOT',11X,'IMAG ROOT'/)
      DO 2 I=1,KO
2     WRITE(5,105) ROOTR(I),ROOTI(I)
105    FORMAT(1H ,D16.10,5X,D16.10)
      WRITE(5,106) IER
106    FORMAT(/1H ,'ERROR CODE = ',I1)
      WRITE(5,150)
150    FORMAT(1H ,'MORE? ',$)
      ACCEPT *,MO
      IF(MO.EQ.1) GO TO 1000
      END
      SUBROUTINE POLRT(XCOF,COF,M,ROOTR,ROOTI,IER)
      IMPLICIT REAL*8(A-H,O-Z)
      DIMENSION XCOF(37),COF(37),ROOTR(36),ROOTI(36)
      IFIT=0
      N=M
      IER=0
      IF(XCOF(N+1)) 10,25,10
10     IF(N) 15,15,32
15     IER=1
20     RETURN
25     IER=4
      GO TO 20
30     IER=2
      GO TO 20
32     IF(N-36) 35,35,30
35     NX=N
```

```
      NXX=N+1
      N2=1
      KJ1=N+1
      DO 40 L=1,KJ1
      MT=KJ1-L+1
40     COF(MT)=XCOF(L)
45     XO=0.00500101
      YO=0.01000101
      IN=0
50     X=XO
      XO=-10.0*YO
      YO=-10.0*X
      X=XO
      Y=YO
      IN=IN+1
      GO TO 59
55     IFIT=1
      XPR=X
      YPR=Y
59     ICT=0
60     UX=0.0
      UY=0.0
      V=0.0
      YT=0.0
      XT=1.0
      U=COF(N+1)
      IF(U) 65,130,65
65     DO 70 I=1,N
      L=N-I+1
      TEMP=COF(L)
      XT2=X*XT - Y*YT
      YT2=X*YT + Y*XT
      U=U + TEMP*XT2
      V=V + TEMP*YT2
      FI=I
      UX=UX + FI*XT*TEMP
      UY=UY - FI*YT*TEMP
      XT=XT2
70     YT=YT2
      SUMSQ=UX*UX + UY*UY
      IF(SUMSQ) 75,110,75
75     DX=(V*UY - U*UX)/SUMSQ
      X=X + DX
      DY=-(U*UY + V*UX)/SUMSQ
      Y=Y + DY
78     IF(DABS(DY) + DABS(DX) - 1.0D-12) 100,80,80
80     ICT=ICT + 1
      IF(ICT-500) 60,85,85
85     IF(IFIT) 100,90,100
90     IF(IN-5) 50,95,95
95     IER=3
      GO TO 20
```

```
100    DO 105 L=1,NXX
       MT=KJ1-L+1
       TEMP=XCOF(MT)
       XCOF(MT)=COF(L)
105    COF(L)=TEMP
       ITEMP=N
       N=NX
       NX=ITEMP
       IF(IFIT) 120,55,120
110    IF(IFIT) 115,50,115
115    X=XPR
       Y=YPR
120    IFIT=0
122    IF(DABS(Y)-1.0D-10*DABS(X)) 135,125,125
125    ALPHA=X + X
       SUMSQ=X*X + Y*Y
       N=N-2
       GO TO 140
130    X=0.0
       NX=NX-1
       NXX=NXX-1
135    Y=0.0
       SUMSQ=0.0
       ALPHA=X
       N=N-1
140    COF(2)=COF(2) + ALPHA*COF(1)
145    DO 150 L=2,N
150    COF(L+1)=COF(L+1) + ALPHA*COF(L) -
     1 SUMSQ*COF(L-1)
155    ROOTI(N2)=Y
       ROOTR(N2)=X
       N2=N2+1
       IF(SUMSQ) 160,165,160
160    Y=-Y
       SUMSQ=0.0
       GO TO 155
165    IF(N) 20,20,45
       END
```

APPENDIX C

CSMP SIMULATIONS

APPENDIX C-1

STEP INPUT TO FIRST LAG-COMPENSATED SYSTEM

```
CONST K1=419.14,P1=.75988,P2=2663.668
CONST W1=290.,W2=2.9,KO=79.432
P2SQ=P2*P2
R2=STEP(0.)
ERR=R2-Z
ERK=KO*ERR
R1=LEDLAG(1./W1,1./W2,ERK)
SZ1=CMPXPL(0.,0.,P1,P2,R1)
SZ=K1*SZ1*P2SQ
Z=INTGRL(0.,SZ)
TIMER FINTIM=.040,OUTDEL=.001,DELMIN=1.E-11
PAGE WIDTH = 80
LABEL Z SLIDE POSITION AND POSITION ERROR VERSUS TIME
OUTPUT Z,ERR
END
STOP
```

Z SLIDE POSITION AND POSITION ERROR VERSUS TIME

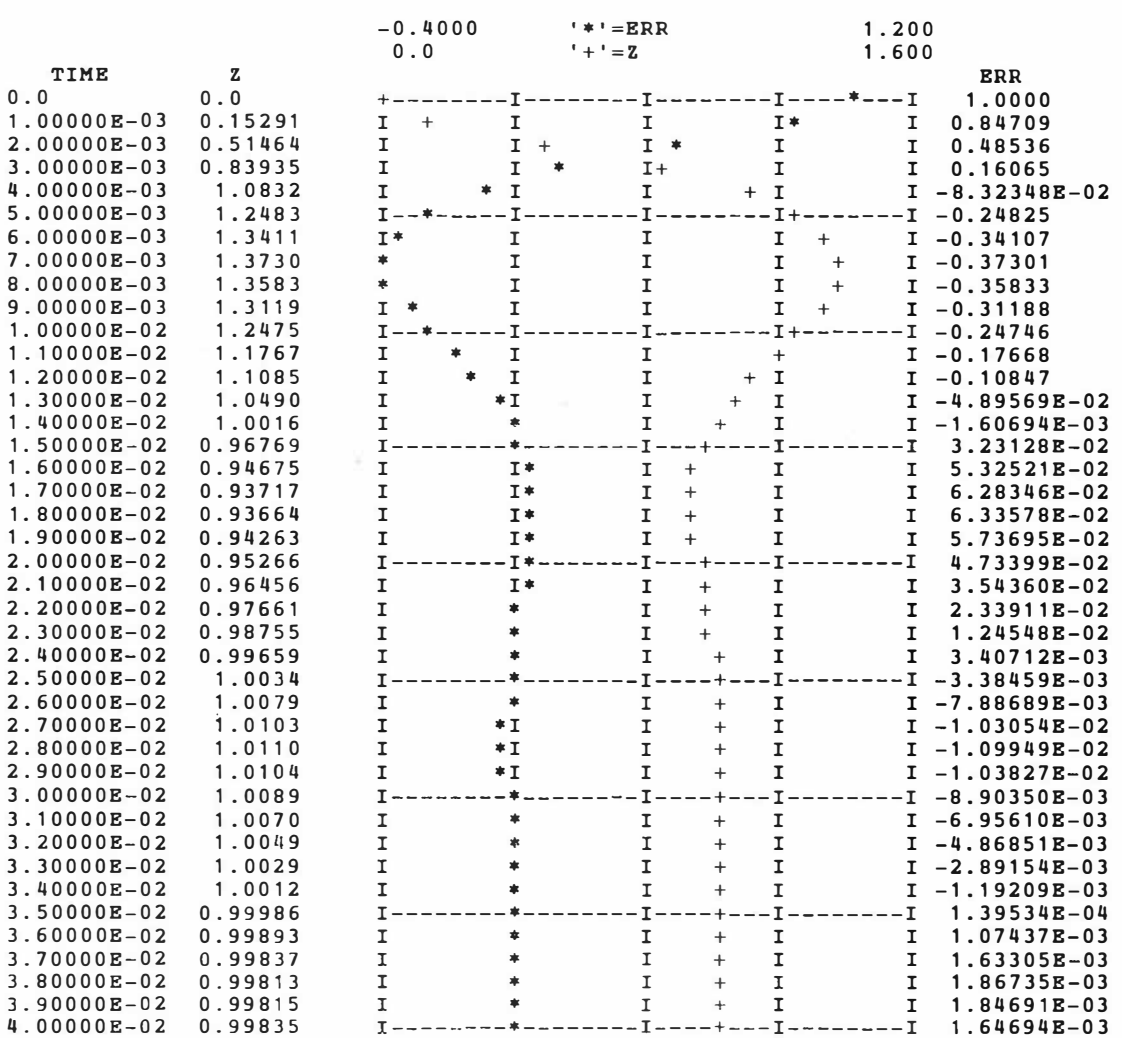

TIME	Z	ERR
0.0	0.0	1.0000
1.00000E-03	0.15291	0.84709
2.00000E-03	0.51464	0.48536
3.00000E-03	0.83935	0.16065
4.00000E-03	1.0832	-8.32348E-02
5.00000E-03	1.2483	-0.24825
6.00000E-03	1.3411	-0.34107
7.00000E-03	1.3730	-0.37301
8.00000E-03	1.3583	-0.35833
9.00000E-03	1.3119	-0.31188
1.00000E-02	1.2475	-0.24746
1.10000E-02	1.1767	-0.17668
1.20000E-02	1.1085	-0.10847
1.30000E-02	1.0490	-4.89569E-02
1.40000E-02	1.0016	-1.60694E-03
1.50000E-02	0.96769	3.23128E-02
1.60000E-02	0.94675	5.32521E-02
1.70000E-02	0.93717	6.28346E-02
1.80000E-02	0.93664	6.33578E-02
1.90000E-02	0.94263	5.73695E-02
2.00000E-02	0.95266	4.73399E-02
2.10000E-02	0.96456	3.54360E-02
2.20000E-02	0.97661	2.33911E-02
2.30000E-02	0.98755	1.24548E-02
2.40000E-02	0.99659	3.40712E-03
2.50000E-02	1.0034	-3.38459E-03
2.60000E-02	1.0079	-7.88689E-03
2.70000E-02	1.0103	-1.03054E-02
2.80000E-02	1.0110	-1.09949E-02
2.90000E-02	1.0104	-1.03827E-02
3.00000E-02	1.0089	-8.90350E-03
3.10000E-02	1.0070	-6.95610E-03
3.20000E-02	1.0049	-4.86851E-03
3.30000E-02	1.0029	-2.89154E-03
3.40000E-02	1.0012	-1.19209E-03
3.50000E-02	0.99986	1.39534E-04
3.60000E-02	0.99893	1.07437E-03
3.70000E-02	0.99837	1.63305E-03
3.80000E-02	0.99813	1.86735E-03
3.90000E-02	0.99815	1.84691E-03
4.00000E-02	0.99835	1.64694E-03

APPENDIX C-2

RAMP INPUT TO FIRST LAG-COMPENSATED SYSTEM

```
CONST K1=419.14,P1=.75988,P2=2663.668
CONST W1=290.,W2=2.9,KO=79.432
P2SQ=P2*P2
R2=RAMP(0.)
ERR=R2-Z
ERK=KO*ERR
R1=LEDLAG(1./W1,1./W2,ERK)
SZ1=CMPXPL(0.,0.,P1,P2,R1)
SZ=K1*SZ1*P2SQ
Z=INTGRL(0.,SZ)
TIMER FINTIM=.040,OUTDEL=.001,DELMIN=1.E-11
PAGE WIDTH = 80
LABEL Z SLIDE POSITION AND POSITION ERROR VERSUS TIME
OUTPUT Z,ERR
END
STOP
```

Z SLIDE POSITION AND POSITION ERROR VERSUS TIME

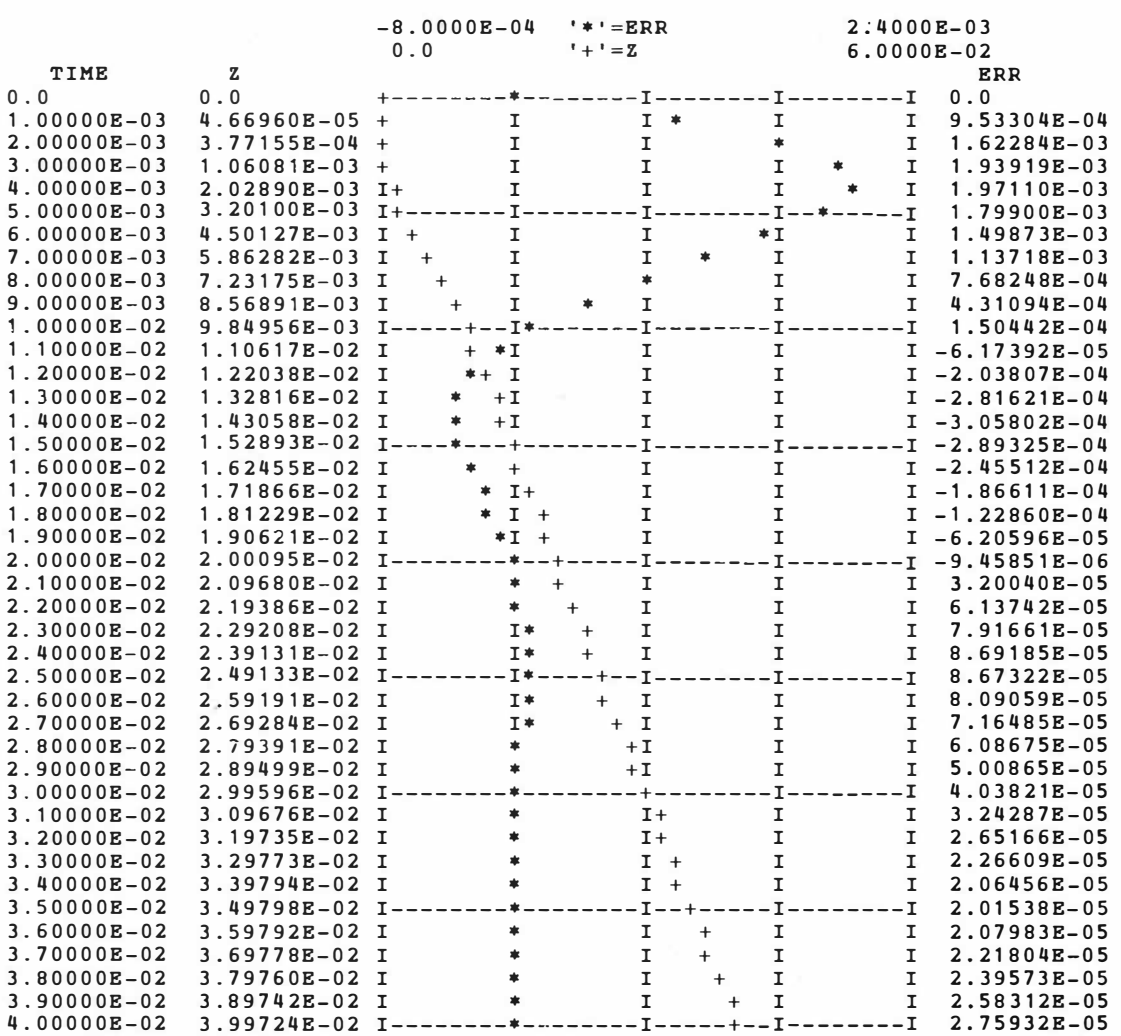

TIME	Z	ERR
0.0	0.0	0.0
1.00000E-03	4.66960E-05	9.53304E-04
2.00000E-03	3.77155E-04	1.62284E-03
3.00000E-03	1.06081E-03	1.93919E-03
4.00000E-03	2.02890E-03	1.97110E-03
5.00000E-03	3.20100E-03	1.79900E-03
6.00000E-03	4.50127E-03	1.49873E-03
7.00000E-03	5.86282E-03	1.13718E-03
8.00000E-03	7.23175E-03	7.68248E-04
9.00000E-03	8.56891E-03	4.31094E-04
1.00000E-02	9.84956E-03	1.50442E-04
1.10000E-02	1.10617E-02	-6.17392E-05
1.20000E-02	1.22038E-02	-2.03807E-04
1.30000E-02	1.32816E-02	-2.81621E-04
1.40000E-02	1.43058E-02	-3.05802E-04
1.50000E-02	1.52893E-02	-2.89325E-04
1.60000E-02	1.62455E-02	-2.45512E-04
1.70000E-02	1.71866E-02	-1.86611E-04
1.80000E-02	1.81229E-02	-1.22860E-04
1.90000E-02	1.90621E-02	-6.20596E-05
2.00000E-02	2.00095E-02	-9.45851E-06
2.10000E-02	2.09680E-02	3.20040E-05
2.20000E-02	2.19386E-02	6.13742E-05
2.30000E-02	2.29208E-02	7.91661E-05
2.40000E-02	2.39131E-02	8.69185E-05
2.50000E-02	2.49133E-02	8.67322E-05
2.60000E-02	2.59191E-02	8.09059E-05
2.70000E-02	2.69284E-02	7.16485E-05
2.80000E-02	2.79391E-02	6.08675E-05
2.90000E-02	2.89499E-02	5.00865E-05
3.00000E-02	2.99596E-02	4.03821E-05
3.10000E-02	3.09676E-02	3.24287E-05
3.20000E-02	3.19735E-02	2.65166E-05
3.30000E-02	3.29773E-02	2.26609E-05
3.40000E-02	3.39794E-02	2.06456E-05
3.50000E-02	3.49798E-02	2.01538E-05
3.60000E-02	3.59792E-02	2.07983E-05
3.70000E-02	3.69778E-02	2.21804E-05
3.80000E-02	3.79760E-02	2.39573E-05
3.90000E-02	3.89742E-02	2.58312E-05
4.00000E-02	3.99724E-02	2.75932E-05

APPENDIX C-3

STEP INPUT TO LEAD-LAG COMPENSATED SYSTEM

(NO VELOCITY FEEDBACK)

```
CONST P1=302.5,P2=3808.,KP=2582.
CONST W1=35.,W2=1.,W3=100.,W4=3500.,KO=7.5
R2=STEP(0.)
ERR=R2-Z
ERK=ERR*KO
EGO1=LEDLAG(1./W1,1./W2,ERK)
R1=LEDLAG(1./W3,1./W4,EGO1)
GP1=KP*R1
GP2=REALPL(0.,1./P1,GP1)
SZ=REALPL(0.,1./P2,GP2)
Z=INTGRL(0.,SZ)
TIMER FINTIM=.040,OUTDEL=.001,DELMIN=1.E-11
OUTPUT Z,ERR
PAGE WIDTH = 80
LABEL Z SLIDE POSITION AND POSITION ERROR VERSUS TIME
END
STOP
```

Z SLIDE POSITION AND POSITION ERROR VERSUS TIME

TIME	Z	-0.4000 '*'=ERR 0.0 '+'=Z 1.200 1.200	ERR
0.0	0.0	+---------I---------I---------I----*---I	1.0000
1.00000E-03	0.68497	I I * I + I I	0.31503
2.00000E-03	1.1017	I * I I I + I	-0.10173
3.00000E-03	0.93065	I I* I I+ I	6.93514E-02
4.00000E-03	0.91793	I I * I I+ I	8.20672E-02
5.00000E-03	0.96146	I---------I*--------I---------I-+------I	3.85364E-02
6.00000E-03	0.96457	I I* I I + I	3.54295E-02
7.00000E-03	0.96707	I * I I + I	3.29300E-02
8.00000E-03	0.97525	I * I I + I	2.47468E-02
9.00000E-03	0.98123	I * I I + I	1.87660E-02
1.00000E-02	0.98596	I---------*---------I---------I--+-----I	1.40432E-02
1.10000E-02	0.99055	I * I I + I	9.44573E-03
1.20000E-02	0.99467	I * I I + I	5.32895E-03
1.30000E-02	0.99827	I * I I + I	1.72883E-03
1.40000E-02	1.0015	I * I I + I	-1.47724E-03
1.50000E-02	1.0043	I---------*---------I---------I--+-----I	-4.32110E-03
1.60000E-02	1.0068	I * I I + I	-6.82735E-03
1.70000E-02	1.0090	I * I I + I	-9.02462E-03
1.80000E-02	1.0109	I *I I I + I	-1.09453E-02
1.90000E-02	1.0126	I *I I I + I	-1.26162E-02
2.00000E-02	1.0141	I--------*I---------I---------I---+----I	-1.40600E-02
2.10000E-02	1.0153	I *I I I + I	-1.52922E-02
2.20000E-02	1.0163	I *I I I + I	-1.63412E-02
2.30000E-02	1.0172	I *I I I + I	-1.72224E-02
2.40000E-02	1.0179	I *I I I + I	-1.79472E-02
2.50000E-02	1.0185	I--------*I---------I---------I---+----I	-1.85394E-02
2.60000E-02	1.0190	I *I I I + I	-1.90058E-02
2.70000E-02	1.0194	I *I I I + I	-1.93644E-02
2.80000E-02	1.0196	I *I I I + I	-1.96238E-02
2.90000E-02	1.0198	I *I I I + I	-1.97916E-02
3.00000E-02	1.0199	I--------*I---------I---------I---+----I	-1.98746E-02
3.10000E-02	1.0199	I *I I I + I	-1.99013E-02
3.20000E-02	1.0199	I *I I I + I	-1.98746E-02
3.30000E-02	1.0198	I *I I I + I	-1.97706E-02
3.40000E-02	1.0196	I *I I I + I	-1.96209E-02
3.50000E-02	1.0194	I--------*I---------I---------I---+----I	-1.94483E-02
3.60000E-02	1.0192	I *I I I + I	-1.92261E-02
3.70000E-02	1.0189	I *I I I + I	-1.89457E-02
3.80000E-02	1.0187	I *I I I + I	-1.86758E-02
3.90000E-02	1.0184	I *I I I + I	-1.83849E-02
4.00000E-02	1.0180	I--------*I---------I---------I---+----I	-1.80473E-02

APPENDIX C-4

RAMP INPUT TO LEAD-LAG COMPENSATED SYSTEM

(NO VELOCITY FEEDBACK)

```
CONST P1=302.5,P2=3808.,KP=2582.
CONST W1=35.,W2=1.,W3=100.,W4=3500.,KO=7.5
R2=RAMP(0.)
ERR=R2-Z
ERK=ERR*KO
EGO1=LEDLAG(1./W1,1./W2,ERK)
R1=LEDLAG(1./W3,1./W4,EGO1)
GP1=KP*R1
GP2=REALPL(0.,1./P1,GP1)
SZ=REALPL(0.,1./P2,GP2)
Z=INTGRL(0.,SZ)
TIMER FINTIM=.040,OUTDEL=.001,DELMIN=1.E-11
OUTPUT Z,ERR
PAGE WIDTH = 80
LABEL Z SLIDE POSITION AND POSITION ERROR VERSUS TIME
END
STOP
```

Z SLIDE POSITION AND POSITION ERROR VERSUS TIME

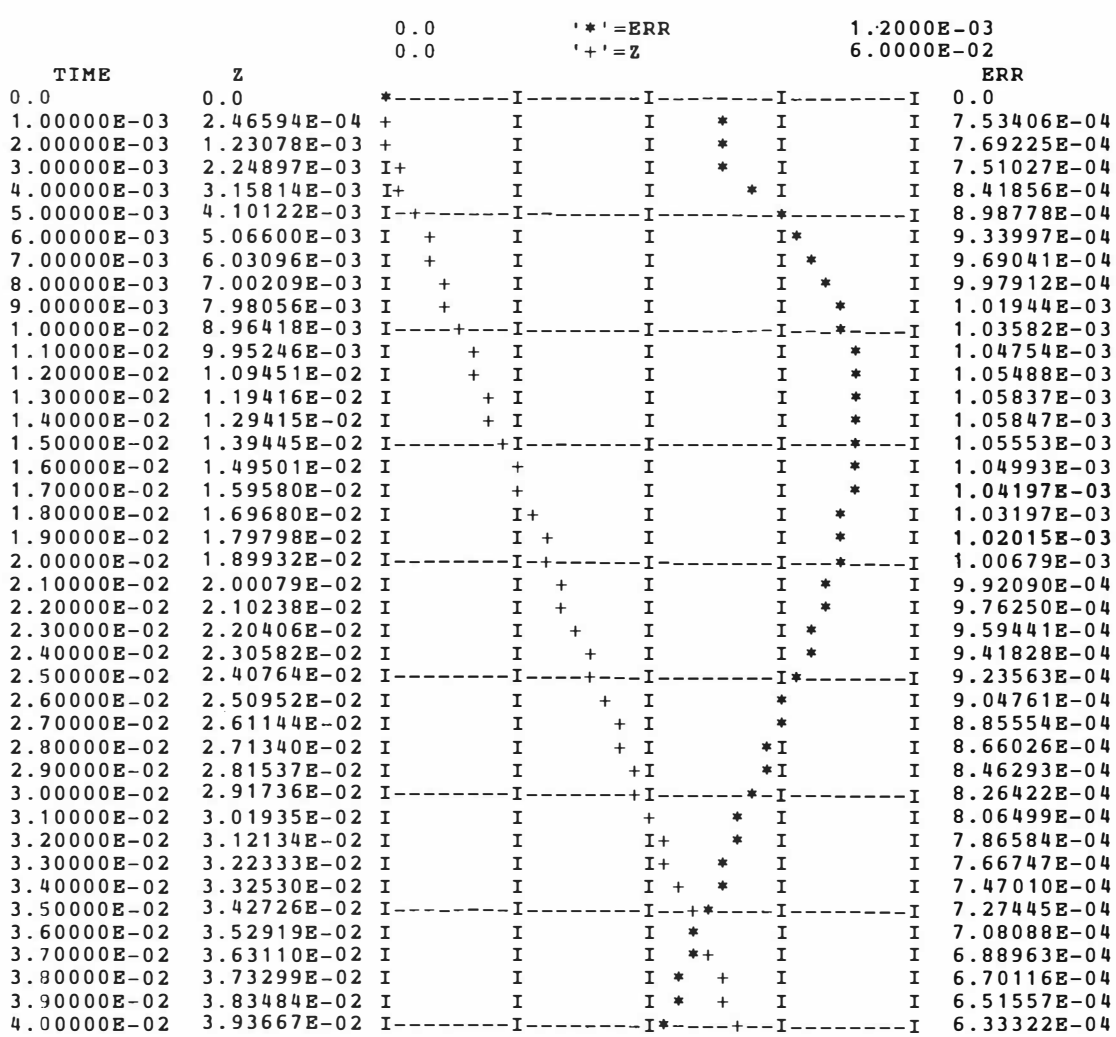

TIME	Z	ERR
0.0	0.0	0.0
1.00000E-03	2.46594E-04	7.53406E-04
2.00000E-03	1.23078E-03	7.69225E-04
3.00000E-03	2.24897E-03	7.51027E-04
4.00000E-03	3.15814E-03	8.41856E-04
5.00000E-03	4.10122E-03	8.98778E-04
6.00000E-03	5.06600E-03	9.33997E-04
7.00000E-03	6.03096E-03	9.69041E-04
8.00000E-03	7.00209E-03	9.97912E-04
9.00000E-03	7.98056E-03	1.01944E-03
1.00000E-02	8.96418E-03	1.03582E-03
1.10000E-02	9.95246E-03	1.04754E-03
1.20000E-02	1.09451E-02	1.05488E-03
1.30000E-02	1.19416E-02	1.05837E-03
1.40000E-02	1.29415E-02	1.05847E-03
1.50000E-02	1.39445E-02	1.05553E-03
1.60000E-02	1.49501E-02	1.04993E-03
1.70000E-02	1.59580E-02	1.04197E-03
1.80000E-02	1.69680E-02	1.03197E-03
1.90000E-02	1.79798E-02	1.02015E-03
2.00000E-02	1.89932E-02	1.00679E-03
2.10000E-02	2.00079E-02	9.92090E-04
2.20000E-02	2.10238E-02	9.76250E-04
2.30000E-02	2.20406E-02	9.59441E-04
2.40000E-02	2.30582E-02	9.41828E-04
2.50000E-02	2.40764E-02	9.23563E-04
2.60000E-02	2.50952E-02	9.04761E-04
2.70000E-02	2.61144E-02	8.85554E-04
2.80000E-02	2.71340E-02	8.66026E-04
2.90000E-02	2.81537E-02	8.46293E-04
3.00000E-02	2.91736E-02	8.26422E-04
3.10000E-02	3.01935E-02	8.06499E-04
3.20000E-02	3.12134E-02	7.86584E-04
3.30000E-02	3.22333E-02	7.66747E-04
3.40000E-02	3.32530E-02	7.47010E-04
3.50000E-02	3.42726E-02	7.27445E-04
3.60000E-02	3.52919E-02	7.08088E-04
3.70000E-02	3.63110E-02	6.88963E-04
3.80000E-02	3.73299E-02	6.70116E-04
3.90000E-02	3.83484E-02	6.51557E-04
4.00000E-02	3.93667E-02	6.33322E-04

APPENDIX C-5

STEP INPUT TO FINAL LAG COMPENSATED SYSTEM

```
CONST P1=1162.4,P2=7634.1,KP=674.
CONST W1=4.16667,W2=.378788,W3=3030.3,KO=6.
R2=STEP(0.)
ERR=R2-Z
ERK=ERR*KO
R11=LEDLAG(1./W1,1./W2,ERK)
R1=REALPL(0.,1./W3,R11)
GP1=KP*R1
GP2=REALPL(0.,1./P1,GP1)
SZ=REALPL(0.,1./P2,GP2)
Z=INTGRL(0.,SZ)
TIMER FINTIM=.040,OUTDEL=.001,DELMIN=1.E-11
OUTPUT Z,ERR
PAGE WIDTH = 80
LABEL Z SLIDE POSITION AND POSITION ERROR VERSUS TIME
END
STOP
```

Z SLIDE POSITION AND POSITION ERROR VERSUS TIME

		-0.4000 '*'=ERR 1.200	
		0.0 '+'=Z 1.200	
TIME	Z		ERR
0.0	0.0	+---------I---------I---------I----*---I	1.0000
1.00000E-03	6.49377E-02	I+ I I I * I	0.93506
2.00000E-03	0.29797	I + I * I	0.70203
3.00000E-03	0.56907	I I +I* I	0.43093
4.00000E-03	0.78981	I I * I + I	0.21019
5.00000E-03	0.93521	I---------I*--------I---------I+--------I	6.47897E-02
6.00000E-03	1.0136	I *I I I + I	-1.36185E-02
7.00000E-03	1.0450	I *I I I + I	-4.50487E-02
8.00000E-03	1.0494	I *I I I + I	-4.93584E-02
9.00000E-03	1.0414	I *I I I + I	-4.14286E-02
1.00000E-02	1.0304	I--------*I---------I---------I---+----I	-3.04127E-02
1.10000E-02	1.0208	I *I I I + I	-2.08416E-02
1.20000E-02	1.0142	I *I I I + I	-1.42231E-02
1.30000E-02	1.0104	I *I I I + I	-1.04465E-02
1.40000E-02	1.0088	I * I I + I	-8.76236E-03
1.50000E-02	1.0083	I---------*---------I---------I---+----I	-8.34751E-03
1.60000E-02	1.0085	I * I I + I	-8.54588E-03
1.70000E-02	1.0089	I * I I + I	-8.93784E-03
1.80000E-02	1.0093	I * I I + I	-9.30214E-03
1.90000E-02	1.0096	I * I I + I	-9.55391E-03
2.00000E-02	1.0097	I---------*---------I---------I---+----I	-9.68933E-03
2.10000E-02	1.0097	I * I I + I	-9.73129E-03
2.20000E-02	1.0097	I * I I + I	-9.71699E-03
2.30000E-02	1.0097	I * I I + I	-9.67026E-03
2.40000E-02	1.0096	I * I I + I	-9.61399E-03
2.50000E-02	1.0096	I---------*---------I---------I---+----I	-9.55677E-03
2.60000E-02	1.0095	I * I I + I	-9.50241E-03
2.70000E-02	1.0095	I * I I + I	-9.45473E-03
2.80000E-02	1.0094	I * I I + I	-9.41086E-03
2.90000E-02	1.0094	I * I I + I	-9.36890E-03
3.00000E-02	1.0093	I---------*---------I---------I---+----I	-9.33075E-03
3.10000E-02	1.0093	I * I I + I	-9.29260E-03
3.20000E-02	1.0093	I * I I + I	-9.25446E-03
3.30000E-02	1.0092	I * I I + I	-9.21631E-03
3.40000E-02	1.0092	I * I I + I	-9.17816E-03
3.50000E-02	1.0091	I---------*---------I---------I---+----I	-9.14001E-03
3.60000E-02	1.0091	I * I I + I	-9.10187E-03
3.70000E-02	1.0091	I * I I + I	-9.06372E-03
3.80000E-02	1.0090	I * I I + I	-9.02557E-03
3.90000E-02	1.0090	I * I I + I	-8.98743E-03
4.00000E-02	1.0089	I---------*---------I---------I---+----I	-8.94928E-03

APPENDIX C-6

RAMP INPUT TO FINAL LAG COMPENSATED SYSTEM

```
CONST P1=1162.4,P2=7634.1,KP=674.
CONST W1=4.16667,W2=.378788,W3=3030.3,KO=6.
R2=RAMP(0.)
ERR=R2-Z
ERK=ERR*KO
R11=LEDLAG(1./W1,1./W2,ERK)
R1=REALPL(0.,1./W3,R11)
GP1=KP*R1
GP2=REALPL(0.,1./P1,GP1)
SZ=REALPL(0.,1./P2,GP2)
Z=INTGRL(0.,SZ)
TIMER FINTIM=.040,OUTDEL=.001,DELMIN=1.E-11
OUTPUT Z,ERR
PAGE WIDTH = 80
LABEL Z SLIDE POSITION AND POSITION ERROR VERSUS TIME
END
STOP
```

Z SLIDE POSITION AND POSITION ERROR VERSUS TIME

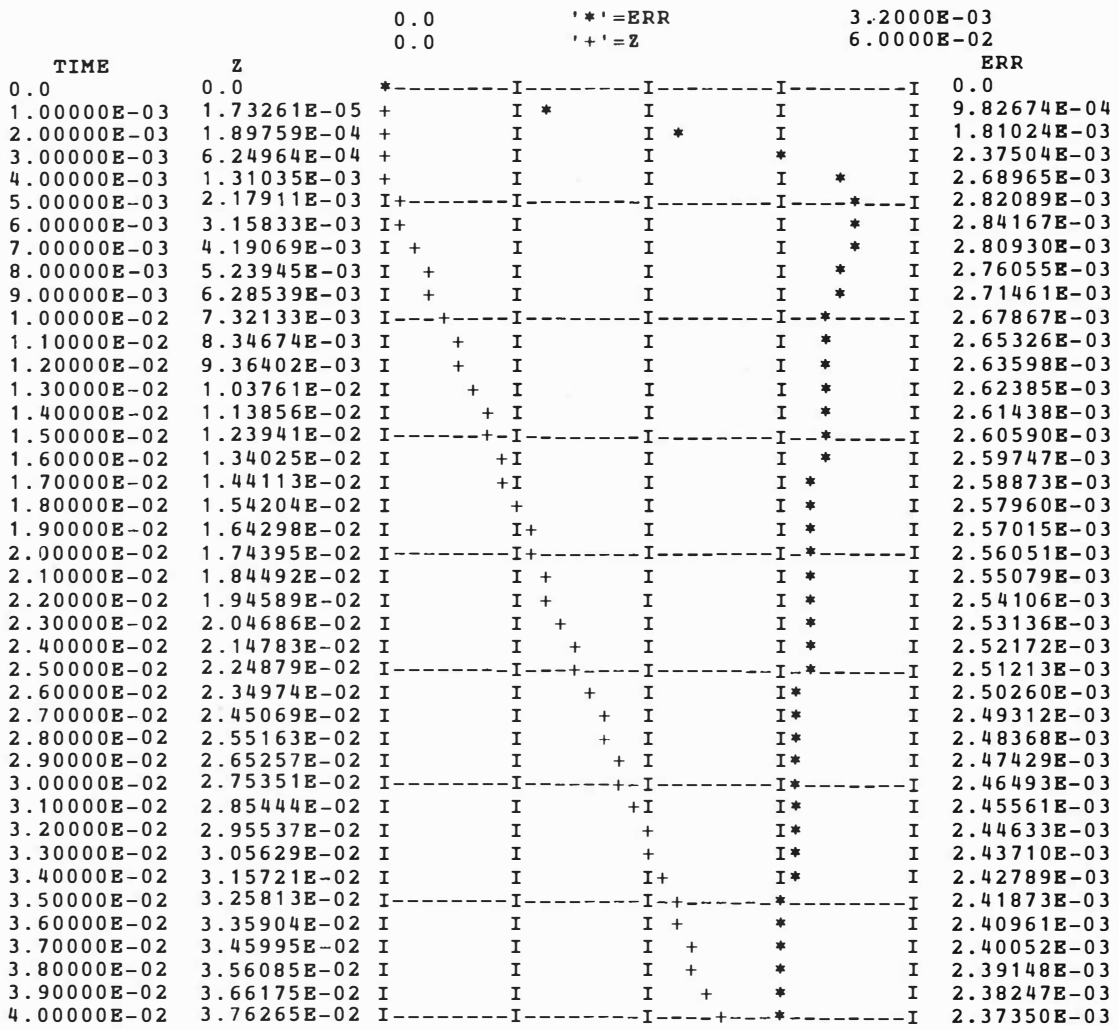

TIME	Z	ERR
0.0	0.0	0.0
1.00000E-03	1.73261E-05	9.82674E-04
2.00000E-03	1.89759E-04	1.81024E-03
3.00000E-03	6.24964E-04	2.37504E-03
4.00000E-03	1.31035E-03	2.68965E-03
5.00000E-03	2.17911E-03	2.82089E-03
6.00000E-03	3.15833E-03	2.84167E-03
7.00000E-03	4.19069E-03	2.80930E-03
8.00000E-03	5.23945E-03	2.76055E-03
9.00000E-03	6.28539E-03	2.71461E-03
1.00000E-02	7.32133E-03	2.67867E-03
1.10000E-02	8.34674E-03	2.65326E-03
1.20000E-02	9.36402E-03	2.63598E-03
1.30000E-02	1.03761E-02	2.62385E-03
1.40000E-02	1.13856E-02	2.61438E-03
1.50000E-02	1.23941E-02	2.60590E-03
1.60000E-02	1.34025E-02	2.59747E-03
1.70000E-02	1.44113E-02	2.58873E-03
1.80000E-02	1.54204E-02	2.57960E-03
1.90000E-02	1.64298E-02	2.57015E-03
2.00000E-02	1.74395E-02	2.56051E-03
2.10000E-02	1.84492E-02	2.55079E-03
2.20000E-02	1.94589E-02	2.54106E-03
2.30000E-02	2.04686E-02	2.53136E-03
2.40000E-02	2.14783E-02	2.52172E-03
2.50000E-02	2.24879E-02	2.51213E-03
2.60000E-02	2.34974E-02	2.50260E-03
2.70000E-02	2.45069E-02	2.49312E-03
2.80000E-02	2.55163E-02	2.48368E-03
2.90000E-02	2.65257E-02	2.47429E-03
3.00000E-02	2.75351E-02	2.46493E-03
3.10000E-02	2.85444E-02	2.45561E-03
3.20000E-02	2.95537E-02	2.44633E-03
3.30000E-02	3.05629E-02	2.43710E-03
3.40000E-02	3.15721E-02	2.42789E-03
3.50000E-02	3.25813E-02	2.41873E-03
3.60000E-02	3.35904E-02	2.40961E-03
3.70000E-02	3.45995E-02	2.40052E-03
3.80000E-02	3.56085E-02	2.39148E-03
3.90000E-02	3.66175E-02	2.38247E-03
4.00000E-02	3.76265E-02	2.37350E-03

VITA

Spivey Stevens Douglass was born in Grenada, Mississippi on January 16, 1939. He attended elementary and high school in that city and was graduated from John Rundle High School in June 1957. The following September he entered Mississippi State University from which he received a Bachelor of Science degree in Mechanical Engineering in June 1961. The following fall he began work on a Master's degree at Mississippi State University while working as a teaching assistant. After completing research for this thesis he began working for the Nuclear Division of Union Carbide Corporation, Oak Ridge, Tennessee, in October 1962. In June 1963 the Master of Science degree was conferred by Mississippi.

Mr. Douglass' doctoral program at the University of Tennessee, Knoxville was conducted both as a full time student working as a research and teaching assistant and also as a part time student while working for Union Carbide. His major fields of study were fluid mechanics and control systems. He received the Doctor of Philosophy degree from the University of Tennessee, Knoxville, in August 1983 and continued his employment with Union Carbide.

Mr. Douglass is married and has four children and lives in Oak Ridge, Tennessee. He is a member of the Society of Manufacturing Engineers and Robotics International.